BIOFUNCTIONALISATION OF ALIGNED FIBRE SCAFFOLDS FOR ANTERIOR CRUCIATE LIGAMENT TISSUE ENGINEERING

A thesis submitted to the University of Manchester for the degree of Doctor of Philosophy in the Faculty of Science and Engineering.

2021

Zara L Smith

Department of Materials

School of Natural Sciences

LIST OF CONTENTS

Final word count: 59,859

ABSTRACT

Anterior cruciate ligament (ACL) tears and ruptures occur in approximately 150,000-200,000 people every year in the USA, costing the health services approximately $7.6 billion USD. Gold standard repair techniques use the patellar tendon autograft, which has a 13% failure rate and associated pain and donor site morbidity. Synthetic grafts have been trialled, but can result in synovial infections and perpetual inflammation. Tissue engineering using biofunctionalised electrospun fibres is a novel method of regenerating ligament tissue by the harnessing physiologically relevant topographical cues, along with biologically relevant attachment sites, which guide cell morphology and reproduction of the native extracellular matrix. Electrospun microfibre scaffolds displayed alignment for across all batches, though showed variable physical (e.g. porosity $p<0.05$, wettability $p<0.001$, surface roughness $p<0.0001$) and mechanical ($p<0.0001$) properties between batches. Scaffolds were plasma treated to improve surface wettability/facilitate protein adsorption, though showed batch variability ($p<0.0001$) between experimental repeats, which appeared to be due to scaffold morphological properties. Scaffolds were incubated with three different fragments of fibrillin-1, where the addition of 1000 ng of PF8 ($p<0.0001$), PF9 ($p<0.0001$) and PF17.1 ($p<0.0001$) appeared to cause an increase in wettability and plasma treated scaffolds showed increased fragment adsorption (PF8 $p<0.0001$, PF9 $p<0.01$, PF17.1 $p<0.0001$). Initial canine anterior cruciate ligamentocyte response to 1000 ng of fibrillin-1 fragments, appeared to show attachment comparable with fibronectin controls (non. sig.), and increased metabolic activity (PF8/17.1, 0 and 1 days, glass substrates, $p<0.05$) and total ECM production (days 1-14, $p<0.05$), though plasma treated scaffolds introduced variability. Human anterior cruciate ligamentocyte response showed differences between donors, though there was some indication of agreement with the canine cell response. Both human and canine cells were capable of producing extracellular matrix proteins on the functionalised scaffolds and the fragments supported the exportation of fibrillin microfibrils into the neo-ECM.

ECM content variation was characterised for degenerative human male anterior cruciate ligaments and was found to be highly variable between donors ($p<0.05$). ECM content was not determined to correlate with age, nor scores reflecting degeneration (non. sig.).

Fibrillin-1 fragment functionalised scaffolds do appear to show promise, and further development of this technology may provide an alternative biofunctionalisation method for ACL tissue engineering.

DECLARATION

No portion of the work referred to in the main body thesis has been submitted in support of an application for another degree or qualification of this or any other university or other institute of learning.

In the appendix of this thesis, there are figures that were present that are from documents previously submitted for MSc Biomedical Materials by Miss M Hu (Appendix 4) and MEng Biomaterials Science and Tissue Engineering by Miss G Crichton (Appendix 2) at the University of Manchester. This work has not been included in the main body of this thesis and is present for justification purposes only.

COPYRIGHT STATEMENT

i. The author of this thesis (including any appendices and/or schedules to this thesis) owns certain copyright or related rights in it (the "Copyright") and s/he has given The University of Manchester certain rights to use such Copyright, including for administrative purposes.

ii. Copies of this thesis, either in full or in extracts and whether in hard or electronic copy, may be made only in accordance with the Copyright, Designs and Patents Act 1988 (as amended) and regulations issued under it or, where appropriate, in accordance with licensing agreements which the University has from time to time. This page must form part of any such copies made.

iii. The ownership of certain Copyright, patents, designs, trademarks and other intellectual property (the "Intellectual Property") and any reproductions of copyright works in the thesis, for example graphs and tables ("Reproductions"), which maybe described in this thesis, may not be owned by the author and may be owned by third parties. Such Intellectual Property and Reproductions cannot and must not be made available for use without the prior written permission of the owner(s) of the relevant Intellectual Property and/or Reproductions

iv. Further information on the conditions under which disclosure, publication and commercialisation of this thesis, the Copyright and any Intellectual Property and/or Reproductions described in it may take place is available in the University IP Policy (see http://documents.manchester.ac.uk/DocuInfo.aspx?DocID=24420), in any relevant Thesis restriction declarations deposited in the University Library, The University

Library's regulations (see http://www.library.manchester.ac.uk/about/regulations/) and in The University's policy on Presentation of Theses.

ACKNOWLEDGEMENTS

Firstly, a huge thank you to my supervisor, Professor Julie Gough, whose guidance and support have been invaluable. Thank you for inviting me into your group and for all the incredible experiences I have had along the way. Thank you also for your patience - for teaching me to trust my own judgement, and for encouraging my independence.

To all those who have collaborated on, and set up the project; Dr Deepak Kumar, Dr Stuart Cain, Dr Pinyuan Tian, Dr Yalda Ashraf Kharaz and Professor Eithne Comerford – thank you all for providing me with the materials for this work, helping me with experiments and for assisting me with getting to grips with the project.

To all the research and technical staff who have assisted me with, or performed analyses for, this work; Marie O'Brien, Dr Louise Carney, Dr Leyla Žilić, Gareth Howell, Dr Andrew Thomas and Dr Marek Nikiel; thank you for all of your advice and help. For taking the time to teach and guide me with methods and for helping me with my analyses.

To Liverpool Musculoskeletal Biobank at Liverpool University for providing me with the human ACL tissue, and to the Henry Royce Institute for Advanced Materials (funded through EPSRC grants EP/R00661X/1, EP/S019367/1, EP/P025021/1 and EP/P025498/1), for the use of the CQ1 cell imaging system.

To the President's Doctoral Scholars Award programme and to EPSRC for the generous funding.

To everyone in the Biomaterials group at the University of Manchester, thank you for support; for all the rants when things got overwhelming, and for discussions about experiments. Above all, thank you for being such encouraging and understanding friends (special thanks to Will Ambler for proofreading parts of this thesis).

To my wonderful partner Wouter, for being my personal crisis manager, even when you had your own thesis to write. For fixing things, writing all the macros I have used for image analysis, proofreading, and for being my greatest source of calm in the more stressful periods of this PhD. Your support has been astounding.

Lastly, to my family; this would not have been possible without the faith you place in me, and your enthusiasm for my pursuits; my achievements are also yours.

LIST OF FIGURES

LIST OF TABLES

LIST OF EQUATIONS

LIST OF ABBREVIATIONS

ACL	Anterior cruciate ligament	**PGA**	Poly-glycolic acid
PCL	Poly-ε-caprolactone	**PLGA**	Poly-lacto-*co*-glycolic acid
FBN1	Fibrillin-1	**-10**	10 ng
MSCs	Mesenchymal stem cells	**-1000**	1000 ng
FN	Fibronectin	**XPS**	X-ray Photoelectron Spectroscopy
COL1	Collagen type I	**FTIR**	Fourier Transform Infra-red Spectroscopy
COL3	Collagen type III	**FBS**	Foetal bovine serum
TCP	Tissue culture plastic	**A/A**	Antibiotics/antimycotics
GC	Borosilicate glass coverslip	**hgDMEM**	High glucose Dulbecco's modified eagles medium
ACL	Anterior cruciate ligament	**LSGS**	Low serum growth factor
ECM	Extracellular Matrix	**CD**	Cluster of differentiation
GM	Genetically modified	**ELN**	Elastin
GAGs	Glycosaminoglycans	**FBLN5**	Fibulin-5
PGs	Proteoglycans	**TEN-C**	Tenascin-C
cACLs	Canine anterior cruciate ligamentocytes	**DEC**	Decorin
hACLs	Human anterior cruciate ligamentocytes	**WLI**	White light interferometry
Saos-2	Human osteosarcoma cell line	**SEM**	Scanning electron microscopy
LARS	Ligament Augmentation Reconstruction System	**IHC**	Immunohistochemistry
PTFE	Polytetrafluoroethylene	**DAPI**	4', 6'-diamidino-2-phenylindole
PET	Polyethylene terephthalate	**DAB**	3, 3'-diaminobenzidine
FDA	Food and Drugs Administration USA	**UV**	Ultra violet light
NIH	National Institute of Health	**BSA**	Bovine serum albumin
TE	Tissue Engineering		
+P	Air plasma treated		
+M	Complete media conditioned		
+N	Sodium hydroxide soaked		
PLA	Poly-L-lactic acid		

AUTHOR INFORMATION

QUALIFICATIONS

2011-2014 BSc Biology (Hons) **University of Hull**

2:1

2014-2015 MSc Nanotechnology & Regenerative Medicine **University College London**

Distinction

2016-2021 PhD Biomedical Materials **University of Manchester**

EMPLOYMENT

2017-2019 Widening Participation Fellow **University of Manchester**

2017-2020 Graduate Teaching Assistant **University of Manchester**

VOLUNTEERING

2016-2020 UCAS Demonstrator **University of Manchester**

2017-2019 Departmental Outreach Volunteer (Materials, EEE) **University of Manchester**

MEMBERSHIP

2017-2021 **Tissue and Cell Engineering Society**

2017-2021 **United Kingdom Society for Biomaterials**

2017-2018 **Tissue Engineering and Regenerative Medicine International Society**

2018-2019 **European Society for Biomaterials**

AWARDS & COMMENDATATIONS

2016-2020 President's Doctoral Scholars Award, **University of Manchester**

2018 Winner - 2nd Year Biomaterials Poster **University of Manchester**

2018 President's Doctoral Scholars Travel Award (£500), **University of Manchester**

2019 Henry Royce Institute Research Grant (~£5300), **University of Manchester**

PEER REVIEWED PUBLICATIONS[*] & PUBLISHED CONFERENCE ABSTRACTS[†]

[†]**Smith ZL**, Kumar D, Ramos Marques D, Hu M, Cain SA, Critchon GS, Ashraf Kharaz Y, Comerford E, Gough JE (2017) Biofunctionalisation of electrospun scaffolds with fibrillin-1 for anterior cruciate ligament repair and regeneration. *eCells & Materials.* eCM Meeting Abstracts 2017. Collection 2. TERMIS EU (P584).

[†]**Smith ZL**, Kumar D, Cain SA, Ashraf Kharaz, Y, Comerford, E, Gough, JE (2018) RGD-containing fibrillin-1 fragments: an initiator protein for anterior cruciate ligament repair and regeneration? *eCells & Materials.* eCM Online Periodical; Collection 4. TCES Conference Abstracts (page 021).

[*]**Smith ZL**, O'Brien M, Williams DA, Gough JE (2021) Histological Extracellular Matrix Characterisation of Degenerative Human Anterior Cruciate Ligament. *Journal of Histology and Histopathology*. **In preparation.**

[*]**Smith ZL**, Kumar D, Ramos Marques D, Cain SA, Ashraf Kharaz Y, Comerford EJ, Gough JE (2021) Fibrillin-1 Functionalised Electrospun Scaffolds for Anterior Cruciate Ligament Repair and Regeneration. *Acta Biomaterialia.* **In preparation.**

CONFERENCE PRESENTATIONS

2017	Tissue Engineering and Regenerative Medicine International Society (Davos, Switzerland)	**Poster**
2017	Tissue and Cell Engineering Society (Manchester, UK)	**Poster**
2018	Tissue and Cell Engineering Society (Keele, UK)	**Oral**
2018	European Society for Biomaterials (Maastricht, Netherlands)	**Oral**

NEXT STEPS

2021-2022 EPSRC Doctoral Prize Fellowship, **University of Manchester**

CHAPTER 1 INTRODUCTION AND PROJECT AIMS

1.1 Introduction

7th September 2008. The New England Patriots had returned to the Gillette Stadium to change their fortune, this time against the Kansas City Chiefs. To help them in this quest; the quarterback and 'Most Valuable Player 2007' Tom Brady. Unfortunately, Brady encountered one of the Chiefs' defensive players, Bernard Pollard, and subsequently took a hit to the left leg. Brady fell and did not get back up[(1)]. Not only that, but he would not set foot on a football field for the rest of the season, following his reconstruction, post-operative infection, and subsequent rehabilitation for an anterior cruciate ligament (ACL) tear[(2)]. This was perhaps one of the most publicised incidences of an ACL injury, viewed by millions of people[(3)]. For the general population, without access to high-end physiotherapeutic care and intense physical rehabilitation training, full recovery from ACL surgery can extend into years as opposed to months.

The ACL is situated inside the knee joint, behind the patellar, and along with the posterior cruciate ligament, is fundamental in the stabilisation of the knee joint. It is generally reported to be made up of two working ligamentous 'bundles'; the posterolateral and anteromedial bundles which support the knee during flexion and extension[(4)]. Consisting primarily of collagen type I and collagen type III in a 9:1 ratio, only 6% of the ACL contains other ECM proteins and cells[(5)]. These cells are of a mainly fibroblastic lineage and are interspersed sparsely throughout the tissue, also lacking the regenerative potential *in situ* to repair the ACL post-injury. This is only exacerbated due to both the presence of inhibitory synovial fluid, and the lack of adequate vasculature. The absence of blood plasma clotting at the injury site means that no preliminary scaffold is formed for the cells to begin the remodelling required to repair the ACL[(6, 7)].

Damage often occurs after forceful valgus movements, with injury occurring at the critical fracture point; a tensile stress of over 24-38 MPa[(8)]. Anterior cruciate ligament (ACL) injuries occur frequently, with 50% of all knee injuries reported as ACL damage[(9)]. Approximately 200,000 ACL injuries occur each year in the USA alone[(10)], resulting in 100,000 reconstructive procedures annually[(11)] at a cost of around $7.6 billion in annual healthcare (2013)[(10)], with $2.6 billion accounting for surgical expenses alone[(12)].

The current 'gold standard' of ligament repair is autograft surgery, requiring muscular tissue from either the patellar tendon or the hamstring. This method however, can result

complications such as donor site morbidity, modular mismatch and graft failure due to loosening of the graft at the bone integration site. Other methods such as allografts, are often taken from cadavers where limitations include; possibility of infection, tissue rejection and limited supply[13]. Since the 1990's synthetic methods have been utilised in an attempt to overcome these issues. They however, also have limitations, such as graft loosening, infection and modular mismatch and lack of biological integration[14].

As all these methods have severe limitations, a tissue engineering approach is currently being explored. The ability to produce functional tissue that has the same modular properties, can integrate biologically, and that can be 'tailored' to the patient, is undeniably attractive. The current methods of repair are bioinert and provide no platform for either integration or regeneration. Furthermore, mechanical properties are somewhat lacking, with current methods such as autografts providing stability for up to 1100 load cycles when 150 N load is applied to simulate walking. When jogging was simulated (450 N), most specimens failed at around 300 load cycles[15]. The preferred graft type, the patellar tendon, although possessing high tensile strength, may still be unsuitable due to the lower ratios of collagen type III present in tendons[16, 17]. Using tissue engineering, it is possible to simulate the exact properties of the ACL, by creating the correct environment in which native cells can be encouraged to reproduce tissue with the correct biochemical composition (i.e. the correct collagen ratios and elastin content). This may lead to a robust neo-ligament with high tensile strength and suitable elasticity. In the following literature review, I will outline the current situation with regards to ACL regeneration and the methods that are currently being explored in the field.

1.2 Identification of the Research Gap

As previously outlined above (section 1.1) there are a number of issues with current methods of ACL reconstruction, which necessitate the exploration into other, potentially more successful methods of reconstruction/regeneration. To this end, tissue engineering of the ACL could be a viable alternative. Many researchers to present have attempted to produce both topographical and biochemical conditions which are optimal to the regeneration of the ACL. Though many have agreed on the use of fibrous scaffolds[18-23], with a diversity of protein components[22, 24-26], though few have attempted to determine the role of RGD fragments in improving the response (namely enhancement of initial cell attachment and

proliferation)[27] of ACL cells. Fibrillin-1 is a glycoprotein present in the native ACL which also contains an RGD motif. This RGD motif interacts with cells, using interacting with similar integrins to fibronectin RGDs[28-30]. Fibrillin-1 is an essential component of the elastic matrix within the ACL and interacts with many other extracellular matrix (ECM) proteins[31-37]. Fibrillin-1 RGD-containing fragments may provide an alternative source for biofunctionalisation of fibrous scaffolds for ACL tissue engineering therapies, and due to interacting with multiple other proteins, and its role in the assembling of late-stage ECM proteins, such as elastin[37], it may further enhance the production (in terms of both acceleration and maturity) of the neo-ACL ECM.

The approach used to address the issues of ACL reconstruction and repair, outlined above, will be tissue engineering-based. This will involve development of a fibrous, biofunctionalised platform scaffold, whereby the use of fibrillin-1 fragments will function as the primary biofunctionalisation method for the novel ACL scaffold. The response of primary ACL fibroblasts to the fibrillin-1 functionalised scaffold can be characterised, for further development of an ACL TE scaffold. This will form the foundation of a functional

construct, which can support the regeneration of the ACL midsubstance by native cells *in vitro*, before implantation into the knee joint as a neo-ligament (illustrated in Figure 1-1).

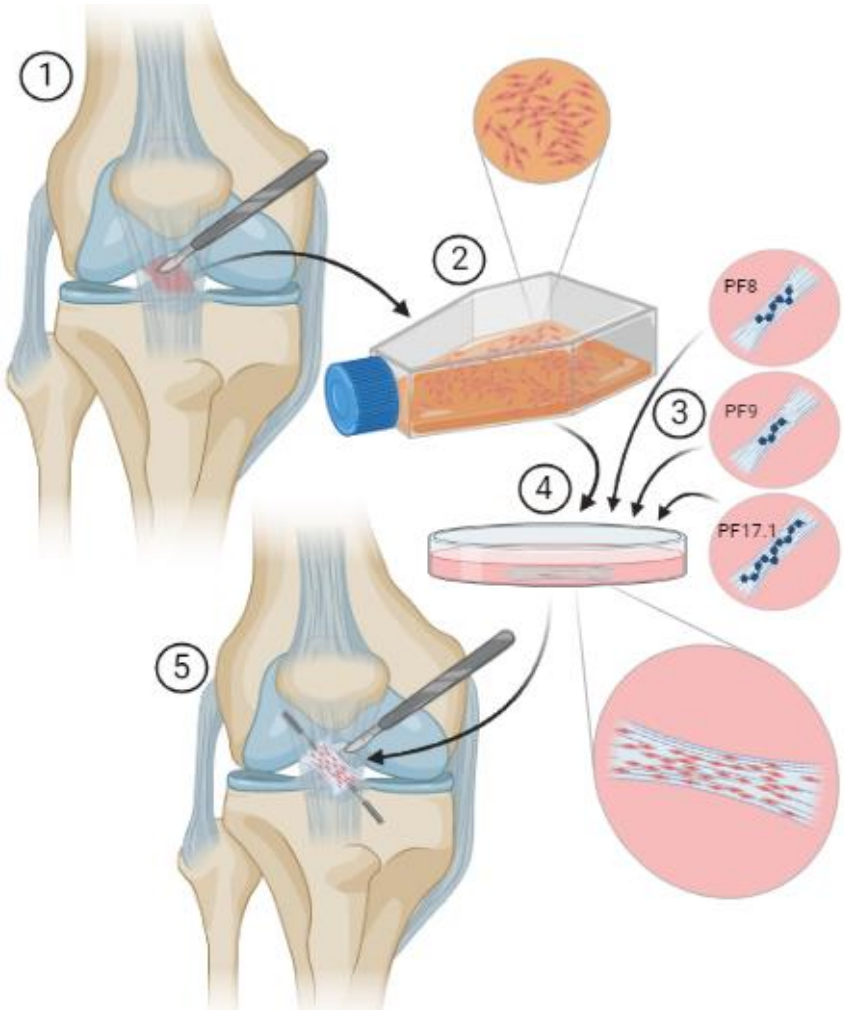

Figure 1-1 Depiction of the proposed approach following the final development of a functional scaffold for ACL regeneration. **(1)** The ACL tissue is excised from the knee joint. **(2)** Cells are isolated from the ligament and expanded in 2D culture. **(3)** The scaffold is functionalised with RGD-containing fragments of fibrillin-1 (PF8/PF9/PF17.1). **(4)** The cultured cells are seeded onto the scaffold and the scaffold is cultured until a mature ECM is formed. **(5)** The tissue-engineered scaffold is replaced into the joint using conventional fixation methods (screws). Created using BioRender.com.

1.3 Thesis Hypothesis

The overall hypothesis of this thesis will be: that an aligned fibre scaffold can be produced which will show limited batch variability. Once biofunctionalised with fibrillin-1 fragments,

these scaffolds will support both canine (from healthy ligament) and human (from degenerative ligament) primary ACL fibroblasts, in retaining more aligned and native morphologies, higher metabolic activity and attachment, and increased ECM protein production, compared to non-biofunctionalised controls.

1.4 Major Aims and Objectives

1.4.1 Aims

The major aims of this thesis will be as follows:

- To fabricate and optimise a reproducible fibrillin-1 fragment functionalised, aligned fibre scaffold suitable for acting as a platform for regeneration of the ACL ECM.
- To determine whether the fibrillin-1 biofunctionalised scaffold is capable of supporting primary native cell behaviour and ECM production.
- To characterise human ACLs and determine whether the biofunctionalised scaffold can support human primary cells isolated from these degenerative ligaments.

1.4.2 Objectives

- Electrospin an aligned fibre scaffold using an FDA-approved synthetic polymer material, PCL.
- Determine batch variability for physical characteristics such as tensile strength (and measures of ductility), porosity, alignment, fibre characteristics, surface roughness, and wettability.
- Determine most appropriate method of surface functionalisation for protein adsorption and cell culture between media-conditioning, sodium hydroxide soaking and air plasma treatment, and ascertain protein adsorption characteristics of the chosen surface functionalisation method for the fibrillin-1 fragments and the combined effect on surface wettability.
- Characterise primary canine ACL fibroblast response to the biofunctionalised scaffolds via morphology, metabolic activity, attachment and neo- collagen type I, fibronectin and fibrillin production with comparisons to negative (no fibrillin-1 fragment) and positive (fibronectin) controls.
- Quantify early-stage orientation of ACL fibroblasts on the biofunctionalised scaffolds.

- Observe specific integrin presence to ascertain attachment of cells to the fibrillin-1 fragments.
- Characterise the ECM content of degenerative human ACL tissue and determine any correlations between protein content and age/degeneration scores.
- Characterise isolated human ACL fibroblast response to biofunctionalised scaffolds via morphology, metabolic activity, attachment and neo- collagen type I, fibronectin and fibrillin production.

CHAPTER 2 LITERATURE REVIEW

2.1 Anatomy of the Anterior Cruciate Ligament

The anterior cruciate ligament (ACL) is one of two ligaments (macro and micro structure displayed in Figure 2-2), which along with posterior cruciate ligament (PCL), perform a stabilising function at the knee joint, preventing conditions such as internal rotation of the joint and anterior tibial translation (ATT)[38]. It is known to be formed of two 'bundles' of tissue – the posterolateral and the anteromedial bundles[39]. These bundles band together and join both at the femoral condyle, and just behind the intercondylar eminence of the tibia[40] to partially secure and form the knee joint. Ligament has a highly hierarchical structure (as depicted in Figure 2-1). The ligament itself is divided into fascicles, long bundles of collagen fibrils that run the length of the ACL.

Current research has discerned that around 65-80% of the ACL is water (wet weight)[41]. In terms of protein components; 85% of the ACL consists of regular, aligned, fibrous collagen type I[16, 39, 42], with collagen type III separating the type I fibrils. Multiple other extra cellular matrix (ECM) proteins, such as elastin and proteoglycans account for a few percent of the ACL composition each[41]. Though sparse, the ligament also contains small amounts of fibroblastic cells (ligamentocytes) which align themselves longitudinally in the interfascicular regions[43]. The purpose of the cellular components are to maintain and repair the ligament tissue[44], though their ability to regenerate is very limited, perhaps due to the ligament fibroblast cells having low proliferative activity[6]. Vascularisation of the ligament has previously been described as poor, which is thought to contribute to its lack of regenerative potential[7]. The main supplier of vasculature to the ACL is the middle genicular artery, which branches off into smaller vessels which vascularise both the proximal and distal ends of the ACL through the epiligament (an outer structure which ensheaths the ACL)[45]. The ACL also possesses a variety of sensory receptors including; free nerve ends, Ruffini corpuscles and Pacinian corpuscles[46]. These receptors, whilst able to detect the changing intensity of mechanical stressors, cannot detect pain. This explains the absence of pain during any incident where the ACL alone suffers traumatic damage[47].

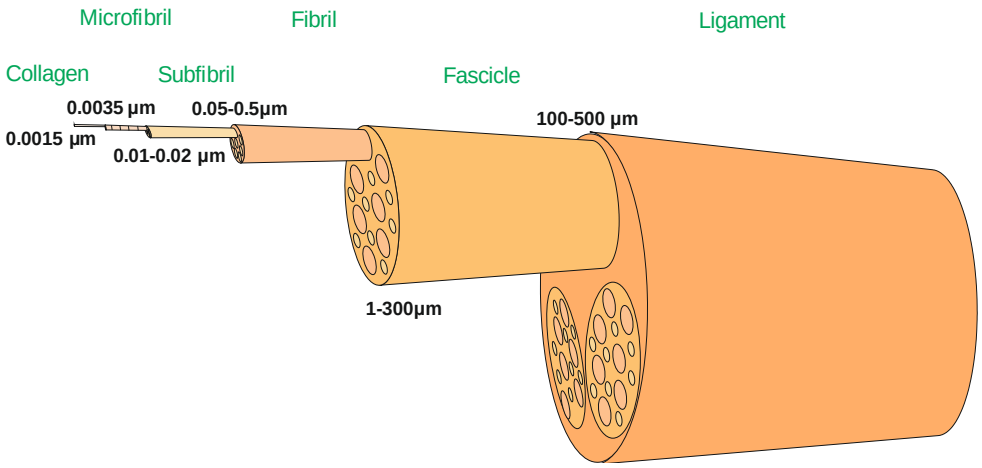

Figure 2-1 A diagram showing the hierarchical structure of ligament tissue. Adapted from Weiss J & Gardiner JC (2001)[48], original by Kastelic J *et al* (1978)[49].

2.1.1 Midsubstance of the ACL

The midsubstance of the ACL (shown in Figure 2-2) is the part that is most widely discussed with reference to the ACL. This section contains the compact collagen fibrils, with their characteristic 'crimped' morphology, that are highly aligned and bundled into clusters, or 'fascicles'. Slowly proliferating fibroblasts, which are elongated in morphology, follow the direction of the collagen fibres, sitting between the fascicles at comparatively low densities. This morphology can appear to change however, during degeneration of the ACL. An increase in ovoid fibrocartilage-like cells be observed in the midsubstance, along with changes in matrix integrity, vascularisation, glycosaminoglycan (GAG) concentration and overall cell density[50]. In normal and healthy ACL midsubstance, the collagen fibrils run longitudinally along the ACL, giving the ligament its high tensile strength. In this section of the ACL, a multitude of proteins have been reported, including: versican and aggrecan (help withstand compression against the PCL during tension[51]), perlecan (associates with elastin and fibrillin-1[52]), decorin and biglycan (interact with elastin and collagen type I fibres[53, 54]), collagen type I (for tensile strength), collagen type III (promotes small amounts of elasticity[51]), tenomodulin (anti-angiogenesis factor[55] and can enhance ligament cell adhesion[56]), tenascin-c (upregulated during injury and perpetuates inflammatory response[57]), fibronectin (form the initial ECM network structure for collagen type I and fibrillin microfibrils[34, 58]), and the components of elastic fibres (containing elastin, fibrillin and fibulins), which align parallel to the collagen bundles in the interfascicular regions[59].

2.1.2 Bone Insertion Sites (Proximal and Distal Ends) of the ACL

The proximal and distal ends of the ACL are much more diverse in their structure and supporting cell populations. Cells that reside in these parts appear osteochondral/fibrochondral, appearing smaller when compared with the cells residing in the midsubstance, and are ovoid in morphology. The proximal end of the ACL (femoral attachment) is characterised by high fibrochondral cells numbers and displays evidence of collagen type II and glycoprotein deposition. However, the distal end of the ACL (tibial attachment) has a collagenous matrix of much lower density, which is arranged into a fine and interconnected net-like weave of fibres, unlike the highly uniform and elongated structure displayed in the midsubstance. The fibrochondral cells which reside here are, unlike at the proximal end, highly active and perhaps due to the local collagen fibre arrangement, possess multiple cell processes which extend equally around the circumference of the cell. At the edge of the ligament-bone insertion site, sat in the interfascicular regions of the ligament, are densely packed lines of chondrocyte-like cells[43, 60-63].

2.2 Biomechanics of the Anterior Cruciate Ligament

As previously mentioned, the ACL consists of two working ligamentous 'bundles'. They work in a partnership where at the bending and stretching of the knee joint, the Posterolateral bundle tightens during extension and the Anteromedial bundle during flexion[4]. As with all ligaments, the biomechanics are entirely dependent on not only the morphology of said ligament, but also mechanical properties of both the ligament tissue (made up of collagen fibrils) and the insertion site (the joining point at which tissue attaches to bone)[64].

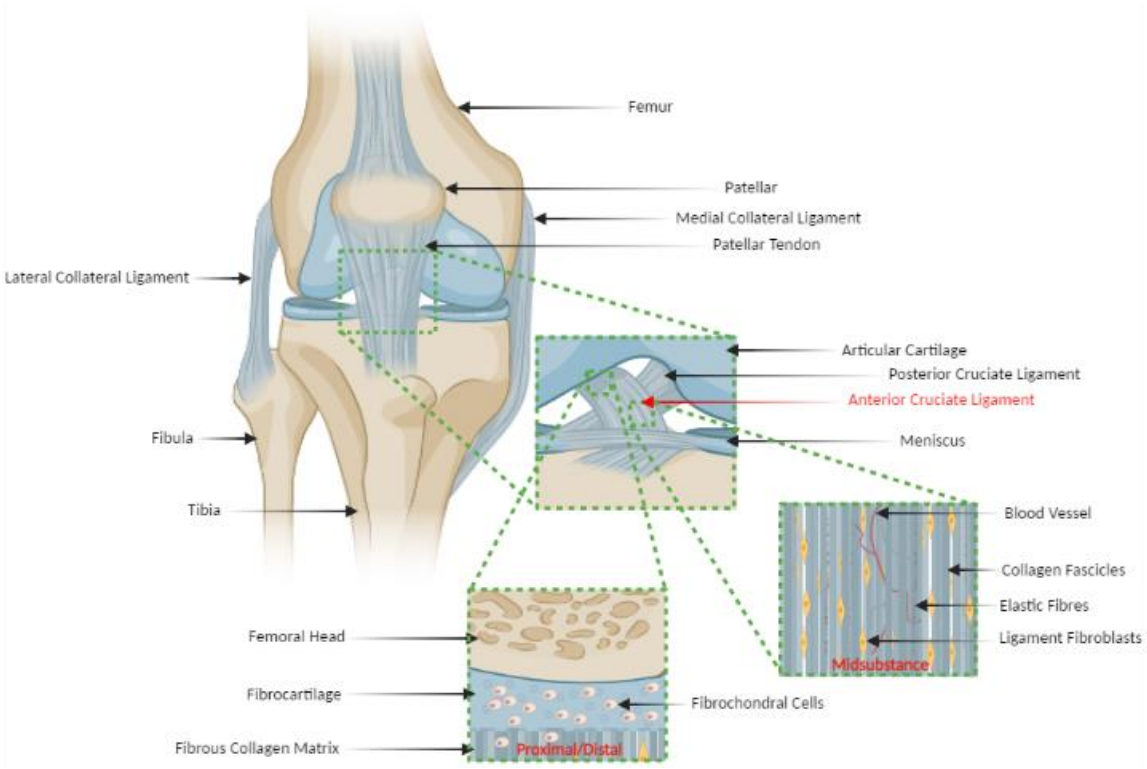

Figure 2-2 A depiction of the position of the anterior cruciate ligament (ACL) within the knee joint and the basic macro and microstructure of the ACL. The ACL sits inside the knee joint, situated behind the posterior cruciate ligament (PCL), forming and X shape across the joint with the PCL. The ACL midsubstance constitutes of highly aligned collagen fibres, sparsely interspersed with elongated, fibroblastic cells. Cells in the bone integration sites (proximal and distal ends) of the ligament tend to be more rounded and of fibrochondral/osteochondral morphology. Image created using BioRender.com.

The primary part of the ACL consists of crimped collagen fibres, designed to withstand and tolerate smaller tensile pressures during axial movement. The subsequent region is one where the collagen fibres are subject to reversible deformation from larger forces. These fibres exhibit a low Young's modulus at low stresses, becoming more resistant to the exerted force at higher stress until their critical stress point and subsequent failure[8]. Butler *et al.* (1992) have reported the figures for the mechanical properties of the ACL, stating a tensile strength of around 24-38 MPa[8] and physiologically normal strain of approximately 10-13% during walking[65] and up to 4.4% during routine exercise[66], due to the presence of elastin in the ligament ECM. However, increased frequency of use in knee joint can cause laxity in the ligaments of the joint after a prolonged period of exercise (when ligaments are stretched and remain so after a consistent load has been applied). This stretching is naturally reversed and original stiffness is regained after a rest period[64].

2.3 Cells of the Anterior Cruciate Ligament: Morphology, Organisation and Activity

The ACL has long been reported to house two distinct cell types; Ligamentocytes, which are usually observed to be aligned along the collagen fibres of the midsubstance of the ACL. However, cells at the distal regions of the ACL can be observed forming small ovoid morphologies and appear to be structurally similar to fibrocartilage cells[5]. Previous research has shown that ligament stem cells reside in the ACL and may even largely contribute to the collagen type I:III ratio that is required to maintain some of the ligament's elasticity. Results revealed that with a 50:50 ligamentocyte and MSC co-culture, subsequent production of the collagen type I:III ECM was closest to 'native'[67].

2.3.1 Inter-Species Differences and Similarities

The ability of cruciate ligamentocytes / stem cells to differentiate into multiple lineages has been shown in humans[68], dogs[69], horses[70] and rabbits[71] with cells shown to be capable of osteogenic, chondrogenic, adipogenic and 'ligamentogenic' (characterised mainly by the production of collagens type I and III, and tenascin-c) differentiation. These ligament stem cells (LSCs) have been discovered to have fibroblast-like phenotypes and have evident inter-species differences between ligament cell markers. While most ACL ligamentocytes express CD90 (Thy-1-GPI-linked glycoprotein receptor), others such as CD105 (endoglin, a type I membrane glycoprotein), CD73 (ecto-5-neucleotidase, enzyme) and CD44 (cell surface adhesion receptor) vary depending on the species analysed, with human and canine ligamentocytes exhibiting the highest expression[72]. With this result in mind, canine cruciate ligamentocytes have also been determined to have the most similar cell morphology with humans, when also compared with those from bovine and ovine sources[73].

2.3.2 Phenotyping the Cells of the ACL

It has long been thought that the ACL predominantly supports cells of a fibroblastic linage. Generally, the cell shape displays that of near 'textbook' fibroblastic morphology. However, these cells appear to express multiple mesenchymal stem cell (MSC) cluster of differentiation (CD) markers, such as; 73, 105, 90, 44, 146 and 166, implying their unusual, but stem cell-like character (popular positive and negative ACL ligamentocyte markers displayed in Table 2-1. They have also been shown to be capable of differentiation into adipogenic, chondrogenic, ligamentogenic and osteogenic cell types[68]. Though it appears that they cannot be selectively differentiated from MSCs, not only in terms of antigen expression and morphology, but also gene expression of integral ACL ECM proteins (such

as collagen type I and III, and tenascin-c). A novel method to assess phenotype, based on the discrimination of surface charge, has been identified. Cells tend to have a net negative surface charge due to the proteins that cover their surface membranes. The electrophoretic mobility of MSCs appears to be significantly higher than ACL ligamentocytes, though this cannot give information about the cells within the population, only identify that the populations themselves are phenotypically different. The protein that contributes to the higher mobility characteristic in MSCs has yet to be identified[74].

Other types of cells, for example $CD34^+$ vascular stem cells and myofibroblasts, migrate into the ligament during healing. While the myofibroblasts have a greater propensity for collagen type III production that normal ligamentocytes, and can be characterised the presence of α-smooth muscle actin[75], $CD34^+$ cells have been shown to contribute to healing at the osteointegration site[76].

Table 2-1 A table describing some commonly used flow cytometry/FACS markers for characterising ACL ligamentocytes, the cells they are commonly found in, and the methods used to detect these markers. IHC – immunohistochemistry, ICC/IF – immunocytochemistry/immunofluorescence, FACS – fluorescent activated cell sorting.

	Marker	Common Name	Cell Type(s) Commonly Detected In	Author(s)	Methods Used for Marker Detection	Justification of Marker Use
POSITIVE ACL LIGAMENTOCYTE MARKERS	**CD90**	Thy1[68]	Fibroblasts, stromal cells[68], activated endothelial cells[77], neurons[78]	Steinert *et al.* (2011)	IHC, FACS	To confirm ACL cell phenotype, determine differences between ACL stem cells and BM-MSCs, observe location of $CD90^+$ cells within ACL tissue, and to detect differences between outgrowth and digested ACL stem cells[68].
				Ogata *et al.* (2018)	FACS, ICC/IF	Ascertain stem cell presence, ACL stem cells-BM-MSC differentiation, identify native location in the ACL, identification of stem cells with ligamentocyte differentiation preference[79].
				Lee *et al.* (2020)	FACS	Confirmation of ACL ligamentocytes cell type[61].
				Zhang *et al.* (2011)	FACS, ICC/IF	To differentiate expression levels between ACL and MCL stem cells, confirmation of stem cell lineage[80].
				Cheng *et al.* (2014)	FACS	To confirm ACL stem cell phenotype[81].

CD73	Lymphocyte-vascular adhesion protein 2[68]	MSCs, endothelial/epithelial cells[68], lymphocytes[82], glioblastoma cells[83]	Steinert *et al.* (2011)	FACS	To confirm ACL cell phenotype[68].
			Ogata *et al.* (2018)	FACS, ICC/IF	To confirm stem cell presence, differentiate ACL stem cells from BM-MSCs, identify location within the ligament, and to identify stem cells with a ligamentocyte differentiation propensity[79].
			Cheng *et al.* (2014)	FACS	To confirm ACL stem cell phenotype[81].
CD29	β1 integrin[68]	MSCs, epithelial, myoepithelial[84], endothelial progenitor cells[85], hepatic progenitor cells[86]	Steinert *et al.* (2011)	FACS	To confirm ACL cell phenotype[68].
			Ogata *et al.* (2018)	FACS	Confirmation of stem cells in ACL tissue[79].
			Cheng *et al.* (2014)	FACS	To confirm ACL stem cell phenotype[81].
CD44	HCAM, hyaluronic acid adhesion molecule[68]	MSCs[68], chondrocytes[87], fibroblasts[88]	Steinert *et al.* (2011)	IHC, FACS	To confirm ACL cell phenotype, determine differences between ACL stem cells and BM-MSCs, observe location of $CD44^+$ cells within ACL tissue, and to detect differences between outgrowth and digested ACL stem cells[68].
			Ogata *et al.* (2018)	FACS	Identification of stem cells[79].
			Zhang *et al.* (2011)	FACS, ICC/IF	Confirmation of mesenchymal stem cell type for both ACL and MCL ligamentocytes[80].
			Cheng *et al.* (2014)	FACS	To confirm ACL stem cell phenotype[81].

	CD105	Endoglin (TGFβ receptor)[68]	MSCs[68], endothelial cells[89], $CD4^+$ T cells[90]	Steinert *et al.* (2011)	IHC, FACS	To confirm ACL cell phenotype, determine differences between ACL stem cells and BM-MSCs, observe location of $CD105^+$ cells within ACL tissue, and to detect differences between outgrowth and digested ACL stem cells[68].
				Ogata *et al.* (2018)	FACS	Identification of stem cells[79].
				Lee *et al.* (2020)	FACS	Confirmation of ACL ligamentocytes cell type[81].
				Cheng *et al.* (2014)	FACS	To confirm ACL stem cell phenotype[81].
NEGATIVE ACL LIGAMENTOCYTE MARKERS	**CD11c**	Integrin alpha X[68]	Monocytes, macrophages, monocyte-derived dendritic cells[91]	Steinert *et al.* (2011)	FACS	To confirm ACL cell phenotype[68].
	CD34	Cell adhesion protein[68]	Haemopoetic stem cells[68]	Steinert *et al.* (2011)	FACS	To confirm ACL cell phenotype[68].
				Lee *et al.* (2020)	FACS	To determine whether there was a $CD34^+$ ACL ligamentocyte stem cell population that resides within the ACL[61].
				Zhang *et al.* (2011)	FACS, ICC/IF	To ascertain whether there were any ACL/MCL stem cells that were of haemopoetic origin[80].
				Cheng *et al.* (2014)	FACS	To confirm ACL stem cell phenotype[81].
	CD45	Antigen for leukocytes[68]	Differentiated haemopoetic cells[68]	Ogata *et al.* (2018)	FACS	Confirm ACL stem cell isolation and purity of population (lack of leukocyte contamination)[79].

				Zhang *et al.* (2011)	FACS, ICC/IF	To confirm the absence of leukocytes[80].
				Cheng *et al.* (2014)	FACS	To confirm ACL stem cell phenotype[81].
	HLA-DR	Human Leukocyte Antigen – DR Isotype[81]	Leukocytes (monocytes, macrophages)[92]	Cheng *et al.* (2014)	FACS	To confirm ACL stem cell phenotype[81].

2.4 Composition of the Extracellular Matrix in the Native Anterior Cruciate Ligament

2.4.1 Fibrous/Structural ECM Proteins

There are three main types of structural proteins that inhabit the ACL; categorised due to their fibrillar nature and their direct effect on tissue mechanical properties. The first of these is collagen. Between species, the overall composition of the ACL can vary. In dogs, collagen content is reported to be lower than that of the human ACL (approximately 85% collagen [16, 42]), with % content of collagen of greyhounds, Labrador retrievers and golden retrievers reported to be 47.7 ± 7.8%, 43.56 ± 5.0% and 53.2 ± 7.3% (mean ± SEM) respectively[93].

The second structural protein is elastin. Elastin is an insoluble and highly fibrillar protein, which aligns itself with collagen along the longitudinal axis of the ligament[59]. The lysyl oxidase enzyme (LOX) mediates its interaction with collagen[94]. As with collagen, there are inter-species differences in elastin content within the ACL, with dogs reportedly having a higher quantity, with dry weight content reported to be 9.86 ± 3.97%[95]. Though when observing the difference in elastic fibre occurrence, with dogs, higher frequency of elastic fibres can be indicative of ACL degeneration[95] or perhaps may alter between breeds or remodelling due to previous long-term exercise regimes[51]. These results could however have been due to the dog breed used, as all were ex-racing greyhounds and mild cruciate ligament degeneration was noted with all participants.

The final structural ECM protein of note is fibronectin. Fibronectin, though also a glycoprotein, is instrumental in the formation of collagen and fibrillin-1 structural networks (which is itself instrumental in elastic fibre formation) and as such, is one of the primary proteins to be deposited by the cells. It has been noted however, that for the maintenance of a structurally sound fibronectin network, mechanical loading is essential[58].

2.4.2 Glycoproteins (GPs), Proteoglycans (PGs) and Glycosaminoglycans (GAGs)

Glycoproteins, such as fibrillin[51], tenascin-c[96], and fibronectin[97] inhabit the ACL. They can be soluble or insoluble proteins to which carbohydrates attach via covalent bonding. Proteoglycans are a subclass of glycoproteins that form a core to which covalently bonded carbohydrates bond. These carbohydrates are amino-containing polysaccharides, and are known as glycosaminoglycans, accounting for 12% of the ACL (dry tissue)[16].

There are four main types of PGs that are reported to exist in the ACL ECM; aggrecan[51], perlecan[52], versican[51] and small leucine rich proteoglycans (SLRPs)[51].

Aggrecan is by far the most common PG in matrix rich tissues, and in the ACL, is predominantly found in the inter-fascicular regions of the midsubstance; aligning alongside the collagen fibre networks[51, 98] and interacting with the collagen fibrils via the agglomeration of hyaluronic acid to its N terminal globular region (G1)[98]. Perlecan is one of very few PGs to associate with the GAG heparan sulphate, and is a predominant PG in elastic microfibril-containing tissues where elastin and fibrillins reside. This is reported to be mediated through electrostatic interactions in the case of elastin, and heparan sulphate binding domains in fibrillin, and supports the regulation of fibrillin-tropoelastin interactions at the fibrillin-1 C terminal[52, 99]. Versican has previously been reported to reside in both the fascicular and interfascicular regions of the ACL[51].

Interestingly, unlike their surrounding tendons in the knee joint, anterior cruciate ligaments comprise of a large proportion of GAGs[51], which also, due to their extremely electronegative surfaces, attract large quantities of water[100] (which in turn accounts for 65-80% of the total weight of the ACL[41]). There are multiple different GAGs (with their covalently bound PGs) that reside in the ACL, detailed in Table 2-2, below. The only one not mentioned in the table, is hyaluronan/hyaluronic acid. Hyaluronan/hyaluronic acid is a GAG that resides in the ACL, and usually can exist independently of a proteoglycan core. It interacts with proteoglycans but does not form any permanent covalent bonds[101].

SLRPs are separated into 5 classes, characterised in part by the organisation of their cysteine-rich clusters[102]. PGs present in class I, such as biglycan and decorin, are most commonly referred to in ACL-related protein analysis[42, 51, 103] as they play integral roles in collagen fibrillogenesis and the homogeneity of fibril diameter[54], though PGs such as lumican and fibromodulin (class II) have also been characterised[103].

Table 2-2 A table to show the different proteoglycans found to be present within the ACL, and their associated glycosaminoglycans.

PROTEOGLYCAN	GLYCOSAMINOGLYCAN SIDE CHAIN(S)
Decorin[104]	Chondroitin sulphate Dermatan sulphate
Perlecan[52]	Heparan sulphate
Biglycan[53]	Chondroitin sulphate

	Dermatan sulphate
Versican[105]	Chondroitin sulphate
Aggrecan[106]	Chondroitin sulphate Keratan sulphate*
Lumican[104]	Keratan sulphate
Fibromodulin[107]	Keratan sulphate

***does not occur on articular aggrecan in rodents[106].

2.5 Damage to the Anterior Cruciate Ligament

2.5.1 Causes of Damage

Damage to this joint is common and occurs due to forceful and repeated valgus movements at the knee. Subsequent damage to this joint can render athletes incapable of performing for up to 12 months[108] and is therefore a serious concern for those who participate in competitive sports. Though it could be assumed that contact sports would show the highest incidence of ACL injury, current research has identified that most ACL ruptures were over three times more likely to be caused by the individual themselves, not in fact, by contact with another person[109].

Biomechanically, ACL rupture is associated with extension, tibial force and tibial torque (depicted in Figure 2-3). Tibial torque is a measure of knee joint rotation, which quantifies how much (muscular) force is needed to cause rotation around a central axis (in this case the knee joint)[110]. This, along with the angle of flexion in the knee, has been directly involved with ACL injury. Within this category, hyperflexion and extension have most commonly been associated, with studies confirming that extension of the joint, wherein increasing interior tibial torque and anterior tibial force markedly increases the risk of ACL injury[111, 112].

Although the regenerative capacity of the ACL is low, due to the inability of platelets to clot, and fibroblastic cells to form a scar (via proliferation) which form the primary regenerative scaffold for cellular remodelling[113], the consequences of ACL rupture will be highly determined by whether or not the patient has suffered a complete or partial tear of the ACL. Patients that present with a complete tear, and some who present with a partial tear, may experience buckling or slackness of the knee and abnormal biomechanical behaviour at the joint. This joint is now categorised as ‘non-functional’[114].

Repeated buckling of the knee will increase the risks of secondary damage to structures such as the medial or lateral meniscus which can in turn cause other, more chronic long term effects; osseous lesions and osteoarthritis[115].

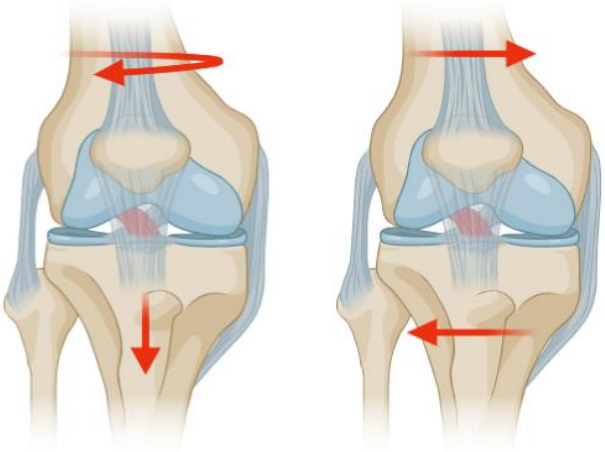

Figure 2-3 Movements by which the ACL can be torn. Image created using BioRender.com.

2.5.2 Physiological Consequences

As aforementioned, due to the lack of pain receptors in the ACL, the sufferer will rarely experience pain at the time of the injury[47]. Although the regenerative capacity of the ACL is low, due to the inability of platelets to clot and fibroblastic cells to form a scar (via proliferation) which form the primary regenerative scaffold for cellular remodelling[113], the consequences of ACL rupture will be highly determined by whether or not the patient has suffered a complete or partial tear of the ACL. To assess this, methods such as the Lachman, Anterior Drawer (movement >10mm towards the opposite side of the knee to the ACL) and Pivot-Shift (above grade 3 on the International Knee Documentation Committee) tests[116], followed by magnetic resonance imaging (MRI) diagnosis[117] are routinely employed. Some of those who have only suffered a partial tear of the ligament will experience no alteration in physiological and biomechanical behaviour of the knee joint, and even with the audible sound of a breaking ligament during the incident, a study has shown that a third of participants who experience ACL tears are unaware that the ligament had been torn until local recruitment of immune cells caused redness, swelling and eventually, pain[118]. In this situation, the ACL is still regarded as a 'functional'. However, patients that present with a complete tear, and some who present with a partial tear, may experience buckling or slackness of the knee and abnormal biomechanical behaviour at the joint. Medically, this joint is now regarded as 'non-functional' and reconstructive surgery would be performed[117].

Rupture of the ACL would also present severe mobility problems, as the knee joint would not be supported and can collapse or buckle. Repeated buckling of the knee will increase the risks of secondary damage to structures such as the medial or lateral meniscus which can in turn cause other, more chronic long term effects[115].

2.5.3 Long Term Effects and Secondary Damage

2.5.3.1 Degenerative Lesions

Degenerative lesions are classed as any damage which can cause loss of function at the site of injury. They can occur in any area of the injury site, as they can affect any part of the knee joint post ACL rupture. Often bone bruising, cartilage wear and meniscal tears are most commonly associated with secondary damage of ACL rupture/tears, with the latter two often being precursors to the development of osteoarthritis of the knee[119].

These lesions often present due to continued biomechanical stress at the injury site, itself due to lack of support by the ACL. Often, this results in meniscal tears and lateral and medial ligament damage, which reduce the amount of support provided to the articular cartilage and surrounding osseous components. This provides a platform for more long term and chronic side effects to develop, with the longer the length of time between injury and resconstructive surgery, the more likely it is that secondary osseous damage will occur[120].

2.5.3.2 Osteoarthritis

Osteoarthritis is a long term side effect of ACL damage, which occurs in 60-90% of ACL injuries requiring, or having had, reconstruction[121]. This often occurs after a ruptured ACL continually buckles. This results in detrimental damage of the medial meniscus, the joint's shock absorber which, with the degradation of the cartilaginous tissue in the joint, can lead to the low-level inflammation that is symptomatic of osteoarthritis. The role of the meniscus in preventing osteoarthritis of the joint is well documented, with a very large proportion of patients who have received/undergone a meniscectomy, having developed osteoarthritic joints[122, 123]. It has been recorded that biomechanical stress and excess load on unstable joints with articular damage may cause the release of inflammatory mediators from chondrocytes[124, 125] (cytokines, interleukins, etc.) which can cause overexpression of immune cells[126]. Mechanosensitive calcium ion channels Piezo 1 and 2 have been shown to be involved in the onset of post-traumatic osteoarthritis[127], with traumatic impact causing influx of Ca^{2+} ions, resulting in chondrocyte death and breakdown of articular cartilage ECM[128].

Another documented risk factor for the development of osteoarthritic tissue is artificial grafts[129]. Dacron grafts have been reported to cause a large increase in the occurrence of osteoarthritis when compared to natural ACL joints[130], with one theory stating that this may be associated with the production of wear particles and the subsequent perpetual inflammation that they induce[131].

2.6 Currently Recommended ACL Treatment Methods

2.6.1 Surgical Grafting

The main objective of ACL reconstructive surgery and associated treatment methods is to stabilise the joint, enable 'normal' biomechanics and to prevent any secondary damage or degenerative conditions. The type of surgical grafting technique that the patient will undergo will depend on the type of tear that is encountered. Due to the preference of keeping as higher percentage as possible of the patient's ACL intact, those suffering from a 'partial' tear (where only one of the two bundles that make up the ACL is torn) will undergo a reconstruction of only the torn bundle (ACL augmentation)[132]. This means that current mechanoreceptors are preserved in the healthy bundle and can continue aiding the brain in locating the orientation and position of the knee joint[133]. By this rationale, the only patients in receipt of a full reconstruction are those who present with a complete tear (both bundles) of the ACL.

Most commonly utilised are autografts. This method involves the extraction of muscular tissue from either the patellar tendons or the hamstring to create a new and functional ACL ligament (as shown in Figure 2-4). Allografting (when muscular tissue is extracted from a cadaver) has recently been declared acceptable in the USA and is now increasing in usage. This method however, cannot be used solely, as the supply is limited and the chance of contracting infection or immune rejection is high[134].

Firstly, a piece of muscular tissue from the patellar tendon is extracted, along with adjoining bone attachment sites. Following this, holes are drilled in diagonally to match the *in situ* orientation of the original ACL ligament, through the tibia and the femur. A guide hook is then passed through these holes to pull the newly inserted pseudo-ligamentous tissue through the knee joint into the correct position. The tissue is then sealed with screws at each insertion site to prevent movement of the graft[135]. Over the subsequent weeks, slow and gentle flexion of the knee joint is performed to increase flexibility and agility in the graft and joint[134].

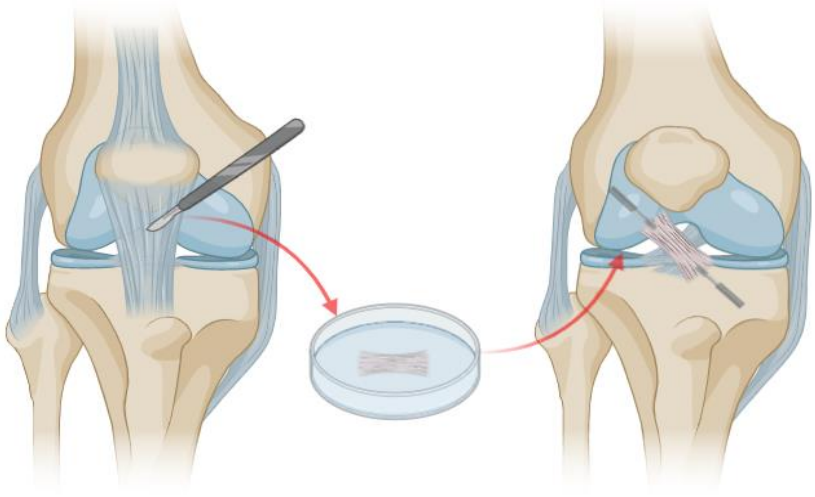

Figure 2-4 A simplified depiction of the 'gold standard' surgical reconstructive procedure, whereby a section of the patellar tendon is grafted into the knee joint to replace the ruptured ACL. The tendon segment is then fixed into place using screws, implanted into the femur and tibia. Image created using BioRender.com.

2.6.2 Disadvantages Associated with the Use of Grafts

Unfortunately, failure rates for grafts in ACL patients are quite high, with up to 13% experiencing autograft failure[136] and allograft failure being reported at around 23%[137]. This could be due to a number of factors, depending entirely on; the origin site of the tissue, whether the tissue is from a cadaver, the material type (if artificial), the position of the graft fixation and the patient's own immunological response. Current research has determined that overall; allografts cause a higher level of morbidity than autografts, perhaps due to immune rejection. Also explored, was the idea that size could be a detrimental and contributing factor to the failure susceptibility of ACL grafts, with results showing that larger grafts elicit a higher risk of morbidity[138].

There are many reports that state that the success of the graft is partly dependent on the origin of the muscular tissue[139, 140] with surgical revision of hamstring grafts being higher, when compared to using patellar tissue[139]. However, when comparisons are made as to the physiological side effects of the reconstructive surgery and not to failure of the graft (laxity), there are alternative opinions which suggest patellar grafts result in higher levels of donor site morbidity, which include pain during activity and when kneeling[141].

Another common and arguably a major problem that occurs upon installation of an ACL graft, is insertion site failure. This is when the femoral and/or tibial insertion site begins to widen[142], with the screws that secure the graft becoming loose, which itself increases the laxity of the joint[143]. This could be due to dislodging during matrix remodelling.

Though allografts are not as commonly used as autografts (the current 'gold-standard' for ACL reconstructive surgery), they do still present with a number of problems; firstly, as they are non-self tissue, they may present the recipient with an immunogenic reaction[144], which may result in an overactive immune response that may either cause the graft to be rejected, or have to be counteracted using immunosuppressant medication. Secondly, if the donor has not been screened effectively, there is a potential risk for disease transmission. Though methods of avoiding failure due to immunogenicity have been tested (irradiation and ethylene dioxide), the methods themselves have been shown to cause side effects once the tissue is *in situ*[145, 146].

2.6.3 Why Artificial Ligaments Fail

Overall, artificial methods fail because they cannot adapt to the biological environment, they are in effect, adaptationally static. In order to integrate into the matrix, cells require biological cues and relevant binding sites, which are not present upon artificial materials. This enables them to initiate their normal cellular behaviour, as well as remodelling their surrounding environment. Another more serious problem, are the side effects of wear particles in a biological environment, and the possible effects they may have systemically. As expected, the body begins to attempt to break down the artificial ligament, which causes weakening and mechanical failure. This also produces wear particles, which upon infiltrating the synovium of the knee joint can lead to serious infections such as synovitis[147]. Additionally, heightened immune activation may lead to a foreign body response and henceforth, fibrotic encapsulation of the artificial ligament, disabling the joint by stiffening[148].

The most popular artificial ligament for use in ACL reconstructive surgery was so called the Ligament Augmentation Reconstruction System (LARS). LARS is a polyethylene terephthalate ACL graft that was developed in France, and immediately gained popularity in Australia, being widely used instead of ACL grafts. This was mainly due to the lack of donor site morbidity and fast healing rates associated with not using autografts. However, recurrent and serious, debilitating and common side effects, such as early onset arthritis, osteolysis of the tunnel integration site and synovitis, have ensured surgical practice involving the use of artificial ligaments was halted over twenty years ago[149].

The most popular artificial ligaments were constructed from a synthetic polyester - polyethylene terephthalate (PET)[150], Dacron and GORE-TEX. Dacron has proven highly unsuitable, with 12.5% of patients developing synovitis[151]. GORE-TEX is produced from polytetrafluoroethylene (PTFE) and has twice the tensile strength of the natural ACL. This polymer has also proven to be 'bio-inert' and non-biodegradable, as well as having been passed by the Food and Drugs Agency (FDA) in the USA for human use[152]. However, rates of synovitis and effusion have been previously recorded as high as 27.6% which is much higher than has been reported for other grafts such as the LARS graft (0.2%)[153]. LARS is perhaps more successful due to the its structure, where the fibres are interlaced at 90 degree angles[154] which provides the material with the ability to withstand faster rates of degradation, and therefore produce fewer wear particles. This in turn, reduces the chance of synovitis[155]. Though first appearing promising, the GORE-TEX graft presented with complications such as presence of wear debris, lack of cellular integration and serious mechanical wear. Long-term follow-ups discerned a failure rate of around 56-70%[149, 156] and a complication rate of 76%[157]. Ultimately due to resultant complications, this graft has been absent from the international market for the past 28 years[156].

Ultimately, though LARS grafts have not been previously successful, PET (the primary component of LARS) has been deemed acceptable for use with a very low failure and complication rate[158] (see Table 2-3). LARS has been undergoing research into providing more long term stability, having previously been recommended for use as short to medium term grafts[155]. This could be due to much higher rates of failure and reports of over 50% showing lack of tissue ingrowth after being observed after longer follow-up periods[14], though it is prudent to note that all patients observed were young, and returned to intense physical activity quickly. Materials lacking biological cues however, are still limited on their

integration potential. Therefore, if these materials were to be improved further, biological approaches could be considered.

Table 2-3 A table to show the major components and failure rates of a selection of ACL artificial grafts[149, 156, 158-160].

IMPLANT TYPE	MAIN MATERIAL COMPONENT	LONG TERM FAILURE RATE (≥ 2 YRS)
LARS	Polyethylene terephthalate (PET)	4-31.5%
GORE-TEX	Polytetrafluoroethylene (PTFE)	56-70%
Dacron	Polyethylene terephthalate (PET)	60%
Kennedy-LAD	Polypropylene (PP)	40-70%
Leeds-Keio	Polyethylene terephthalate (PET)	28%

2.7 Tissue Engineering for Ligament Repair

2.7.1 An Introduction to Tissue Engineering

Tissue engineering (TE) is defined by Langer and Vacanti (1993), as an *"interdisciplinary field which applies the principles of engineering and the life sciences toward the development of biological substitutes that restore, maintain, or improve tissue function"*[161]. It is a field that originates from biomaterials research and combines various other scientific disciplines in an interdisciplinary approach; to aid in the production of novel, revolutionary, and personalised medical therapies for the regeneration of tissues. TE often uses the TE triad, whereby three main components are required to achieve a TE approach; a scaffold (made from either natural or synthetic materials), a cell source to produce the tissue components (i.e. ECM), and bioactive signalling cues (to direct cell growth, phenotype and ECM production)[18, 19, 22, 25, 162].

Often the tissues most targeted by this field either have a low regenerative capacity, or are those which have been damaged beyond their critical point of repair. This novel method of refunctionalision enables the body to regenerate its own tissues, therefore avoiding any potential immunological activation that may be observed in non-biodegradable ligaments and allografts, or any donor site morbidity that may be experienced after autografting.

There are multiple methods that are utilised in TE to create scaffolds for tissue repair, though for tissues that require stronger tensile properties and highly aligned matrices, electrospun fibres are a preferred platform. TE often incorporates the use of biodegradable scaffolds,

which are often seen to be preferred over non-degradable structures. Though non-biodegradable materials are often stronger and retain that strength over time (as opposed to biodegradable materials, which lose stability over time due to hydrolysis, enzymatic breakdown, etc.), they are (similarly to current synthetic grafts) adaptationally static. This becomes of concern when one considers that almost 50% of ACL injuries occur in young people under the age of 25 (this age group also has the highest injury incidence rate per 100,000 person-years)[163]. Growth of the ligament could be impaired by a static graft, and would require multiple surgical interventions. The use of these biodegradable materials works upon the basis that the new tissue will eventually replace the scaffold and in line with this, would have a degradation rate that is directly proportional to the production rate of new tissue. In practice however; this is extremely unlikely. Material degradation rates are susceptible to many external stimuli, e.g. pH, temperature and enzymatic breakdown instigated by immune reactions. Another essential component is mechanical viability. Mechanical properties must be compatible with natural tissue to avoid failure or negative reactions due to occurrences such as stress shielding (seen mainly in bone) where tissue remodels due to removal of load bearing activity. In order for cell attachment to occur, a biomaterial must enable the adsorption of proteins to its surface, therefore enabling integrin-specific cell-protein binding. However, super hydrophilic materials appear to inhibit protein binding, as proteins must then compete with water molecules. In reality, an intermediate hydrophilicity is considered the most appropriate. Bioactivity of a TE scaffold is also important, as many synthetic materials lack biological recognitions sites, cells lack their appropriate, native responses[164].

For anterior cruciate ligament tissue, there are highly specific requirements. The material must be able to withstand large tensile forces of 24-38 MPa[8], must be able to undergo recoverable strain of around 5%[165] (to enable the ductile properties of ligament), and should be aligned to guide and assist with the organisation of a highly aligned, (and mainly) collagenous matrix. Despite ligament not being known for its vascular nature, must be able to support limited vasculogenesis and be sufficiently porous for supplying oxygen to the surrounding cells, due to the diffusion depth for oxygen being limited to 100-200 μm[166]. It has been reported, that for this reason, the maximum depth for a TE scaffold should be no more than 1 mm[166], unless they have properties that could negate the requirement for reliance on oxygen diffusion alone. The scaffold must also support the cells in their elongated ‘spindle-like’ forms to enable appropriate function and gene/protein

expression[167, 168]. For these reasons, electrospinning of TE scaffolds is a popular and somewhat successful approach for ligament repair and regeneration[169, 170].

2.7.2 Electrospinning Biomaterials for Ligament Tissue Engineering

As most tissues have a collagenous ECM, electrospinning is an extremely popular way of replicating the native environment, partly due to it being an inexpensive procedure that is easily tailorable for producing a variety of morphologically compatible materials. This is primarily due to its ability to mimic the topographical cues of the native ECM (including structure, fibre diameter, porosity, etc.), exhibiting important contact guidance cues for cells from highly fibrous tissues. It requires three fundamental parts; a polymer source, a high voltage supply and a collector. The polymer solution is usually formed by the dissolution of polymeric particles in either solvent or acid, unless melt electrospinning/electrowriting is being used which requires only the polymer itself. Acids (such as formic acid) have been popular for use with silk fibroin, due to its ability to produce thinner fibres than comparative silk solutions with solvent (1, 1, 1, 3, 3, 3-hexafluoro-2-isopropyl alcohol; HFIP)[171]. Solvents have more widespread use for preparing electrospinning polymer solutions and are selected based on their dielectric constant/relative permittivity[172]. Simply put, the dielectric constant of a solvent is a measure of the ease by which molecules within the solvent polarise when exposed to an external electric field (i.e. the ease of the polymer solution overcoming the surface tension at the needle tip), as depicted in Figure 2-5[173]. Hence, the higher the dielectric constant, the more readily molecules will polarise, and the more attracted the polymer will be to the collector. Use of a solvent with a high dielectric constant can therefore result in fibres with smaller diameters, due to the increased speed at which the polymer solution moves from the needle tip towards the collector[174].

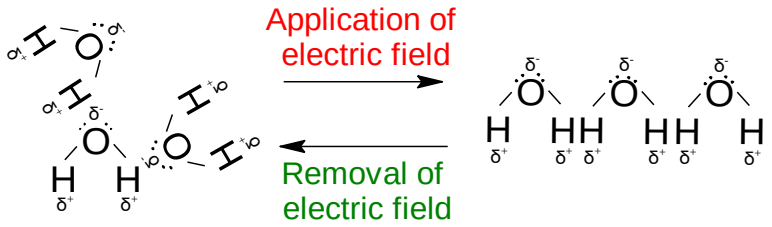

Figure 2-5 The process by which a dielectric constant is determined in solvents. For simplicity, water molecules exemplify the process. The diagram shows the reorientation of water molecules into a uniform conformation,

in response to an externally applied electric field. This confomation is highly unstable and molecules will relax into their orginal state once the electric field is removed.

The voltage supply is connected to the needle in order to polarise the polymer solution (mechanism detailed above). A grounding connector/earth is attached to the collector in order to create an electric potential between the needle and the collector. When the electric potential overcomes the surface tension of the polymer solution droplet at the end of the needle, the solution is drawn from the tip of the needle towards the collector. Fibres can be tailored to match the ECM of the tissue they are required for – highly anisotropic orientation is usually achieved by the use of a mandrel (a rotating cylinder) where fibres are stretched out around the mandrel. This technique is often used for the creation of TE scaffolds for muscle or nerve tissues. The other type of fibre orientation is 'random', where the fibres are collected on a flat plane and result in the creation of a non-woven mesh, suitable for tissue types such as skin[175].

Electrospinning is an extremely popular method of scaffold fabrication for ligament tissue[169, 176-178]. Its production of materials with a highly fibrous composition enables the recapitulation of the native collagenous environment, delivering the appropriate topographical cues to the cells (see Figure 2-6). For this reason, with anterior cruciate ligament, highly aligned matrixes are preferentially used. Lee *et al.* (2005) found that high degrees of alignment encouraged native morphology in human ligament fibroblasts which in turn encouraged a significant increase in the production of collagenous matrix[179]. Utilisation of this method can enable the production of scaffold with high tensile properties that are required for repair of ligament tissue and adequate porosity to enable optimal cell integration.

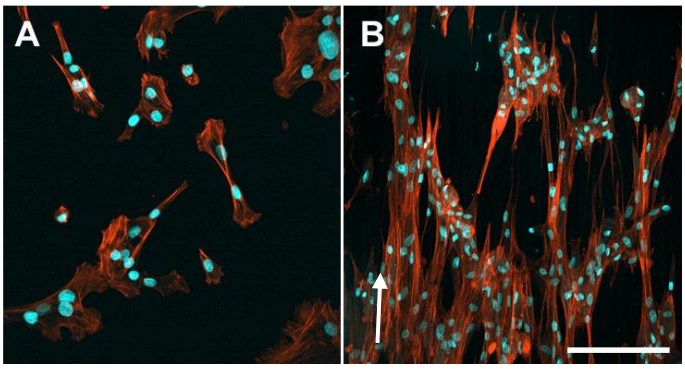

Figure 2-6 Canine ACL ligamentocytes (stained with DAPI (cyan) and phalliodin (red)) on flat 2D glass substrate (**A**) and on plasma treated aligned microfibres (**B**). Arrow indicates fibre direction and scale bar represents 200 µm.

2.7.2.1 Natural or Synthetic Polymer Scaffolds?

Table 2-4 A table to show the related advantages and disadvantages of using a selection of natural polymers as scaffolds for tissue regeneration.

MATERIAL	ADVANTAGES	DISADVANTAGES
Collagen (Type I)	• Naturally high elastic and tensile strength[180]. • Enhances cellular adhesion and migration[181]. • Abundantly available[182]. • Haemostatic (promotes coagulation)[183]. • Non-toxic[182]. • Biodegradation rate can be somewhat tailored[184].	• Antigenic – can produce an immune response[183]. • High production cost[181]. • Fast degradation rate[182]. • High batch to batch variability[181]. • Low tensile strength when commercially produced[184].
Silk Fibroin	• Biodegradable[185]. • Non-harmful degradation products[185]. • Highly biocompatible[186]. • Replicates connective tissue elasticity and strength[186].	• Non-removal of sericin can cause immunogenicity[187]. • Inflammatory response observed upon implantation *in vivo*[188]. • Degradation behaviour can be difficult to control[185].
Alginate	• Good haemostat[189]. • Non-toxic[190]. • Biodegradable[190]. • Similar in structure to GAGs[190].	• Biodegradability is molecular weight dependant[191]. • Gelates rapidly – difficult to electrospin[190]. • Requires copolymer interaction for electrospinning[190].
Gelatin	• Can alter Isoelectric points (IEP) at different pH[192]. • FDA approved material[193]. • Excellent haemostat[193]. • Cell proliferation enhancing properties[194].	• Can be immunogenic, but very low generally[195]. • Evidence of necrotic activity in cells following modification[196]. • Poor mechanical strength (7.5% w/v – 41 µm fibre mat, < 5 MPa)[197]. • Not bioadhesive without crosslinking[195]. • Low production cost[195]. • Has to be electrospun at high temperatures to avoid gelation[197]. .
Chitosan	• Solubility and strength can be easily tailored[198]. • Excellent haemostat and is bioadhesive[199]. • Is inherently antibacterial[199]. • Non-cytotoxic[199].	• Can cause immunogenicity[198]. • Degradation rate is highly sensitive to changes in pH[198]. • Long systemic retention time[198].

The debate as to whether natural or artificial materials are better for use as tissue engineering scaffolds has not yet been concluded. Natural materials like collagen, are topographically suited for TE scaffolds, with some (collagen, gelatin, etc.) providing integrin binding sites for enhanced cell attachment[200]. Generally, it is reported that the mechanical properties of natural polymers are not suitable for the engineering of tissues which are subject to high tensile stresses, as they are mechanically weak and deform with relatively little force[201, 202]. However, these scaffolds can be removed by the body with relative ease, and with little side effect, compared to synthetic materials, which due to their chemical composition, can cause localised negative effects via acidification of their environment upon degradation[203]. Synthetics however, are much more mechanically viable, especially for tissues such as ligament which are subject to high tensile stresses and need to be mechanically able to resist stresses of ≤ 38 MPa[8]. This also means they have a much slower rate of degradation than natural polymers, which tend to degrade faster, and are often very sensitive to temperature and pH[198]; inappropriate for the ACL, where scaffolds have to be able to resist deformation of high tensile stress during tissue regeneration.

Though mechanical matching is an imperative part of the selection process, natural polymers have unique characteristics that prove useful when applying them for use as TE scaffolds. Along with alginate and collagen, chitosan is haemostatic, enabling the formation of blood clots in tissue, a feature essential for aiding in tissue regeneration, hence why it has been used as a popular option for research into enhanced wound dressings. In terms of ligament tissue, Collagen Type I would appear to be the most logical, with it making up ~81% of the total ACL ECM. Having promising ACL healing capacity *in vivo*[204] and enhancement of cell response, which is further evidenced by the lack of fibrosis/necrosis when compared to gelatin (denatured collagen) scaffolds[205], make it appropriate for use as a ligament scaffold (see Table 2-4)[202, 206]. However, though collagen appears to be a good match for use in scaffolds, its disadvantages, which include high cost of production, may not make it feasible for production on a commercial scale[207]. The development of silk fibres for ligament tissue engineering has been highly popular in recent years, which is likely due to its high levels of 'biocompatibility' and its excellent mechanical and architectural features[185]. Altman *et al.* (2002) created silk scaffolds showing remarkably similar stiffness and elongation values to that of the native human ACL[186], though the fibres created were very much larger (10 to 40 times larger in diameter) than collagen fibres present in the native ACL and would not provide similar topographical cues. Cells showed increased collagen type I and III

production with enhanced proliferative responses of bone marrow stromal cells (BMSCs), with this also implying the differentiation of these cells into ACL-like cell types[186]. However, immunogenic reactions upon the implantation of silk fibroin have been noted, with immunological reactions being sustained for multiple weeks[188].

Synthetic polymers are the alternative to using natural constituents, eliciting (mainly) good biodegradation profiles and non-immunogenicity, with most showing excellent and easily tailorable mechanical properties. However, some of these polymers struggle to degrade, or degrade too quickly in biological environments. There are however, many which have been researched widely as potential tissue engineering scaffolds, as they are either available as the major component in medical devices and technologies, or have been shown to have limited or little negative effects both *in vitro* and *in vivo* (Table 2-5). Polymers such as polylactic acid (PLA), polyglycolic acid (PGA), polylactic-co-glycolic acid (PLGA) and polycaprolactone (PCL) for example, which has become extremely popular for use in biomaterials science, perhaps due to their prior approval for use in medical and clinical technologies by the FDA[208-210]. However, though PGA has excellent mechanical strength, its rapid biodegradation rate, prevents it from being used alone for the regeneration of load bearing tissues. Combining it with PLA however, is a trade-off, PLA stabilises the material to certain extents, but makes the material more hydrophobic by addition of extra exposed ester groups[210]. Other concerns include the initiation of immune response triggered by environmental acidification during polymer resorption. Limited efforts have been made to use PLGA or any of its derivatives for ACL TE, instead it having to be highly crosslinked with other synthetic or natural polymers which offer improvement on functionalisation or mechanical properties[211, 212]. PCL however, is extremely popular in the field of ACL regeneration, with its mechanical properties matching almost exactly those of the native ACL. Though it is an extremely hydrophobic biomaterial with a contact angle of around 130°[194], its surface properties are easily modifiable by using techniques such as plasma treatment or chemical binding agents such at poly(ethylene terephthalate) (PET) or even chemical processes such as alkaline hydrolysis[213]. Though its degradation time is long, this enables the support of load-bearing tissue whist regeneration occurs. This property alone gives PCL the advantage over its synthetic and natural counterparts, with high levels of biocompatibility aiding its advantage. This is evidenced by many recent research groups, with all reporting positive outcomes such as biological integration[169], adequate cell attachment[214] and increased cell proliferation and collagen type I production when

compared to blends with natural polymers[167] *in vivo* and *in vitro* when observing the responses of native ACL cells.

Table 2-5 A table to elucidate on the main advantages and disadvantages of popular synthetic materials for the production of ligament TE scaffolds.

MATERIAL	ADVANTAGES	DISADVANTAGES
Poly-ε-caprolactone (PCL)	• FDA approved for a range of medical devices[208]. • Highly biocompatible[215]. • Surface properties are easily modifiable[215]. • Has a high tensile strength that is similar to the ACL (up to 39 MPa – 1.5 µm diameter fibres)[216]. • High copolymer compatibility[217]. • Is soluble in many organic solvents[218]. • Complete biodegradation requires long periods of time (2-3 years)[219] .	• Highly hydrophobic without surface modification[215]. • Contains no biological integration sites[208].
Poly-Lactic Acid (PLA)	• FDA approved for various medical applications[210]. • Bioresorabable[220]. • Good mechanical properties (65-72 MPa)[203]. • By-products can be cleared easily by the body[221]. • Can take up to 5 years to resorb[220].	• Highly hydrophobic without surface modification[210]. • Poor solubility in solvents (crystalline PLA)[222]. • Acidification of environment post degradation[203]. • Can cause immune response[210].
Poly-Glycolic Acid (PGA)	• Excellent mechanical properties (up to 1.1 GPa)[223]. • FDA approved as biodegradable sutures[224]. • Bioresorabable[223]. • By-products are non-toxic and are easily removed by the body[224].	• Low solvent solubility[224]. • Loses mechanical properties within 1-2 months[225]. • Loses mass within 6-12 months[226]. • Slightly hydrophobic without surface modification[227]. • Acidification of environment post degradation[228]. • Can cause immune response[228].
Poly-Lactic-*co*-Glycolic Acid (PLGA)	• Popular for use as a composite material[209, 229]. • Highly biocompatible[209]. • Bioresorabable[230].	• Hydrophobic without surface modification[209]. • Fairly weak materials – too weak for ACL

	• Tailorable mechanical properties[230]. • High solubility in a range of solvents[209, 229].	reconstruction (~42 kPa – single fibre Young's modulus)[231]. • A cause immune response[232]. • Often have to be copolymerised for use as load bearing scaffolds[211]. • Acidification of environment post degradation[231].

2.7.3 Cell Sources Used for ACL TE

Generally, within ACL TE, two main types of cells are used; primary anterior cruciate ligamentocytes and bone marrow mesenchymal stem cells (BM-MSCs). The popular use of BM-MSCs is in part due to their similarities in both size and character to ACL ligamentocytes, but also due to their ability to produce an ECM that contains many of the major ECM components of ligament without having to be differentiated nor induced. ACL ligamentocytes, like BM-MSCs, also display trilineage differentiation (and express almost identical CD markers), although appear to be less efficient at producing integral ECM proteins, such as collagen types I and III, and proliferate less quickly[233]. Other stem and progenitor cell types have been explored for ACL TE, with human umbilical cord derived MSCs showing promise at regenerating the bone-integration site[234] and human amnion-derived MSCs being able to be differentiated into ACL ligamentocytes by use of a co-culture-growth-factor-stimulation method for tissue engineering purposes[235].

Other cell types such as human dermal fibroblasts have been explored, and have been shown to produce relevant ligament-associated ECM proteins such as scleraxis and tenascin-c[236], and have previously been shown by van Eijk *et al.* (2004) to produce higher quantities of collagen, and show faster rates of proliferation, when compared to native ACL ligamentocytes[233]. Other stem cell types, such as embryonic stem cells (ESCs; naturally pluripotent stem cells) and induced pluripotent stem cells (iPSCs; stem cells that possess pluripotency by induced overexpression of pluripotency-associated genes) have been briefly trialled in knee and ACL-related regeneration strategies[237, 238]. While pluripotent stem cells may sound attractive with their ability to differentiate into a vast number of adult cell types, their ability to form teratomas is problematic for tissue engineering therapies[237]. ESCs also have added complications, due to their origin in embryonic tissue. Ethical debates around the use of human embryonic tissue are ongoing and current, with permissions varying from

country-to-country and between regulatory bodies. The use of cells derived from embryonic tissue must consider stringent ethics, which must be accounted for upon their use[239].

Use of these other cell types whilst useful for demonstrating ACL TE *in vitro*, may come with disadvantages upon translation. Similarly to justification for the abandonment of allografts in favour of patellar autografts, if anterior cruciate rupture occurs, use of the patient's own ACL cells will produce a graft that is non-immunogenic to the host system. Other cell types will require operative extraction from the patient or donation from an external host. In an effort to reduce surgical procedures and chances of immunogenicity, it would be ideal to optimise the use of materials and biofunctionalisation components for ACL ligamentocytes.

It is however, a valid concern, that the condition of the cells used in the tissue engineering protocol may cause significant problems with subsequent cell performance and TE graft production. Hasegawa *et al.* (2013) explored the expression of stem cell markers and integral ACL ECM proteins from between young/healthy, old, and degenerative ACLs to determine whether the condition of the knee and age of the patient affected the expression of the cells (and subsequently their ability to perform integral functions in the ACL). Results showed that in fact degenerative ACLs contained a higher proportion of stem cell-like ligamentocytes, and that more cells could be acquired that from those of young/healthy or aged donors[50]. Subsequent studies, exploring the effect of age on ACL ligamentocyte properties/expression, have determined that though there appear to be no differences in proliferative ability and differentiation potential, specific cytoskeletal genes are downregulated compared to younger donors[240] and could ultimately affect ECM assembly and cell migration[58].

Ruptured ligaments have been considered as a cell source, and studies that have compared them to 'normal' ligament have found that though there may be differences between the two in terms of α-smooth muscle actin and integrin subunit expression in culture, these aforementioned differences in response equalised when seeded onto biomaterial scaffolds. However, it is important to note that in this study; 'normal' ligaments were from patients also affected with osteoarthritis. Comorbidities such as this may (as highlighted above) present other variables that might confound the results[241]. Another study has shown that a greater proportion of CD34+ ligamentocytes reside at the rupture site in ACLs, which themselves showed higher differentiation and proliferative potential than cells from non-

rupture sites[242]. This result inferred the potential of cells from ruptured ACLs to be used in ACL TE, despite current surgical methods, which retain the ruptured stumps for superior graft integration[243].

2.8 Cell Guidance Techniques Used in Scaffolds for the ACL

In recent years, a variety of cell guidance techniques have been employed to encourage the responses of cells in regenerative scaffolds. This enables a high level of cytocompatibility and provides an environment that not only mimics the ECM, but also reduces the chances of negative reactions. Tailoring these components appropriately is arguably the most important part of producing a TE scaffold, as the material can guide the cells, providing them with a matrix where they will respond as if they are in an *in vivo* environment[22, 24, 178, 244-246].

2.8.1 Surface Topographical Structure

The most appropriate scaffolds for topographical replication will continue to be allografts. As the tissue taken is native ACL tissue, the ECM is native and designed perfectly for function. However, due reasons mentioned in section 2.6.2, the aim of TE scaffolds is to be able to replicate, as closely as possible, the native ECM of the ligament.

Topography can be defined as the particular patterning at nano or micron level on the surface of a substrate. Topographical cues are especially important for cells as they aim to emulate the native matrix and can guide a multitude of cell responses, including (but not limited to); alignment (as shown in Figure 2-7), adhesion, migration and differentiation[244, 245]. As collagen forms the majority of the ACL ECM, electrospinning provides the means to enable the replication of the collagenous structure. This is integral in the forming of ligament ECMs, where fibre alignment can alter the expression and production of ECM proteins[247].

Lee *et al.* (2005) have successfully discovered the effect of fibre alignment, stating that it has the ability to determine cell shape, with primary ACL cells exhibiting native 'spindle' like morphology when cultured on aligned polyurethane scaffolds[179]. Not only this, but cells also orientated themselves in the direction of alignment and produced a more collagenous ECM when exposed to aligned fibres. On a much smaller scale, studies have been performed that explore the effects of submicron topographical features on anterior cruciate ligament cell behaviour. Wang *et al.* (2013) has demonstrated that independent of surface chemistry, the morphological response of ACL cells can be tailored with surface pattern alone, with results that show higher frequency of cellular elongation and alignment was observed on grove depths of around 700 nm. Surface patterning however, did not appear to effect spreading and proliferation, which was more responsive to surface chemistry. Another interesting observation was that cells on deeper grooves (with appropriate surface chemistries) produced more collagen type I, and in comparison to smaller 100 nm grooves, was highly aligned with surface topography[248]. This may perhaps be due to the ability of the 700 nm groves to more accurately represent a fibrous 3D environment, prompting the cells to respond more accordingly.

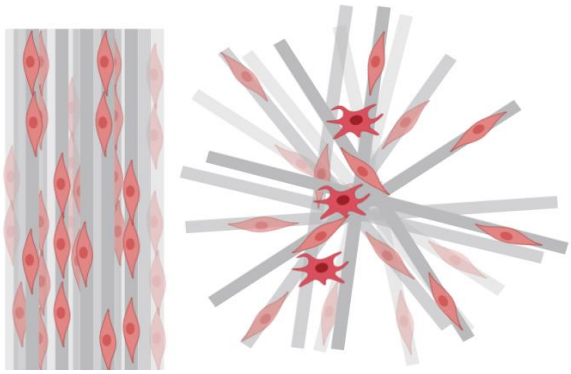

Figure 2-7 Depiction of how fibre alignment can affect cellular orientation on a tissue engineering scaffold. Image created using BioRender.com.

2.8.1.1 Micro or Nano Fibre Diameters?

When creating fibres for a tissue it is important to consider the native architecture of that tissue. For this reason, nano or microscale fibres are used. In ligament tissue engineering, there have been reports of both being utilised to guide ligament cell alignment and mimic the collagen fibres present in the ECM. Fibres of truly nanoscale proportions, defined by The United States National Nanotechnology Initiative as 1-100 nm[249, 250], are rarely employed[18]. Instead, what the literature appears to refer to as nanoscale (300 nm to ~900 nm) are often utilised for ACL TE[179, 251-253], with this diameter enabling comparison with

that of collagen fibrils in the ACL ECM. Interestingly with PCL, acid combinations, and not solvents, have resulted in the smallest fibre diameters (especially when the % concentration of PCL is ~12-15%). Acetic/formic acid in a 1:1 ratio have proven superior for the formation of 'nanofibres' (~230 nm) when compared to solvents such as chloroform/methanol, though this combination did also produce fibres under 1 µm in diameter (~810 nm)[254].

Microscale fibres have been previously divided into categories in order to categorise the differing magnitudes they encompass. Microscale (10-15 µm), small-microscale (5-10 µm) and sub-microscale (0.1-1 µm) have been termed by Thapa *et al.* (2003)[255]. All forms of microscale fibre are also popular in ligament TE. As defined by the above, small-microscale fibres have demonstrated promise in ligament TE, having been shown promote cell spreading and demonstrate good cell viability (4.18-6.44 µm diameters)[256]. Chen *et al.* (2008) have shown great promise for microscale fibres in ACL TE, with their 10 µm diameter fibres demonstrating good *in vivo* compatibility by means of cell ingrowth, regeneration of the midsubstance of the ACL and no inflammation/swelling in the joint[19]. Interestingly, direct comparisons of fibre diameters on MSCs found that up to 3 days, 2.6 µm diameter fibres supported cell metabolic activity better than fibres of 300 nm or 5.2 µm in diameter[257].

Interestingly, fibre diameter has previously been determined to have more of an effect of MSC differentiation into a ligamentocyte phenotype than fibre alignment. Cardwell *et al.* (2012) have determined that when comparing aligned fibres of ~500 nm, ~1.1 µm and ~2.1 µm and random fibres of ~300 nm, ~1.5 µm and ~3.6 µm in diameter, they found that collagen type I and scleraxis expression was significantly higher on the largest fibre diameter for both orientations. They also determined that after 9 days in culture, fibre diameters of ~1.5-2.1 µm (random and aligned respectively) supported the highest cell density, with the same fibre diameters also best supporting cell elongation/projection[258].

Fibre diameter has also been linked with properties such as tensile strength and porosity of the tissue engineering scaffold. Higher tensile strength with decreasing fibre diameter has long-since been reported in electrospun polymer scaffolds[259, 260], as well as the obvious benefits of high surface area to volume ratios[261], whilst increasing fibre diameter has been previously related to increasing scaffold porosity[218]. It appears that in deciding which fibre diameter to utilise, there is a payoff between these properties (high tensile strength and high porosity), both of which are required features in ACL scaffolds. Despite nanoscale fibres

often being preferred for tissue engineering scaffolds, due to increased surface area to volume ratios, the ACL cells' preference for various microscale fibre diameters may be due to the positioning of the cells in their native ECM. Ligamentocytes generally sit within the interfascicular regions. Fascicles in the ACL are large bundles of collagen fibres and are heterogeneous in size, measuring anywhere between 1-300µm in diameter[262].

Despite there being evidence of the ideal fibre diameter for cells used for ACL TE being ~2 µm in diameter[257, 258], there is the marked heterogeneity of fascicle diameters in the native ACL to consider. This consideration has led to the exploration of constructs which reflect this, where a mixture of fibre diameters are present[22, 170, 187]. This may also reduce the payoff with previously outlined physical characteristics (strength and surface area vs. porosity), whilst retaining the ability to recapitulate the native ACL architecture.

2.8.1.2 Influence of Topography on Cell Behaviour and ECM Orientation

It is well characterised that cells will respond to physical cues in their environment, and orientate themselves accordingly. Topographical cues have been reported to influence cell morphology through contact guidance effects; random substrate morphologies have been reported to result in randomly oriented cells, whilst aligned substrates have caused cell elongation along the direction of substrate alignment[263].The elongation of the cell results in intracellular signalling which moderates the upregulation of genes, via a process known as mechanotransduction. More specifically, mechanotransduction is the transference of signals through cell surface receptors to the nucleus, stimulated by mechanical forces. These forces can be either entirely external (cyclic straining on a cell-seeded material or the whole tissue)[264], or caused by the cells themselves (exerting tension on the ECM). They are usually moderated by the interaction of integrin receptors at the cell membrane, which are mechano-receptive. This mechanical stress on the integrins results in the upregulation of the intracellular RHO and MAPK pathways, which are essential for the formation of stress fibres and focal adhesions[264].

Mechanotransduction is essential for cells to move through and adapt to their environment. It governs a cell's ability to differentiate and attach to/interact with, the ECM, as well as upregulate essential genes through the mechanical stimulation of the nucleus. As briefly alluded to in section 2.7.1, ligament cells in the ACL midsubstance should retain a spindle-like, elongated morphology as the regulation of essential genes required for survival and

ligament-associated ECM production can be altered by cell shape[42, 167, 168], and by the addition of mechanical force (which also alters cell shape)[42]. Topographical cues, such as aligned fibres have been shown to guide the elongation of fibroblasts along the longitudinal axis of the construct. Though many studies show this as a result of the application of tensile strain on the constructs, evidence for cells adopting these conformations in static environments are available. It may be worth noting however, that there is the possibility these constructs had been placed under tension in order to mount them for cell culture, therefore making them stiffer. This is especially relevant when considering the findings of Checa *et al.* (2015) and Rens & Merks (2020) who determined that cells in stiffer environments have a tendency to form chains, or elongated morphologies[265, 266], implying the observed morphologies may not be due to topography alone. Elongation occurs due to focal points of ECM stress forming under the polarised protrusions of the cell. Strong stresses under the protrusions cause stabilisation of focal adhesions and prevent retraction of the polarised protrusions. Continuation of focal adhesion stabilisation further pulls the polarised ends of the cell outwards, destabilising adjacent adhesions and resulting in a stretched and elongated cell[266].

Interestingly, cell alignment has been shown to result in neo-ECM alignment[267]. As ECM alignment has been shown to increase both the speed and persistence of the cell along the ECM fibres[268], the effect of which has been shown to be successfully recapitulated in 3D aligned matrices[269]. Though there appears to be no confirmed explanation for why the alignment of both cell and neo-ECM are linked, perhaps the forward trajectory of the cell at increased speed is enabling the deposition of highly aligned fibres. In contrast, the cell on a non-aligned substrate[269], which has limited directionality, will display randomly oriented and highly disorganised neo-ECM.

2.8.2 Surface Chemistry Modification

2.8.2.1 Plasma Treatment

Plasma treatment is a popular and widespread method of altering the surface chemistry (10-1000 Å[270]) of a material by means of oxidation. This is primarily due to the exposure of chemically unstable ions/free radicals, usually generated by the application of a radio frequency field. Most often performed using oxygen, this procedure can also utilise ammonia (NH_3)[215], monomeric compounds and air to perform hydrophilisation on the surfaces of a variety of substrates. Plasma is often a preferred method of surface chemical modification due to it causing very little damage to the bulk material[270], though it has been shown, in

some cases (usually after longer treatment times), to compromise the tensile properties of materials, possibly due to the nanoscale 'etching' effect that occurs during treatment[271, 272].

Plasma treatment relies on the ability of ionised particles it generates to collide with a material surface. Due to this, common methods of plasma generation (e.g. RF glow discharge plasma), and subsequent treatment, often occurs at low pressure. This is primarily to reduce the mean free path of the charged ions/electrons in the plasma. Mean free paths are the distance that an ion/electron of a given diameter (depends on the element in question that is being ionised) can travel before it undergoes a collision. Reduction of parameters such as pressure and temperature can reduce the mean free path, increasing the frequency and number of collisions with the material of interest over a given amount of time, therefore increasing the probability of a treatment-saturated surface[273, 274].

Many popular polymer substrates used in tissue engineering have hydrophobic surface properties, rendering them unsuitable for adequate cell attachment[210, 231, 275, 276]. Plasma treatment will alter the surface chemistry of the polymer, enabling it to be more conducive to cell attachment. However, this particular surface treatment method produces highly unstable chemical bonding which, if not stabilised with additional covalent bonding (i.e. proteins, conjugation chemistries, other polymers etc.) will enable the material to undergo hydrophobic recovery within relatively short time frames[276]. Another disadvantage to this method is that it can render materials super-hydrophilic (water contact angle ~0°)[277]. Super-hydrophilic materials can encounter issues with protein adsorption and cell attachment due to the surface's strong attraction of water, creating a highly competitive environment for protein/cell surface interaction[278].

2.8.2.2 Hydrolysis

Within the literature, soaking in various chemicals appears to be a moderately popular method to improve the wettability of a biomaterial. Acid/alkaline hydrolysis, also referred to as etching, is a method by which nanoscale topography is etched into the material means of corrosion. This method increases the wettability of a material by producing $H^+_{(aq)}$ or $OH^-_{(aq)}$ ions which attack ester (R-O-R) or carbonyl (C=O) groups to produce exposed –OOH groups on the substrates, either through additional reactions with water (acids) or alone (bases)[279, 280].

Unlike plasma treatment, mentioned above (section 2.8.2.1), this method affects the bulk material, as opposed to solely the surface, with ionic penetration through the bulk material

increasing with increasing acid/base concentration. As this method effects the bulk properties of the material, it can also have significant weakening effects on the mechanical properties of the material and has been shown to decrease scaffold mass and thickness[279]. Most commonly, this is performed with basic solutions, such as sodium hydroxide, with a wide variety of concentration and exposure times being utilised[281-284]. Though acid hydrolysis with mineral[285] acids are reported in the literature, their use is less commonplace, perhaps owing to the superior performance of basic catalysts in performing hydrolytic reactions[286].

2.8.3 Growth Factors Supplementation/Release

Growth factors (GF) are a highly effective method of directing cellular migration and differentiation. Their effectiveness however, depends on not only their concentration, but also their release kinetics. Controlled release of GFs can also ensure a concentration gradient, which in turn can provide guidance to the cells for directional migration and time dependant differentiation[287]. The most popular method of controlled release is achieved by containing the factors inside fabricated biomaterials, which are degraded by the body at different rates. The method of controlled release will depend on the period of time the growth factor is desired[288]. Commonly appearing in the literature relating to ACL TE is basic fibroblastic growth factor (bFGF). Methods of release included degradation of GF-impregnated hydrogels and coatings on electrospun fibres[22]. In these instances, the addition of bFGF increased the stiffness of newly formed tissue and increased proliferation with the hydrogel-releasing scaffolds *in vivo*, reporting an increase in collagen deposition compared to the control[21]. Meaney-Murray *et al.* (2003) performed a comparison study as to the most appropriate growth factor to use whilst attempting to stimulate regeneration of the ACL. Transforming growth factor β (TGF-β1), FGF-2, platelet derived growth factor (PDGF)-AB and epidermal growth factor (EGF) was released from a lyophilised, highly porous scaffold. Though it was found that GF addition did not affect the rate of migration into the scaffold, PDGF-AB and FGF-2 both positively influenced proliferation. However, upon the analysis of collagen ECM deposition, both PDGF-AB and TGF-β1 exposed cells produced over three times the amount when compared to controls[289], suggesting that PDGF-AB may be the most appropriate GF. PDGF, along with collagen is highly implicated in the formation of scar tissue, which is why both cell proliferation and collagen production happen sequentially, implying a healing response in the ACL from exposure to this scaffold[289].

2.8.4 Protein Adsorption

Protein adsorption is considered extremely undesirable in a number of biomedical applications (for reasons including sterility, thrombogenicity, etc.)[290] however, for biomaterial success, it is considered essential. Protein adsorption is one of the primary stages of biological integration, enabling the cells to begin to populate the material. It is used primarily in biomaterial fabrication as a technique used to adhere a tertiary amino-acid structure to a surface to support cell attachment and subsequent bioactivity. Here, proteins adsorbed to biomaterials act as anchorage sites for cells, providing them with stable and more permanent attachment motifs, as opposed to the weak intermolecular force interactions they experience when binding to an exclusively chemically modified biomaterial surface[291].

Proteins are complex tertiary structures, which fold in a manner that is most energetically favourable/stable. What determines this, are the specific amino acids that form the structure. Each of the possible 20 amino acids have different chemical characteristics and can be divided into 4 groups (determined by their side chains):

- Electrically charged: lysine, arginine (positively charged), glutamic acid, aspartic acid (negatively charged) and histidine
- Polar and uncharged: serine, threonine, asparagine and glutamine
- 'Different' chemical character: histidine (aggregates, no ordered secondary structure), glycine (no side chains), proline (excitation couplets, cyclic constraints in the carbon backbone)
- Hydrophobic: alanine, valine, isoleucine, leucine, methionine, cysteine (non-aromatic), phenylalanine, tyrosine, tryptophan (aromatic side chains)[292]

A protein's adsorption kinetics will depend on a number of factors: its arrangement of amino acid sidechains, the surface chemistry of the target material[293] and the topography of said material[294] to name but a few. It has been previously well reported that proteins adsorb more successfully to hydrophobic materials, through inter-molecular interactions (such as van der Waals forces[295]), as their competition for surface interaction with water molecules is greatly reduced[293]. It should be noted however, that strong hydrophobic adsorption can permanently denature the protein[294], preventing interaction with cells.

A preference for hydrophobic materials is true for many proteins, including as collagen[296], fibrinogen, and bovine serum albumin[297]. It is know that proteins deform on strongly hydrophobic surfaces, losing their tertiary structure and unfolding onto the material surface.

Fibrinogen has been reported to lose its secondary structure when adsorbing to hydrophobic surfaces rather than hydrophilic[294]. However, at the risk of understating the complexity of protein adsorption, it must be highlighted that multiple factors can affect the interaction kinetics of a protein with a surface, other than the degree of wettability/surface energy of a material surface. Factors such as; protein concentration[298], protein size[295, 297, 298], solution pH[299], atmospheric temperature[300] and surface topography[294], to name but a few, have been previously reported.

Moreover, these parameters cannot exist in isolation and therefore cooperatively change the adsorption profiles of proteins. Solutions containing differing sizes of proteins can cause adsorption and desorption kinetics of differing size ranges to alter. Known as the 'Vroman effect', it indicates that in a heterogeneous solution, smaller proteins of higher concentrations with weaker surface affinity will first be adsorbed and subsequently desorbed and replaced by larger ones with stronger affinity[298].

2.8.4.1 Integrin-Mediated Cell Attachment to Proteins

When attaching to proteins/ligands, cells do so by means of specific attachment. This is facilitated by integrin receptors, which are small transmembrane proteins, promoting the attachment of cells to ECM proteins, which is integral for not only cell survival in adherent cell populations, but also for matrix remodelling, a process whereby the cells actively participate in the general upkeep of their surrounding ECM. Upon their attachment to ECM ligands, they also become responsible for the triggering of protein complexes, which recruit specific molecules (kinases, phosphatases etc.) responsible for the behaviour of the cells. Integrins are comprised of two subunits, one α and one β. In total there are 18 α subunits and 8 β subunits which, in different combinations can form 24 different types of integrin. Interestingly, integrin receptors can cluster and interact with different α-β subunit compositions, forming focal adhesions. For example, the integrin αvβ3, which is heavily involved in mechanotransduction and binding of RGD motifs in vitronectin[301] and fibrillin-1[30], can co-localise with multiple different types of ligand, though α5β1 (facilitates the attachment of cells to RGD motifs in fibronectin), can only co-localise with a few[301]. Their interactions with the RGD motifs in ECM proteins such as fibronectin, collagen, vitronectin and fibrillin are largely responsible for the success of biofunctionalised materials. Enabling specific attachment to these immobilised proteins, which are more stable than the non-specific interactions with chemical modifications (i.e. plasma treatment), enables subsequent

protein deposition and neo-ECM formation, and therefore faster cell integration and tissue formation.

2.8.5 ACL-Related Proteins for Scaffold Biofunctionalisation

Table 2-6 A brief summary of studies that utilise the incorporation of proteins to biofunctionalise materials used for ACL repair and regeneration.

AUTHOR	MATERIAL DESCRIPTION	FUNCTIONALISATION PROTEIN	CELL TYPE	STUDY OUTCOMES
Ruan *et al.* (2019)[24]	Knitted Collagen-Silk	Collagen type I	Rabbit ACL fibroblasts	*In vivo* study; formation of ordered collagen fibrils, presence of COL1 and TENC positive staining, lack of immunogenic response.
Yu *et al.* (2020)[26]	Air plasma treated braided PLLA	Fibronectin	MSCs	Increased cell attachment and proliferation, supports ECM deposition and correct cell morphology.
Leong *et al.* (2015)[22]	Aligned electrospun PCL	Collagen type I/bFGF	Human foreskin fibroblasts	*In vivo*; aligned collagen fibrils, little immunologic reaction, good cell infiltration, bFGF promoted enhanced stiffness compared to controls.
Leong *et al.* (2014)[25]	Aligned electrospun PCL	bFGF/Heparin	Human foreskin fibroblasts/Rat ACL model	Significantly higher proliferation with functionalised scaffolds *in vitro*, collagen fibre production within the graft *in vivo*. Tensile strength of graft proved insignificant to the negative control following *in vivo* implantation.
Lu *et al.* (2005)[302]	Braided PLLA/ PGA/PLAGA fibres	Fibronectin	Rabbit ACL fibroblasts	Fibronectin increased cell attachment and long-term (14 days) matrix production on PLLA and PLAGA scaffolds.
Shen *et al.* (2014)[303]	Silk fibroin knitted sponges	Collagen type I	Rabbit MSCs	Increases attachment and migration of cells, improved bone-graft healing, architecturally similar to normal ligament, protected cartilage surface.
Yoshikawa *et al.* (2006)[304]	Ovine patellar tendon graft	VEGF	Native ovine ACL cells	Increases vascularisation but decreases graft stiffness, promoting early phase graft laxity in the joint.
Pauly *et al.* (2017)[305]	Electrospun PCL bundles	CTGF	Ovine/porcine MSCs	Increased cell number on functionalised scaffolds, supported the production of collagen type I/III (*in vitro* and *in vivo*) and GAGs.

2.8.5.1 Fibrillin

The fibrillins are an ancient family of glycoproteins that are well conserved between species. They are often associated with elastic tissues and occur three isoforms. Fibrillin-1, which contains a proline rich region and is expressed throughout the organism's lifetime, fibrillin-2, which has a glycine-rich region and expression predominantly in the developmental period[306, 307], and fibrillin-3, which contains a region that is glycine and proline rich, and is expressed within the same time-frame as fibrillin-2[307, 308].

Fibrillin is a disulphide rich, hydrophilic protein, separated by highly regular epidermal growth factor-like (EGF) domains (of which the vast majority are calcium binding and contain regular disulphide bonding). It also contains seven transforming growth factor β binding protein-like domains (or TB domains), which are 8–cysteine domains, of which one (TB4 - FBN1) or two (TB4 and TB3 - fibrillin-2/3) contain an RGD site[307]. These RGD motifs mediate cell interactions by binding with integrins $\alpha_5\beta_1$, $\alpha_v\beta_3$ and $\alpha_v\beta_6$[309] and are moderated by a synergy site in cbEGF domains 19-21[310]. They have recently been found to mediate integrin binding, actin binding and growth factor expression through the RGD-integrin interaction with miRNAs[311].

Also present are multiple heparan sulphate binding sites, one of which resides in TB5. These binding sites mediates fibrillin interactions with perlecan, a heparan sulphate-containing glycoprotein, which appears to assist in the formation of microfibrils[36]. Fibrillin deposition is highly dependent on the assembly of fibronectin and is one of the later proteins to be deposited into the ACL ECM[34]. This relatively large, beaded 350 kDa protein is highly fibrillar, forming 10-12 nm microfibrils[312] and self-assembles around the newly deposited elastin fibrils, performing its role as a supportive structure, and acting as a template for elastin deposition[306]. In terms of cell binding, Sakamoto *et al.* (1996) hypothesised that there may be a second type of non-RGD binding site on fibrillin as cells maintained levels of adhesion despite the presence of RGD inhibitors[309]. Another type of binding, essential to fibrillin assembly, is mediated through heparan sulphate and their proteoglycan, perlecan. Heparan sulphate binding sites have been discovered in TB domains and have been found to be mediated through the calcium binding EGF domains playing a critical role in fibrillin assembly. Heparan sulphate can mediate the interaction between C and N terminal domains, disenabling the multimerisation of fibrillin-1, without effecting fibronectin interactions[313].

Upon a review of current literature, fibrillins 1 and 2 do not appear to have been directly involved in the tissue engineering of anterior cruciate ligaments. However, the use of fibrillin-1 in vascular applications is popular, where the responses of endothelial and smooth muscle cell types have proven positive[30, 314, 315], and unlike fibronectin[316], appears to be anti-thrombogenic[315]. Testing with immobilised fibrillin-1 fragments (RGD containing) however, have elucidated on the potential of fibrillin to increase the biocompatibility of synthetic polymer substrates, with potential for utilisation in TE scaffolds[315].

2.8.5.2 Elastin and Tropoelastin

Simply put, tropoelastin is the ~20 nm monomeric form of elastin. This 60 kDa protein can be credited for the many of the elastic properties of the ECM, with it usually produced in foetal development/early childhood and rarely in adulthood. It contains alternating polar and non-polar domains, with the hydrophobic regions contributing heavily to protein flexibility by creation of three types of β-type labile turns. This monomer is highly elastic, with a tensile stress of 3 kPa and the ability undergo reversible elastic deformation to 8 times its resting length[317]. Mature elastin has also been found to colocalise with perlecan (heparan sulphate containing glycoprotein) and it has been hypothesised to assist with cell attachment to elastin fibrils[52]. In addition to perlecan and fibrillin-1, elastin also interacts with fibulin-5. Fibulin-5 has previously been determined to be essential for elastogenesis[318, 319] and mediate cell interactions with elastin via their RGD motif[319]. The C terminal has been found to play an essential in the crosslinking, coacervation (driven by hydrophobic interactions) and microfibril deposition, whilst the N terminal mediates the interaction of tropoelastin with fibrillin-1 via domain 4 and is essential for tropoelastin deposition and subsequent integration into the ECM[37].

There have been multiple efforts to incorporate elastin derivatives into TE scaffolds, though with mixed results. Tropoelastin coatings result in increasing wettability of polyethylene, and subsequent cell spreading, have been reported with fibroblast cells[164]. Endothelial cells have also been shown to exhibit increased attachment and proliferative responses when exposed to tropoelastin and elastin[320-322]. Reports in the literature of using elastin-like peptides (ELPs) (peptides similar in structure to tropoelastin) on TE scaffolds have proven successful, with aligned ELP-coated scaffolds found to cause upregulation of elastin production by fibroblasts[247]. Though it is possible to discover elastin-coated scaffolds, very few have been designed to relate to ligament TE. The one example that is known (to the knowledge of the author) utilises tropoelastin coatings on the scaffold/graft fibres and

reported better osteointegration at the graft insertion point[323]. The limited amount of elastin-coated scaffolds is perhaps due to low solubility of elastin and the addition of elastin to a scaffold decreasing the capacity for tensile strength[321]. In addition to this, elastin/tropoelastin itself bears no attachment motifs to which cells can directly attach, and relies heavily on GAG mediation to facilitate cell interaction[324]. This may indicate that elastin might not be the most viable option for ACL regeneration.

2.8.5.3 Fibulin

The fibulins are a versatile, yet small family of calcium binding proteins, known to interact with different components of the ECM, including elastic fibres, to aid in cellular interaction and fibre assembly. Of these, fibulins 4 and 5 are most relevant to ligament tissue. Lack of these can cause severe elastogenic effects in utero[325] and worsening deformation in all elastic tissues throughout the body[318], respectively. Recent attention has been focused on fibulin-5. Fibulin-5 is a protein that is upregulated by TGF-β and interacts directly with elastic fibres and their constituents, organising and assembling elastic fibres by interaction of its RGD motifs with cells. Nakamura *et al.* (2002) showed that fibulin-5 negative mice exhibit elastic fibre deformation possibly due to lack of cell binding and subsequent lack of remodelling[318], implying that whilst fibulin-5 does not prevent the formation of elastic fibres, it inhibits the structural assembly. There are records that confirm the production of fibulins 1, 3 and 5 by ACL fibroblasts, with fibulin-5 being produced at relatively higher levels when cells were placed in an environment with a damaged ECM[241]. There have been efforts to incorporate increased expression of this protein into a TE scaffold. Endothelial cells, which had undergone virally induced overexpression of fibulin-5 were cultured in an expanded PTFE TE scaffold, where fibulin-5 expression increased attachment, but decreased proliferation[326]. Though very little of the literature reports the use of any type of fibulin in connection with ligament regeneration or tissue engineering technologies, perhaps due to fibulin's latent expression, when compared with other elastic forming proteins such as fibrillin and tropoelastin, or its need interact directly with microfibrils and elastic fibres in order to achieve cell attachment; conjugation to materials will inhibit its effects.

2.8.5.4 Fibronectin

Fibronectin is a protein integral for ECM assembly, with assembly of fibronectin fibril formation dependent upon cellular interactions with the N terminal via $\alpha_5\beta_1$ integrins which proceeds the self-assembly of fibronectin and regulates the formation of ECM microfibrils. Through this mechanism, fibronectin has been shown to be integral for elastic fibre

formation as it governs the assembly of fibrillin in the ECM[34]. Fibronectin is also highly cell-adhesive, with Lotz *et al* (1989) showing that fibroblasts in particular elicit high levels of strong binding to fibronectin coated surfaces, with 100% binding within 15 mins of incubation (37°C)[327]. This study was confirmed using rabbit ACL cells which displayed a significant preference for fibronectin in further attachment studies[328]. Instances of utilising fibronectin as a coating to enhance cell response are widely reported in the literature, with it being used as an enhancement technique for current artificial ligament grafts. Li *et al.* (2014) has reported that fibronectin promoted cellular integration into the graft and upregulated collagen type I genes, enabling the formation of collagen-heavy matrices on the polyethylene terephthalate (PET) grafts by MSCs. This useful knowledge may be applicable to the new LARS graft to enhance biocompatibility, due to PET being the major component[329]. In terms of developing novel TE scaffolds and the enhancement of their success, the effect of utilising fibronectin has been explored; Hu *et al.* (2005) reported that coating PLA/PGA/PLGA fibres with fibronectin improved ACL fibroblast attachment and proliferation, delayed scaffold degradation of PGA fibres, and increased ECM production[302].

2.8.5.5 Collagen

As the ACL comprises of 85% collagen, this protein has been a firm favourite when selecting functionalising proteins for ACL TE. Collagen is one of the most abundant proteins in the mammalian body and can be found over 28 forms. Types I and III are fibrillar collagens and dominate the ACL ECM, with collagen type II present at the terminal ends where osteochondral integration occurs[5]. The integration of collagen type III in the ACL matrix is reported to give the ACL some of its elastic properties, reducing stiffness of tissue and causing thinner fibres. This could be caused by delayed N terminal processing in collagen type III which is hypothesised to control shape and diameter of fibrils[330]. Collagen type I production in the ACL is reported to be mediated by actin fibre stretching which shifts the location of integrin $\alpha_v\beta_3$ and causes stress activated gene expression, enabling collagen type I production[264]. Collagen coatings have previously been investigated for use with the anterior cruciate ligament, starting with attempts to improve biological integration of BMSCs with PET ligament grafts at the osteochondral integration site. Results showed a highly increased rate of proliferation and adherence and cells appeared to adopt ACL fibroblast native 'spindle' morphology[331] indicating graft suitability for the ACL. Leong *et al.* (2015) also demonstrated high levels of proliferation of human foreskin fibroblasts on

collagen-only coated PCL scaffolds, with cell number quadrupling within a week[25]. However, collagen is preferentially used as an electrospun scaffold, as mentioned in section 2.7.2.1, with instances of its use showing positive and encouraging responses, such as enhanced attachment[200].

2.8.5.6 Glycosaminoglycans (GAGs)

GAGs are characterised as monomeric, (usually sulphated) polysaccharides which attach to a proteoglycan (PG) core. Within the ACL, there are multiple PGs, which interact with multiple different proteins within the microfibrillar environment. Biglycan (a dermatan sulphate linking PG) interacts directly with microfibrils[53] whilst perlecan (heparan sulphate containing) interacts with fibrillin-1 and microfibrils in the basement membrane, directly effecting assembly[36]. Another PG present in the ACL, decorin, appears to function slightly differently, forming complexes with both fibrillin-1 and microfibril-associated glycoprotein-1 (MAGP-1), indirectly affecting fibrillar structure[53].

A popular GAG studied in connection with the ACL is heparin/heparan sulphate (HS). This particular GAG is of critical importance in ligament tissue, due to its association with fibrillin-1 and its direct effect on the interactions between fibrillin-1 and tropoelastin/MAGP-1. It consists of glucuronic acid and *N*-acetylglucosamine repeats and is always found covalently linked to PGs *in situ*. Its interactions with proteins however, are highly dependent on the degree of sulphation of each repeating unit. For example, only highly sulphated HS will undergo interactions with fibrillin-1. Fibrillin-1-HS interaction domains are highly specific and binding of HS is mediated by multimerisation of fibrillin-1, or rather HS limits the multimerisation of fibrillin-1, suggesting its use as a regulation mechanism for microfibril assembly[313].

Though there have been previous studies which have shown highly encouraging results when using GAGs on biomaterials to support attachment and proliferation in adipose stem cells[332] and neural and chondrogenic differentiation in embryonic stem cells [333] and MSCs [334, 335] respectively, there have been very few efforts to incorporate GAGs into scaffolds for ligament repair. While some have only used synthetic GAGs to aid in the adsorption of other growth factors to the scaffold[25], others have used them as the main bioactive component of the scaffold. This study, authored by Murray *et al.* (2001) employs the use of chondroitin sulphate, for repair at the terminal ends of the ligament and enhanced osteo-integration. In the instances reviewed, chondroitin sulphate has been incorporated directly into the

scaffolds, rather than applied as a coating. Cells have been found to be able to migrate into the scaffold, whilst expressing contractile actin[336]. Another, more recent endeavour by Gouveia *et al.* (2021) has used core-shell collagen-PCL fibres for the controlled release of GAGs (chondroitin sulphate, dermatan sulphate) into the media to enable more successful fibre integration and matrix production. Chondroitin sulphate incorporation appeared to be highly successful, and was determined to enhance matrix production above other conditions tested[337].

2.9 Formulated and RGD-containing Peptides

Isolating regions of interest within a protein can be highly beneficial to optimising cell responses or desired outputs of a biomaterial. The majority of these fragments reported in the literature are those containing RGD motifs[27, 248, 309, 310]. RGD motifs are a specific cell attachment site formed by three amino acid residues – arginine, glycine and aspartic acid, and are widely utilised in a number of cell types. They enable the attachment of cells through 8 of the 24 known integrins (mainly α_v subunits and β_1 subunits, with the exception of $\alpha_{11b}\beta_3$), whose use varies depending on the host protein[338].

There are multiple instances of RGD-containing peptides being utilised for the enhancement of ACL ligamentocyte response. Chen *et al.* (2003) determined that EDC/NHS conjugated RGD fragments on silk fibres increase ACL ligamentocyte metabolic activity, attachment, spreading and upregulated collagen type I production[27]. Wang *et al.* (2012) also determined that RGD functionalisation increased cell spreading over than of oxygen plasma functionalised surfaces and RGD peptide conjugation successfully directed the orientation of cells along 100 nm groves over oxygen plasma and dopamine conjugation[154]. From a review of the literature, it appears that RGD fragments are primarily used as a method of early stage attachment and little is reported about longer-term effects >14 days[248, 310, 339, 340].

Recently, although performed with a focus on the ACL, but not performed using ligament cells (with hamstring-derived tenocytes, which are somewhat similar), TGFβ1 peptides have been used as surface-conjugated methods for enhancing cell response due to their ability to sequester other proteins and growth factors and are conducive to cell proliferation and ECM production. Use of the covalently bonded TGFβ1 peptide was found to upregulate TGFβ1-associated proteins at early time points, such as aggrecan and collagen type I, but interestingly, perpetuated the upregulation of collagen type III over time. Use of these

fragments *in vivo*, produced tissue that mimicked native ligament characteristics (cell morphology, fibre alignment) and showed adequate tissue density[208].

2.10 Conclusions

To conclude; ACL tears are a relatively common and debilitating issue. With young people heavily effected and prognoses of recurrent graft failure, current outcomes are not desirable. Moreover, with increasing numbers of women participating in sports (and having a higher risk of ACL tears), it is becoming increasingly more of an urgent issue within today's society. There have been many reports in the literature of methods for encouraging the repair and regeneration of ACL tissue. These techniques have employed a variety of methods; however biofunctionalisation of a architecturally mimicking scaffold appears to hold the most potential. This potential lies in the biofunctionalised scaffolds' ability to topographically guide cells whilst providing ECM-relevant cues and attachment sites for the formation of a functional neo-ECM.

Fibrillin-1 has shown great promise as a biofunctionalisation component, with marked success in endothelial cells and human dermal fibroblasts[310, 315]. As fibrillin-1 is also present in the ACL ECM, is equipped with RGD-cell binding sites, and is a component of later-stage, maturity-indicating ECM components, i.e. elastic fibres[306], it may show promise as a method of encouraging ACL ligamentocyte regenerative response.

In this literature review the author has aimed to provide relevant and thorough information, which will guide the understanding of the research performed in this thesis.

CHAPTER 3 FABRICATION AND CHARACTERISATION OF AN ALIGNED FIBRE POLYMER CONSTRUCT WITH FIBRILLIN-1 FRAGMENTS

3.1 Overview

3.1.1 Introduction

Over the past decade, there have been multiple promising studies detailing the effectiveness and success of aligned polymer scaffolds on ACL regeneration. The necessity of appropriate topographical guidance cues that can mimic the native ECM structure can impact heavily on ACL cell morphology and subsequent neo-ECM production, as well as overall matrix alignment[179].

Poly-ε-caprolactone is a semi-crystalline polymer with exceptional viscoelastic properties and the ability to be manipulated into a variety of different scaffold morphologies[218, 341-343]. As PCL has previously been FDA approved for wound healing dressings, and has ample evidence in its success as an electrospun scaffold, it was a logical place to start. Large amounts of optimisation regarding the electrospinning parameters, solvent type and polymer concentrations, including investigations into the suitability of random vs. aligned fibres for canine ACL cell culture, were previously explored by Dr D Ramos Marques and Miss G Crichton (unpublished, see Appendix 1[344] and 2[345]). This optimisation work lead to stable parameters which enabled the production of the fibrous platform which was used for this work.

3.1.2 Statement of Novelty

According to the literature, the majority of ACL regenerative techniques using electrospinning focus highly on the fabrication of nano- and sub micron- scale fibres. This chapter will introduce the use of a microscale fibrous scaffold, functionalised with RGD motif-containing fibrillin-1 glycoprotein fragments. This will function as a platform for the regeneration of the ACL using canine cruciate ligamentocytes. It will also determine which surface treatment (from a range found in the literature) is most appropriate for increasing the wettability of micron-fibre PCL scaffolds and which treatment (in combination with the scaffolds) is most suitable (in terms of cell viability) for culture of primary canine ligamentocytes. Analysis of the effect on these specific fragments on the scaffolds, and how they alter scaffold properties, will also be performed.

3.1.3 Hypothesis

It is hypothesised that an aligned fibrous scaffold can be produced that will demonstrate high levels of anisotropic fibre orientation, with fibre diameters that are suitable for guiding the morphological response of ACL cells, and that these will remain consistent between batches.

It is also expected that the method of surface treatment selected will demonstrate suitable hydrophilicity to encourage native cell morphology, efficient protein adsorption and will retain high levels of cell viability. It is predicted that the selected treatment method will demonstrate little variation in its protein-fragment adsorption ability, and adsorbed fragments will be observable.

3.1.4 Aims & Objectives

- Reproduction of a suitable platform scaffold which is capable of emulating the highly aligned native architecture of the ACL.
- Determination of character of the produced electrospun scaffold, as an average and between individual batches, in terms of:
  - The average fibre diameter of the scaffolds produced using SEM and image analysis, ensuring they are suitable for topographical ACL cell guidance in terms of their size.
  - Level of anisotropic orientation of the scaffold fibres.
  - Scaffold thickness and roughness of the surface topography by interferometry for determination of dimensional structure and surface topographical architecture.
  - Porosity of the scaffolds to enable cellular integration by gravimetric analysis.
  - Mechanical properties by tensile testing for determining the strain at which the platform will tolerate for recovery, for performing experiments under tensile strain.
- Discern the most suitable treatment method for the scaffolds, taking into account:
  - Wettability for protein adsorption and cell attachment.
  - Protein/fragment adsorption capabilities of the scaffold post treatment.
  - Cell viability, morphology and alignment for the different treatment methods.
- Determination of the success and variability of the chosen treatment method using a multitude of analytical methods.
- Visualisation of the adsorbed fibrillin-1 fragments on the scaffolds and their controls.
- Determination of whether treated scaffolds adsorb higher amounts of fibrillin-1 fragments compared to untreated and glass controls.

- Determination of any variation between batches of treated scaffolds in their ability to adsorb fibrillin-1 fragments.
- Observation of effect of fibrillin-1 fragments on scaffold wettability.

3.2 Materials & Methods

3.2.1 Materials

3.2.1.1 Chemicals

Chloroform (277106P, BDH, VWR, UK), PCL (poly-ε-caprolactone (PCL, M_n 80,000 g mol^{-1}, 440744, Sigma Aldrich UK), borosilicate glass coverslips (No.1, 101000, Marienfeld-VWR Germany), silicone RTV multi-purpose sealant (732, clear, Dow Corning UK), gelatin from cold water fish (G7041, Sigma Aldrich UK), glycine (G8898, Sigma Aldrich UK), 2, 2'-azino-bis(3-ethylbenzothiazoline-6-sulfonic acid (ABTS) solution (002024, Invitrogen™ Novex™ UK), ProLong™ Diamond Antifade Mountant (P36970, Invitrogen UK), DMSO (dimethyl sulphoxide, D5620, Sigma Aldrich UK), 10% neutral buffered formalin (HT501128, Sigma Aldrich Germany), sodium hydroxide (10192863, Fisher Scientific UK), 4X LDS loading buffer (NuPAGE, NP0007, Invitrogen UK), 10X sample reducing agent (NuPAGE, NP0004, Invitrogen UK), Bis-Tris gel (4-12%, 1mm, NP0321, Invitrogen UK), 1X MOPS SDS running buffer (NP0001, NuPAGE, Invitrogen UK), PrecisionPlus Protein AllBlue Standard (L0001647 A, BioRad USA), InstantBlue staining solution (ISB1L, expedeon UK), Resazurin salt (R7017, Sigma Aldrich UK), dichloromethane (10750862, Acros Organics UK).

3.2.1.2 General Cell Culture

Trypsin/EDTA solution 1X (0.05% trypsin, 0.02% EDTA in Hanks' balanced salt solution, 59417C, Sigma Aldrich UK), bovine serum albumin (BSA; A7906, Sigma Aldrich UK), Dulbecco's phosphate buffered saline (PBS, D8537, Sigma Aldrich UK), Dulbecco's Modified Eagles Media (DMEM, high glucose, 4500 mg L^{-1} glucose, 584 mg L^{-1} L-glutamine, 3700 mg L^{-1} sodium bicarbonate, D5796, Sigma Aldrich UK), fetal bovine serum (FBS; F9665, Sigma Aldrich USA), Antibiotic-Antimycotic 100x (A/A; 10,000 U penicillin, 10 mg streptomycin, 25 µg amphotericin B ml^{-1} A5955, Sigma Aldrich UK).

3.2.1.3 Assays

LIVE/DEAD solution (LIVE/DEAD Viability kit, L3224, Life Technologies Ltd. UK).

3.2.1.4 Antibodies

Mouse anti-6His (MAB050, R&D Systems USA), goat anti-mouse IgG (whole molecule) peroxidase (A4416, Sigma Aldrich UK), goat anti mouse 568 nm secondary antibody (ab175473, Abcam UK).

3.2.2 Electrospinning of Aligned Fibre Scaffold

1.5 g of poly-ε-caprolactone (PCL) pellets were mixed with 10 ml chloroform to form a 15% (w/v) solution and stirred overnight in a glass vial with a magnetic stirrer.

The solution was spun from a 10 ml syringe (BD Plastipak, UK) using a flattened 21G syringe needle. The needle was purged of air and secured for spinning. The mandrel used for collection was covered in greaseproof paper and earthed. The cable delivering the voltage source was attached to the base of the needle. A latticed wire plate was then hung from the needle to further ensure fibres were directed towards the collector (as illustrated in Figure 3-1). Atmospheric temperature was sustained at 20-22°C and relative humidity between 30-45%. The parameters used for the electrospinning protocol are described in Table 3-1.

Table 3-1 Parameters for electrospinning 15% PCL scaffolds (distance is measured from the needle tip to the closest edge of the mandrel).

PARAMETER	VALUE
Polymer solution volume	1.5 ml
Polymer solution flow rate	1.5 ml/hr
High voltage	18.0 ± 0.1 kV
Mandrel rotation	1400 ± 10 rpm
Mandrel diameter	ø130 mm
Mandrel surface width	50 mm
Distance from collector	200 mm
Time spinning	20 mins

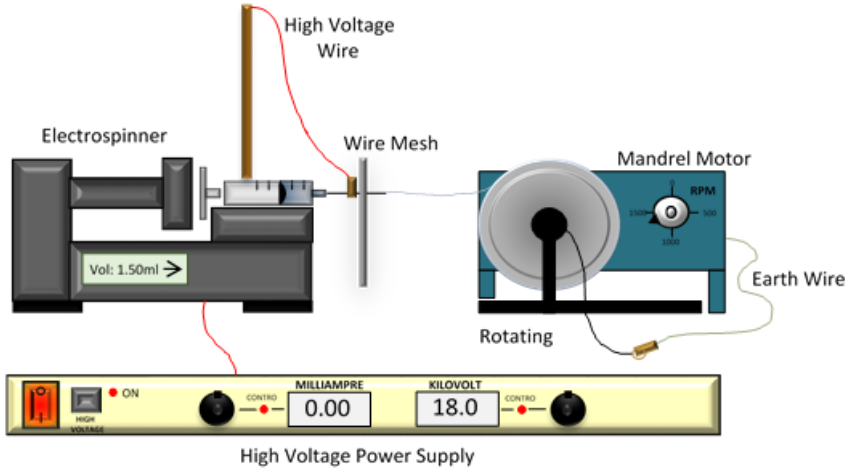

Figure 3-1 Depiction of the electrospinner set up for spinning the aligned fibres scaffolds. A relatively simple set-up was used, housed in a fume cupboard.

3.2.2.1 Mounting the Scaffolds

For all experimentation (unless otherwise indicated), scaffolds were mounted on 12 x 12 mm No.1 borosilicate glass coverslips, using an FDA-approved silicone RTV multi-purpose sealant.

3.2.3 Characterising Electrospun Fibre Dimensions

3.2.3.1 Fibre Diameter and Orientation

SEM images were taken of scaffolds from six batches (n=4) with a Tescan Vega3 with Tescan Essence™ software. Sputter coating was performed with 3 nm depth of Gold/Palladium (60:40, Quorum Q105T ES).

3.2.3.2 Diameter

FIJI ImageJ was used to analyse fibre diameter. The scale was set, and fibres were measured manually, using the line tool. A total of 500 fibres per batch were measured to determine both the mean diameter and standard deviation.

3.2.3.3 Orientation

FIJI ImageJ was used to determine the distribution of fibre orientation. Lines were drawn over the fibres using the line tool and angle measurements were processed in Graphpad prism (version 7) by performing a frequency distribution analysis. A minimum of 50 measurements were taken per scaffold and each measurement was repeated for n=4 scaffolds per batch to confirm degree of anisotropy.

3.2.3.4 Pore Size / Interfibre Spacing

FIJI ImageJ was used to threshold n=12 images per batch (giving approximately 8035 data points per batch). Particles were analysed with 0.1-Infinity μm^2 area as the threshold for detection. To calculate the diameter of the pores/interfibre spacing, Equation 3-1 was used.

Equation 3-1 The equation used to calculate the pore diameter (Ø)/interfibre spacing from area information outputs given by FIJI ImageJ.

$$\emptyset = \left(\sqrt{\frac{Area}{\pi}} \right) x\ 2$$

3.2.4 Scaffold Topographical Properties

Scaffold depth was characterised by use of white light interferometry (ContourGT, Veeco, Bruker). A 3% threshold was applied for imaging, with a 50 x lens. For wider scope fibre imaging a 0.55 x zoom was applied, for closer, more detailed images, a 2 x zoom was used. Vision64 software was used to analyse the images. Thickness data was acquired via the maximum height function (Sz) where height between highest peak and lowest pit were measured. Surface roughness data was collected using the arithmetical mean height (Sa) function. This function expresses the height difference of each point compared to the arithmetical mean of the surface as an absolute value (as illustrated in Figure 3-2). Four scaffolds were measured per batch to give a total of 12 measurements per batch.

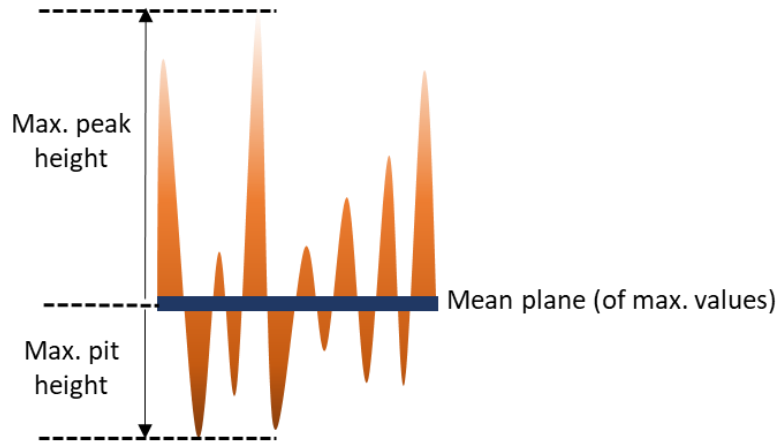

Figure 3-2 A depiction of how the scaffold total thickness (sum of max. peak height and max. pit height) and surface roughness (arithmetical mean of max. values) are calculated by the software. Based on, and adapted from illustration by Keyence[346].

3.2.5 Mechanical Properties of the Aligned PCL Fibres

In order to calculate mechanical properties, such as the Young's modulus and ultimate tensile strength (UTS) of the electrospun scaffold, the scaffold dimensions had to be determined. Scaffolds (n=6) were secured into a paper mould where the window of fibre tested was approximately 25 mm x 5 mm in dimension. The thickness of the scaffold was measured by use of a digital thickness gauge (0-12.7x30mm, 0.001mm, Digital Micrometers Ltd.). Scaffolds were then tested on an Instron Tensile testing system 3344 (Bluehill Universal software) at a strain rate of 5 mm min^{-1} with a 10 N load cell. In order to determine batch variability, six different batches were tested (n=6 per batch).

For ultimate tensile strength, highest stress value was taken before failure. The elastic strain and stress are the final values at which the material is still undergoing elastic deformation. The Young's modulus was calculated using the elastic linear region, with the toe region being removed.

3.2.6 Gravimetric Analysis for % Relative Porosity of Scaffolds

To calculate the % relative porosity of the electrospun PCL scaffolds, Equation 3-2 was used (published by Kim *et al.* 2014)[347].

Equation 3-2 The equation used to determine % relative porosity (ϕ) using weight measurements of the scaffolds. The symbol ϕ is used to describe relative porosity.

$$\phi = \left(\frac{1 - M}{\rho V}\right) x\ 100$$

Where **M** is the mass of the produced scaffold, **ρ** is the relative density of PCL, reported as 1.135 g cm^{-3}[347] and **V** is the calculated volume of the scaffold (*length x width x depth*). Fibres were cut into 1 x 1 cm squares for measuring. Ten batches were measured with an n=6 per batch.

3.2.7 Wettability of Aligned PCL Fibres

Contact angle measurements were performed on 9 different batches of PCL scaffolds (n=3 per batch). This procedure was performed with distilled water at room temperature (20ºC), using a Krüss DSA100 Drop Shape Analysis System goniometer (1.50 µl drop, 399 µl/min rate). Measurements were analysed using Drop Shape Analysis software (static sessile drop type, circle method). Three measurements were taken per sample (3 samples/condition). Imaging parameters were kept consistent throughout the study.

3.2.8 FTIR for Determining the Presence of Chlorine

Samples were prepared as above (section 3.2.2) and were allowed to dry for a period of one hour to prevent spectral saturation with O-H peak due to water. FTIR spectrophotometer Omic SmartOrbit software was used. For these samples, a diamond source (30,000 – 200 cm-1) was selected and background was read every 30 mins during experimentation. The instrument itself collected an average of 32 readings per analysis (total of 192 readings per condition).

3.2.9 Treatment methods for Improving the Function of PCL Fibres

For this experiment, popular treatment methods (Sodium hydroxide soaking and media conditioning) were compared against air plasma treatment and were subjected to cell viability assessment for their cellular compatibility.

Sodium hydroxide ($NaOH_{(aq)}$) was sterile filtered (0.22 µm filter; MillexGP PES membrane, SLGP033RS, Fisher Scientific UK) used at a 1 M concentration, with scaffolds submerged in 2 ml for 30 mins, before being removed and rinsed away with 1 ml deionised sterile $H_2O_{(l)}$ ($dH_2O_{(l)}$) 5 times to ensure the removal of any potentially toxic reagents[348, 349].

Media conditioning was performed using high glucose DMEM (10% FBS, 1% antibiotic/antimycotic). Scaffolds were soaked overnight in 2 ml media at 37ºC / 5% $CO_{2(g)}$ / 95% humidity[350, 351].

Plasma treatment was performed using an RF glow discharge air plasma treatment instrument at 20 W for 1 min (detailed further in section 3.2.10.2).

All scaffolds were sterilised with procedures detailed in section 3.2.10.1 and 3.2.10.3. Post treatment, they were dried for 1 hour before further analysis/cell culture.

3.2.10 Sterilisation and Treatment of Scaffolds

3.2.10.1 Ethanol Sterilisation of Scaffolds

Scaffolds were sterilised by submergence in 70% ethanol (1 ml, 1 hr). Ethanol was then removed, and scaffolds were left to dry (1 hr, room temperature).

3.2.10.2 Plasma Treatment

Plasma treatment was performed using a radio frequency (RF) generator (RFG 100-13, 13.56 MHz, Coaxial Power Ltd. UK; see Figure 3-3 for schematics) to generate glow discharge (low vacuum, air) plasma at 20 W. The instrument was used at a pressure between $1.5x10^{-1}$

and $9x10^{-2}$ mBar, generated by using a RV5 two-stage rotary vane vacuum pump (A65301906, Edwards UK). Scaffolds were exposed for 1 min (room temperature).

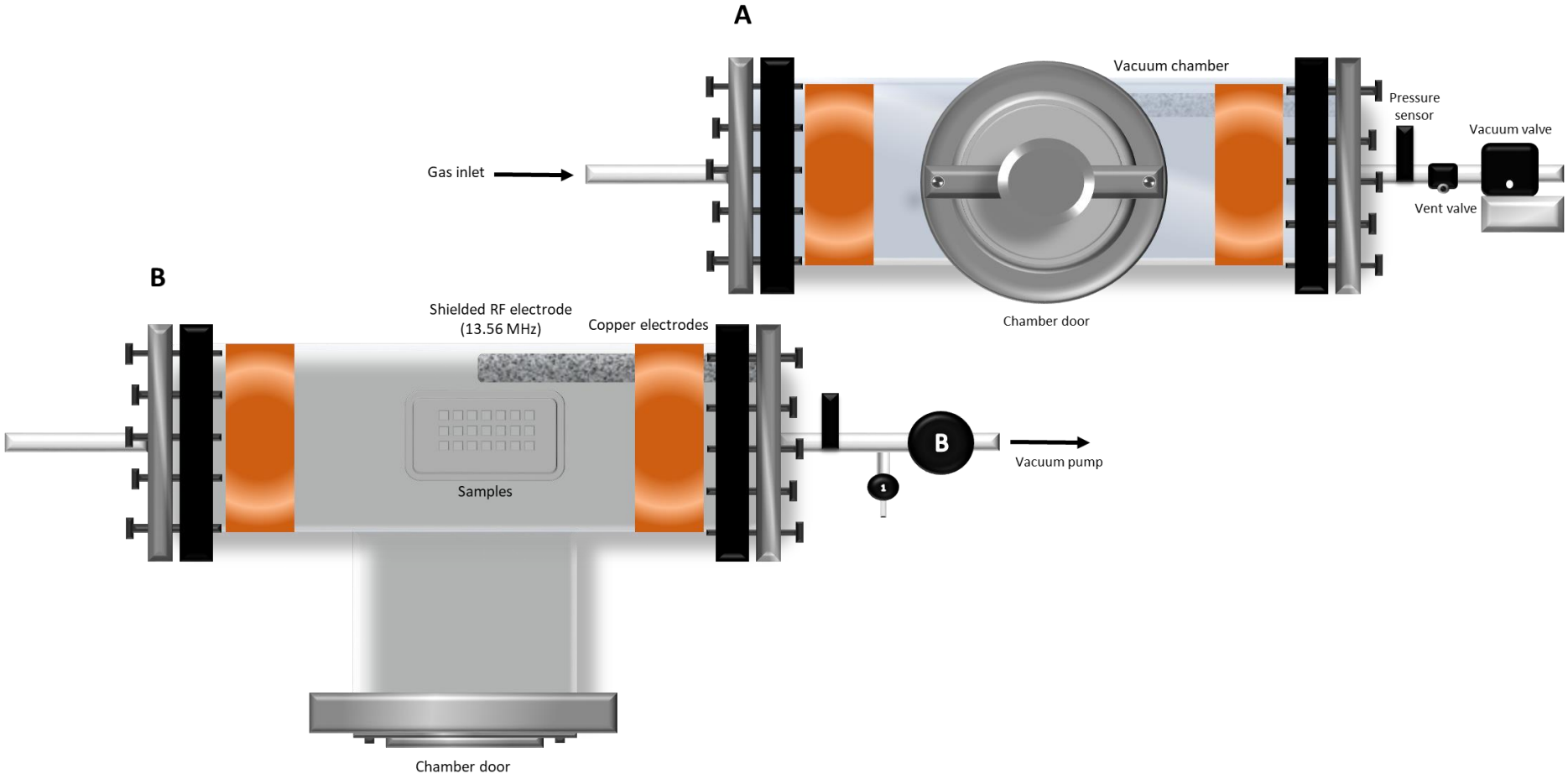

Figure 3-3 Plasma instrument schematics. Drawings show the RF glow discharge air plasma instrument both from the front (**A**) and above (**B**). For this work, only air plasma was used, so the gas inlet was not connected to any external gaseous source (i.e. $O_{2(g)}$ or $NH_{4(g)}$). This instrument was originally assembled by Dr K Meade (University of Manchester).

3.2.10.3 Ultra Violet Light Sterilisation

Ultra Violet (UV) light sterilisation was performed using the UV function in the Thermo Fisher MSC-ADVANTAGE Microbiological Safety Cabinets (1hr, room temperature).

3.2.10.4 Fibrillin-1 Fragment Coating

Coating with fibrillin-1 was performed using a 0.2 or 20 µg ml^{-1} solution in PBS (50 µl $sample^{-1}$) of 3 different fibrillin-1 fragments (recombinant human fibrillin-1 fragments PF8, PF9 and PF17.1, generously donated by Dr Stuart A Cain, School of Biological Sciences, University of Manchester, UK). The coated scaffold was then incubated (4°C, overnight) to facilitate adsorption.

3.2.11 Effectiveness of Plasma Treatment

3.2.11.1 Effect of Plasma Treatment on Wettability

This procedure was performed as above in section 3.2.7.

3.2.11.2 SEM Imaging

SEM images were taken to further confirm plasma treatment of the samples. Images were taken on a Hitachi TM4000 bench-top SEM using 5 kV voltage. Images were taken at an n=3 (1 image per magnification) for two scaffolds per condition.

3.2.11.3 X-Ray Photoelectron Spectroscopy

XPS measurements were performed by Dr Andrew Thomas and Dr Marek Nikiel (School of Natural Sciences, Faculty of Science and Engineering, University of Manchester). Scaffolds were fabricated and mounted on silica wafers, which had previously been cleaned using sonication in acetone/isopropanol. They were sterilised as above (sections 3.2.10.1 and 3.2.10.3) before analysis. Scaffolds were then mounted on silica wafers and placed in the high vacuum analysis chamber under approximately 2.09 x 10^{-9} mBar pressure for analysis, using the parameters listed in Table 3-2 and Table 3-3.

Scaffolds (n=3) were used to collect quantitative data regarding the % relative atomic concentration at the material surface. CASAXPS v2.3 19PR1.0 (with Kratos library) software was used to analyse atomic concentrations within the survey and carbon spectra.

Table 3-2 Parameters used for producing the x-ray energy.

Focus Voltage	**15.0 kV**

Anode	Al K α (1486.71 eV)
Power	120 W

Table 3-3 Parameters used for creating the elemental spectra.

Spectrum Range	**1200 to -5 eV**
Step	0.5 eV
Delay	0.2 s
EPass	Survey: 70 Elemental: 20

3.2.11.4 Longevity of Plasma Treatment

To test the longevity of plasma treatment effect on the scaffolds, samples were prepared as in sections 3.2.10.1, 3.2.10.2 and 3.2.10.3. Samples (n=3) were measured over 48 hrs and 7 days and data was collated. The samples were stored dry at 4°C between measurements.

This procedure was performed as in section 3.2.7.

3.2.12 Testing for Variation of Plasma Treatment with by Contact Angle

To perform variation tests of plasma treatment, 12 samples were made from a single batch of electrospun fibres to limit any variability. Three batches of 4 samples were independently treated with air plasma and the surface wettability and protein adsorption capability were assessed. Sample batches were plasma treated separately and stored overnight before testing wettability to mimic conditions before cell seeding. Measurements were taken with a Krüss DSA100 Drop Shape Analysis System goniometer (1.50 µl drop, 399 µl/min rate). Measurements were analysed using Drop Shape Analysis software (static sessile drop type, circle method) with imaging parameters remaining consistent throughout the experiment. Three measurements per sample were taken, with a total of 12 measurements per batch.

To further analyse plasma variation, flat PCL films were cast. A 7% solution of PCL in dichloromethane (DCM; 4 ml) was stirred in a glass vial for 45 mins, before being put aside to rest for a further 10 mins. The resulting solution was poured gently (to avoid bubbles forming) into a 15 cm diameter glass dish, covered and left to dry overnight. The film was collected the next day and tested both before and after plasma treatment (n=3 batches, n=8 samples, 2 measurements/sample).

3.2.13 Fibrillin-1 Fragment Functionalisation

3.2.13.1 Indirect ELISAs for Protein Adsorption

For determining differences in adsorption to the various material substrates, the majority of the protocol as detailed below was replicated from a publication by Hajian *et al.* (2014)[315] and antibody concentrations were optimised. All steps in this procedure were performed at room temperature unless otherwise stated.

Firstly, 1.5 µg of fibrillin-1 fragment (amount optimised for sufficient signal) was adsorbed to the scaffolds overnight (protocol detailed in section 3.2.10.4) following sterilisation (as in section 3.2.10). Excess protein solution was removed from the materials before beginning the experiment. Samples were blocked with 200µl of 3% BSA (1 hr). Mouse anti-histidine primary (200 µl, 1:500 PF8, PF9; 1:1000 PF17.1) in 3% BSA was added for a further 1 hr. Post PBS washing (thrice), 200 µl goat anti-mouse peroxidase (200 µl, 1:1000 PF8, PF9; 1:2000 PF17.1) in 3% BSA was added (1 hr) before additional washing. ABTS solution (120 µl) was incubated with samples (45 mins, protected from light). Sample reactions were analysed from 100 µl aliquots (after transferring to a clean, clear 96 well plate) using a Labsystems Multiskan Ascent plate reader at an absorbance maximum of 412 nm.

Standard curves shown in Figure 3-4 were produced on TCP to evidence the linearity of detected absorbance and fragment concentration.

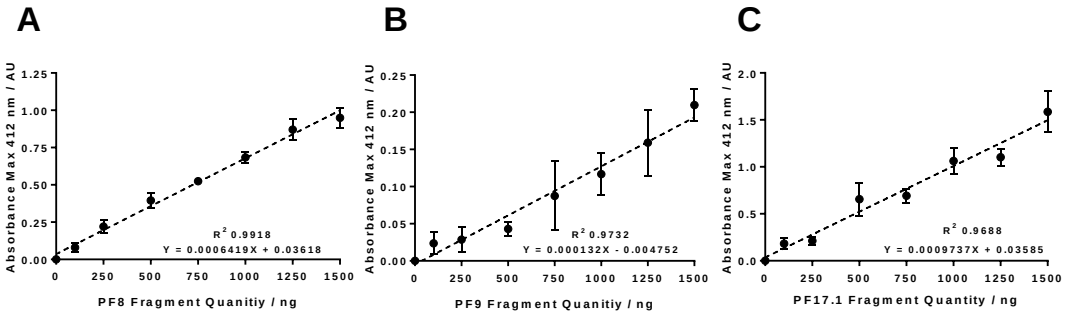

Figure 3-4 Standard curves on TCP were produced to demonstrate the linearity of the relative adsorption ELISAs for fibrillin-1 fragments PF8 (**A**), PF9 (**B**) and PF17.1 (**C**).

3.2.13.2 Immunohistochemistry for Fibrillin-1 Fragment Visualisation

During the isolation and purification of proteins that are to be used in biotechnology, often tagging with specific sequences/amino acids (GST, His etc.) are performed. This enables the detection and/or quantification of those proteins in an assay or by immunohistochemical staining.

Sterilisation and coating steps were performed as in sections 3.2.10 and 3.2.10.4 respectively, with 250 ng of fibrillin-1 fragments, to enable sufficient signal. Scaffolds and controls were fixed with 10% NBF and washed with PBS. Quenching with 0.2M glycine was performed (5 mins) before washing twice. Histidine-tagged fibrillin-1 fragments (PF8, PF9 and PF17.1; 250 ng substrate^{-1}) were detected by use of a mouse anti-histidine tag primary antibody (200 µl, 1:400 in 2% FSG) post blocking with 2% fish skin gelatin. Scaffolds were then incubated overnight (4ºC) before being washed thrice with PBS. Secondary antibody (goat anti-mouse 568 nm) was used to stain the scaffolds for the visualisation of fibrillin-1 (200 µl, 1:800 in 2% FSG, 2 hrs, room temperature). Removal of the secondary antibody was followed with thrice washing in PBS and application of ProLong™ Diamond Antifade Mountant. Substrates were imaged on a Leica DM2500 LED microscope (Leica DFC3000 G camera), using Leica LAS software.

3.2.14 Cell Culture and Maintenance

3.2.14.1 Cell Maintenance

Canine cruciate ligament cells (cACLs) were maintained in T75 flasks with 15 ml DMEM high glucose media (Dulbecco's Modified Eagle's Medium - high glucose, 4500 mg L^{-1} glucose, 584 mg L^{-1} L-glutamine, 3700 mg L^{-1} sodium bicarbonate), supplemented with 10% fetal bovine serum (FBS) and 1% Antibiotic-Antimycotic (A/A). Media was fully changed every 2-3 days.

For all the experiments in this chapter, primary canine cruciate ligamentocytes were used. A total of 10 donors (at passage 1) were acquired from the Comerford Group (Institute of Ageing and Chronic Illness) at the University of Liverpool. The cells were from donors with identical inclusion criteria and had previously been characterised[69]. Cell isolation was performed by mincing the cruciate ligaments, and digesting with 0.1% collagenase type II, overnight, at 37°C. Cells were then strained and resuspended in complete DMEM (10% FBS and 1% A/A - 100 U ml^{-1} penicillin, 100 µg ml^{-1} streptomycin and 2 µg ml^{-1} amphotericin

B) before seeded at a density of $1.2x10^3$ cells cm^{-2} onto fibronectin coated (20 µg ml^{-1}) plates[69].

In previous work performed on these cells, donor to donor variability tests were performed. The findings detailed that the inter-donor variability in the trend of response was small, and that donors could be pooled for further experiments[352]. As per the protocol recommended by Liverpool University, cells were passaged at 90-95% confluence in order to maintain the fibroblastic phenotype.

For long term storage, cells were resuspended in a 90% FBS and 10% dimethyl sulfoxide (DMSO) solution and frozen to -80ºC at a rate of -1ºC min^{-1} in an isopropanol container (Nalgene UK). Cells were retained in -80ºC conditions until further use.

3.2.14.2 Cell Seeding for Experimentation

cACLs were detached from flasks using trypsin-EDTA (2 ml, 3 mins, 37°C, 5% CO_2, 95% humidity) and centrifuged at 300 g for 4 mins. Cells were resuspended in fresh hgDMEM for seeding. Cell suspension was prepared to a concentration of 6×10^5 cells ml^{-1} and were subsequently seeded at a density of 6×10^4 cells per scaffold, in a 100 µl media droplet. Cells were retained in the droplet during incubation (37°C, 5% $CO_{2(g)}$, 95% humidity) for 2 hrs, before flooding of the wells with a further 2 ml of media and culturing to specified time points. cACLs were used between passages 3-5 for all experiments.

cACL data was pooled for analysis due to previous donor variability experiments showing only minor variations in the overall trend of the responses (Appendix 4)[352].

For all viability-related experiments, borosilicate glass coverslips were used as positive material controls, justified by their use as such in the literature[353, 354].

3.2.14.3 LIVE/DEAD Viability Assay

LIVE/DEAD assay contains two labelling dyes: calecin AM, which is metabolised to calecin in live, metabolically active cells and is green fluorescent, and ethidium homodimer-1, a red fluorescent labelling dye that binds to genetic material, by movement into the cell through compromised cell membranes. This enables the observation and detection of live and dead cells within a sample[355].

LIVE/DEAD solution was produced by the dilution of ethidium homodimer-1 1:500 (λ_{exc}517 nm, λ_{em}617 nm) and calecin-AM 1:2000 (λ_{exc}494 nm, λ_{em}517 nm) with phosphate buffered

saline (PBS). cACL-seeded scaffolds were removed from incubation, washed with PBS and 200 µl of LIVE/DEAD reagent was added before incubation (20 mins, 37°C, 5% CO_2, 95% humidity). Seeded scaffolds were rewashed with PBS and imaged on a Nikon Eclipse 50i microscope with Nikon digital camera DXM1200F using Lucia G/F software.

3.2.14.4 Alamarblue Metabolic Activity Assay

Resazurin is a non-toxic chemical, which can be reduced to resorufin by cell metabolic NADH pathways (shown in Figure 3-5). Resazurin itself is blue in colour and non-fluorescent, however its reduction product resorufin, it highly red fluorescent and is linearly related to cell metabolic output[356].

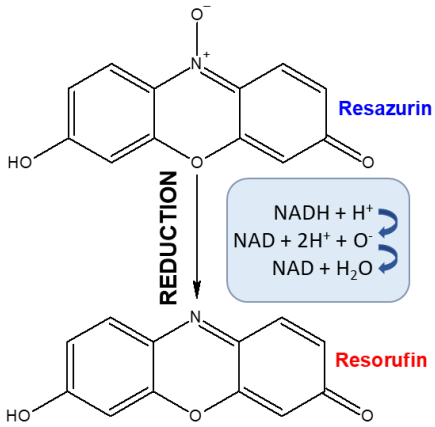

Figure 3-5 Chemical formula and reduction reaction non-fluorescent blue resazurin into highly red fluorescent resorufin. Diagram adapted from Matsuura *et al.* (2019)[356].

Resazurin salt solution was prepared using a 1:80,000 dilution (w/v) of resazurin powder in sterile PBS and sterile filtered (0.5 mM stock solution). Working solution was prepared using a 1:10 dilution of resazurin salt solution in fully supplemented media. Working solution (1ml) was added to each well and was incubated in darkness for 2 hrs (37ºC, 5% CO_2, 95% humidity). Solution was removed (triplicate per sample) into a clear 96 well plate. Samples were then read on a FLUOstar OPTIMA fluorescent plate reader at λ_{exc}544 nm and λ_{em}590 nm. Samples were washed with sterile PBS and replenished with media before returning to incubation.

3.2.15 Statistical Analysis

Data was checked for Gaussian distribution, using the D'Agustino-Pearson omnibus normality test. If this assumption was satisfied, one way ANOVA (with Tukey HSD Post-

Hoc test) for single time points, or two way ANOVA (with Sidak Method or Tukey post-hoc test) for multiple time points were selected. If normality was not satisfied, corresponding Kruskal Wallis H Test was applied. Giesser-Greenhouse corrections were applied to all tests to counter any heterogeneity of variances. Minimum alpha levels of $p<0.05$ were accepted as significant. Value of n denotes number of sample repeats per experiment and each batch number is taken as a single experimental repeat. Each experimental data set is based on a minimum of 2 experimental repeats, unless otherwise stated.

3.3 Results

3.3.1 Characterisation of Electrospun Fibre Dimensions

To characterise fibre diameters and overall scaffold orientation, SEM imaging was performed. These measurements were taken to elucidate on the more intricate characteristics of the fibre scaffolds.

3.3.1.1 Fibre Diameter

Fibre diameter was calculated by measuring 500 individual fibres per batch. Calculated batch diameters all displayed in Figure 3-6. Measurements from 3000 fibres showed a total mean average of 2.127 ± 0.6597 µm, with the range between means exceeding no more than 0.558 µm; from 1.977 ± 0.7802 µm to 2.535 ± 0.4572 µm. Such large variation in fibre diameter may be due to multiple conditions, such as inconsistent humidity, small changes in temperature and minor fluctuations mandrel rotation speed.

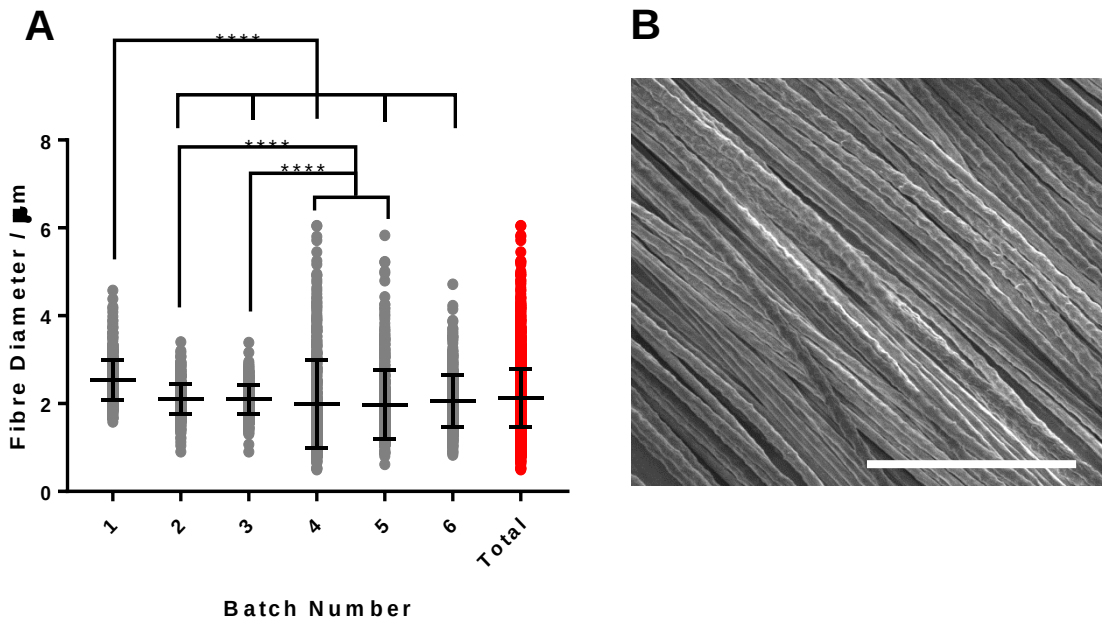

Figure 3-6 (**A**) Fibre diameter and subsequent standard deviation was calculated from 500 fibres (over 8 images) per batch (n=4). Individual data points are shown with the means and standard deviations. Kruskal Wallis H test was performed with rank comparison tests. ****p<0.0001. (**B**) SEM micrograph showing fibre morphology; though heterogeneous on the micron scale, did appear to vary slightly on the sub-micron scale with varying degrees of individual fibre roughness. White arrow indicates fibre direction and scale bar denotes 50 µm. SEM micrograph taken at x2780 mag.

3.3.1.2 Fibre Orientation

To produce aligned fibrous scaffolds, from which data can be pooled following cell culture, it is imperative to ascertain whether there are any inter-batch variations that may disrupt cell response. High degrees of orientation in ligament-emulating scaffolds are essential to deliver the correct topographical cues to the ligament cells.

Fibre orientation was determined using parameters detailed in section 3.2.3.3. Each of the six images displayed are representative of their individual batches and all show high levels of fibre anisotropy. The electrospinning method provided (developed by Dr Douglas Ramos Marques), produced fibres with high levels of alignment, capable of emulating the topography of the collagen fibres present in the native ACL. Narrower distributions on the graphs represent smaller variation in fibre orientation, as illustrated in Figure 3-7.

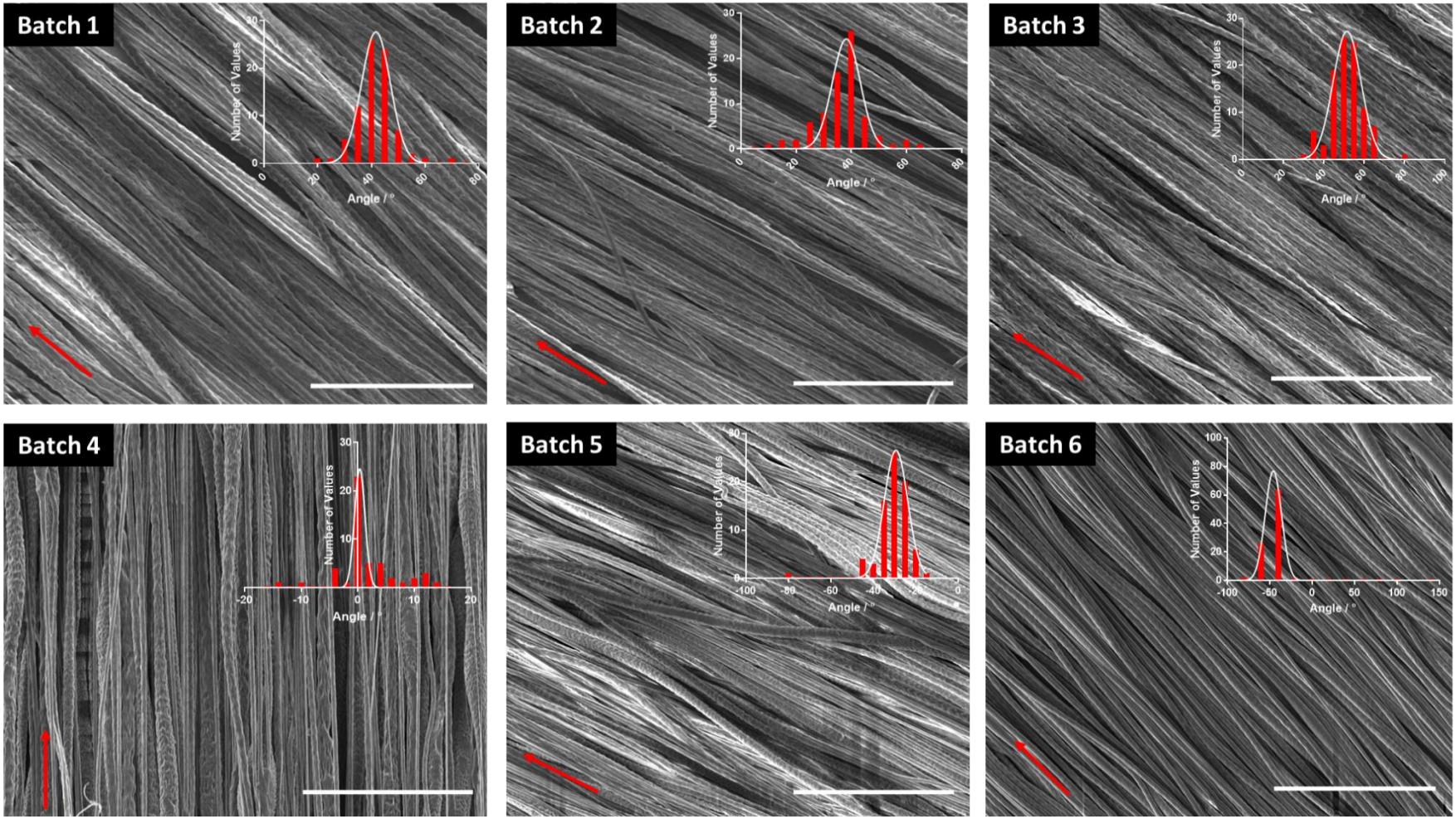

Figure 3-7 SEM micrographs above show the representative distribution of alignment of the electrospun fibres (n=4) from 6 independent batches. Increased and narrow peaks on the graph show high levels of anisotropy in the fibre orientation. Scale bar represents 50 µm and red arrows show the direction of alignment. Images taken at x2780 mag.

3.3.1.3 Pore Size

Pore sizes of the scaffolds were shown to be relatively small, with all batches producing median pore sizes under 1 µm in diameter. All batch pore sizes showed logarithmic distribution, and similar general trends, with large variations in pore size distribution (diameters extending up to 69.5 µm for batch 1, 39.2 µm for batch 2, 40.8 µm for batch 3, 29.8 µm for batch 4, 64.9 µm for batch 5 and 50.3 µm for batch 6), as shown in Figure 3-8. However, the vast majority of these measurements fell under 15 µm, with only 0.82, 0.51, 0.32, 0.20, 0.27 and 0.29% of diameters being recorded as above 15 µm in batches 1, 2, 3, 4, 5 and 6 respectively. Total median diameter of pores across all batches was determined to be 0.67 µm. This result does not appear to agree with previous results of electrospun PCL fibrous scaffolds reported in the literature, which all display larger diameters[357, 358].

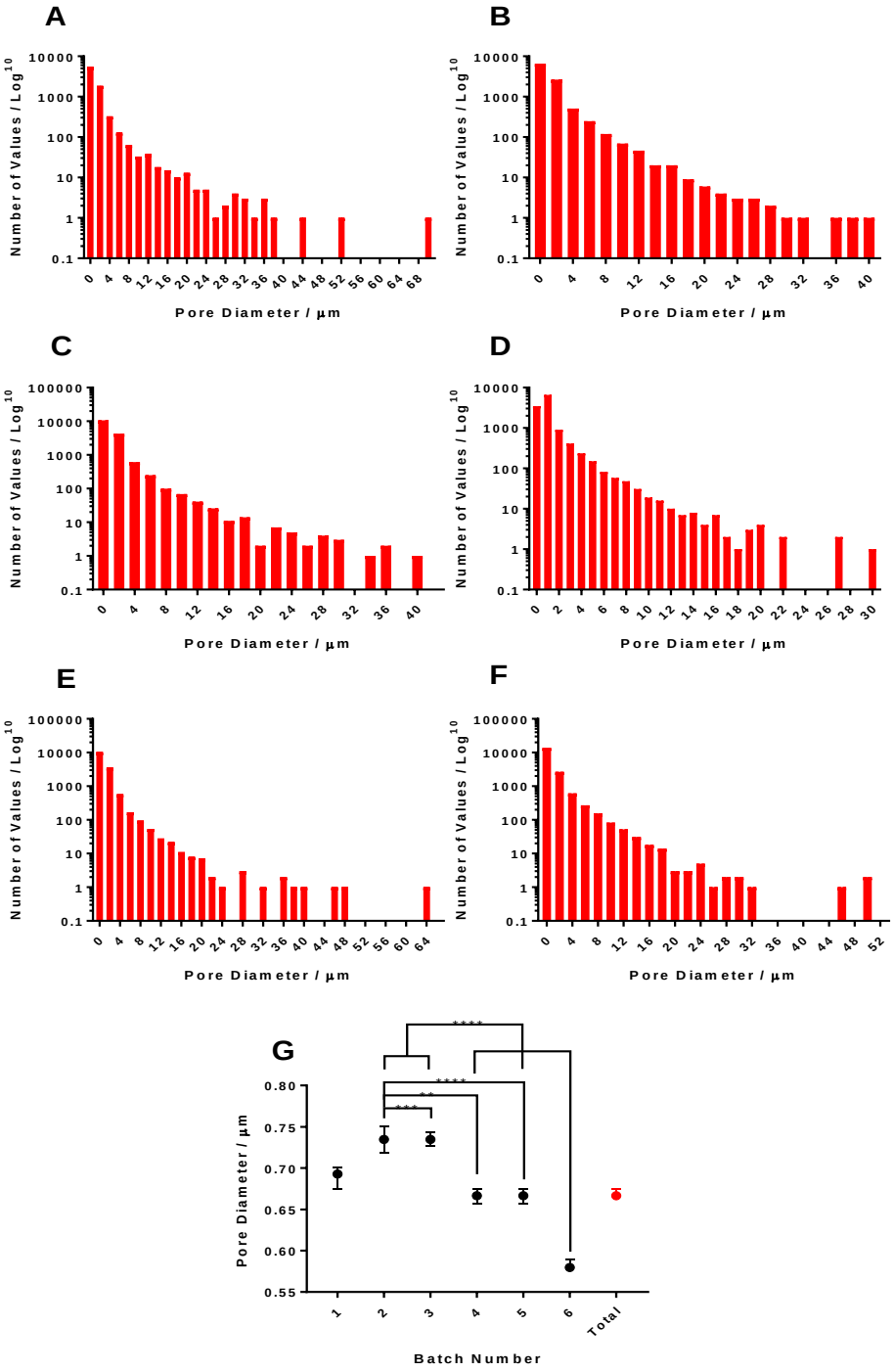

Figure 3-8 Distributions of pore diameter/interfibre spacing between batches (**A**-1, **B**-2, **C**-3, **D**-4, **E**-5, **F**-6) as measured via ImageJ thresholding of SEM images (n=4) Spaces on the graphs (**A** – **F**) show diameters where no data was recorded. **G** shows the average and ranges of pore diameter/interfibre spacing for each batch, where the symbols represent the median values and error bars demonstrate the 95% confidence interval. A Kruskal Wallis H test was performed with rank comparisons for non-parametric data. **p<0.01, ***p<0.001, ****p<0.0001.

3.3.2 Scaffold Topographical Properties

White light interferometry determined scaffolds to have micro-topographical features at the substrate surface, with the average total surface roughness of the scaffold, across all batches determined to be 5.24 ± 1.82 µm (with a range of 4.06 µm between batch measurements), as shown in Figure 3-9B. Though relatively similar, there were significant differences between batches, with batches 6, 7 and 8 displaying a larger degree of surface roughness than the first 5 batches measured ($p<0.0001$, $p<0.05$ and $p<0.05$ respectively). This imaging analysis enables visualisation of the surface topography as the cell would interpret it and will display undulations in the fibre position. Thickness measurements, depicted in Figure 3-9A, were taken from the images and averages were calculated. Overall thickness was recorded as 43.3 ± 8.22 µm, with a range between batch means of 11.1 µm. However, there was very little variation between batches in this instance, with only batches 2 and 8 showing significantly different thicknesses ($p<0.05$).

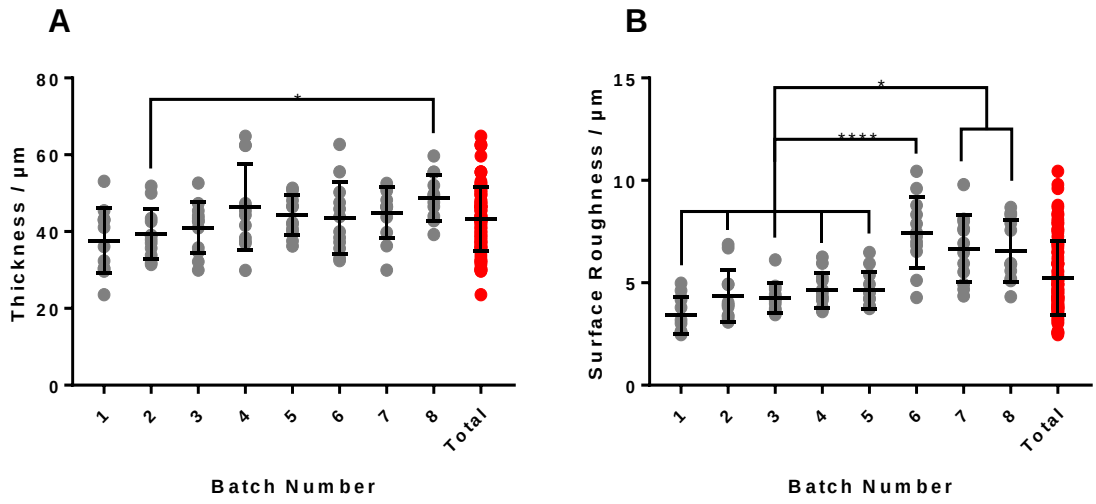

Figure 3-9 Scaffold thickness (**A**) and surface roughness (**B**) over eight individual batches (n=4, 3 measurements per batch). Measurements were taken using white light interferometry and calculated using Vision64 software. Mid-lines show means and error bars, standard deviations. Both datasets were analysed using one way ANOVAs, with Tukey HSD post hoc tests. * $p<0.05$, ** $p<0.01$, **** $p<0.0001$.

Though this technique is a popular method of topographical visualisation, the measurements referring to thickness of the scaffold may be somewhat inaccurate as it may not be able to visualise all the fibres. As seen in Figure 3-10D, there are black spaces between some fibres, where fibres were not detected, or fragmented images of some fibres indicate only partial detection, both of which may have had an effect on the accuracy of the overall

measurements. However, as observed in Figure 3-10, fibres appear highly anisotropically aligned, with mostly uniform, and somewhat compact fibre morphologies. Red colouring of fibres shows those closer to the top of the scaffold, with darker blue indicating those at the bottom.

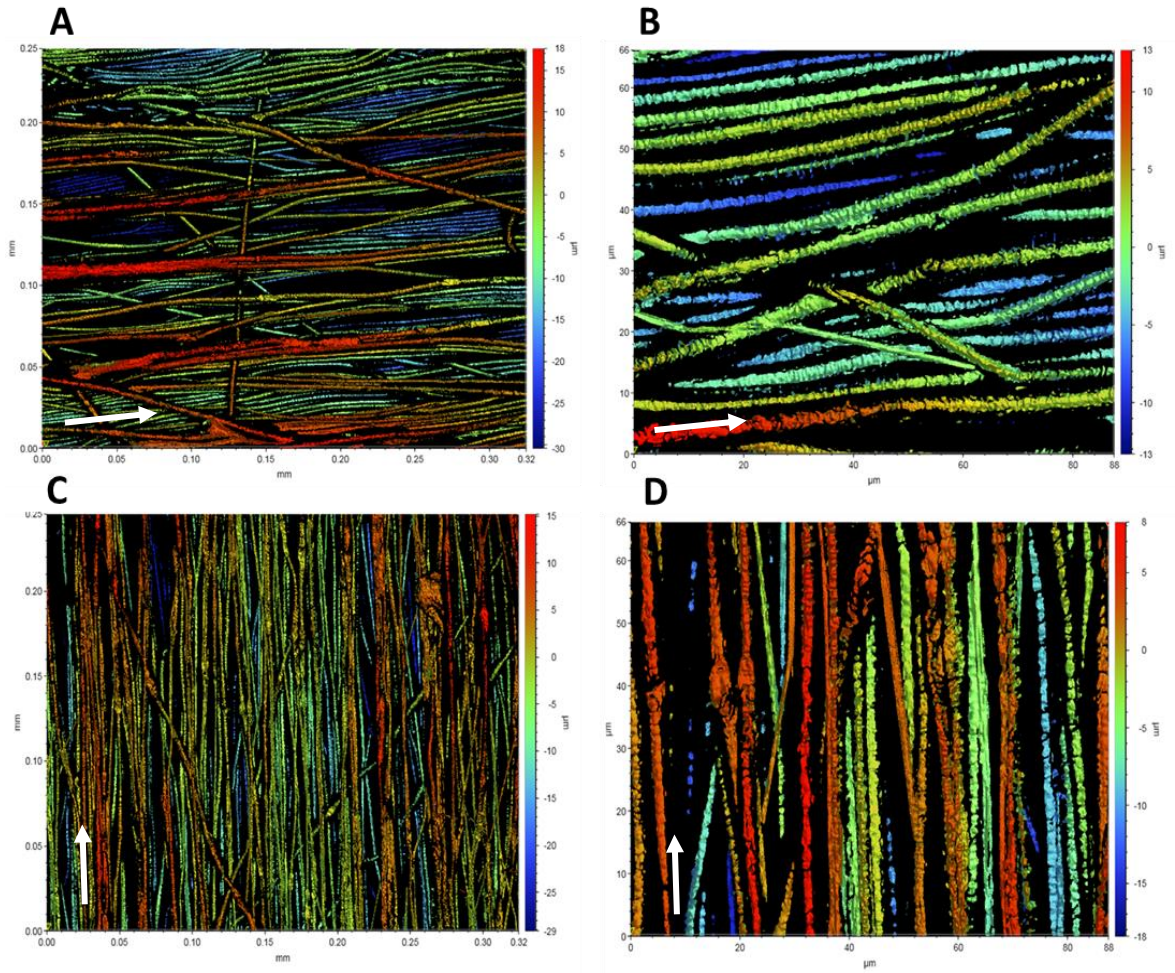

Figure 3-10 White light interferometry images were taken to determine scaffold topography. Images **A** and **C** were taken at 0.55 x zoom, whilst **B** and **D** were taken at 2 x zoom to enable determination of fibre topography from a much closer perspective. Red colouring indicates fibres closer to the top of the construct and dark blue for those at the bottom. White arrows indicate direction of the fibres.

3.3.3 Mechanical Properties of the Aligned PCL Fibres

To assess the mechanical properties of the electrospun PCL aligned fibres, fibres were subject to tensile testing at a strain rate of 5 mm/min. Fibres showed an average ultimate tensile strength of 5.23 ± 1.65 MPa with a range of 4.25 MPa between batches, due to the unusually high values from batch 5. Excluding batch 5 data, range between batches reduces

by approximately 50% to 2.39 MPa, whilst the mean remains fairly similar at 4.78 ± 1.41 MPa. Interestingly, fibres could withstand a maximum strain of 6.20 ± 1.43% at 2.81 ± 0.685 MPa when strained at 5 mm/min and did not appear to have much variation between batches. Young's modulus showed no significant variation between batches, resulting in an overall batch total of 54.9 ± 25.5 MPa. Strain at failure however, varied significantly between more than one batch, with batches 2 and 5 showing significantly higher strain % at failure than other batches (minimum $p<0.05$). Batch 5 appeared to have unusually high levels of compliance compared with other batches, straining in plastic deformation for almost 3 times longer than other batches (Figure 3-12). For mechanical properties testing, six individual batches were tested (n=6) to determine batch to batch variability. It appears that though the ultimate tensile strength of the material (Figure 3-11F) is similar between batches, there are some differences in mechanical properties when the compliance of the material is quantified. The electrospun PCL fibres appear to be highly compliant, in some cases, straining up to 8 times their original length before failure occurs (Figure 3-11A). Though compliance varies significantly between batches, this may again be due to inconsistent atmospheric conditions whilst electrospinning the fibres, but did not appear to be related to fibre thickness.

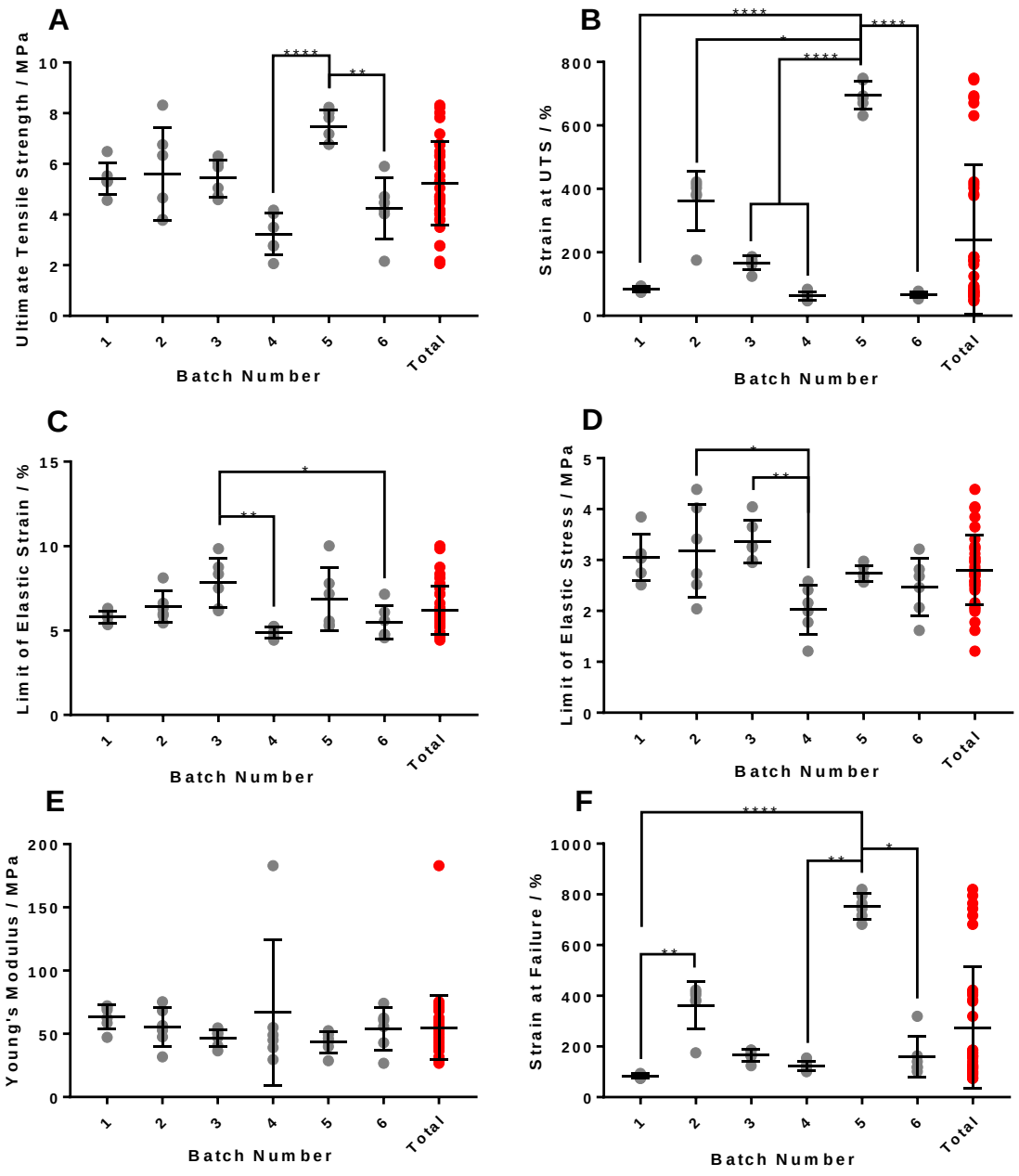

Figure 3-11 Ultimate tensile strength (**A**), strain at ultimate tensile strength (**B**), strain at elastic deformation limit (**C**), maximum amount of strain performed before elastic deformation limit was overcome (**D**), Young's modulus (**E**) and strain at failure (**F**) are depicted above for each of the six batches tested (n=6). Data points for each samples, with means and standard deviations are displayed. All data sets, with exception of **F**, were

statistically analysed using one way ANOVAs with Tukey HSD post hocs. Data set **F** was analysed using Kruskal Wallis H test with compared ranking. * $p<0.05$, ** $p<0.01$, **** $p<0.0001$.

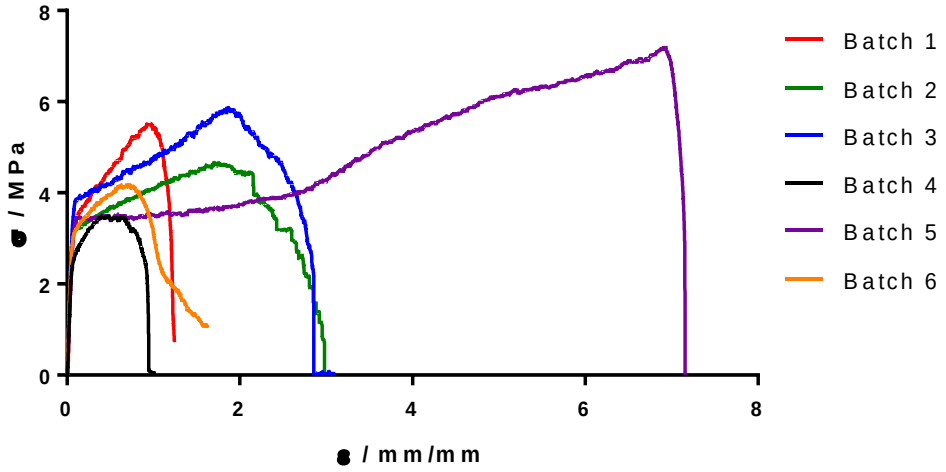

Figure 3-12 Example stress-strain curves from each of the 6 batches tested.

3.3.4 Gravimetrically Determined Porosity of Aligned Fibre Scaffolds

Relative porosity is determined by calculating the theoretical mass of a solid sample of PCL (at given sample dimensions) and then calculating the ratio of given weight of your sample versus the theoretical sample weight to determine what percentage of the sample is 'empty space'. As shown in Figure 3-13 all average porosities for every batch were between 60-85%, with the mean total determined to be 74%. This value falls in agreement with Semitela *et al.* (2020) who reported their PCL fibre scaffold porosity as approximately 71%[358], but lower than those seen elsewhere in the literature for aligned fibres. The variation of porosities observed between batches implies that within the scaffolds, approximately two thirds (and above) of the scaffold consisted of empty space. Though present, significant differences between scaffold porosities appeared not to be commonplace, with only batch 7 showing significantly higher relative porosity than batches 1, 2 and 3 ($p<0.05$). This data can be used to determine that the scaffolds produced are highly porous – suitable for cellular integration, where literature has suggested that a minimum of 50% porosity must be achieved to enable adequate cellular integration[252].

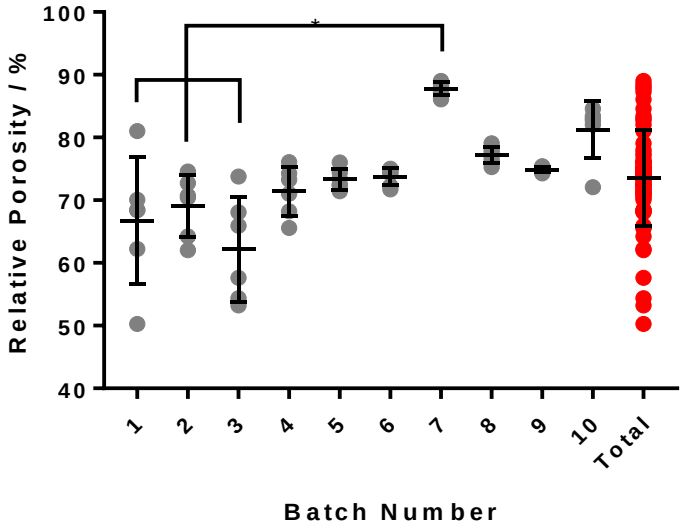

Figure 3-13 Variability of % relative porosity between ten individual batches (n=6). Kruskal Wallis H test was performed with comparative ranking. Error bars presented show standard deviation and mid line represents the mean values. * $p<0.05$.

3.3.5 Wettability of Aligned Fibres

Wettability of the fibres appeared rather consistent, with the averages of all batches falling within a 12° angle range, as shown in Figure 3-14. This variation could be explained by multiple reasons; the porosity of the scaffold or how thin the fibre mat was, causing the wettability to be affected by the glass coverslip that they were mounted upon. Due to the variation in age of the mounted scaffolds, there could be some residual chloroform still present on the fibres which may also have increased the wettability. However, all results appear to be lower than the average often reported in the literature, which often state contact angles of between 130-140°[359, 360]. This again may be due to the scaffold thickness and porosity, or indeed to the type of measurement method used. The film however, in agreement with the literature, appeared to be much more hydrophilic than the aligned fibres. This may have been due to surface roughness, causing the droplets to spread outwards.

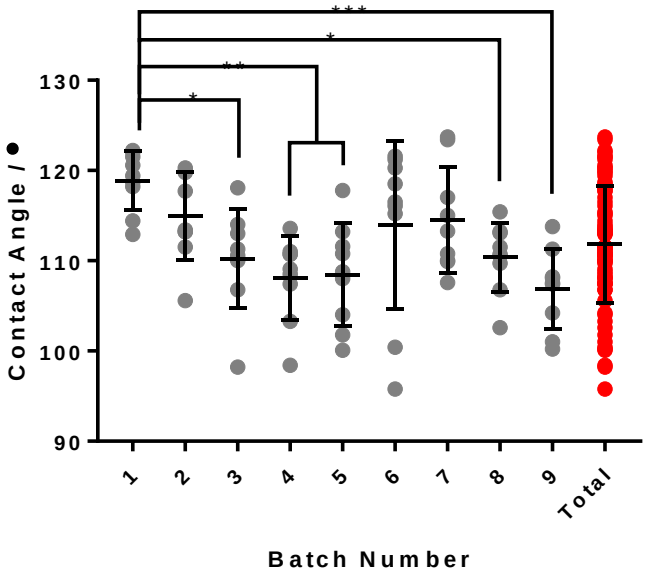

Figure 3-14 Batch to batch variation of the wettability of aligned PCL fibres. Fibres were spun and mounted on glass coverslips before measurements were taken (n=3, 3 measurements per sample). A one-way ANOVA with Tukey HSD post hoc tests were performed to determine statistical significances. Error bars shown represent standard deviation and mid line indicates the mean. *p<0.05, **p<0.01, ***p<0.001.

3.3.6 Verifying Lack of Chloroform Contamination in Electrospun Fibres

FTIR was used to determine whether chloroform contamination was present in the fibres. All characteristic peaks of PCL were displayed on the spectra (Figure 3-15B) and correlated with bonding types present in the PCL chemical structure, as shown in Figure 3-15A. The strong C-Cl peak between 550-800 cm^{-1} was not detected (purple dashed box on spectra, Figure 3-15B), implying good processibility of PCL for electrospinning, using chloroform as a solvent. Bonding behaviours characteristic of PCL were present and agreed with those reported in the literature by Can-Herrera *et al.* (2016)[361] and Gurlek *et al.* (2017)[214], such as: elongation of C=O (1720 cm^{-1}), asymmetric and symmetric stretching of CH_2 (2950 cm^{-1}) and saturated esters stretching C(=O)-O (denoted as C-O at 1160 cm^{-1}), which are labelled on the spectra in Figure 3-15B below. Other behaviours detected in the spectra were; asymmetric deformation of CH_2 (1470 cm^{-1}), asymmetric deformation of residual CH_3 (1360 cm^{-1}), C-O/C-C stretching in crystalline phase (1290 cm^{-1}), asymmetric C-O-C stretching (1240 cm^{-1}), O-C-C group (1100 cm^{-1}) and C-O/C-C stretching in amorphous phase (1040 cm^{-1}) [362].

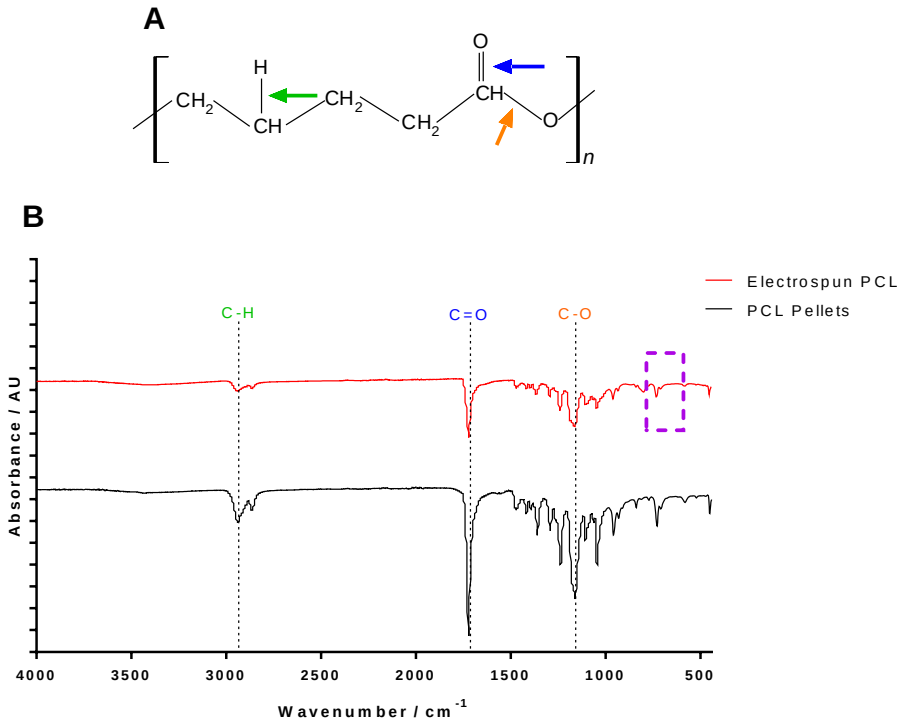

Figure 3-15 FTIR spectral analysis on PCL before and after the electrospinning process. The chemical formula of PCL is displayed above (**A**) with coloured arrows corresponding to bonding type highlighted on the spectra below (**B**). Purple dotted box indicates the position of a potential C-Cl bonding peak (n=3, 2 measurements/sample).

3.3.7 Selection of an Appropriate Treatment Method

3.3.7.1 Determining Effect of Treatment on Sample Wettability

Contact angle was performed to discern the success of each treatment type on reducing the hydrophobicity of PCL. The 'no treatment' condition was used as a negative control, whilst borosilicate glass coverslips were used as a positive, due to their well-documented ability to facilitate cell attachment and growth[363]. As displayed in Figure 3-16, both air plasma ($p<0.0001$) and media conditioning ($p<0.001$) treatments significantly reduced the contact angle of the PCL scaffolds, rendering them hydrophilic (contact angles <90°), with mean angles of 35.01° and 39.32° respectively, similar to that of the glass coverslips at 42.98°. However, soaking with sodium hydroxide did not appear to alter the wettability of the scaffolds as much, when compared with air plasma and media soaking, resulting in a contact angle of 98.67°, which indicates retained hydrophobicity.

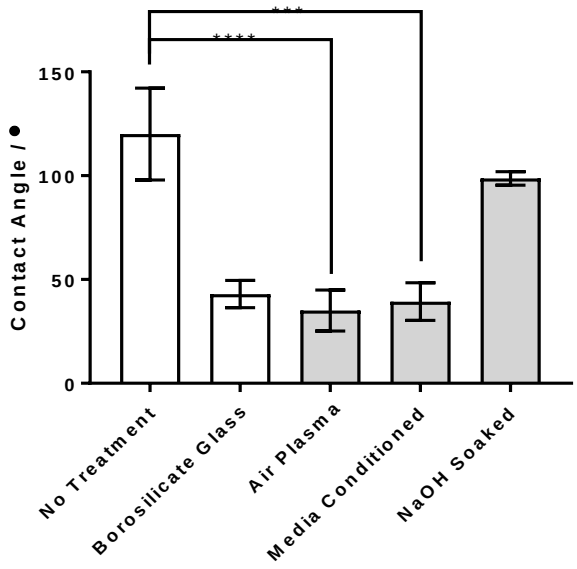

Figure 3-16 Changes in wettability due to different surface treatments of PCL. 'No treatment' was the sterilised PCL alone and here acted as a negative control, whilst the borosilicate glass samples were used as positive controls (n=3, 3 measurements/sample). Kruskal Wallis H test with rank comparisons were used to identify significant differences between groups, results based on 1 experiment. The bars display means and error bars show standard deviations. ***p<0.001, ****p<0.0001.

3.3.7.2 Protein Adsorption Ability of Sample Treatment Methods

Protein adsorption was required for treatment consideration due to having to adsorb fibrillin-1 fragments to the surface of the material. Here, fibronectin and one of the fibrillin-1 fragments (PF8) was used to perform a test to understand further the capacity of each treatment to facilitate protein binding. Figure 3-17 shows fibrillin-1 fragment PF8 adsorption, and shows that sodium hydroxide treatment was able to adsorb the most fibrillin-1 fragment. Throughout both experiments, media conditioned samples consistently adsorbed less fibrillin-1 when compared to all other conditions ($p<0.0001$). This may largely be due to the prior adsorption of FBS and other serum proteins onto the scaffold surface during the overnight soaking, resulting in a surface saturation of protein.

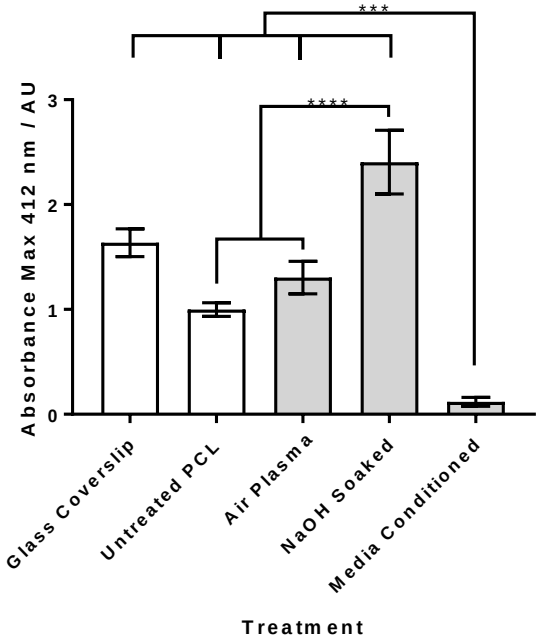

Figure 3-17 Potential of each treatment to facilitate protein adsorption. Fibrillin-1 fragment PF8 was used to determine which of the treatments were best suited to protein adsorption (n=3). One-way ANOVAs with Tukey HSD post hoc test were used to identify significances. Means ± SD are displayed. Performed once. *** $p<0.001$, **** $p<0.0001$.

3.3.7.3 Ligamentocyte Reponses to Treatment Methods

Primarily, two experiments were performed to discover an appropriate treatment method which could be used for continuing studies. Two viability protocols were used to determine both the cytotoxicity and cell morphology/alignment on the individual treatment methods previously assessed.

3.3.7.3.1 Metabolic Activity of cACLs to Surface Treatment Methods

Metabolic activity was tested to determine the cell viability across different surface treatment methods (Figure 3-18). This was performed to determine to which treatment method would result in the highest metabolic activity of the cell population on the samples, and infer which (if any) method resulted in cytotoxicity. Untreated PCL (which was used as a negative control) appeared to consistently display the lowest metabolic activity at all time points, as expected, due to it having the lowest wettability (as observed in Figure 3-16). Interestingly, air plasma treatment significantly exceeded all other conditions in cell viability up to day 1 ($p<0.0001$), and displayed cell viability equal with that of glass at day 7, whilst retaining significantly higher viability than untreated, media conditioned or sodium hydroxide soaked scaffolds ($p<0.0001$).

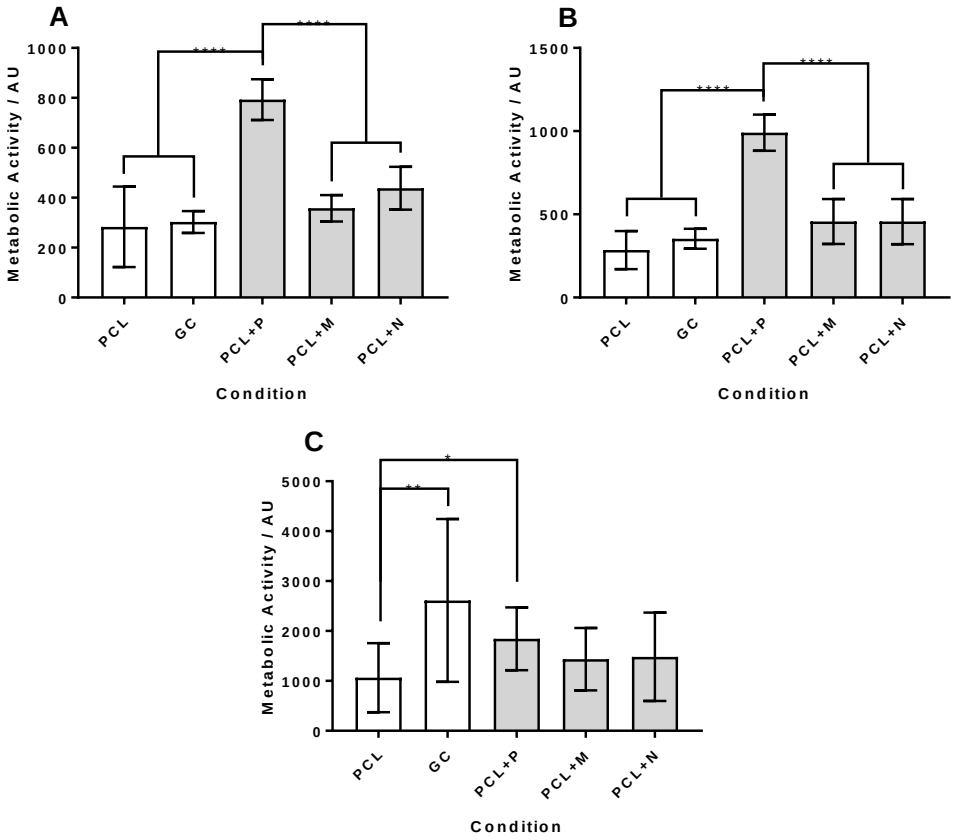

Figure 3-18 Metabolic activity (resazurin reduction assay) of the cells on PCL scaffolds at 0 (**A**), 1 (**B**) and 7 (**C**) days, subject to different treatments (n=3). 0 day time point was measured 4 hours post seeding. Letters following 'PCL' indicate method of treatment: 'P' air plasma treatment (1 min), 'M' high glucose DMEM + 10% FBS (1% A/A) overnight conditioning (37°C), 'N' sodium hydroxide soaking (30 mins, room temp). Statistical tests were performed using one-way ANOVAs and Tukey HSD post hoc, with exception of day 7 time point which was analysed with a Kruskal Wallis H test and rank comparisons. A total of 2 experimental repeats are included in the analysis. Bars show means and error bars show standard deviations. *$p<0.05$, **$p<0.01$, **** $p<0.0001$.

3.3.7.3.2 Effect of Surface Treatment Methods on Cell Morphology and Cytotoxicity

LIVE/DEAD assay imaging was performed to visualise cell death and morphology over the different treatment methods, using glass coverslips (GC) as positive controls for cell viability and untreated (PCL) scaffolds as negative controls for cell viability. Depicted in Figure 3-19, air plasma treated scaffolds were the only samples which displayed good cell distribution and evidence of alignment at all time points tested, displaying no indication of cell death on any of the samples. Early time points (4 hrs post seeding) for both media soaked (PCL+M) and sodium hydroxide soaked (PCL+N) showed marked evidence of cell death, whilst untreated PCL showed only sporadic and isolated occurrences. Clustering of cells occurred

at early time points (4 hrs, 24 hrs) on all conditions, with the exception of air plasma treated scaffolds. All scaffold samples appeared to show some evidence of cell orientation at day 7.

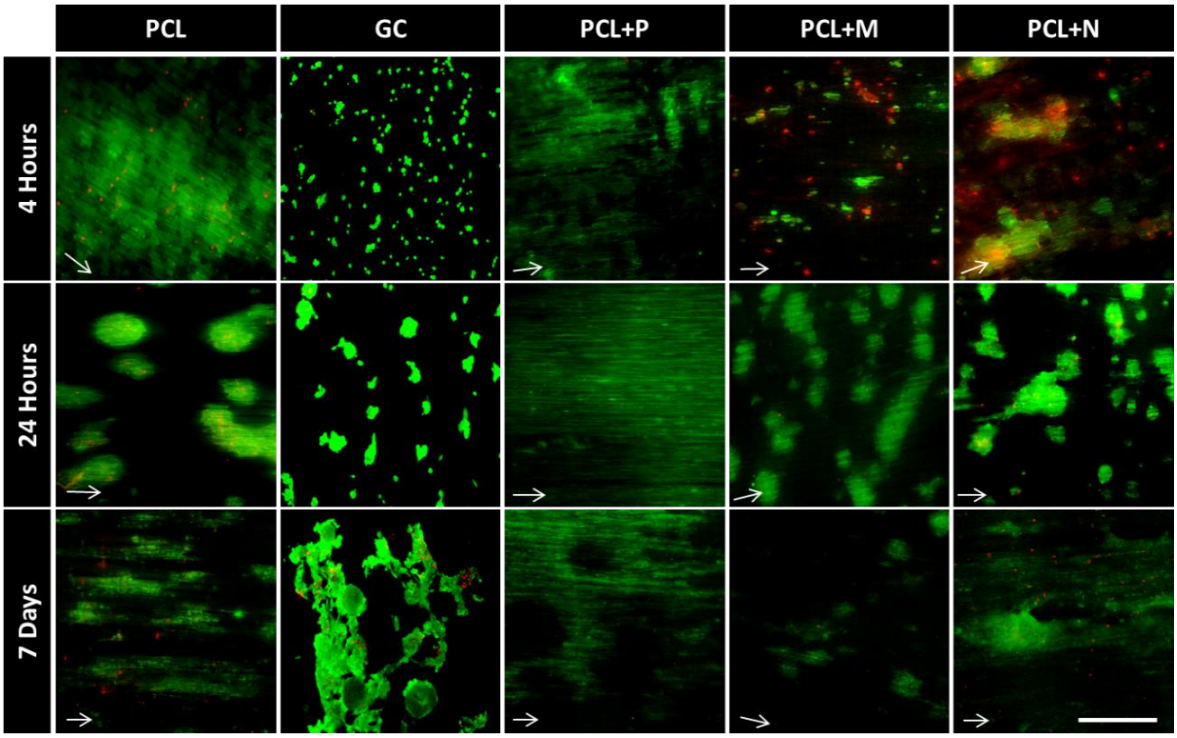

Figure 3-19 Glass coverslips (GC) were used as a positive control for observing viability of the cells (n=3), representative of 2 experiments. Plasma treated samples (PCL+P) showed good cell dispersion and viability at all time points compared to untreated (PCL), media conditioned (PCL+M) and sodium hydroxide soaked (PCL+N). Green staining represents live cells, and red staining shows cell death. White arrows indicate overall fibre direction and scale bar represents 250 µm.

3.3.8 Examining Evidence for the Effectiveness of Plasma Treatment on the Scaffolds

3.3.8.1 X-ray Photoelectron Spectroscopy (XPS) Confirmation of Air Plasma Treatment

XPS was performed to determine whether plasma treatment at the surface had been successful. The plasma used was generated from atmospheric air, of which the majority is nitrogen. However, it can be observed in the graphs below that the element reacting with the fibre surface was oxygen, and is depicted on the graphs B, D and E (Figure 3-20). It is displayed as an increase in the surface concentration of oxygen. Nitrogen peaks were not observed on the survey spectra of plasma treated PCL (Figure 3-20B) and could not be identified above any background readings on the elemental spectra at the expected N 1s

binding energy (Figure 3-20G). This corroborated with existing literature which also determined that any increases in nitrogen surface concentration are negligible or extremely small, and that oxygen is responsible for the increase in wettability of the scaffold[364, 365]. The experiment was repeated thrice to enable quantitative analysis. Peaks were identified to have a slight red shift in the plasma treated samples compared to the peak positions of the non-treated samples, characteristic of charging effects due to increased surface electronegativity[366].

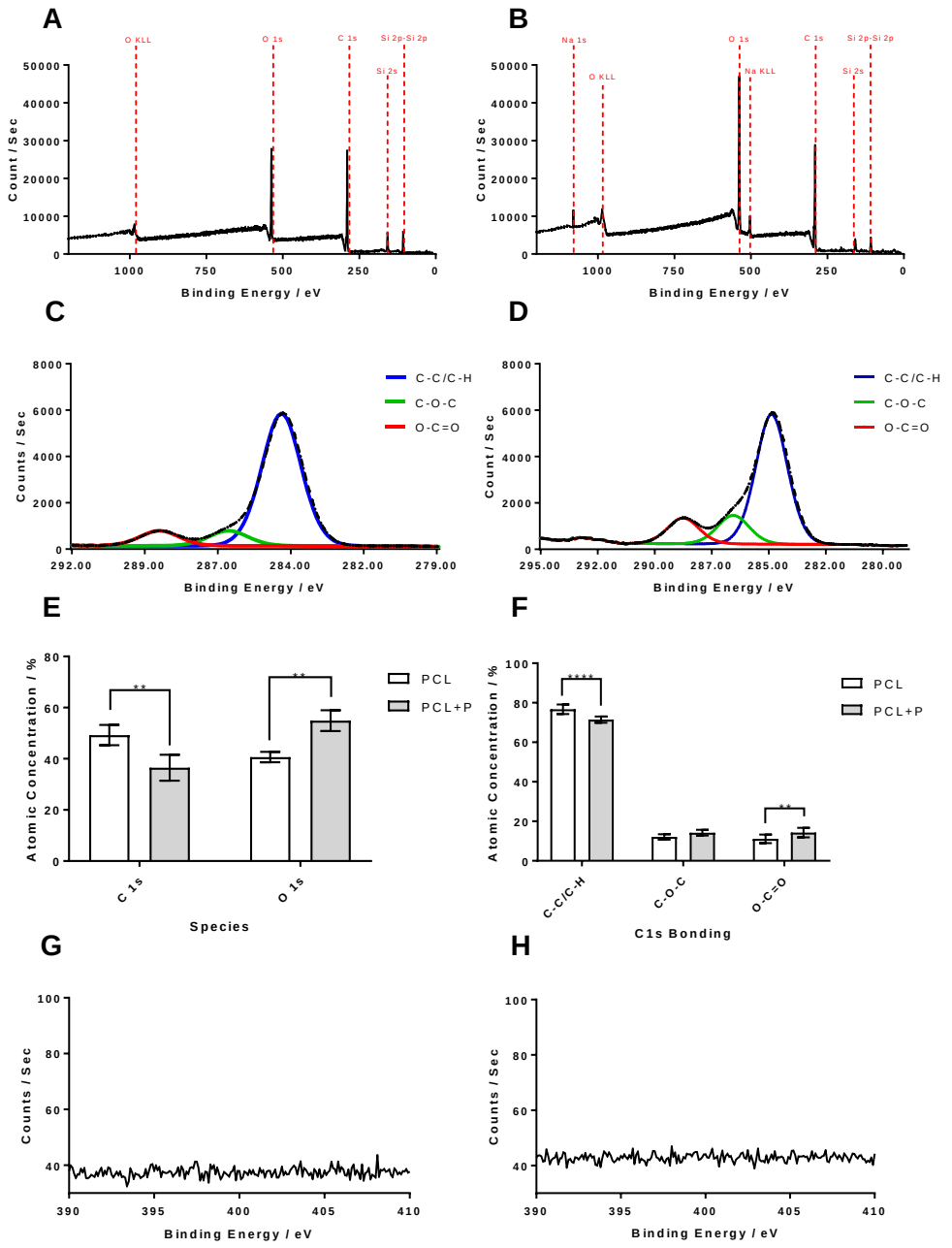

Figure 3-20 XPS spectra of non-plasma treated (**A**, **C**) and plasma treated scaffolds (**B**, **D**). Surveys show much larger increases in oxygen peaks in plasma treated samples (**B**) than non-plasma treated ones (n=3). Carbon bonding spectra of non-plasma treated samples (**C**) vs. plasma treated samples shows an increase in carbon-oxygen bonding at the surface. XPS analyses show relative concentrations of carbon 1s to oxygen 1s at the surface during an elemental survey (**E**) and further analyses on types of bonding present in carbon during a more focused scan (**F**). Elemetnal scans of the expected position of nitrogen peaks were taken to determine whether any nitrogen was contributing to the increase in hydrophilicity of the PCL, both before (**G**) and after (**H**) plasma treatment. To discern statistical significance, two-way ANOVAs were used with Sidak's multiple

comparisons tests. Bars show means (n=3) and error bars show standard deviation. Graph **F** is representative of 2 experimental data sets (n=3). ** p<0.01, ****p<0.0001.

3.3.8.2 Effect of Plasma Treatment on Fibre Morphology and Topography

Upon observing the images taken of the produced PCL aligned scaffolds using scanning electron microscopy (SEM) in Figure 3-21, it is clear that plasma treatment increases surface roughness by a chemical etching process, supported by Kuzminova *et al.* (2017)[367], where it has been reported that plasma etching can cause the formation of grooved patterns of approximately 10 nm[368]. The difference in nanoscale topography at the fibre surface is clearly depicted at the higher magnification (x 2000) where plasma-treated fibres retain more grooved and irregular surfaces than those that have not been subject to treatment. This may increase the overall surface area, with the roughness not only increasing wettability but also providing a larger surface area upon which biological molecules (i.e. proteins) can adsorb.

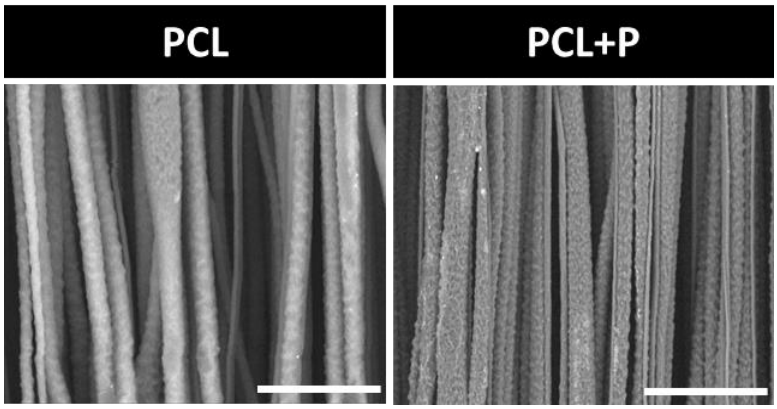

Figure 3-21 SEM images reveal the surface topography of the electrospun aligned PCL scaffolds. Plasma treatment appeared to create a more topographically irregular surface. Scale bars represent 20 µm, images taken at x2000 mag.

3.3.8.3 Longevity of Plasma Treatment on Scaffolds

To determine the length of time in which surface plasma treatment was stable for, scaffolds were plasma treated and contact measurements were taken (n=3) for the 0 hours condition. Untreated PCL was measured in parallel as a negative control. The 0 hours functioned as the positive control for this experiment. The same samples underwent repeated measurements. Data presented in

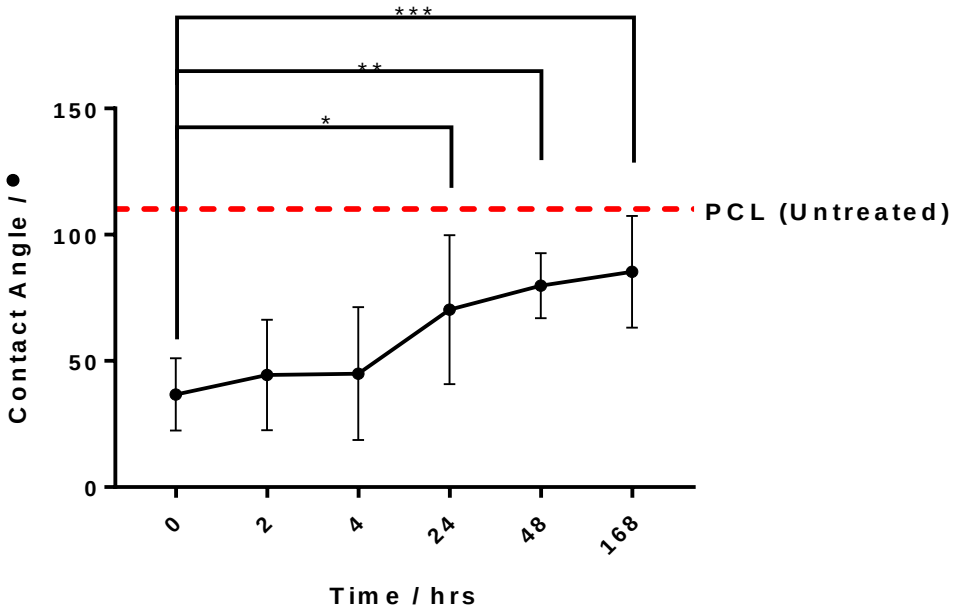

Figure 3-22 shows that the scaffolds underwent significant hydrophobic recovery after 24 hours ($p<0.05$), but began to undergo recovery by 2 hrs following plasma treatment. Within the first 24 and 48 hours, the scaffolds recovered by 34° and 43° degrees on average. These results appear to show moderate agreement with data reported by Jokinen *et al.* (2012), where it was reported that PCL will undergo (up to) 33° recovery within the first 48 hours[276]. For this reason, it was determined that scaffolds were to undergo fibrillin-1 fragment adsorption immediately following plasma treatment and subsequent UV sterilisation (within 1.5 hrs post plasma exposure).

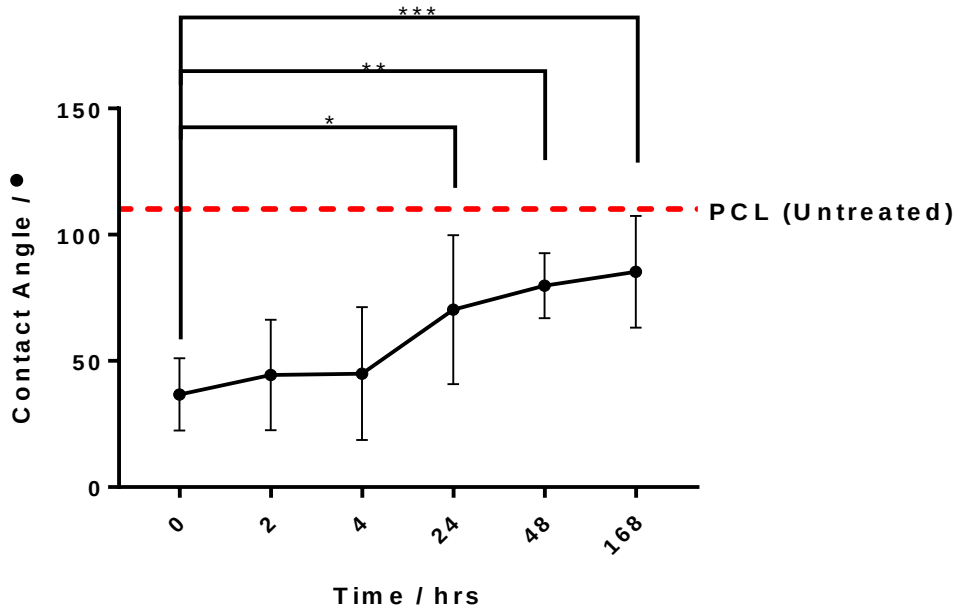

Figure 3-22 The longevity of plasma treatment on dry-stored samples was assess via contact angle measurements (n=3, 3 measurements/sample). Hydrophobic recovery of samples over a 7 day (168 hr) time period is shown. The 0 hr time point measurements were taken immediately following sterilisation treatment. Untreated plasma scaffolds were measured and the mean is shown as a dotted red line (standard deviation ± 7.322º). Error bars show standard deviations, results were analysed using ANOVA repeated measures test with Tukey HSD post hoc. * $p<0.05$. ** $p<0.01$, *** $p<0.001$. Performed only once to determine where significant recovery takes place.

3.3.9 Plasma Treatment Variation

Variation both between batches and within batches was observed. In order to remove any variables due to changes in fires structure/porosity affecting the experiment, each dataset was performed using scaffolds made from the same electrospun batch (shown in Figure 3-23B). Maximum amount of variation between means of scaffold batches was 47.53° (as shown in Figure 3-23A. This is likely due to the variation in both surface topography and porosity between the fibres, subsequently changing the exposed treatable surface area of the scaffold. In order to determine whether this could be ruled as the cause, flat, 2D PCL films were cast to remove any variation due to the fibre morphologies. Displayed in Figure 3-23C, wettability was determined both before and after plasma treatment and no notable or statistical differences between treated batches could be determined.

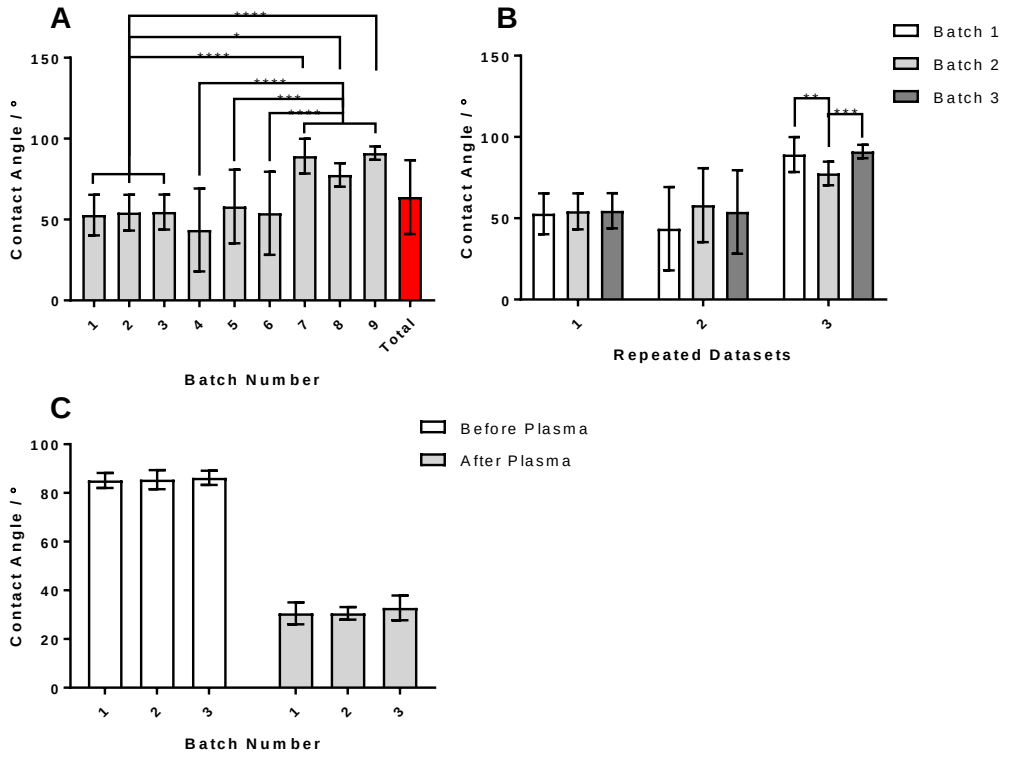

Figure 3-23 Determination of batch-to-batch variation of plasma treatment of electrospun fibrous scaffolds (n=4, 3 measurements/sample). Due to significant variations in the wettability between batches of the fibrous scaffolds (**A, B**), 3 independent batches of PCL films were cast, plasma treated and wettability analyses were performed (n=8, averaging 2 measurements/sample) (**C**) to determine whether the effect may be due to variations in fibre structure and porosity. One-way ANOVA was performed with Tukey HSD post hoc test for fibrous scaffolds and a two-way ANOVA with Sidak's multiple comparisons for films to determine differences between groups. Bars display means and error bars display standard deviations. *p<0.05, **p<0.01, ***p<0.001, ****p<0.0001.

3.3.10 Fibrillin-1 Fragment Functionalisation of the Scaffold

3.3.10.1 Effect of Fibrillin-1 Fragments on Scaffold Wettability

As displayed in Figure 3-24, PCL scaffold samples were tested immediately following the final stage of the protein adsorption protocol. Plasma treated samples, as expected, retained high levels of hydrophilicity when compared with the non-plasma treated samples ($p \leq 0.0001$). Interestingly both 1000 ng of PF8 and PF9 appeared to significantly reduce the water contact angle of glass coverslips ($p<0.05$ and $p<0.0001$ respectively) however, for non-plasma treated scaffolds, this was shown in all 1000 ng fragments (PF8 $p<0.05$, PF9 $p<0.0001$ and PF17.1 $p<0.01$). The trend observed of 1000 ng fragments increasing

wettability however, held true for all conditions, with all 1000 ng functionalised plasma treated substrates showing significantly higher levels of hydrophilicity when compared to the non-biofunctionalised controls (all $p<0.0001$). Unexpectedly, 10 ng of PF8 appeared to significantly increased and PF17.1 significantly reduced the wettability of the plasma treated scaffold, though these effects did not occur on any other substrate. The effect of 10 ng PF17.1 did not translate on plasma treated scaffolds when the adsorbed concentration was increased to 1000 ng per scaffold.

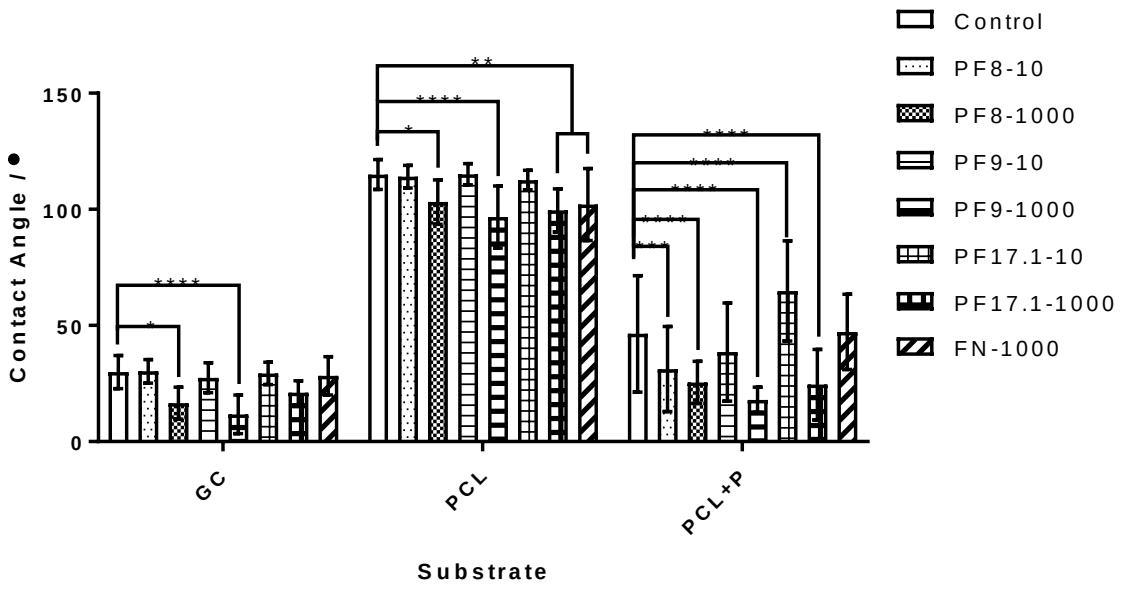

Figure 3-24 Representative contact angles of functionalised PCL scaffolds and glass controls when tested with deionised water (n=3, 3 measurements/sample). '+P' is indicative of plasma treated samples, whilst those beginning PF' have been treated with fibrillin-1 fragments. FN represents those treated with fibronectin. Numbers '10' and '1000' indicate the amount of fibrillin fragment in ng that has been adsorbed to the substrates. Two-way ANOVA was performed, with Tukey's multiple comparisons test to determine individual significances. Bars show means and error bars, standard deviations. *p<0.05, **p<0.01, ****p<0.0001. 10 ng conditions performed thrice and 1000 ng, twice.

3.3.10.2 Visualisation of Adsorbed Fragments using Immunohistochemistry

Evidence of fibrillin-1 fragment adsorption was achieved by immunochemical staining of 6his-tagged fragments with an anti-histidine antibody. Images could not be consistent between substrates due to extreme variation in brightness, but were kept consistent within substrate groups and for their respective negatives. Figure 3-255 clearly depicts the adsorption of fragments on both PCL and plasma-treated PCL. Adsorption was evident due to bright staining in the protein samples and lack of staining in the controls which had

undergone no protein coating. Staining could be observed on the glass samples as a faint 'glow' where PF17.1 and PF8 are clearly visible and PF9 is faintly so. Staining on the scaffolds appeared to align with fibre orientation and fibrous architecture remained clearly visible, which implies that fragments did not form a film over the fibres, nor disrupt the topographical cues required for cell alignment. These findings show agreement with work performed by Lin *et al.* (2021)[369], which show similar immunofluorescent staining patterns of bioadhesively-adsorbed proteins to PCL fibres. Though not observable in the micrographs below, the fluorescent staining of non-plasma treated samples was concentrated in one small area, as opposed to the plasma treated and glass samples, which had evenly distributed staining throughout.

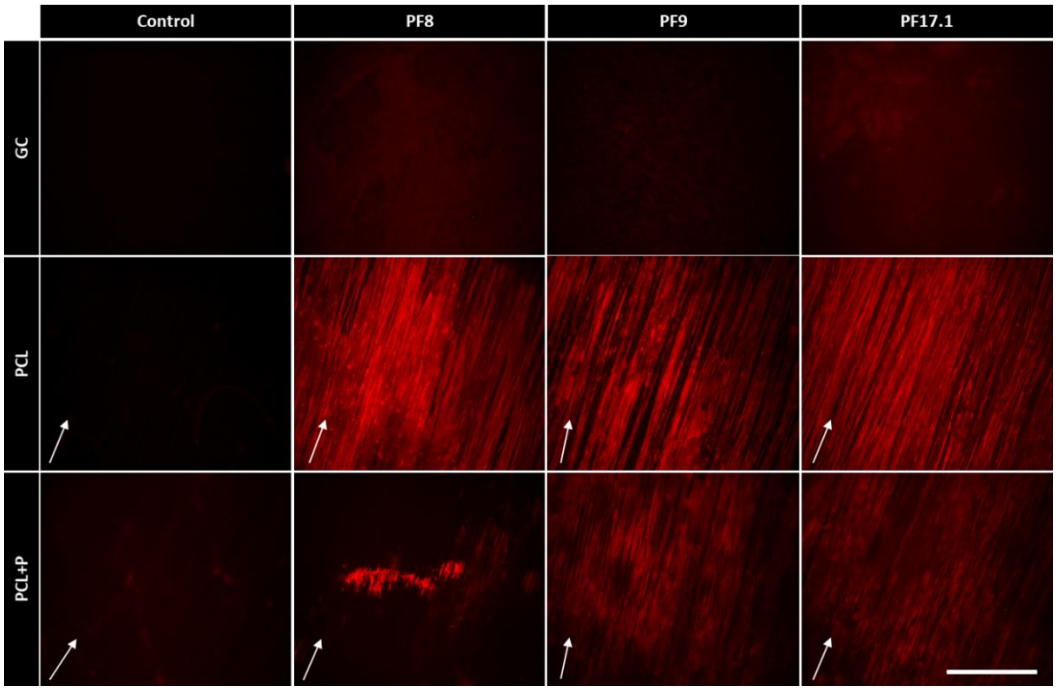

Figure 3-255 Immunochemical staining images of 6His-tagged fibrillin-1 fragments on PCL fibres under various treatments (non-plasma and plasma treated). Imaging parameters were kept consistent within the substrate groups and their negatives, images were universally enhanced in brightness (+ 40%). Scale bar represents 500 µm and arrows indicate fibre direction. Images representative of 2 experiments.

3.3.10.3 Relative Protein Adsorption Profiles of Fibrillin-1 Fragments

In order to determine which substrates adsorbed the fibrillin-1 fragments more successfully, indirect ELISAs were performed on the adsorbed fibrillin and relative adsorption was

compared between substrates. In all cases, it appeared that the plasma-treated scaffolds adsorbed the fibrillin-1 fragments the most successfully when 1.5 µg of fragment was added to each substrate, with PF8 (Figure 3-26A) and PF9 (Figure 3-266B) displaying significant differences when compared to all other substrates ($p<0.0001$). PF17.1 (Figure 3-266C) however, appeared to adsorb almost equally well to the glass coverslips, plasma treated scaffolds and TCP, but retained significantly higher adsorption on plasma treated scaffolds when compared to those which were not plasma treated ($p<0.01$).

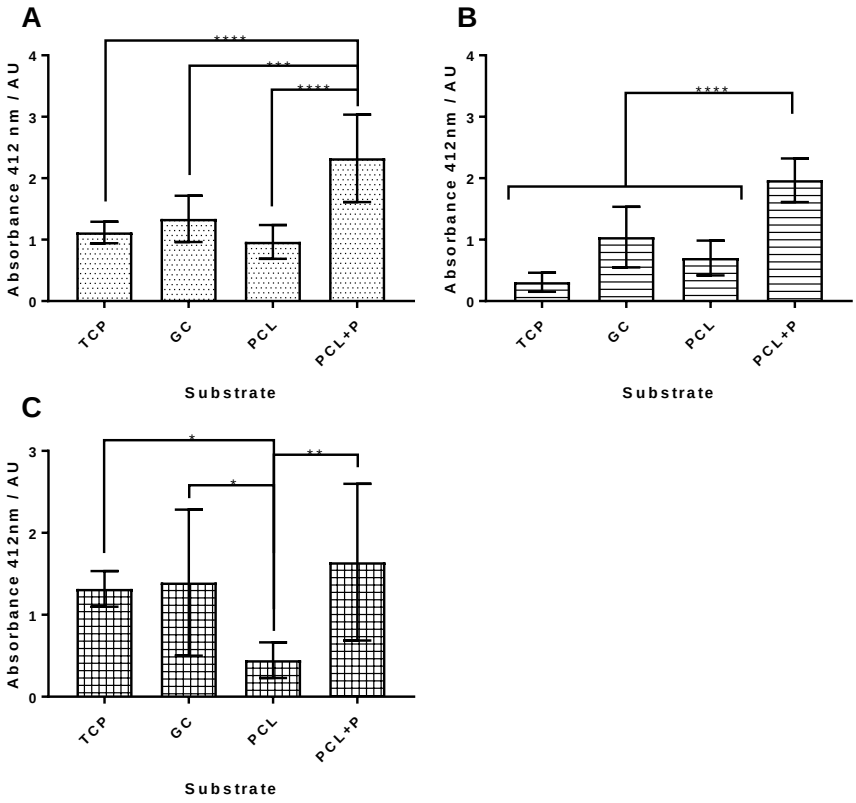

Figure 3-266 Indirect ELISAs were performed to give an indication of relative protein adsorption between substrates for PF8 (**A**), PF9 (**B**) and PF17.1 (**C**). Means ± SD are displayed. One-way ANOVAs with Tukey's post hoc tests were performed to determine statistical significances. *p<0.05, **p<0.01, ***p<0.001, ****p<0.0001. Each experiment was performed thrice.

3.3.10.4 Batch-to-Batch Protein Adsorption Profile of Plasma Treated Scaffolds

Six batches of plasma treated scaffolds were tested for effect of wettability variation on fragment adsorption. Indicated by the graphs below (Figure 3-27A, B and C), the effect of wettability variation on protein adsorption was non –significant. However, the conclusion

that the effects of variations in wettability on hydrophilic surfaces, in this circumstance, cannot be deemed negligible. Though insignificant, there are variations in the mean amounts of protein adsorbed, which may lead to difference in cell response during experimentation. Due to the inability to formulate a standard curve from which the exact adsorption of the fragments can be calculated (due to the nature of an indirect ELISA measuring surface adsorption), the scale of the differences in adsorption cannot be determined.

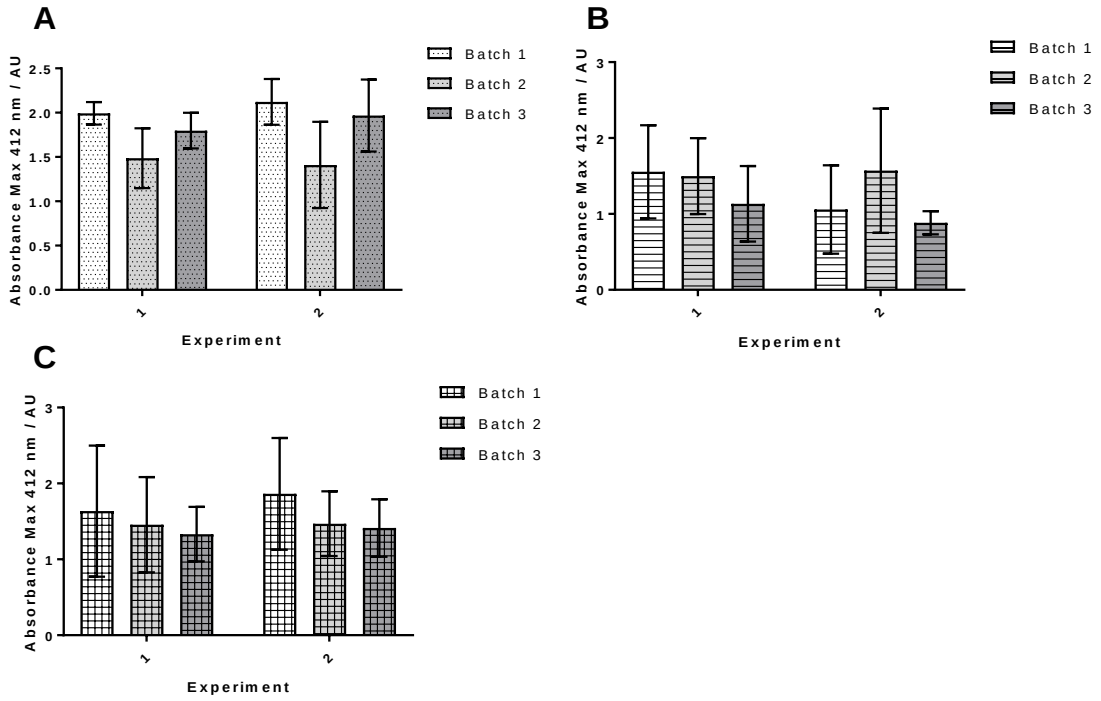

Figure 3-277 Variation in plasma-induced protein adsorption variation on PF8 (**A**), PF9 (**B**) and PF17.1 (**C**) adsorption (n=3). One-way ANOVA with Tukey's post hoc tests were performed. No statistical significances observed. Bars show means and error bars indicate standard deviations.

3.4 Discussion

For the production of aligned PCL scaffolds, the electrospinning method was previously optimised by Dr D Ramos Marquez where the parameters were compared to (also optimised) randomly oriented fibres (Appendix 1). The fibres produced from this method exhibited highly aligned orientations. It is well documented that the alignment of tissue engineering scaffolds can have a large impact on the orientation of ligament cells and their neo-ECM and as such, highly aligned substrates have been extremely popular for ligament tissue engineering in recent literature[177, 252, 253, 370], demonstrating superior ability to support larger cell numbers and guide native cell morphology when compared to their randomly oriented counterparts[253].

Fibres produced displayed a mean fibre diameter of 2.13 ± 0.660 μm and showed significant variation between batches ($p<0.0001$). This could have possibly been due to inconsistency in atmospheric conditions; Ghobeira *et al.* (2018) have previously reported an observable increase in fibre diameter with increasing relative humidity[218]. Interestingly, larger fibre diameter has been associated with both an increase in surface roughness and an increase in porosity. These factors have been reported to cause decreases in water contact angle due to air entrapment[218], and could therefore explain the variation in wettability between batches observed in this study. It has been previously reported in the literature that the efficacy of micro-fibres for connective tissue TE is inferior to that of nanofibers due to lower surface area to volume ratios and subsequently, less protein attachment[261]. Some studies however, have shown that microscale (~3 μm) fibres can increase cell alignment, density, area and aspect ratio of fibroblasts, in addition to supporting protein adsorption on individual fibres (resulting in cell extension and alignment on the fibres) compared to their nanoscale (~100 nm, ~700 nm) counterparts[229]. It is also known that increasing fibre diameter relates proportionally to scaffold porosity, which facilitates cellular infiltration into the scaffold and is therefore capable of supporting higher cell densities. One study found that MSCs had higher levels of attachment to microfibers of 2.6 μm diameters when compared to those at 0.3 and 5.2 μm[257], implying there may be a trade-off for cells between surface area and porosity.

Pore sizes are usually measured by mercury porosimetry, a highly accurate method for determining scaffold porosity and pore dimensions. However, due to the fragile nature of the scaffolds produced for this work, it was unlikely that they would withstand the system pressure. It has been previously reported that this method is inadequate for scaffolds where

the fibre diameter is under 3 μm[341]. Pore size was therefore measured using SEM micrographs, and analysed with FIJI ImageJ. Median pore sizes were presented due to trend being highly logarithmic with a large range of pore sizes measured and presented as 0.67 μm when diameters across all batches were averaged. Adequate porosity in a tissue engineering scaffold is required for diffusion of nutrients and waste products into, and out of, the scaffold. The most appropriate pore size for cellular integration appears to be highly dependent on cell type; with 11 μm pores facilitating the integration of dermal fibroblasts into elastin fibre scaffolds with relatively low porosity (34.4%)[371], whilst osteoblasts have shown a preference for larger pore sizes (100 μm) over smaller ones (40 μm)[372]. Cooper *et al.* (2005) have previously concluded that through the results of their research, a pore size of 100-300 μm is required to facilitate ligament tissue in growth *in vivo*. Taking these values into consideration, the scaffold produced in this study yielded an average pore size that is too small for cell integration or tissue formation, according to the above reports. The measurement method (SEM/ImageJ) may have underestimated scaffold pore size due to the single z-plane upon which the images were taken, and the inability to observe the 2.5D structure of the scaffold (fibres laying on top of one another). Small numbers of larger pores were observed however, ranging between 30 and 70 μm, through which the cells may have migrated. This could be observed by the blurred colour of the cells present in LIVE/DEAD cytotoxicity imaging which shows that fibres present are covering the cells (as seen in Figure 3-19), perhaps due to the presence of the much larger pores.

White light interferometry (WLI) was utilised to assess the thickness and surface roughness of the electrospun scaffolds. Though atomic force microscopy (AFM) is often a favoured method of measurement, the fibres were large enough to accurately use an alternative method and as a result, WLI was considered adequate. 'Sa', a measure of difference in height from the arithmetic mean of the sample's peaks and troughs was calculated to determine roughness (graphically represented in section 3.2.4) and has been utilised previously in the literature[373, 374]. Data revealed that in general, scaffolds were relatively similar in thickness between batches, though surface roughness did appear to vary significantly ($p<0.01$), with the surface topography accounting for roughly 12% of the overall thickness. Thickness was determined (on average, over all batches) to be 43.26 μm. The term '3 dimensional' is used widely in literature, but with most examples varying between hundreds of microns to mm thick[21, 22, 289, 347, 370, 375], with those less than 100 μm being reformed (i.e. rolled/braided/knitted) to give them much larger thicknesses[177]. It was determined that this

scaffold could be categorised as 2.5 dimensional; in microstructure, it appeared that the cells did not interpret the scaffold as entirely 2D, curving around the fibres and treating them (almost) as 3 dimensional structures. Interestingly, though fibre wettability appeared to be rather consistent before plasma treatment, surface roughness appeared to have rather a large effect on the overall wettability of the fibres post treatment, as shown by the comparison to flat PCL films which retain similar wettability between groups before and after surface treatment.

Once the fibres were fabricated, it was imperative to determine whether there was any residual chloroform present, which could potentially result in higher levels of cytotoxicity during cell culture. To determine this, FTIR was performed and checked for any peaks which might correspond to C-Cl bonding. No peaks were identified, hence it was ascertained that all chloroform had evaporated during the electrospinning procedure and/or during ethanol sterilisation. This was imperative to ascertain, as chloroform ($CHCl_3$) can change the organisation of the lipid bilayer in cellular membranes[376]. It be oxidised by cytochrome P450 into trichloromethanol, resulting in the spontaneous decomposition into phosgene ($COCl_2$), a harmful and highly reactive molecule. Phosgene binds covalently to lipids, reduced glutathione and proteins, causing breakdown of lipid membranes and cellular oxidative stress[377].

Although the parameters have been optimised to recreate the highly aligned and fibrillar structure of the ACL ECM (with an overall fibre diameter of 2.13 ± 0.660 μm, which could mimic the sub-fascicular units which are 1-20 μm in diameter[378]), PCL retains a highly hydrophobic surface chemistry. Three popular methods were tested to determine which would simultaneously; increase the hydrophilicity (for both fragment adsorption and cellular adhesion), display high levels of protein fragment adsorption and provide a non-toxic environment, suitable for normal cellular activity. Though all of the conditions appeared to reduce the contact angle, it appeared that the media soaking could not adsorb sufficient quantities of protein fragment, possibly due to adsorption and subsequent saturation of serum proteins from the media, leaving less available surface area for the fragments to adsorb. Both cell compatibility assessments showed air plasma treatment to be the most appropriate method, encouraging cell distribution and encouraging elevated levels of cellular metabolic activity and lack of cytotoxicity. As a result, the method preferentially used for following experiments was air plasma treatment. This enables exposure of carboxyl groups (-COOH) though reactions with ionised plasma and reactive oxygen species, which enable the

formation of stronger hydrogen bonds with exposed electronegative elements within the fibrillin-1 protein fragments. Other methods to increase the adsorption of proteins, such as amination have been explored in recent research, where amide groups are either chemically conjugated to the material or introduced via plasma treatment with ammonium ions to further improve protein adsorption[379]. Due to the electronegativity of nitrogen, this reaction process would presumably have a similar effect on the hydrophilicity and subsequent adsorption profile of the protein, but would increase cost when compared to using air as a plasma source.

Porosity of scaffold was measured using gravimetric analysis as previously described in literature[347]. This method was chosen due to the mechanical instability of the fibres. Mercury-based porosimetry measurements would have likely deformed the fibres, giving highly inaccurate results and has been reported in the literature[341]. Helium pycnometry and μCT were considered, however, time and access to the instrument proved to be highly limiting factors. Scaffolds appeared to exhibit an overall average of 73.77 ± 8.307 % porosity, with a range of 25.63% between batch means. None of the batches displayed mean porosities below 60% and was therefore above the reported 50-60% minimum threshold required to facilitate cell infiltration[252]. However, the fibres appeared to have a lower porosity compared with reports of architecturally similar scaffolds, which appeared to average at approximately 90%[257, 341, 380].

Mechanical properties show that the fibres themselves have moderate tensile strength and can exhibit extremely high levels of compliance (up to ~800% elongation in batch 5). The strain limit of the elastic region has proven to be ~5%, similar to that of native ACL tissue[165] (with a strain rate of 5 mm/min). The fibres also showed their properties to be strain rate dependent, however this did exclude limit of elastic strain, which proved to be insignificantly different with each increasing strain rate (Appendix 3). Though not mechanically suitable for use as an actual graft, these properties will enable the aligned fibrous scaffold to be used as a further platform in a bioreactor setting for further testing in relative physiologically applicable environments (strain rate, relative displacement).

Plasma treatment, sodium hydroxide soaking and media conditioning are all popular methods to increase the wettability of hydrophobic polymers, and often referenced in academic literature. Interestingly, all three methods function on the basis of differing principles to improve wettability. Plasma (as aforementioned) uses primarily oxygen free radicals to increase the content of electronegative atoms/polarise the surface, making it easier

for cells to attach via stronger intermolecular bonding (this also causes nanotopographical 'etching' at the surface). Conversely, media conditioning uses protein adsorption to achieve a similar result, with serum proteins providing specific binding sites for cell attachment. Sodium hydroxide however, performs a hydrolytic etching process at the surface, increasing surface area and therefore the wettability. Considering the three different methods attempted for selection of an appropriate treatment method, the specific requirements in place for a suitable cellular scaffold meant that air plasma treatment proved itself the resoundingly clear choice. Though both media soaked and plasma treated conditions had high wettability, only air plasma treatment could adsorb high levels of protein compared to the media soaked. This may be due to the adsorption and subsequent saturation of FBS on the surface of the scaffold. Short-term cellular compatibility tests showed the apparent cell preference for plasma treated scaffolds, with no cytotoxicity observed at any of the time points and high metabolic activity throughout. It should be noted however, that the LIVE/DEAD assay, though a visually informative method which informs on not only cytotoxicity, but on morphological response of the cells, can be inaccurate. This is due to dead anchorage-dependent cells detaching and being washed away during the final steps of the assay, giving inaccurate visual live to dead cell ratios. This can be somewhat overcome by determination of the quantity of remaining live cells, however this method requires knowledge of cell number present on each sample, and subsequent normalisation. The other assay used in this chapter to determine potential cytotoxicity and suitability of the scaffold treatment method, was the resazurin reduction assay. The resazurin reduction assay, more commonly known as Alamarblue, is a quantifiable assay, which requires the reduction of resazurin (blue non-fluorescent salt) to resorufin (red, highly fluorescent salt) by the cells. This can then be translated into a measure of cell metabolic activity. It is important to be aware however, that interference of bioactive molecules introduced to the media can cause inaccurate readings due to interactions with the resazurin salt in solution. Additionally, it is beneficial to be aware that some cell types will display inverse behaviours to cytotoxicity to what is usually observed, increasing intracellular metabolism with an increase in presence of cytotoxic agonist. This can be due to tolerance of the particular agonist. This effect has been documented in cells derived from liver, kidney, colon and lung tissue[381].

Plasma treatment was determined the most appropriate method for using in further studies and was verified for sufficient treatment and longevity of treatment effect on the scaffolds. XPS, FTIR and SEM micrographs were the selected methods used for testing this. All of the

above methods displayed expected results, reported in the literature[364, 365, 367]. Variation between batches of plasma treated scaffolds however, was found to differ significantly when analysed with water contact angle measurements. Upon the further analysis of flat cast PCL films, which showed no variation, it was determined that this was perhaps due to minor differences in fibre structure or porosity of the individual scaffolds.

Plasma treatment longevity was investigated to ascertain for how long the treated scaffolds could be stored for experimentation, without affecting the quality of the treatment. Hydrophobic recovery is commonplace in hydrophobic polymers often used in tissue engineering[276] and can change the cell behaviour and protein adsorption kinetics of the scaffold. This process has been reported to occur through two mechanisms; diffusion and/or molecular reorientation. The former supposedly occurs due to the higher concentration of polar groups at the polymer surface, which eventually are pulled into the bulk material. The second occurs when the modified surface molecules are larger. Due to their size, they cannot diffuse into the bulk, and instead only the polar groups are pulled downwards, leaving the non-polar groups remaining at the surface[382]. Jokinen *et al.* (2012) found that PCL begins recovery within 2 days of treatment[276], the materials used were cast films, and the time taken for hydrophobic recovery can differ on a number of parameters. Polymer type[276, 364], treatment substance (i.e. oxygen, nitrogen, air)[276], treatment length and power[276] and polymer morphology (fibres have been proposed to have shorter recovery times due to increased surface area)[383] have all been reported to alter recovery time.

For wettability testing, the fibrillin-1 fragments were adsorbed at a concentration of 10 ng and 1000 ng per scaffold. This concentration was selected due to results described by Sakamoto *et al.* (1996)[309] and Hajian *et al.* (2014)[315] and was performed in preparation for cell culture. Contact angle measurements were performed immediately following protein adsorption and utilised fibronectin as a positive control due to its superior adhesion properties[384]. Contact angle data of the scaffolds, acquired following fibrillin-1 fragment adsorption, showed no significant differences between 10 ng fragments and controls, which was partially expected due to the fragment concentration being so low. Interestingly, when the PCL is plasma-treated, 10 ng of PF17.1 fragment slightly increases the material hydrophobicity when compared to the other fragments and controls.

This could possibly be due to both the adsorbed fragment concentration and the presence of cbEGF domains, which have been reported to undergo hydrophobic interactions due to their

increased density of methyl groups[385]. As PF17.1 contains a larger proportion of cbEGF domains than either PF8 or PF9, there would be more hydrophobic interactions occurring. The second explanation (which would occur in tandem with the first), is that lower concentrations of proteins may be conducive to the unfolding of the tertiary structure, when adsorbing to the substrate surface. Lower concentration of proteins may give the proteins themselves (relatively) more surface upon which to adsorb, and subsequently more space upon which to unfold. This unfolding might more effectively expose the cbEGF domains, promoting hydrophobic interactions and decreasing the surface wettability of the scaffold.

In order to observe 6His tagged fibrillin-1 fragments on the scaffolds and the glass controls, fragments were adsorbed at 250 ng per scaffold and immunofluorescent staining was performed. Evidence of small amounts of clustering on the fibres was observed, yet the proteins did not appear to disrupt the fibrous architecture, which was clearly visible on the micrographs. Higher intensity of staining was observed on the untreated PCL fibres, which necessitated the reduction in exposure time during imaging. This may have been due to a larger amount of the fragments adsorbing to a smaller area. Due to the extreme hydrophobicity of PCL, lack of spreading of the protein solution was observed, concentrating adsorption to a smaller surface area that was seen in either glass or plasma treated PCL. Interestingly, it has long been determined that hydrophobic surfaces have superior adsorption kinetics for most proteins[293, 296, 297]; however, when tested for differences in adsorbed protein amount between substrates, hydrophilic plasma treated surfaces adsorbed the most fibrillin-1 fragment overall. It is possible that this was due to the increased available surface area upon which to adsorb (as opposed to protein being concentrated in a smaller area as in non-plasma treated samples, rather than being spread around the scaffold as with plasma treated substrates), and not a favourable interaction with hydrophobic surface chemistry. Hence, this may explain the visualisation of higher intensity staining on the untreated materials. Confirmation of this theory could be achieved by the production of a concentration curve for untreated scaffolds to determine at which concentration protein saturation occurs. By comparing this to plasma treated (hydrophilic) substrates, it would be possible to determine whether surface area is the limiting factor for protein adsorption. Other highly sensitive methods of protein quantification, such as a sandwich ELISA could not be performed due to the fragment only containing one tag and the lack of other antibodies that could act as a paired set for both capture and detection. The NanoOrange assay were briefly investigated, but it appeared that protein detection was

reliant on fragment size, and in order to quantify adsorbed fragments, they would require removal with components such as SDS or triton-X-100, neither of which are tolerated by the NanoOrange assay[386].

3.5 Chapter Conclusions

The primary objective of anterior cruciate ligament scaffolds is to emulate the native collagenous matrix, enabling native cell morphology, which subsequently determines the alignment of the neo-ECM. This study has shown that aligned microscale fibrous scaffolds, functionalised with fragments of fibrillin-1, can be produced. Though these scaffolds have a relative porosity of between 60-85%, which has been reported to support cell integration[252], but were not mechanically stable enough for further development as grafts. Morphologically, the scaffolds showed batch-to-batch variation in pore size, fibre diameter, wettability, porosity, thickness and surface roughness ($p<0.05$), for which fluctuations in atmospheric conditions, such as humidity and temperature, were attributed to these differences. Plasma treatment was shown to increase hydrophilicity, support native cell morphology and increase metabolic activity over other treatment options, and was determined to effect the scaffold surface chemistry by increasing surface oxygen concentration. Plasma treatment of scaffolds did however, show rapid hydrophobic recovery (63.8% recovery within 24 hrs and 77.4% within 1 week of treatment, as determined by contact angle measurements) which implied lack of suitability for longer-term storage, due to instability of surface chemistry. Plasma treated samples also showed batch-to-batch variation in wettability, but it was determined that this was likely due to differences in porosity and/or surface roughness, through validation of this theory with flat PCL films.

Fibrillin-1 was shown to adsorb to the scaffolds, further improving wettability when adsorbed at 1000 ng ($p<0.05$). The fragments were determined to coat the fibres, with more staining visualised on non-plasma treated samples, perhaps due to the superior adsorption abilities of hydrophobic surfaces[297]. It was demonstrated that plasma treated scaffolds had the highest adsorption capacity for all fragments, though showing small, but non-significant variation in adsorption between different plasma treated batches.

CHAPTER 4 EFFECT OF FIBRILLIN-1 FRAGMENT SCAFFOLD BIOFUNCTIONALISATION ON CANINE ANTERIOR CRUCIATE LIGAMENTOYTES

4.1 Overview

4.1.1 Introduction

Fibrillin-1 is instrumental in the assembly of elastic fibres and play a supportive role, both acting as a template for elastin deposition and coacervating assembled microfibrils (collectively known as 'oxytalan fibres'[59]) around elastin to afford support[306]. They also provide RGD binding sites for cell attachment to the elastic fibres, and to enable matrix remodelling[30]. Such fibres can be found throughout the ACL matrix, as without them, the tissue could not recover from repeated cyclic strain.

Fibrillin has been previously been determined to interact with multiple ECM proteins, including elastin[306], fibulin-5[33], fibronectin[34], perlecan[52], MAGP-1[306], heparan sulphate[99], TGFβ1[32] and decorin[35]. These interactions implicate fibrillin-1 in a multitude of roles within ECM assembly, and as such, imply influence of fibrillin-1 in the development and maturity of the neo-ECM.

In this chapter, four fibrillin-1 fragment-functionalised PCL aligned fibre scaffolds will be seeded with canine cruciate ligamentocytes to attempt to encourage higher cell viability and increase the amount, and subsequent maturity, of the newly formed ECM, for ACL TE applications.

Two amounts of fibrillin-1 were selected: 10 and 1000 ng. The rationale for these choices were based on two publications by Sakamoto *et al.* (1996)[309] and Hajian *et al.* (2014)[315], where each showed enhanced attachment of fibroblastic ligament/chondroblast and endothelial cell types respectively. Following this rationale, the use of these fibrillin-1 fragments (compared to non-fibrillin-1 functionalised scaffolds and 2D controls) is anticipated to increase cACL attachment profiles, increase the metabolic activity of the cells (implying positive cell interactions with the scaffold), assist in the retention of 'native' cell morphology, and ultimately, bring about an increase in quantity and maturity of the neo-ECM produced. If these criteria are met, the scaffold will be determined to have been successful.

Cells were acquired as per the method depicted in Figure 4-1, and collected from the Comerford Group at the Institute of Ageing and Chronic Disease, University of Liverpool, UK. They were previously fully characterised[387].

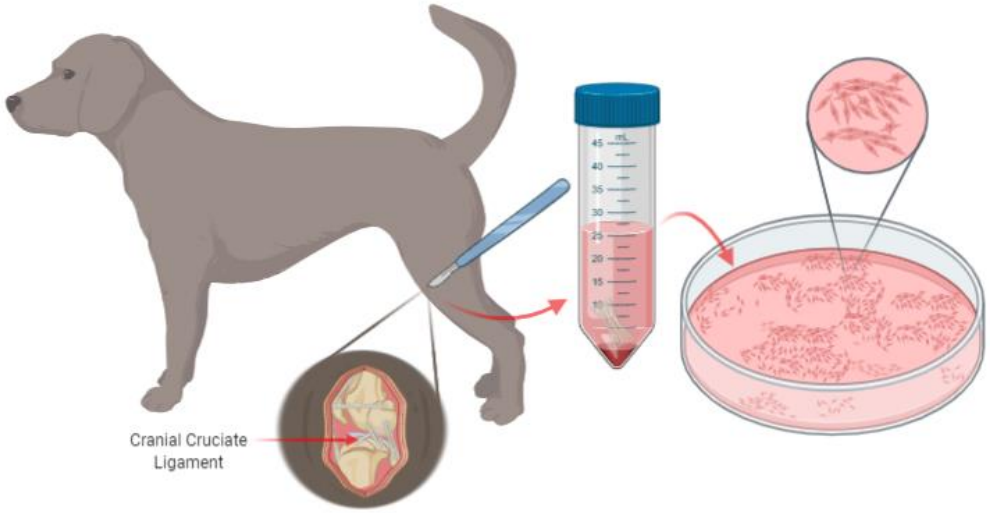

Figure 4-1 A depiction of the cell extraction protocol performed by Comerford group at the University of Liverpool. All cells used in this chapter were harvested from the cranial cruciate ligament. Image adapted from Kharaz (2014)[388]. Image created using BioRender.com.

4.1.2 Statement of Novelty

The work in this chapter aims to be the first that has characterised the response of ACL cells from canines to fibrillin-1 fragments (RGD-containing), immobilised on aligned microfibre scaffolds.

4.1.3 Hypothesis

The expectation is that cells will retain native 'spindle-like' morphologies and have a uniform dispersion amongst the fibres. It is also expected that functionalisation of the fibrous scaffold will increase metabolic activity, and that this will correlate with both cell imaging and the attachment results for testing individual fragments and concentrations with the cells. It is finally expected that all conditions will support the production of collagen type III and that functionalised scaffolds will increase the production of other ACL-integral ECM proteins (fibronectin, collagen type I and fibrillin).

4.1.4 Aims & Objectives

- Determination of the regenerative capacity of canine ACL cells.
- Colony forming unit assay, performing with crystal violet staining to determine the formation of cell colonies.

- Visualisation of any changes in morphology that may have been due to fibrillin-1 fragment functionalisation of fibrous scaffolds.
  - Use of the LIVE/DEAD labelling assay to determine appropriate cell morphology and appropriate cell dispersion and orientation throughout the scaffold.
  - SEM imaging to determine morphology of cells with respect to the fibres.
- To determine whether fibrillin-1 RGD functionalisation has an effect on the metabolic activity of the canine ACL cells.
  - Use of a resazurin reduction solution (Alamarblue) to infer cell attachment and viability.
- Whether fibrillin-1 fragment functionalisation has an effect on the levels of early-stage attachment in canine ACL cells.
  - Early (1 hr) interactions with fibrillin-1 fragments on TCP.
  - Quantify % attachment using QuantIT Picogreen assay to measure and comparing to normal TCP as 100% attachment control.
- Verification of integrin-mediated attachment of canine ACL cells to the fibrillin-1 RGD.
  - Immunofluorescent staining of integrins $\alpha_v\beta_3$ and $\alpha_5\beta_1$ at 1 hr to visualise integrins.
  - Blocking of integrins $\alpha_v\beta_3$ and $\alpha_5\beta_1$ and culturing to 1 hr to determine the effect on cell attachment to fibrillin-1 fragments and fibronectin controls.
- Observation of ECM deposition/production by canine ACL cells which may be due to fibrillin-1 RGD.
  - Use of immunofluorescent staining to detect integral ECM proteins; collagen type I, fibronectin and fibrillin.
  - Semi-quantification of the above proteins to determine any effects of the fibrillin-1 fragments on cell ECM protein production.
  - Immunofluorescent staining of collagen type III to ascertain whether the biofunctionalised scaffolds are capable of supporting cACL collagen type III production.

4.2 Materials & Methods

4.2.1 Materials

4.2.1.1 General Cell Culture

Trypsin/EDTA solution (0.05% trypsin, 0.02% EDTA in Hanks' balanced salt solution, 59417C, Sigma Aldrich UK), bovine serum albumin (BSA; A7906, Sigma Aldrich UK), Dulbecco's phosphate buffered saline (PBS, D8537, Sigma Aldrich UK), Dulbecco's Modified Eagles Media (DMEM, high glucose, D5976, 4500 mg L^{-1} glucose, 584 mg L^{-1} L-glutamine, 3700 mg L^{-1} sodium bicarbonate, D5796, Sigma Aldrich UK), fetal bovine serum (FBS; F9665, Sigma Aldrich UK), Antibiotic-Antimycotic (A/A; 10,000 U penicillin, 10 mg streptomycin, 25 µg amphotericin B ml^{-1} A5955, Sigma Aldrich UK), goat serum (GS, PCN5000, Novex, Thermo Fisher UK / G6767, Sigma Aldrich UK).

4.2.1.2 Chemicals

Sodium hydroxide (10192863, Fisher Scientific UK), 10% neutral buffered formalin (HT501128, Sigma Aldrich Germany), gelatin from cold water fish (G7041, Sigma Aldrich, UK), glycine (G8898, Sigma Aldrich UK) , Sigma Aldrich UK), Triton-X-100 (T8787, Sigma Aldrich UK), ProLong™ Diamond Antifade Mountant (P36970, Invitrogen UK), resazurin salt (R7017, Sigma Aldrich UK), VECTASHIELD® mountant (H-1200, Vector USA), ProLong™ Gold antifade mountant with DAPI (P36931, Thermo Fisher UK), DMSO (dimethyl sulphoxide, D4540, Sigma Aldrich UK), 1-Step™ pNpp substrate solution (37621, Thermo Fisher UK), Assay buffer (K412-500-1, Biovision USA), ALP enzyme (K412-500-3, Biovision USA), EDTA (E6758, Sigma Aldrich UK), Tris-base (M02623, Fluorochem UK).

4.2.1.3 Assays

Quant-IT™ PicoGreen™ dsDNA Assay Kit (P7589, Thermo Fisher UK), LIVE/DEAD solution (LIVE/DEAD Viability kit, L3224, Life Technologies Ltd. UK).

4.2.1.4 Antibodies

Rat anti-$\alpha_5\beta_1$ integrin [5H10-27(MFR5)] (ab25251, Abcam UK), mouse anti-human $\alpha_v\beta_3$ [LM609] (ab190147, Abcam UK), goat anti-mouse 568 nm (ab175473, Abcam UK), goat anti-rat 546 nm (A11081, Thermo Fisher UK), phalliodin Alexa Fluor 488 nm (8878S, Molecular Probes, Cell Signaling Technology), DAPI (D1306, Thermo Fisher Scientific UK), mouse anti-fibrillin (MAB1919, Millipore UK), rabbit anti-fibronectin (F3648, Sigma Aldrich UK), goat anti-type I collagen (UNLB, 1310-01, Southern Biotech USA), donkey

anti- mouse IgG Alexa Fluor 633nm conjugate (SAB4600131, Sigma Aldrich UK), donkey anti-rabbit IgG (H+L) Alexa Fluor 594 nm (A31572, Thermo Fisher Scientific UK), donkey anti-goat IgG (H+L) Alexa Fluor 488 nm (A11055, Thermo Fisher Scientific UK), rabbit polyclonal primary anti-Collagen III (ab7778, Abcam UK), goat anti-rabbit IgG 488 nm secondary (A11034, Invitrogen™ UK), Alexa Fluor™ 488 goat anti-rabbit (A31627, Thermo Fisher UK).

4.2.2 Fibrillin-1 Fragments

4.2.2.1 Background

The human fibrillin-1 fragments have been produced and purified by Dr Stuart A Cain and Dr Pinyuan Tian (School of Biological Sciences, Faculty of Biological Sciences, Medicine and Health, University of Manchester, UK). There are three RGD-motif containing fragments, all of which overlap in amino acid sequence and have been produced by a mammalian expression system in HEK293-EBNA cells[30] and tagged using an N terminal His_6[389]. All fragments were previously validated for purity using western blotting, approximation of monomeric mass via SDS-PAGE, and confirmed for correct cbEGF domain folding by electrophoretic shifts in response to calcium, post EDTA treatment[390-392].

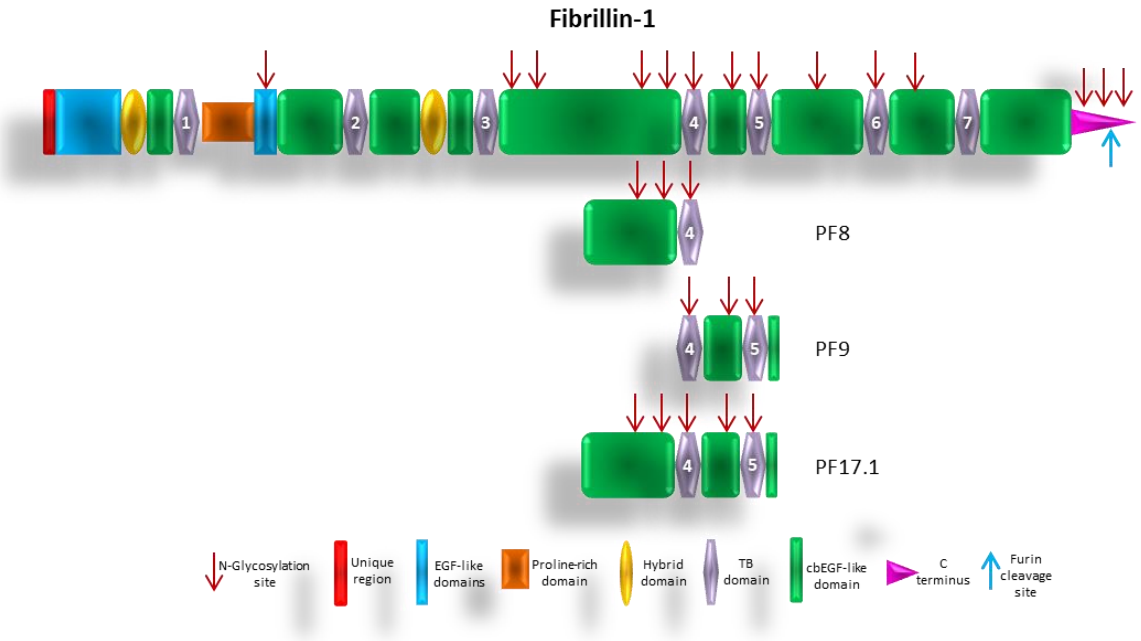

Figure 4-2 A diagrammatic representation of where each fragment used in the subsequent experiments lies within the fibrillin-1 protein and which active sites and domains it contains. This diagram is based on illustrations previously published by Bax *et al.* (2007)[310] and Cain *et al.* (2012)[392].

The first, termed PF8, is a small 367 amino acid fragment corresponding to amino acids 1238-1605. Within this region are 7 calcium binding epidermal growth factor-like (cbEGF) domains and TB4, including the cbEGF22 which has a synergistic effect on TB4 and is necessary for triggering signalling events downstream[393]. It is in this TB4 domain, that the RGD motif is located. PF9, along with TB4 and three cbEGF domains, also contains the TB5 domain, which hosts a heparin/heparan sulphate binding site. This is the smallest of the three fragments, consisting of only 279 amino acids (residues 1528-1807). PF17.1 is the final fragment, measuring 569 amino acids in length. This fragment corresponds to residues 1238-1807 within the fibrillin-1 protein, meaning that it contains all the active sites and domains of both PF8 and PF9.

4.2.3 Cell Culture and Maintenance

4.2.3.1 Cell Maintenance

Ligamentocyte maintenance was performed as in Chapter 3, section 3.2.14.1.

4.2.3.2 Cell Seeding for Experimentation

Ligamentocyte seeding was performed as in Chapter 3, section 3.2.14.2.

4.2.4 cACL Viability Testing on Fibrillin-1 Functionalised Scaffolds

4.2.4.1 Cell Cytotoxicity and Morphology

Protocol was performed as in Chapter 3, section 3.2.14.3.

For imaging however, samples were imaged using a CQ1 cell imaging system (Yokogawa, Japan). Scaffolds were imaged as stacks using a 5 µm step, gain and exposure parameters were kept consistent throughout the experiment.

4.2.4.2 Cell Metabolic Activity

Protocol was performed as in Chapter 3, section 3.2.14.4.

4.2.5 Determination of Cell Attachment to Fragments

Wells were coated with fibrillin-1 fragments at densities of 7 ng cm^{-2} and 700 ng cm^{-2} overnight at 4°C. Wells were then exposed to 200 µl of 10 mg ml^{-1} BSA for 1 hr at 37°C (method adapted from a protocol by Bax *et al.* (2014) [394]). Following the removal of the BSA solution, wells (n=3) were seeded with cells (1.5 $x10^4$ cells $well^{-1}$) for each condition. Cells were removed from incubation at 1 hr post seeding and washed with PBS to remove any unattached cells. Post washing, cells were lysed with a 1% Triton X-100 solution in 1X TE Buffer (10 mM Tris-base, 1 mM EDTA) for 15 mins (200 µl) and frozen until analysis. Supernatant was collected and 50 µl was pipetted into a clear 96 well plate (with 50 µl X1 TE buffer), before being mixed with Quant-IT™ PicoGreen™ dsDNA Assay Kit detection dye (1:200 dye in 1X TE buffer) and analysed on a fluorescent plate reader at λ_{exc}485 nm and λ_{em}520 nm.

4.2.5.1 Blocking and Staining of cACL Integrins for Attachment to RGD Motifs

To confirm RGD interaction with known fibrillin-1 RGD integrins, cACLs were trypsinised (as above) and resuspended in serum-free media either supplemented with rat anti-$\alpha_5\beta_1$ integrin or mouse anti-human $\alpha_v\beta_3$ [LM609] at a 1:50 dilution (cell concentration of 2 x 10^6 cells ml^{-1}) or without. The suspension was incubated (37ºC, 5% CO_2, 95% humidity) for 45 mins before seeding. The antibodies were used to block integrins which facilitate RGD motif binding as per the method used by Zhou *et al.* (2009)[395]. cACLs were seeded at a density of 1 x 10^4 cm^{-2} onto 1000 ng pre-coated glass coverslips (PF8 or fibronectin, as described in Chapter 3, section 3.2.10.4; surface blocked for 1 hr at 37°C, with 10 mg ml^{-1} sterile filtered BSA) and cultured for 1 hour in serum free media. Media was then removed and cells were washed with sterile PBS, fixed with 10% neutral buffered formalin and stored in PBS at 4°C. For imaging of samples, cells were permeabilised and quenched using 0.5% triton-x-100/0.2 M glycine (in PBS) for 5 mins, washed twice with PBS and blocked with 2% FSG (30 mins). Non-integrin blocked samples were subsequently stained with the above antibodies (100 µl, 1:200 for mouse anti-$\alpha_v\beta_3$ or 1:100 for rat anti-$\alpha_5\beta_1$, in 2% FSG, overnight, 4°C) before being washed thrice and stained with 100 µl of secondary antibody (1:400, goat anti-mouse 568 nm or 1:200, goat anti-rat 546 nm). All samples were stained with 100 µl phalloidin (1:200) and DAPI (1:1000) for 2 hrs (in 2% FSG, room temperature).

After 3 PBS washes, all samples were mounted with ProLong™ Diamond Antifade Mountant and imaged on a Leica DM2500 LED microscope (Leica DFC3000 G camera)

with either a dry (x10) or an oil immersion (x100) lens. Imaging parameters were kept consistent.

4.2.6 Cell Morphology on the Scaffolds (Scanning Electron Microscopy Imaging)

Scaffolds were prepared as in section 4.2.3.2 and dried for 1.5 hrs at room temperature. Scaffolds were then sputter coated with a 3 nm gold/palladium (60:40) mix using a Quorum Q105T ES instrument, after mounting on an SEM stub with carbon adhesive. SEM analysis was performed on a Hitachi High- Technologies S-3000N with PC-SEM V10-11 2252 software.

4.2.7 ECM Protein Analysis

4.2.7.1 Immunofluorescent Staining for Detection of ECM Proteins

Scaffolds were cultured with cACLs for set time points (1, 7, 14 and 28 days), media was removed, and cells were washed with PBS. Cells were fixed (10% neutral buffered formalin, 1 ml, 1 hr) and stored in PBS (4°C). Fluorescent immunostaining protocol was optimised by Dr Stuart Cain (School of Biological Sciences, Faculty of Biology, Medicine and Health, University of Manchester). Scaffolds were quenched and permeabilised in 0.2 M glycine and 0.5% triton X-100 in PBS (500 µl, 5 mins) before washing twice with PBS. Scaffolds were blocked with 2% FSG in PBS (300 µl, 30 mins, room temperature) and exposed to primary antibodies (mouse anti-fibrillin, rabbit anti-fibronectin, goat anti-type I collagen; 200 µl scaffold^{-1}, 1:200 with 2% FSG), and incubated (4ºC, overnight). Primary antibody was removed, and scaffolds were washed thrice with PBS before labelling with secondary antibody (donkey anti- mouse IgG Alexa Fluor 633nm conjugate, donkey anti-rabbit IgG (H+L) Alexa Fluor 594 nm, donkey anti-goat IgG (H+L) Alexa Fluor 488 nm, 200 µl, 1:200 in 2% FSG, 2hrs, room temperature). All scaffolds were counterstained with DAPI (1:2000). Secondary antibody was removed, and scaffolds were washed thrice with PBS. The samples were then mounted on glass imaging slides using ProLong™ Diamond Antifade Mountant.

A CQ1 Cell Imaging System (Yokogawa, Japan) with x20 dry lens was used to perform ECM imaging. Three stacks (2.5 µm step) were imaged for each sample. The gain and exposure settings were retained for all samples. FIJI ImageJ was used to quantify nuclei counts (Appendix 11.1) and % area of staining. Individual channels were semi-quantified for % area function using '**MeasureMacro**' (details in Appendix 11.2). The three individual

channels were then sample-matched, stacked, and Z-projected using '**ECMImageCompiler**' (details in Appendix 11.3) before being quantified for total % area ECM protein coverage, as above.

4.2.7.2 Immunocytochemical Staining for Fluorescent Detection of Intracellular Collagen type III

Scaffolds seeded with cACLs were cultured for set time points (1, 7 and 14 days). Quenching and permeabilising protocol was performed as above (section 4.2.7.1) Scaffolds were then blocked with 5% goat serum (GS, Thermo Fisher for 10 ng; Sigma Aldrich for 1000 ng samples) in PBS (1hr, room temperature) and rabbit polyclonal primary, anti-Collagen III (100 µl, 1:100 in 5% GS) was incubated with the scaffolds overnight at 4°C. Samples were washed thrice with 1 ml PBS before incubation with 100 µl goat anti-rabbit IgG 488 nm secondary (Invitrogen™ UK for 10 ng, Thermo Fisher UK for 1000 ng, both 1:1000 in 5% GS, 1hr, room temperature), protected from light. A fluorescent mounting solution containing DAPI (VECTASHIELD® for 10 ng samples, ProLong™ Gold antifade mountant with DAPI for 1000 ng samples) was also added to the scaffolds.

Imaging was performed on a Ziess Axia AX10 Imager M1 with Axo Cam MRm using green (λ_{exc}400-418nm) and blue (λ_{exc}478-495nm) filters for 10 ng samples and CQ1 cell imaging system (Yokogawa, Japan) for 1000 ng samples using the same filters. All imaging parameters were kept consistent within the two condition batches.

4.2.8 Orientation Analysis of cACLs on Fibrillin-1 Functionalised Scaffolds

In order to determine initial cell orientation, .tiff images from the day 1 time point, showing only intracellular collagen 1A1, were used to determine initial cell orientation on the biofunctionalised scaffolds.

For analysis, a total of 9 images per condition were imported into ImageJ software, where OrientationJ (plug-in for Fiji ImageJ)[396] was used. Parameters used for the software were as detailed in Rezakhaniha *et al.* (2012)[397].

4.3 Results

4.3.1 Cell Response to Fibrillin-1 Coated PCL Scaffolds

4.3.1.1 Determination of Cell Morphology, Alignment and Viability

LIVE/DEAD assay was again used to determine the morphology and indicate any potential cytotoxic response of the cACL cells on the PCL/fibrillin-1 functionalised scaffolds. As depicted in Figure 4-3B, untreated PCL samples showed clustering of cells, whilst plasma treatment enabled cell spreading and more even distribution (Figure 4-4C). Interestingly, the addition of 10 ng of PF8/PF9/PF17.1 to glass coverslips did not encourage spreading of cells when compared to the control at either time point. However, 1000 ng of fibrillin-1 fragments PF8 and PF17.1 appeared to cause enhanced attachment to the glass coverslips and clustering of cells at very early time points (4 hrs, shown in Figure 4-3A). Notably, 1000 ng of fragment appeared to have a definite effect on cell morphology and spreading on untreated PCL scaffolds. Micrographs taken at 4 hrs show slightly increased cell number, however the most positive effect can be observed at 24 hrs post cell seeding. 1000 ng of PF8 appears to have caused cell alignment and spreading along the fibres, removing the clustering formation that can still be observed on the 10 ng conditions (with exception of PF17.1) and the negative control. Both PF9 and PF17.1 show that cells have adopted a degree of alignment and extension, resulting in more native-like morphologies. Fibronectin controls (1000 ng) at 24 hrs display complete lack of clustering on untreated PCL scaffolds and single-cell extensions along the fibres can be observed.

Plasma treated PCL scaffolds, functionalised with 10 ng of fibrillin-1 fragment showed no morphological enhancement when compared to the negative control samples at 24 hrs. However, the addition of 1000 ng of both the fibrillin-1 fragments and fibronectin, resulted in extension of the cells along the fibres and a very high degree of linearity and orientation along the longitudinal fibre axis.

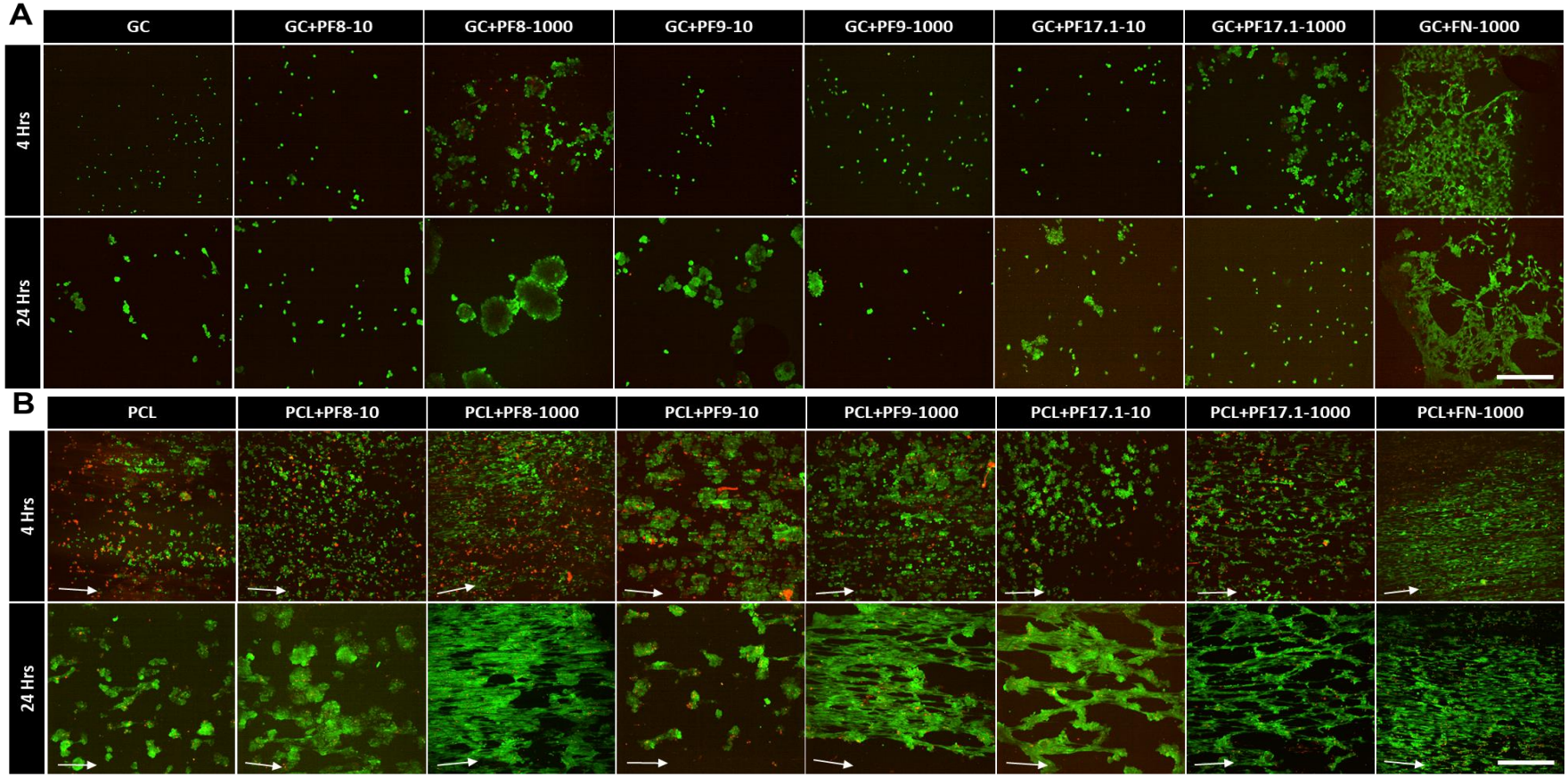

Figure 4-3 LIVE/DEAD cytotoxicity images showing viability of cACL cells on untreated PCL scaffolds (**B**) and glass controls (**A**), coated with fibrillin-1 fragments PF8, PF9 and PF17.1 (n=3). Gain and auto exposure were kept consistent across all samples. Scale bars represent 500 µm and white arrows indicate the direction of the fibres. 10 ng conditions (-10) have been performed twice and 1000 ng conditions (-1000), once.

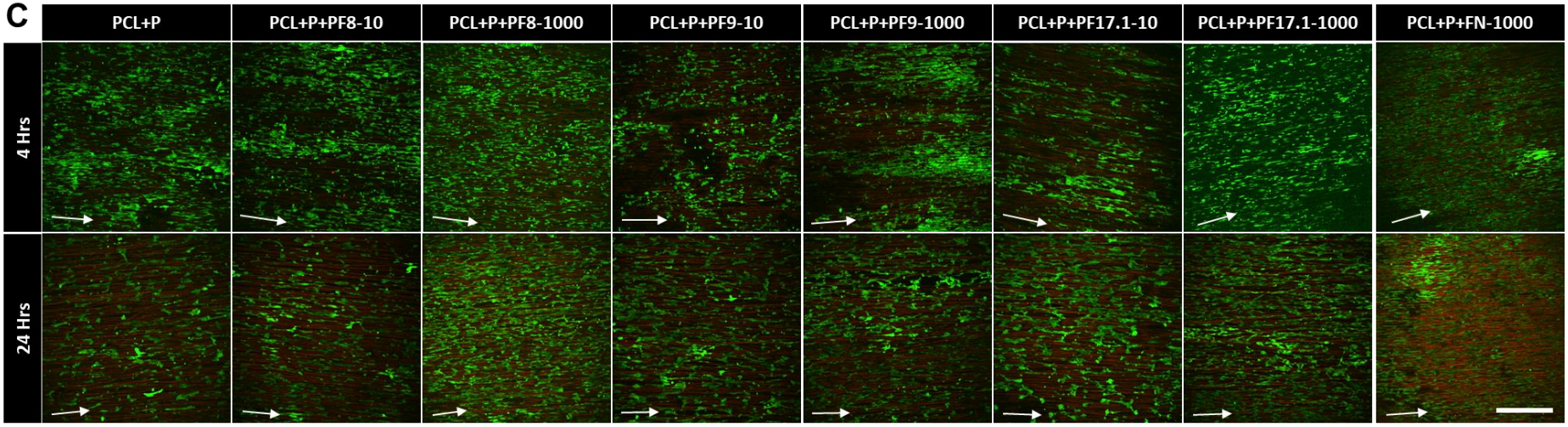

Figure 4-4 (Continuation of Figure 4-3) Fluorescent micrographs of LIVE/DEAD cytotoxicity images showing viability of cACL cells on and plasma treated PCL (**C**), coated with fibrillin-1 fragments PF8, PF9 and PF17.1 (n=3). Gain and auto exposure were kept consistent across all samples. Scale bars represent 500 µm and white arrows indicate the direction of the fibres. 10 ng conditions (-10) have been performed twice and 1000 ng conditions (-1000), once.

4.3.1.2 Metabolic Activity of cACLs on Fibrillin-1 Functionalised Scaffolds

Metabolic viability was tested by the detection of resazurin reduction, using borosilicate glass coverslips (GC) as positive controls substrates. Untreated scaffolds acted as negative substrate controls with each substrate coated with fibrillin-1 (each had a fibrillin-1-negative scaffold as a control). Blanks (negative controls of media and resazurin solution only) were used for this experiment to remove any background and to normalise all data procured.

As shown in Figure 4-5A, C, E and G, scaffolds coated with 10 ng of fibrillin-1 fragments (PF8, PF9 and PF17.1) each had a fibrillin-1-negative scaffold or glass coverslip as a control. Though marginally lower at all time points when compared to the fragments (especially at 7 and 14 days) plasma treated scaffold conditions all remained non-significantly different to one another. Significances were observed at 14 days on the glass substrate between the non-functionalised controls and PF9 ($p<0.001$)/PF17.1 ($p<0.01$).

On the scaffolds and glass controls functionalised with 1000 ng of fibrillin-1 fragments (shown in Figure 4-5B, D, F, H), significant differences were observed on the glass controls and non-plasma treated scaffolds. The glass controls showed significantly higher metabolic activity at 4 hrs post seeding when functionalised with PF8 ($p<0.05$) and PF17.1 ($p<0.01$) than with the negative controls, with fibronectin also displaying significantly higher metabolic activity ($p<0.01$). Non-plasma treated scaffolds showed higher metabolic activity at the same time point on PF8 functionalised scaffolds when compared to the negative controls ($p<0.05$). Interestingly, the glass controls maintained significantly greater differences in metabolic activity up to 1 day, when they began to plateau at 7 days. At 14 days however, significantly higher metabolic activity was observed all fragments on glass compared to the negative controls (PF8 $p<0.0001$, PF9 $p<0.001$, PF17.1 $p<0.0001$). Non-plasma treated scaffolds retained a similar trend to what was observed 4 hours post seeding, but comparisons to the negative controls were non-significant. Similarly, with plasma treated, biofunctionalised samples, fibrillin-1 fragment functionalised scaffolds supported marginally higher metabolic output up to 1 day post culture, though these differences remained non-significant. Interestingly at day 7, the negative control appeared to support higher metabolic activity than that of the fibrillin-1 functionalised scaffolds (PF8 $p<0.05$, PF9 $p<0.0001$, PF17.1 non-significant).

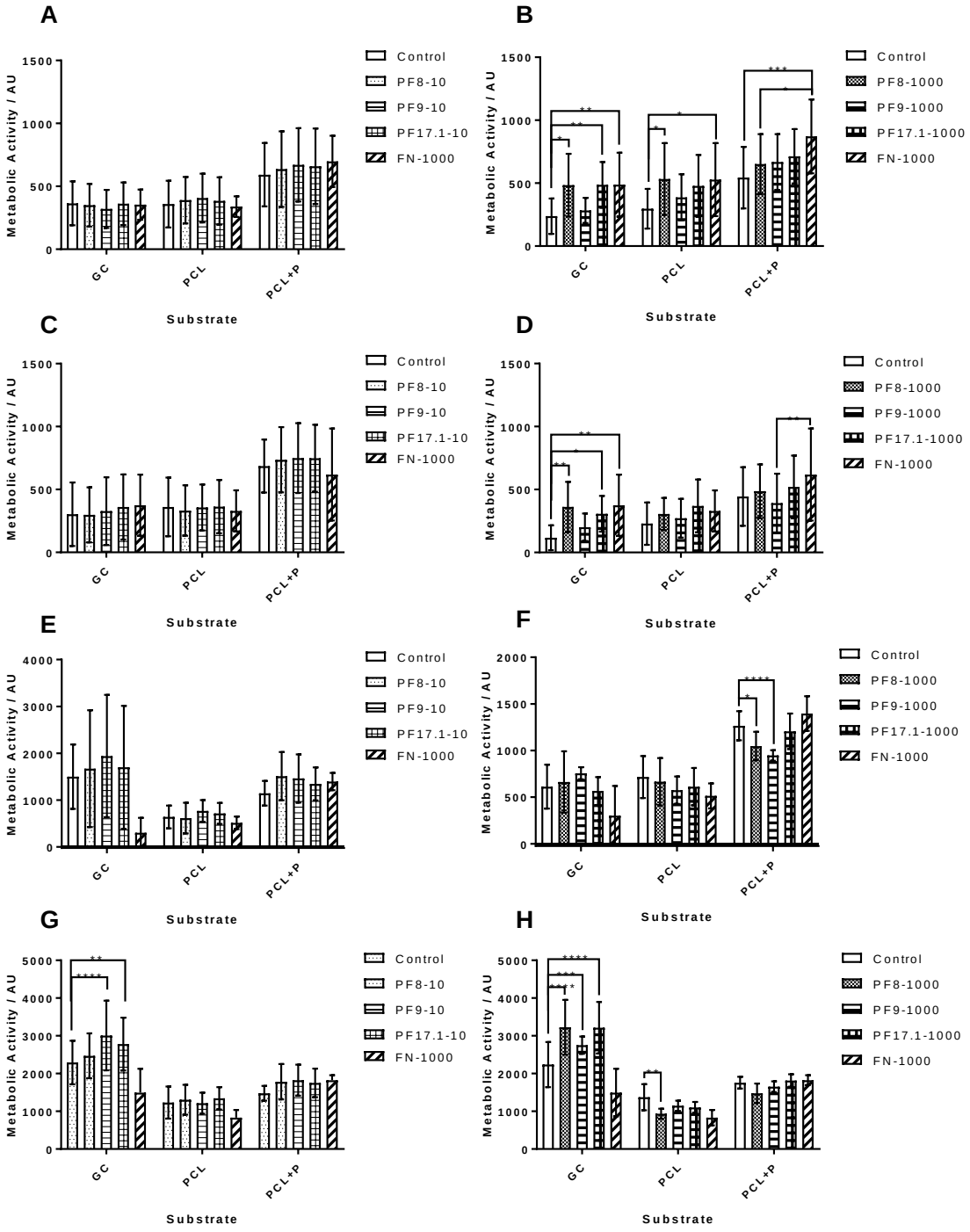

Figure 4-5 Metabolic activity of cACLs on fibrillin-1 biofunctionalised substrates (n=3). Data shown is pooled from n=3 experiments for 10 ng samples and n=2 experiments for 1000 ng samples. Metabolic activity is shown for 10 ng (**A**, **C**, **E**, **G**; 3 experiments) and 1000 ng (**B**, **D**, **F**, **H**, 2 experiments) of fibrillin-1 fragment. Metabolic activity at 0 (4 hrs post seeding, **A**, **B**), 1 (**C**, **D**), 7 (**E**, **F**) and 14 (**G**, **H**) days are displayed. Two-way ANOVAs with Tukey's multiple comparisons test were performed. Means ± SDs are displayed. *p<0.05, **p<0.01, ***p<0.001 ****p<0.0001.

4.3.1.3 Morphology of cACLs on PF8 Coated Scaffolds

SEM images were performed to observe the exact morphology of the cells on the fibres at one early (24 hrs) and one later (7 days) time point to observe cell morphology on the fibres. Shown in **Error! Reference source not found.**, though no obvious differences could be observed between time points on the glass slides, it appeared that cell density was higher on the PF8 coated slides. The hydrophobic environment of the untreated PCL appeared to cause cells to lift away from the fibres, sitting on top of them rather than displaying the highly integrated appearance that can be observed in plasma treated PCL (PCL+P) conditions. This again will be primarily due to surface wettability. Highly wettable surfaces will increase cell adhesion by non-specific binding through polar carboxylic and carboxyl groups, exposure during plasma treatment whilst the non-polar surface of untreated PCL and associated energetics will cause cells to attach to each other and form tight surface clusters.

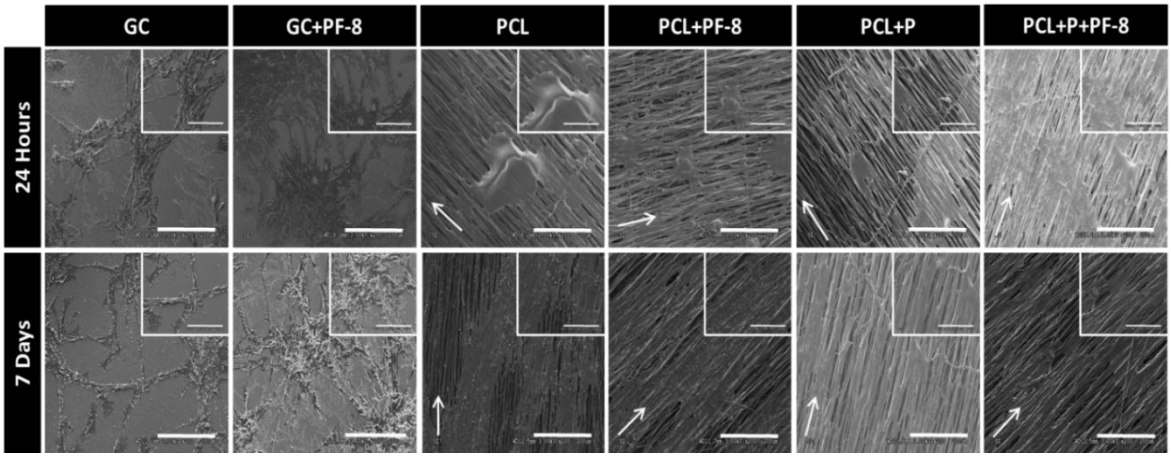

Figure 4-6 SEM images of cACLs seeded onto low concentration PF8 fragment-coated scaffolds. Scale bars in this image represent 200 µm in the larger images and 100 µm in the smaller images. Contrast was enhanced universally by +20%. Arrows indicate direction of the fibres.

4.3.2 Early-Stage Attachment of cACLs to Fibrillin-1 Fragments

For assessing the attachment of the cACLs to the substrates mediated by fibrillin-1 fragments, Quant-IT Picogreen assays were performed. Attachment was first normalised to BSA-only control wells and a TCP 'Control' condition was used for approximating 100% attachment. This enabled the calculation of % attachment to the substrate.

As depicted in Figure 4-7, positive controls with no BSA treatment were used to approximate 100% attachment and fragment/fibronectin-control conditions were examined with respect to TCP. BSA controls were used as to normalise the conditions for any residual cell attachment that was not due to the fragments or fibronectin themselves, as they appeared to

effectively deter cell attachment at the 1 hr time point. Though significantly lower attachment occurred on the equivalent-10 ng coated surfaces ($p<0.05$ apart from fibronectin), it does appear that low densities of fibrillin-1 facilitate some attachment. PF8 and PF9 demonstrated cell attachment levels of 48 and 49% respectively whilst PF17.1 appeared to enhance attachment further with a mean of 72% attachment. Interestingly, though at low densities, cells appear to respond similarly to PF8 and PF9, this trend does not translate to higher density functionalisation. At 1000 ng-equivalent densities, PF8 facilitates 97% attachment of cells (PF8 in agreement with Hajian *et al.* (2014)[315]), whilst PF9 only supports 70%. Superior attachment can be observed with higher densities of both PF17.1 and fibronectin, which support 107 and 126% of the TCP control respectively.

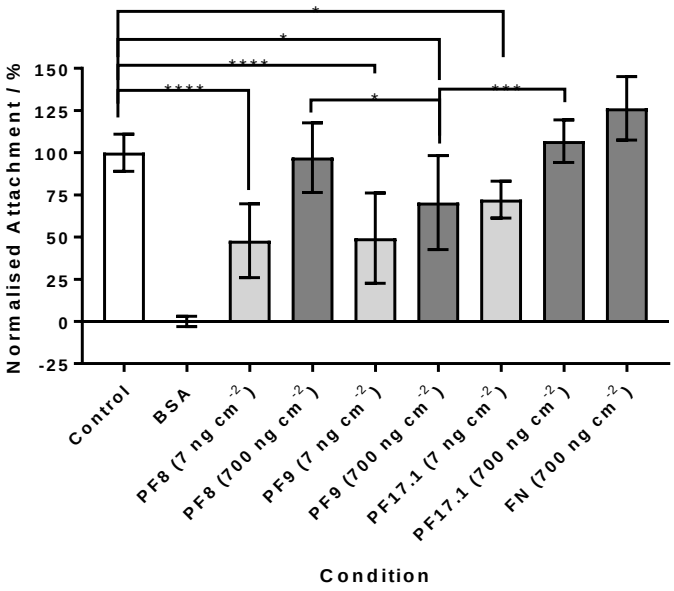

Figure 4-7 cACL attachment to fibrillin-1 fragment coated TCP (blocked with 10 mg ml^{-1} BSA). Bars show means and error bars indicate standard deviations. Graph is based on 2 experimental repeats (n=3). One-way ANOVA was performed with Tukey HSD post hoc tests to determine significances. *$p<0.05$, ***$p<0.001$, ****$p<0.0001$.

4.3.3 Assessing Integrin Binding of cACLs to RGD Motifs in Fibrillin-1 Fragments

In order to confirm cACL integrin attachment via the RGD binding motif present in the fibrillin-1 fragments, previously reported fibrillin-1-binding integrins $\alpha_5\beta_1$ and $\alpha_v\beta_3$[30] were blocked and stained to positively determine cell interaction with the fibrillin-1 fragment RGD motif. The fragment PF8 was selected to determine this owing to its higher concentration of RGD motifs per unit of mass and the presence of the upstream synergistic site. Fibronectin was utilised as a positive control (due to the well characterised interactions

of its RGD motif with cell integrins $\alpha_5\beta_1$[28, 398] and $\alpha_v\beta_3$[29, 399]), and the effect of blocking these cell integrins was assessed by determination of the cell shape and detection of the integrins themselves in unblocked samples at 1 hr post seeding.

In Figure 4-8A below, it can be clearly observed that integrin-blocked cells display a more rounded morphology when compared to the non-blocked cells as they are unable to interact with the RGD ligands present in the fibrillin-1 fragments and in the fibronectin controls and therefore cannot attach to the surface. As expected, this effect was also observed on the BSA-coated glass surface, confirming the role of the RGD-containing fragments in the cell's ability to attach to the substrate surface.

Integrins were also observed in unblocked examples (yellow arrowheads) as small clusters within the cell, and around the edges of the cell membrane, similar to previously reported $\alpha_v\beta_3$ intracellular localisation in both human ACL fibroblasts, by Tetsunaga *et al.* (2009)[264] and human endothelial cells by di Blasio *et al.* (2015)[400]. However, though $\alpha_5\beta_1$ integrins were faintly observed by fluorescent microscopy, their blocking did not appear to have any effect on the attachment of cACLs to fibronectin controls, though it did appear to retain some effect on the attachment of cACLs to PF8 (evidenced by rounded morphology in Figure 4-8A). Controls without BSA coating were performed to demonstrate the use of BSA as an appropriate surface blocking agent and show very little inhibition of attachment, as displayed by the numerous spreading cells in the fluorescent micrograph (Appendix 10).

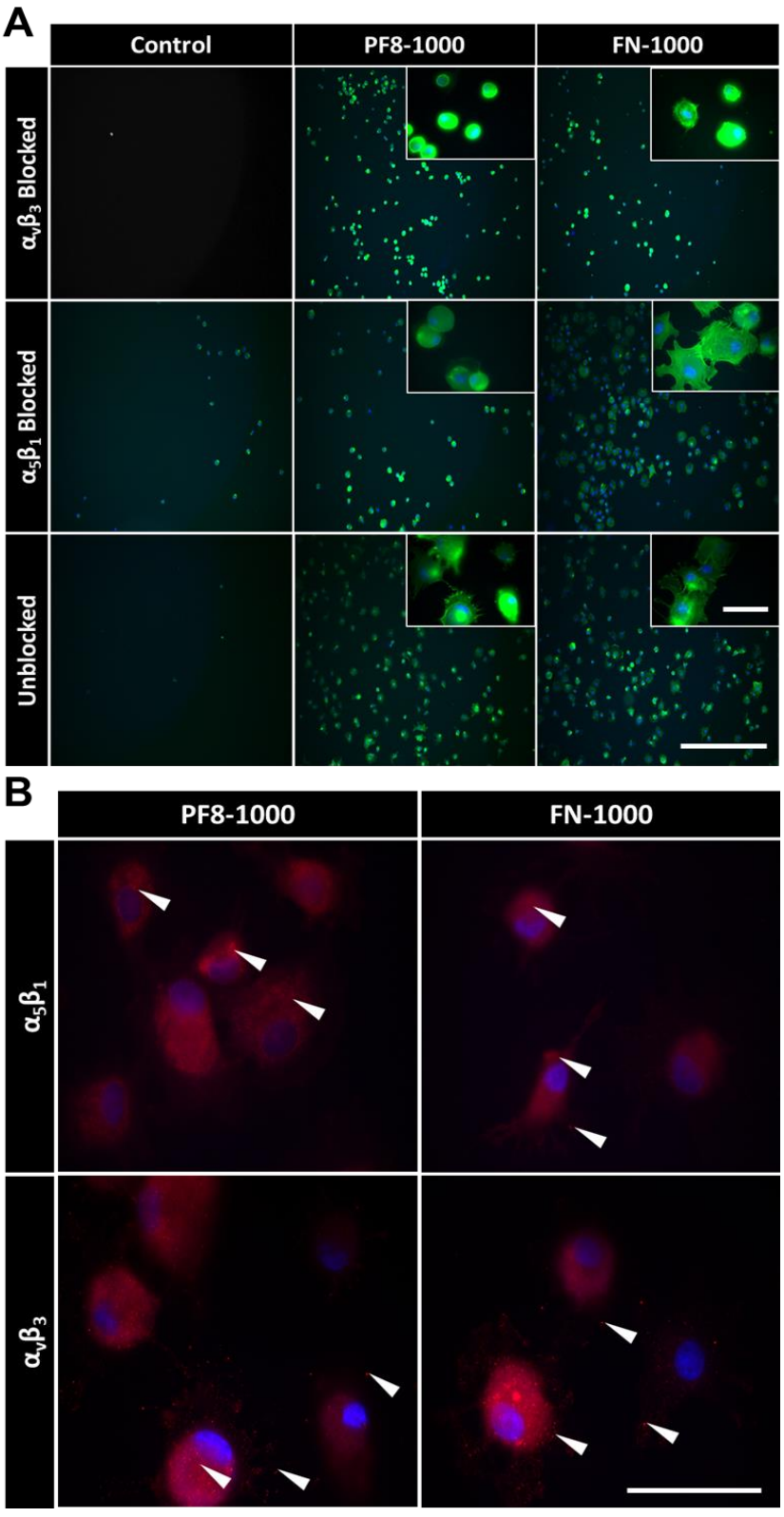

Figure 4-8 Fluorescent micrographs of integrin blocking (**A**) and integrin staining (**B**). Coverslips were blocked with BSA to ensure the attachment was to PF8 fragments and FN exclusively. Scale bars represent 500 µm for primary images and 50 µm for those in the smaller windows (**A**). White arrowheads indicate clusters of integrins and scale bar represents 50 µm (**B**).

4.3.4 ECM Matrix Production on Fibrillin-1 Functionalised PCL Scaffolds

4.3.4.1 Nuclear Count

Nuclear count was performed from blue channel (DAPI) fluorescent micrographs at 1, 7, 14 and 28 days (Figure 4-9A, B, C and D respectively). Though no scaffold displayed significantly different nuclear counts at 1 day post seeding, at 7 days, significantly higher cell number (inferred by the nuclear count) was detected on PF8, PF9 and PF17.1-functionalised scaffolds, compared to the negative control ($p<0.05$, $p<0.01$ and $p<0.001$ respectively). Higher counts were observed in the non-plasma treated scaffolds with 1000 ng of PF8, PF9 and PF17.1, though these were not significant. At 14 days, cell number further increased on plasma treated samples and the trend observed on day 7 perpetuated. Significantly higher cell number was detectable on 1000 ng of PF8 ($p<0.01$), PF9 ($p<0.0001$) and PF17.1 ($p<0.0001$) compared to the control samples. At day 28, it was observed that non-significant increases in cell number on non-plasma treated scaffolds occurred with all 1000 ng fibrillin-1 fragments plasma treated scaffolds however, decreased in cell number, with 1000 ng of PF9 showing significantly lower cell counts than the negative control ($p<0.01$).

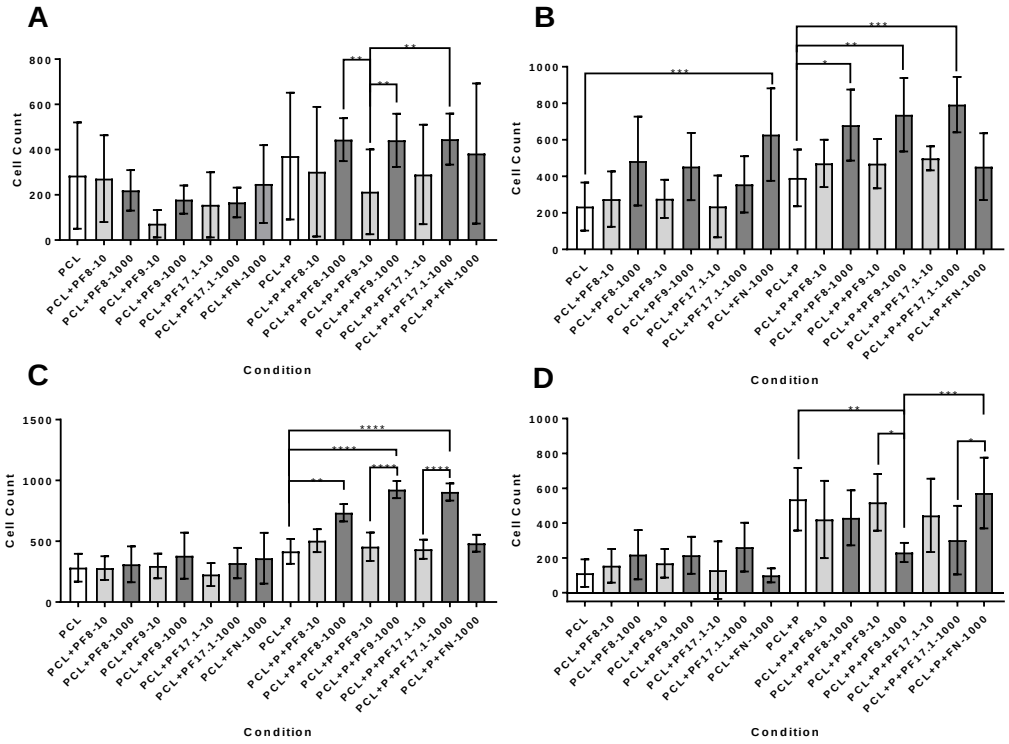

Figure 4-9 Cell counts at 1 (**A**), 7 (**B**), 14 (**C**) and 28 (**D**) days on scaffolds functionalised with fibrillin-1 fragments (PF8, PF9, PF17.1), acquired by analysing DAPI-stained cell nuclei per image taken. One-way

ANOVA was performed per time point and Tukey's post hoc test was applied. Mean ± SD displayed. * $p<0.05$, ** $p<0.01$, *** $p<0.001$, **** $p<0.0001$.

4.3.4.2 Total ECM Protein

Immunostaining of fibronectin (green), collagen type I (cyan) and fibrillin (red) showed visible differences in matrix maturity between the scaffold conditions (as depicted in Figure 4-10). Non-plasma treated PCL scaffolds showed largely random and disorganised matrices, with a seemingly low degree of cell and matrix alignment compared to plasma treated samples. Samples that were plasma treated also appeared to exhibit faster ECM development from the first time point, continued to deposit ECM proteins in a regular, and aligned fashion throughout the experiment. Such high level of both fibronectin and fibrillin may indicate a latent production of fibrillin due to fibronectin having to be deposited before fibrillin can be incorporated into the ECM[34].

Analysis was performed on all three fragments of fibrillin-1 (PF8, PF9, PF17.1) using a very low quantity (10 ng) and higher quantity (1000 ng). Fibronectin functionalised and untreated scaffolds acted as positive and negative controls respectively. To determine the effects of combination plasma treatment with the fibrillin-1 fragment functionalisation, non-plasma treated scaffolds were used as a comparison. As expected, non-plasma treated samples exhibited clustering of the cells (due to the hydrophobic nature of the material). Though the effect appeared to lessen at the 7 day time point, evidence of early stage clustering effects could still be observed at later time points.

Moreover, a correlation between nuclear count and ECM density can be observed on the immunofluorescent images tabulated below in Figure 4-10 and Figure 4-11. Plasma treated samples show obvious increased matrix maturity at 7 (both non-treated and treated with plasma) and at day 14 (plasma treated samples) when 1000 ng of fragment was adsorbed. Density of the ECM network appears much increased on day 14 when using 1000 ng fibrillin, however, appears to be subject to much more rapid degradation of the ECM at later (28 day) time points when compared to 10 ng samples and non-treated and fibronectin controls. Graphs of total ECM production, show that 1000 ng of fibrillin-1 fragment (all fragments) can increase ECM from 1 to 14 day time points, and can induce higher levels of matrix production that the fibronectin positive control at mid time points (7 and 14 days), though this effect is lost at 28 days.

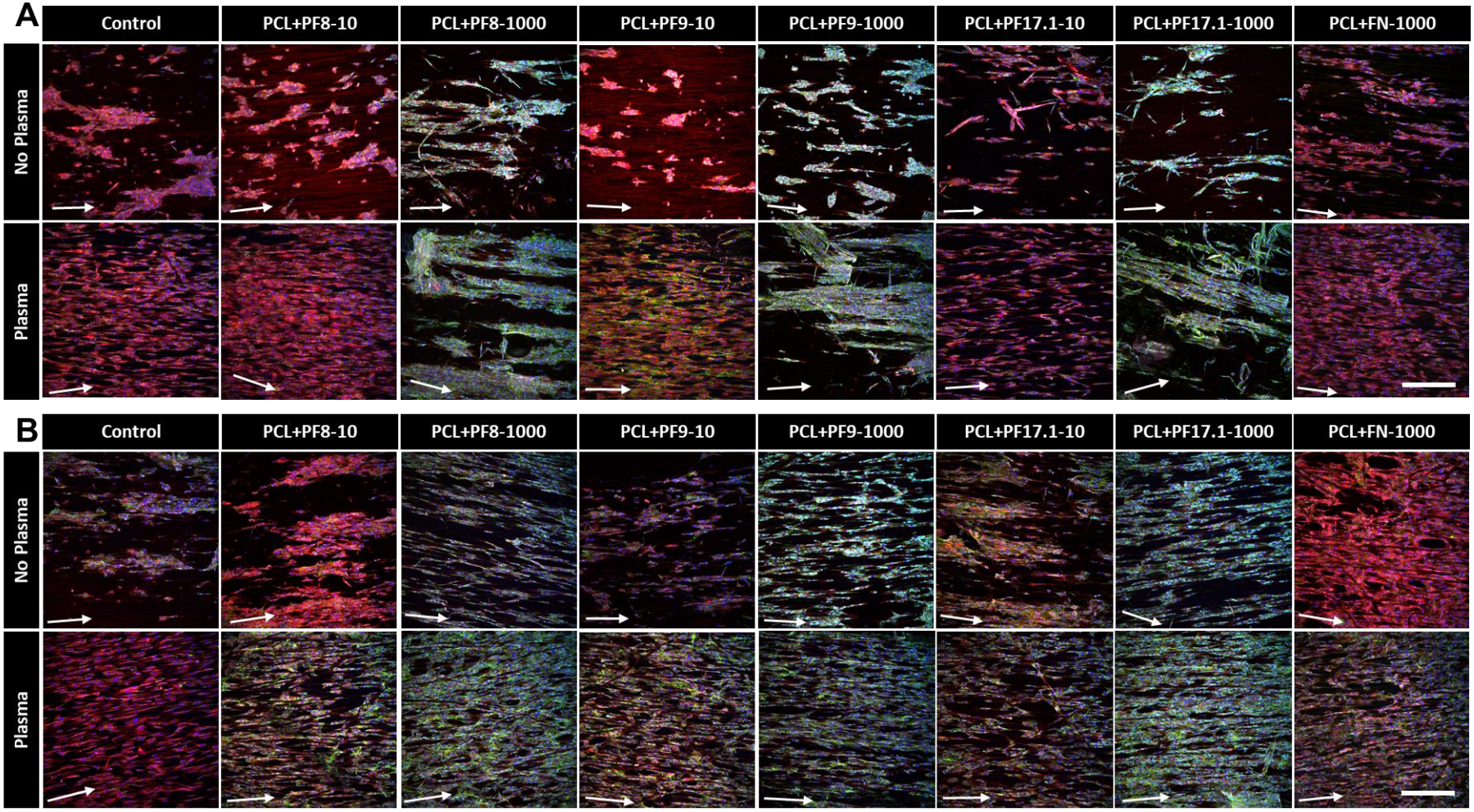

Figure 4-10 Fluorescent micrographs show the development of the ECM at 1 (**A**) and 7 (**B**) days. ECM components collagen type I (cyan), fibronectin (green) and fibrillin (red) were immunofluorescently stained to show ECM development over time. All samples were counterstained with DAPI (blue) to show cell nucleus and provide an approximate cell count for each condition. Arrows on the images show the orientation of the fibres. Scale bar represents 250 µm.

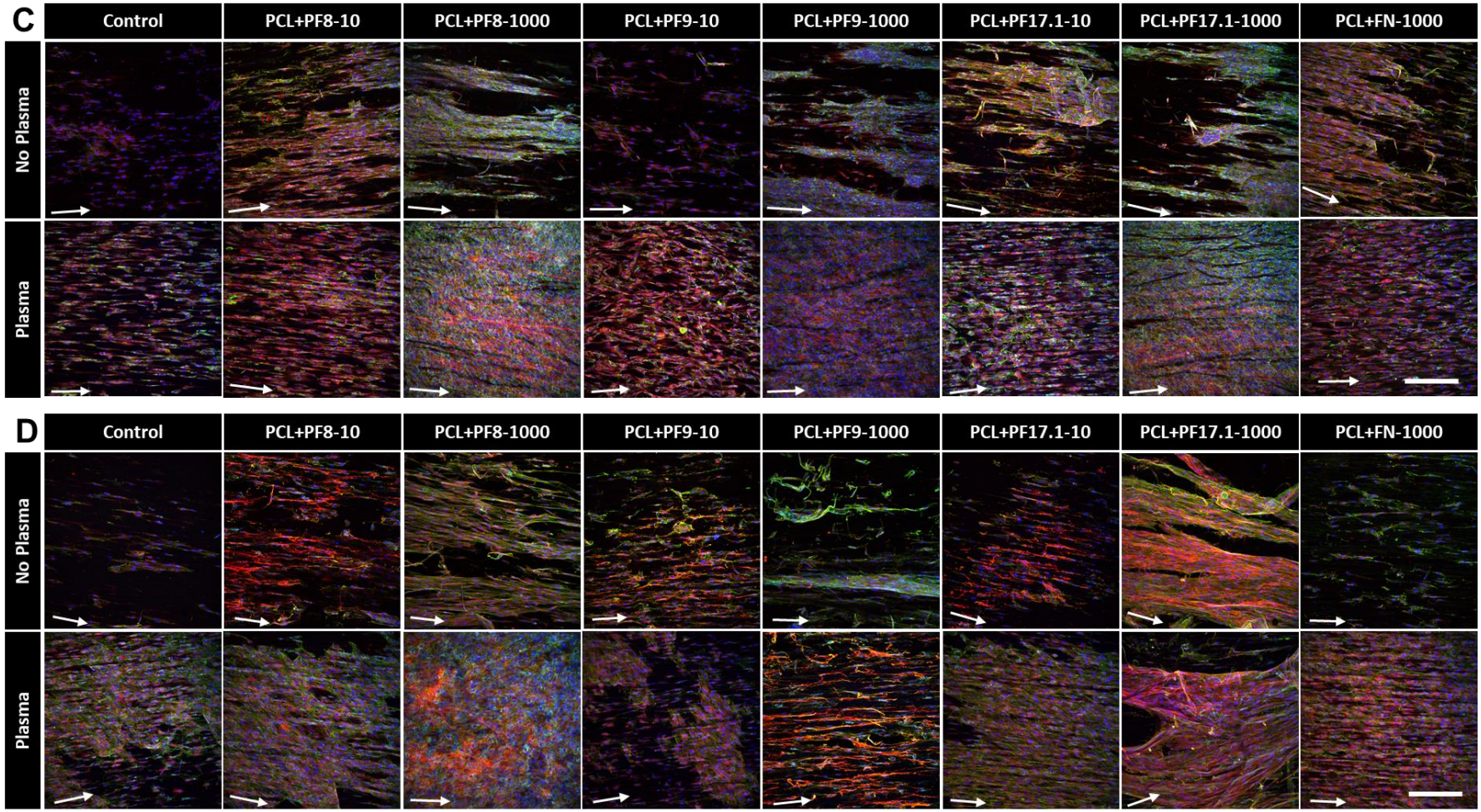

Figure 4-11 Montages of micrographs taken to show the development of the ECM at 14 (A) and 28 (B) days. ECM components collagen type I (cyan), fibronectin (green) and fibrillin (red) were immunofluorescently stained to show ECM development over time. All samples were counterstained with DAPI (blue) to show cell nucleus and provide an approximate cell count for each condition. Arrows on the images show the orientation of the fibres. Scale bar represents 250 µm.

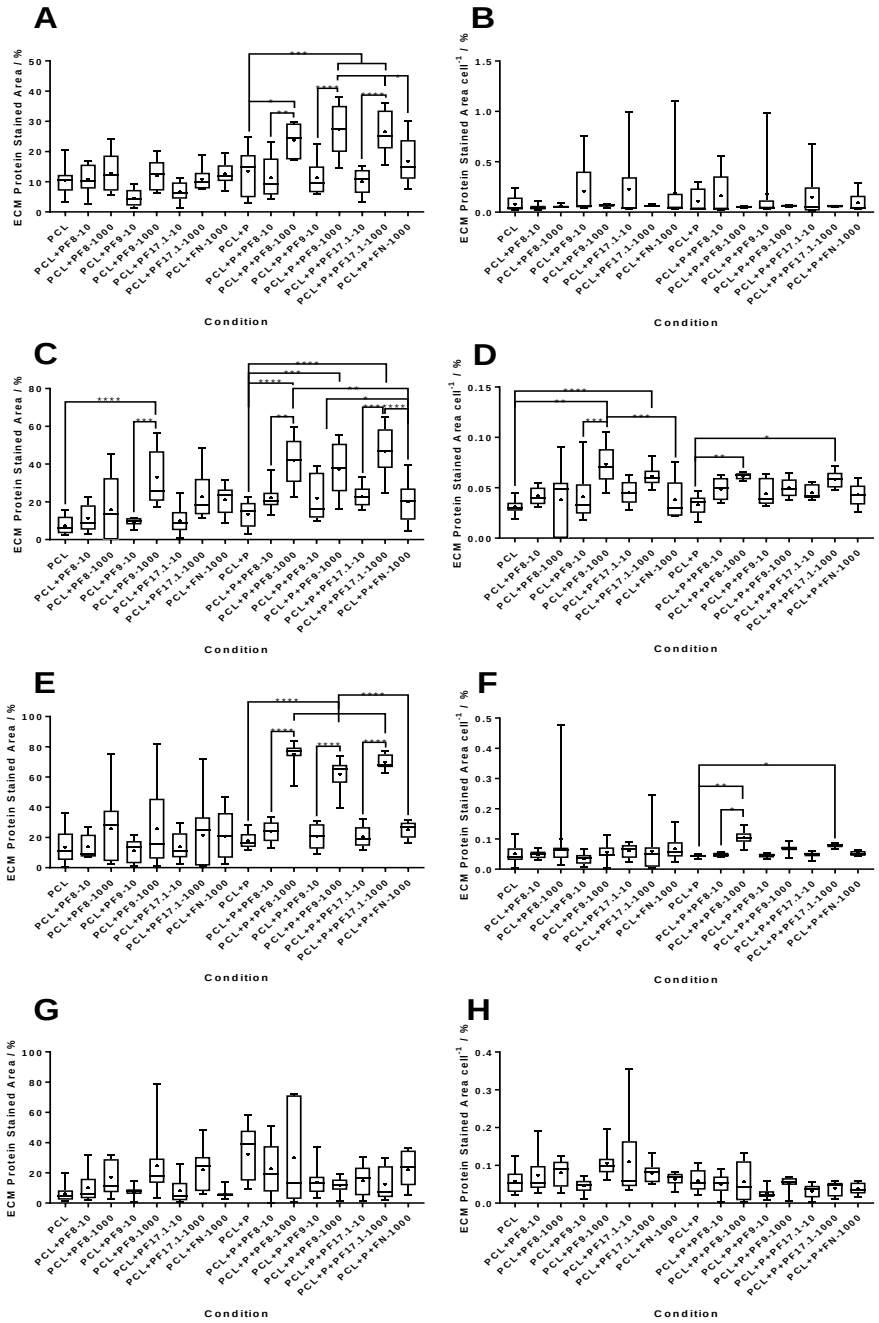

Figure 4-12 Total ECM proteins produced and analysed as % area at 1 (**A**, **B**), 7 (**C**, **D**), 14 (**E**, **F**) and 28 **(G**, **H**) day time points. Graphs were produced that detail total % area of ECM proteins (**A**, **C**, **E**, **G**) and % area when normalised to cell number (**B**, **D**, **F**, **H**). Box and whisker plats show the interquartile range, median and mean. Error bars show ranges. One-way ANOVA (with Tukey HSD post hoc tests) were performed on all graphs except B, F and H, which were subject to Kruskal Wallis H tests (with rank comparisons). Geisser-

Greenhouse corrections for non-sphericity were applied to every test. * $p<0.05$, ** $p<0.01$, *** $p<0.001$, **** $p<0.0001$.

4.3.4.3 Collagen Type I Production

Collagen type I, though produced at an intracellular level throughout the experiment, developed into fibrils, which were only observed at day 28 (Figure 4-14D), and were more prevalent in 1000 ng fibrillin-1 fragment conditions than 10 ng or controls (both negative controls and fibronectin controls). They appeared on non-plasma treated conditions with all fragments at 1000 ng, however could only be observed with the use of 1000 ng PF17.1 on plasma treated samples.

As shown by the graphs in Figure 4-15 below, collagen type I production was higher overall (non-significant) at 1 day post seeding on 1000 ng fibrillin-1 functionalised scaffolds than on the 10 ng counterparts (Figure 4-13A), though interestingly, the 10 ng conditions retained higher collagen type I production per cell (non-significant) at the same time point across both non-plasma treated and plasma treated scaffolds (Figure 4-15B). At day 7, production of collagen per cell appeared to stabilise amongst all conditions (Figure 4-15C), though total collagen appeared significantly higher on 1000 ng PF9 functionalised non-plasma treated scaffolds ($p<0.01$) and on all 1000 ng fragments on plasma treated scaffolds, compared to their respective negative controls (PF8 $p<0.01$, PF9 $p<0.05$, PF17.1 $p<0.0001$, Figure 4-15D). After 14 days in culture, 1000 ng fibrillin-1 fragment functionalised (plasma treated) scaffolds appeared to have increased collagen type I expression on the scaffolds, and maintained significantly higher expression than either the non-biofunctionalised controls or fibronectin-functionalised controls (all $p<0.0001$, Figure 4-15E). Though non-plasma treated scaffolds also demonstrated this trend, fibronectin functionalisation appeared to be of equivalent effectiveness for total collagen type I production, and all conditions, though increased, were non-significant to the negative controls. Production of collagen type I per cell appeared slightly higher than 10 ng conditions, negative and fibronectin controls on plasma treated conditions at this time point (Figure 4-15F), it was determined to be non-significant. At 28 days following cell seeding only 1000 ng PF8 appeared to have greater total collagen type I % area than the control on plasma treated scaffolds, whilst all 1000 ng conditions on non-plasma treated scaffolds showed similar effects on non-plasma treated samples (all non-significant, Figure 4-15G). Interestingly, this partially translated to production per cell (Figure 4-15H), where 1000 ng PF9 and PF17.1 produced significantly more collagen type I per cell than the negative controls ($p<0.01$ and $p<0.05$ respectively).

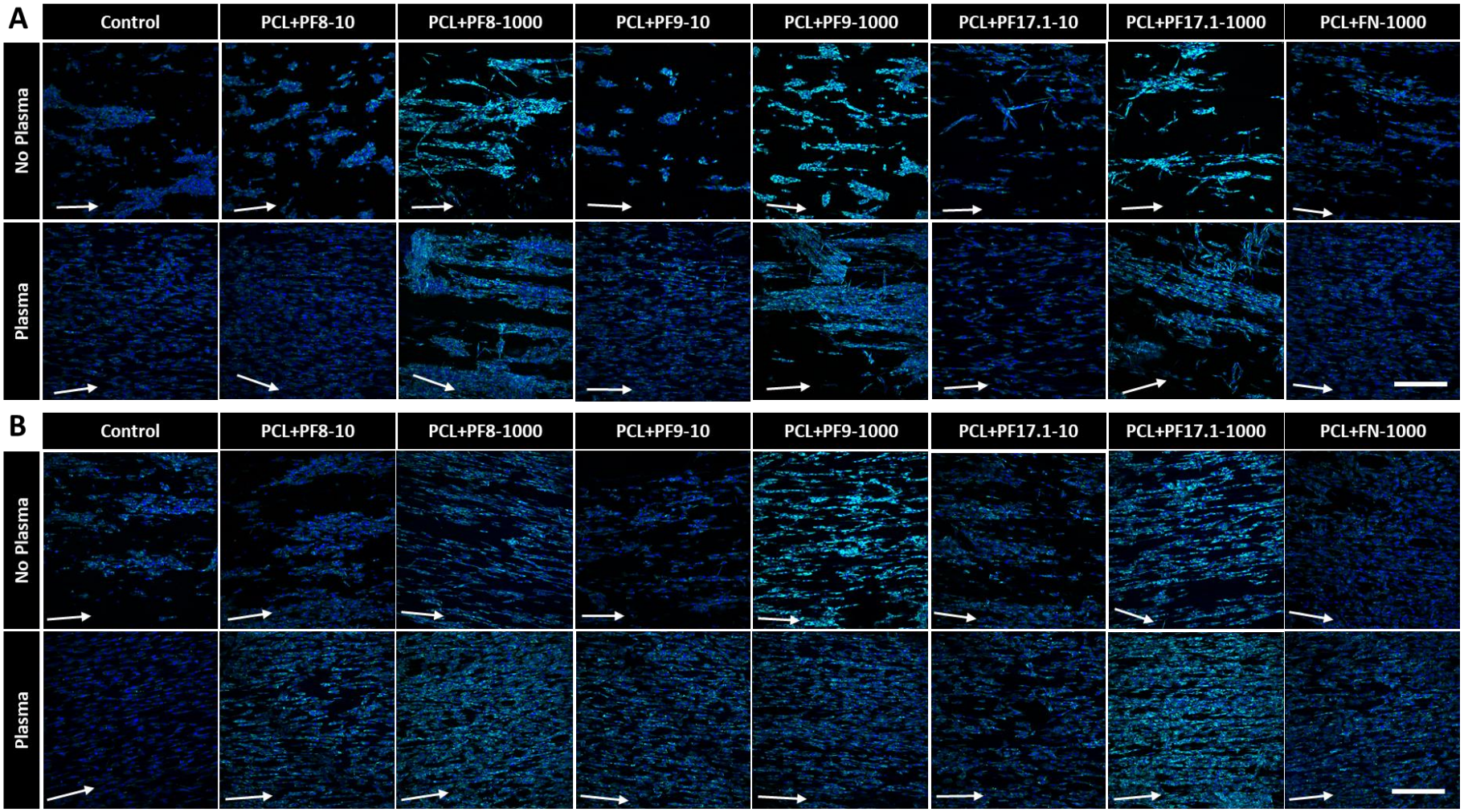

Figure 4-13 Montages of micrographs taken to show the production of Collagen type I (cyan) at 1 (A) and 7 (B) days. Collagen type I can be seen at early time points intracellularly. All samples were counterstained with DAPI (blue) to show cell nucleus and provide an approximate cell count for each condition. Arrows on the images show the orientation of the fibres. Scale bar represents 250 µm.

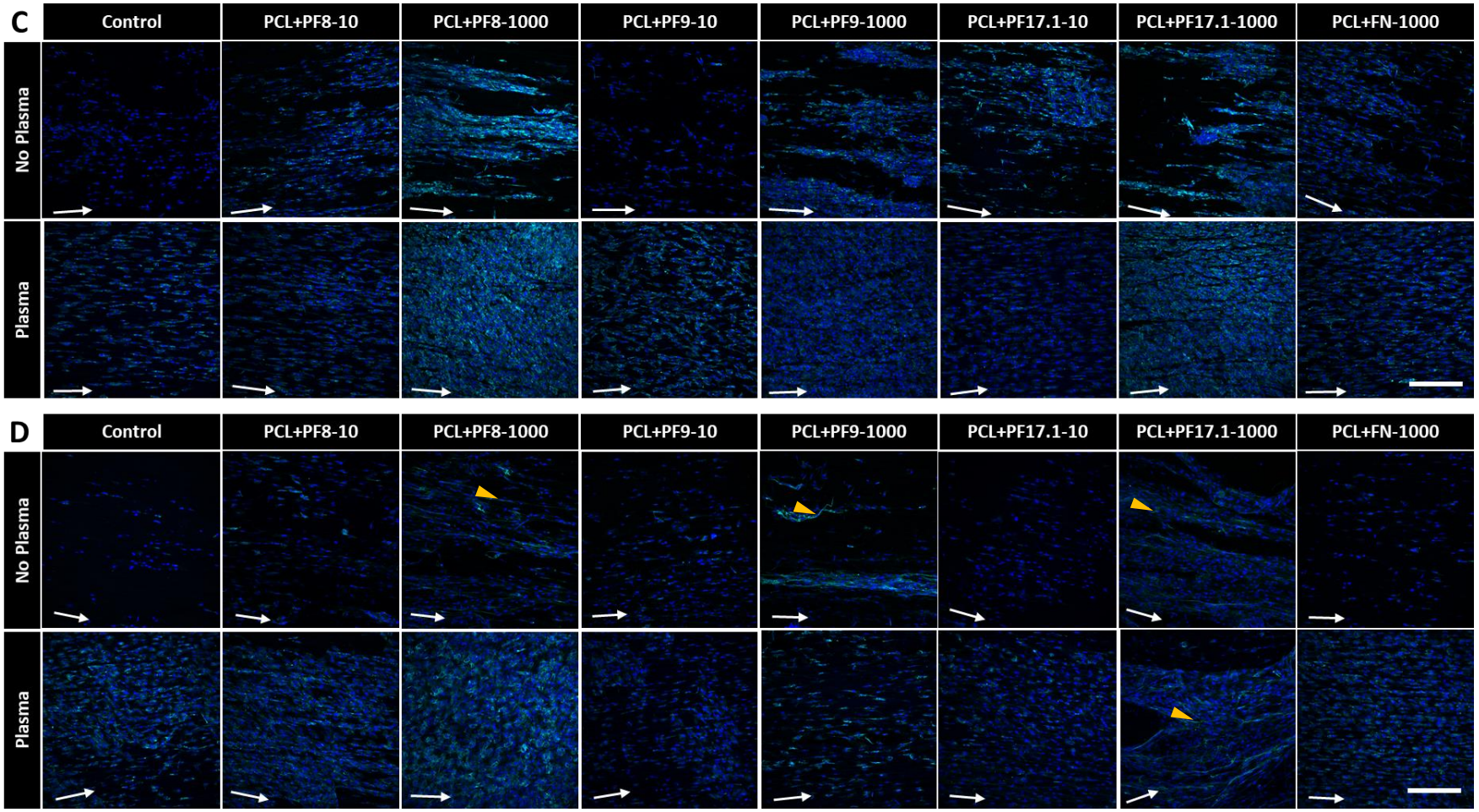

Figure 4-14 (Continued from Figure 4-13) montages of micrographs taken to show the production of Collagen type I (cyan) at 14 (**C**) and 28 (**D**) days. Collagen type I can be seen at later time points both intracellularly and as extracellular fibres in 28 day time point micrographs. All samples were counterstained with DAPI (blue) to show cell nucleus and provide an approximate cell count for each condition. White arrows on the images show the orientation of the fibres. Yellow arrowheads indicate collagen type I fibrils. Scale bar represents 250 µm.

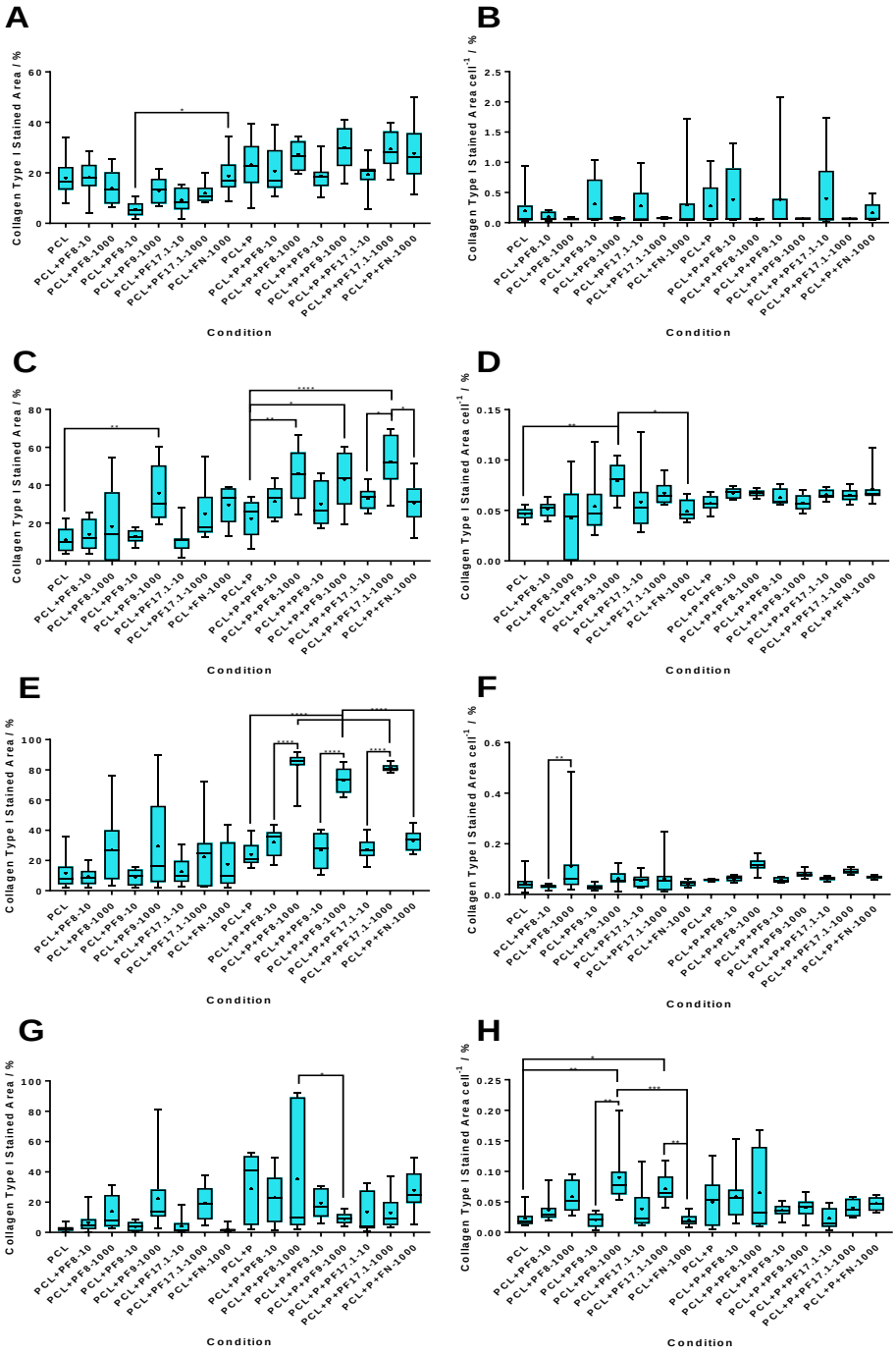

Figure 4-15 Collagen type I % area analysis of immunofluorescently stained cellular scaffolds at 1 (**A**, **B**), 7 (**C**, **D**), 14 (**E**, **F**) and 28 (**G**, **H**) day time points. Graphs were produced that detail total % area of collagen type I (**A**, **C**, **E**, **G**) and % area when normalised to cell number (**B**, **D**, **F**, **H**). Box and whisker plats show the interquartile range, median and mean. Error bars show ranges. One-way ANOVA (with Tukey HSD post hoc tests) were performed on **A**, **C**, **E**, **F** and **G**, with **B**, **D** and **H** subject to Kruskal Wallis H test (with rank

comparisons). Geisser-Greenhouse corrections for non-sphericity were applied to every test. * $p<0.05$, ** $p<0.01$, *** $p<0.001$, **** $p<0.0001$.

4.3.4.4 Fibronectin Production

Fibronectin is one of the preliminary proteins to be deposited into the neo-ECM, as it is integral for wound healing, and as the extracellular fibrils form template structures for both collagen[58] and fibrillin[34] deposition, it was expected that extracellular fibrils would be observed from a relatively early time point.

As such, fibrils appear at 7 days in the neo-ECM (Figure 4-16C), independent of the condition observed. At the first time point (1 day following seeding) total fibronectin density appeared much higher on the plasma treated, 1000 ng functionalised scaffolds than the negative controls ($p<0.0001$, Figure 4-18A). This trend was perpetuated with PF8 and PF9 on non-plasma treated scaffolds ($p<0.01$) however, PF17.1, though having a higher fibronectin % area than the control, was not significant in difference. Interestingly, PF17.1 (along with PF9) did appear to have produced more fibronectin per cell (Figure 4-18B) on the non-plasma treated scaffolds than the negative controls, where 1000 ng PF8 remained higher, but not significantly different. These trends were perpetuated to 7 days, with the exception of 1000 ng PF17.1 on non-plasma treated scaffolds, which produced significantly higher densities of fibronectin than the control, rather than PF8 (which now produced a non-significantly higher density than the negative control scaffolds, Figure 4-18C). All production per cell at 7 days, mirrored total production (Figure 4-18D).

By day 14, total fibronectin using the 1000 ng fibrillin-1 fragments, retained significantly higher densities on plasma treated scaffolds (PF8 $p<0.0001$, PF9 $p<0.001$, PF17.1 $p<0.0001$) when compared to both the negative controls and fibronectin (Figure 4-18E). On non-plasma treated samples, fibrillin functionalised scaffolds showed higher % area of fibronectin when compared to the negative controls, this was determined to be non-significant. Only 1000 ng PF8 on plasma treated scaffolds produced more fibronectin per cell than the negative control, PF9 and PF17.1 were increased, though remained non-significantly different (Figure 4-18F).

At 28 days, negative control scaffolds appeared to have the highest total area of fibronectin present (Figure 4-18G), but this was only significant to 1000 ng of PF9 on plasma treated scaffolds ($p<0.05$). No other significant differences were observed at this time point.

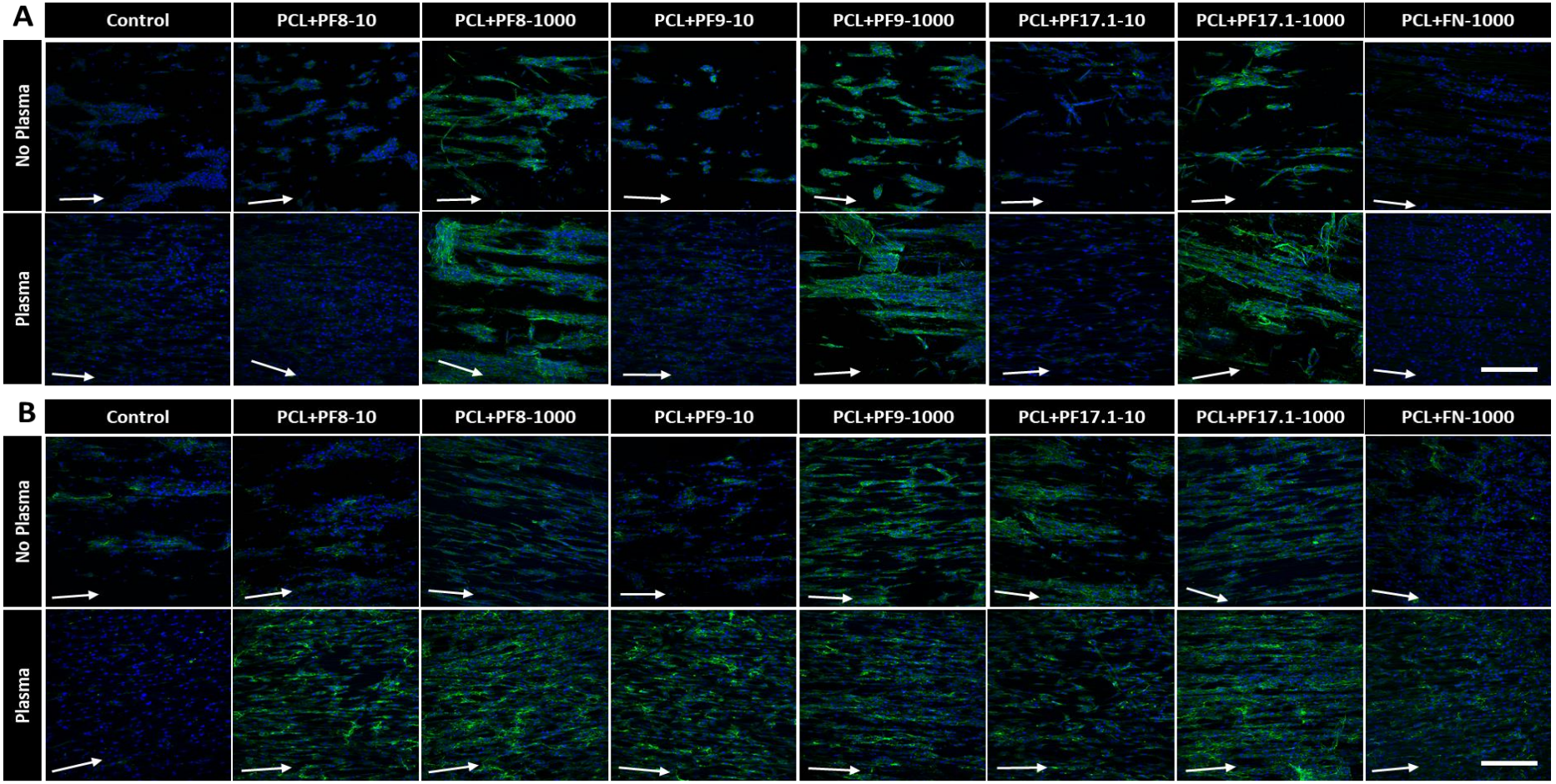

Figure 4-16 Montages of immunofluorescent micrographs which show the production of fibronectin (green) in the neo-ECM at 1 (A) and 7 (B) day time points. All images were counterstained with DAPI for clarity of cell position and for cell counting. All white arrows indicate the direction of construct fibre alignment and the scale bar represents 250 µm.

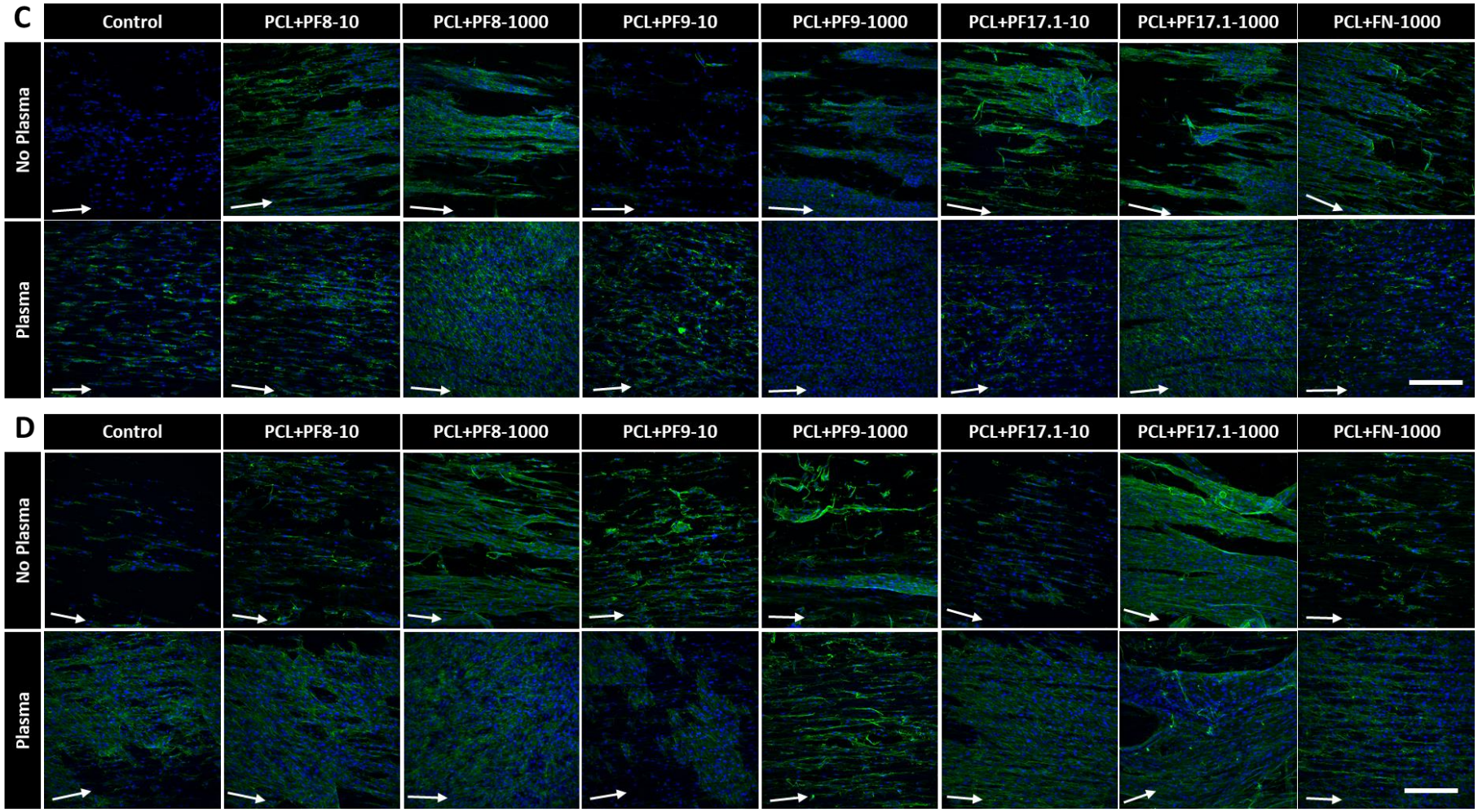

Figure 4-17 (Continued from Figure 4-16) montages of immunofluorescent micrographs which show the production of fibronectin (green) in the neo-ECM at 14 (C) and 28 (D) day time points. All images were counterstained with DAPI for clarity of cell position and for cell counting. All white arrows indicate the direction of construct fibre alignment and the scale bar represents 250 µm.

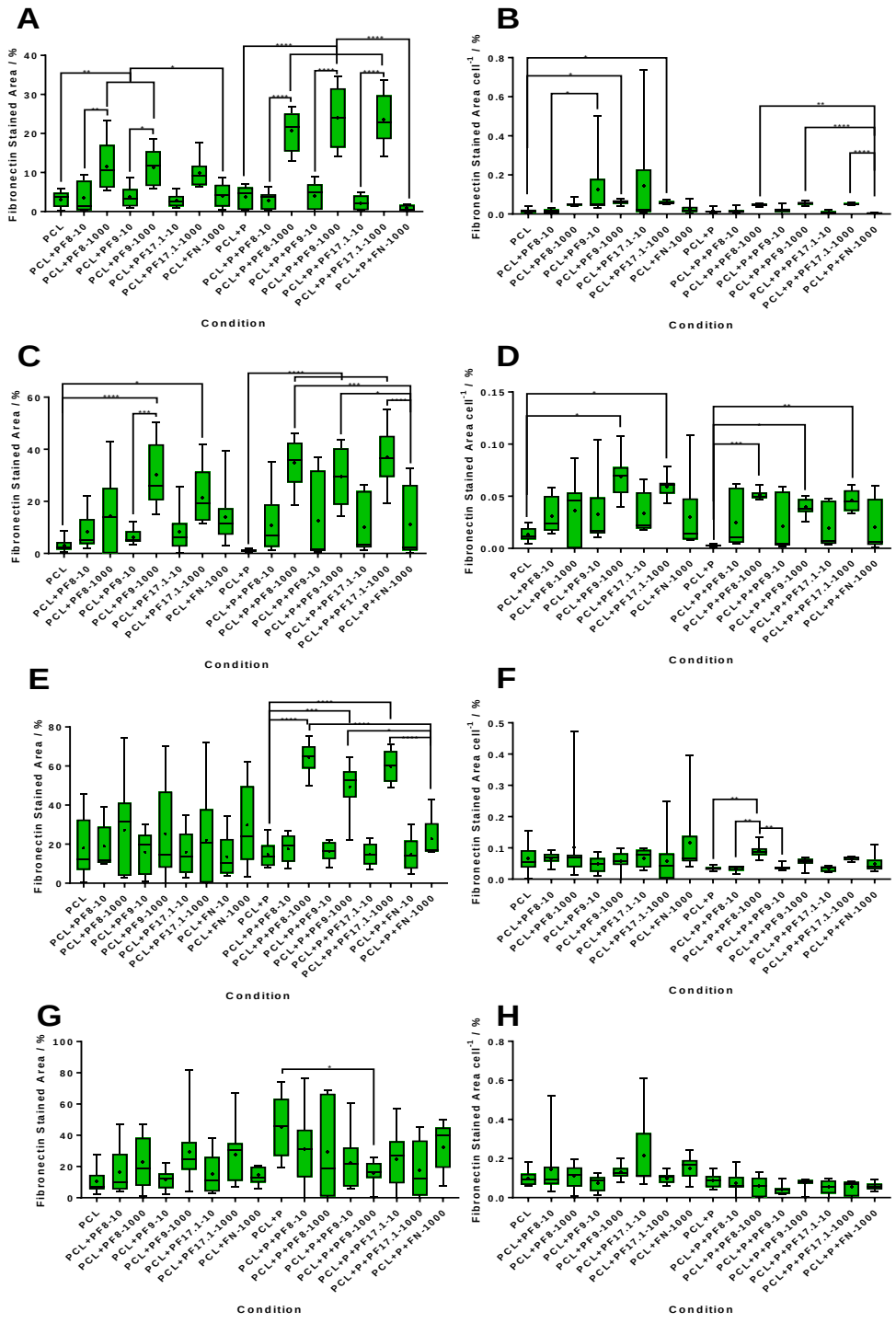

Figure 4-18 Graphs show the % area of fibronectin produced on each fibrillin-1 fragment functionalised scaffold at 1 (**A**, **B**), 7 (**C**, **D**), 14 (**E**, **F**) and 28 (**G**, **H**) day time points. Graphs were produced that detail total % area of fibronectin (**A**, **C**, **E**, **G**) and % area when normalised to cell number (**B**, **D**, **F**, **H**). Box and whisker plats show the interquartile range, median and mean. Error bars show ranges. One-way ANOVA (with Tukey HSD post hoc tests) were performed on **A**, **C**, **E**, **G** and **B**, **D**, **F**, **H** were subject to Kruskal Wallis H test (with

rank comparisons). Geisser-Greenhouse corrections for non-sphericity were applied to every test. * $p<0.05$, ** $p<0.01$, *** $p<0.001$, **** $p<0.0001$.

4.3.4.5 Fibrillin Production

Fibrillin is a later-stage ECM protein, associated with elastic fibre development, as the fibrils form a template for elastin deposition[306]. It appeared that all conditions showed evidence of cell-surface associated fibrillin-1[312] from 1 day post seeding (as observed in the fluorescent micrographs in Figure 4-19).

Interestingly however, 10 ng fibrillin-1 functionalised scaffolds appeared to support the production of more fibrillin up to 7 days (where fibrillin production remained either intracellular on localised with the cell, Figure 4-21A and C). Though 1000 ng PF9 appeared to perform equally to that of the 10 ng samples, on the non-plasma treated samples, but did not appear to produce the same quantities of fibrillin per cell.

At 28 days however (Figure 4-21G), 1000 ng PF9 did appear to produce significantly enhanced quantities of fibrillin compared to the negative controls ($p<0.05$) on non-plasma treated scaffolds, and though this trend did translate to production per cell, it was determined to be non-significant. It was noted however, that fibrillin production per cell did appear significantly increased to fibronectin-functionalised samples on plasma treated scaffolds (Figure 4-21H).

Fibrillin microfibrils can be observed on the fluorescent micrographs in Figure 4-20 from as early as 14 days with 1000 ng fragments on plasma treated scaffolds. It is clear to see however, that the microfibrils formed at 28 days on non-plasma treated 10 ng fibrillin-1 fragment scaffolds are short and somewhat disjointed compared to those on the plasma treated scaffolds (and the ones supported by 1000 ng of PF17.1), despite appearing to have directionality. The microfibrils formed using 1000 ng of all fragments on plasma treated scaffolds, show high degrees of directionality and have maintained an elongated and much less fragmented conformation.

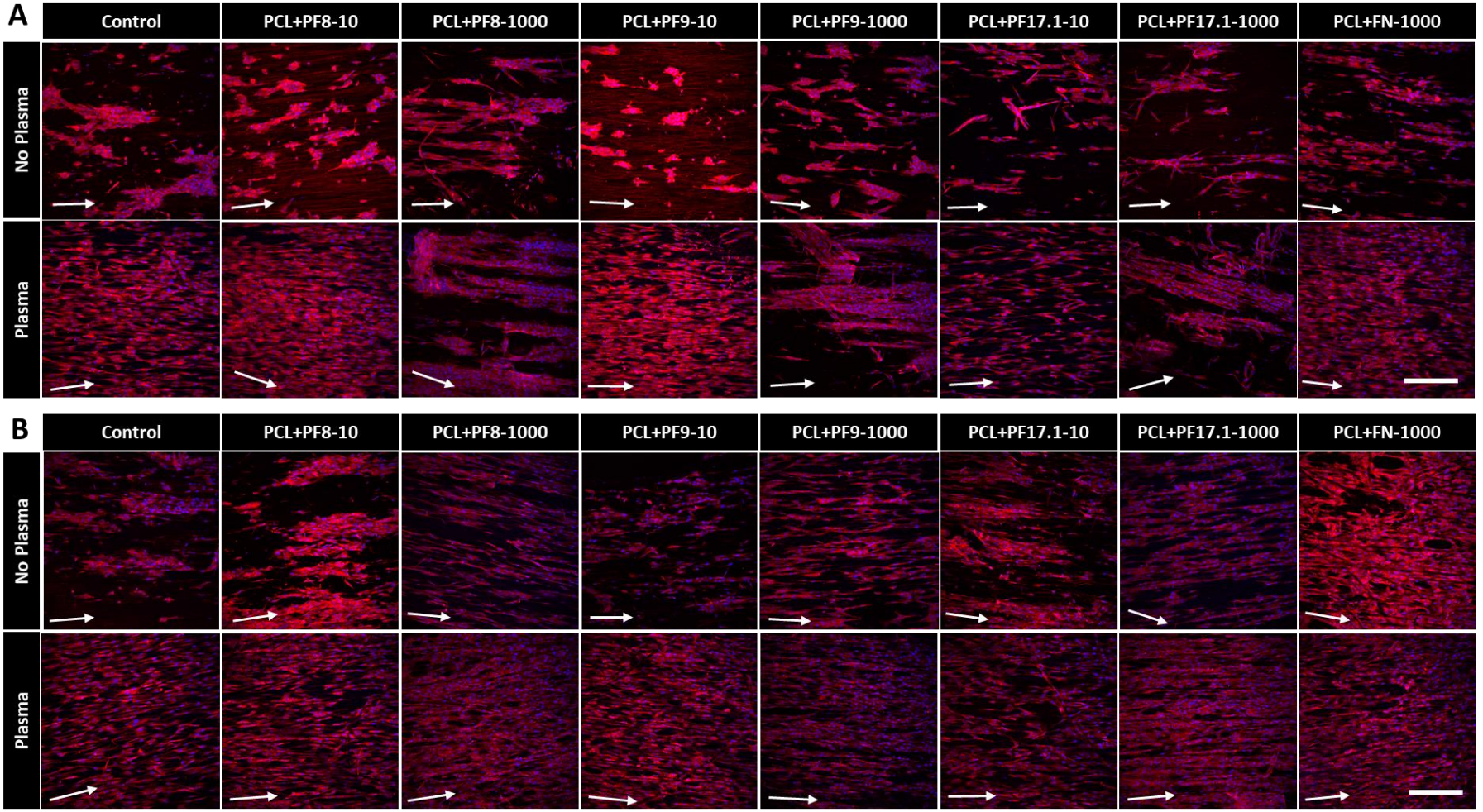

Figure 4-19 Montages of fluorescently stained neo-fibrillin production (red) by cACLs. Staining shows faint intracellular neo-fibrillin production at 1 (**A**) and 7 (**B**) days. All samples were counterstained with DAPI (blue) to provide cell locations and for cell number analysis. White arrows indicate fibre direction and the scale bar represents 250 µm.

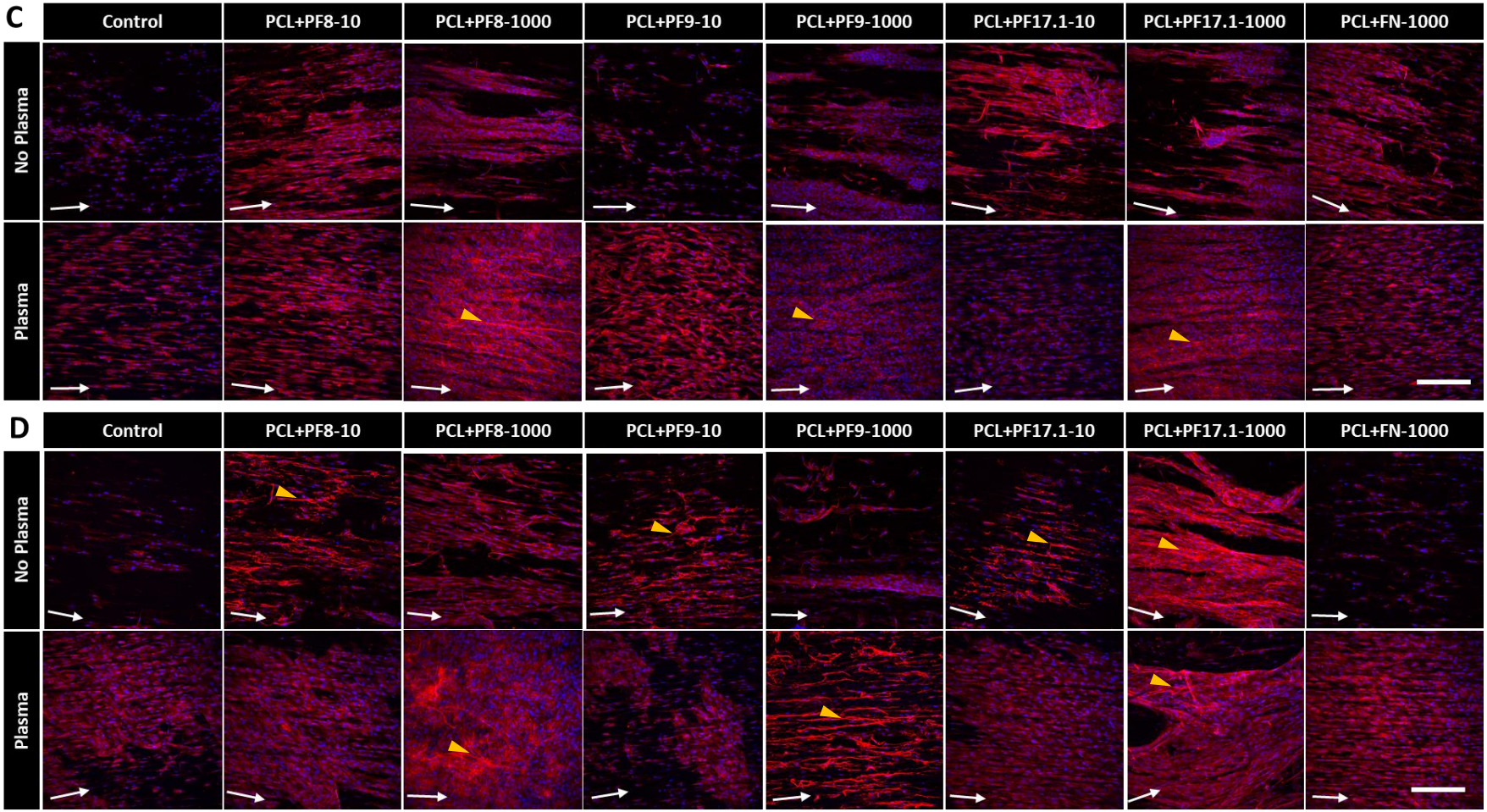

Figure 4-20 (Continued from Figure 4-19) montages of fluorescently stained neo-fibrillin production (red) by cACLs. Staining shows intracellular and fibrilliar extracellular neo-fibrillin production at 14 (**C**) and 28 (**D**) days. All samples were counterstained with DAPI (blue) to provide cell locations and for cell number analysis. White arrows indicate fibre direction and yellow arrowhead show fibrillar fibrillin-1 formation. Scale bar represents 250 µm.

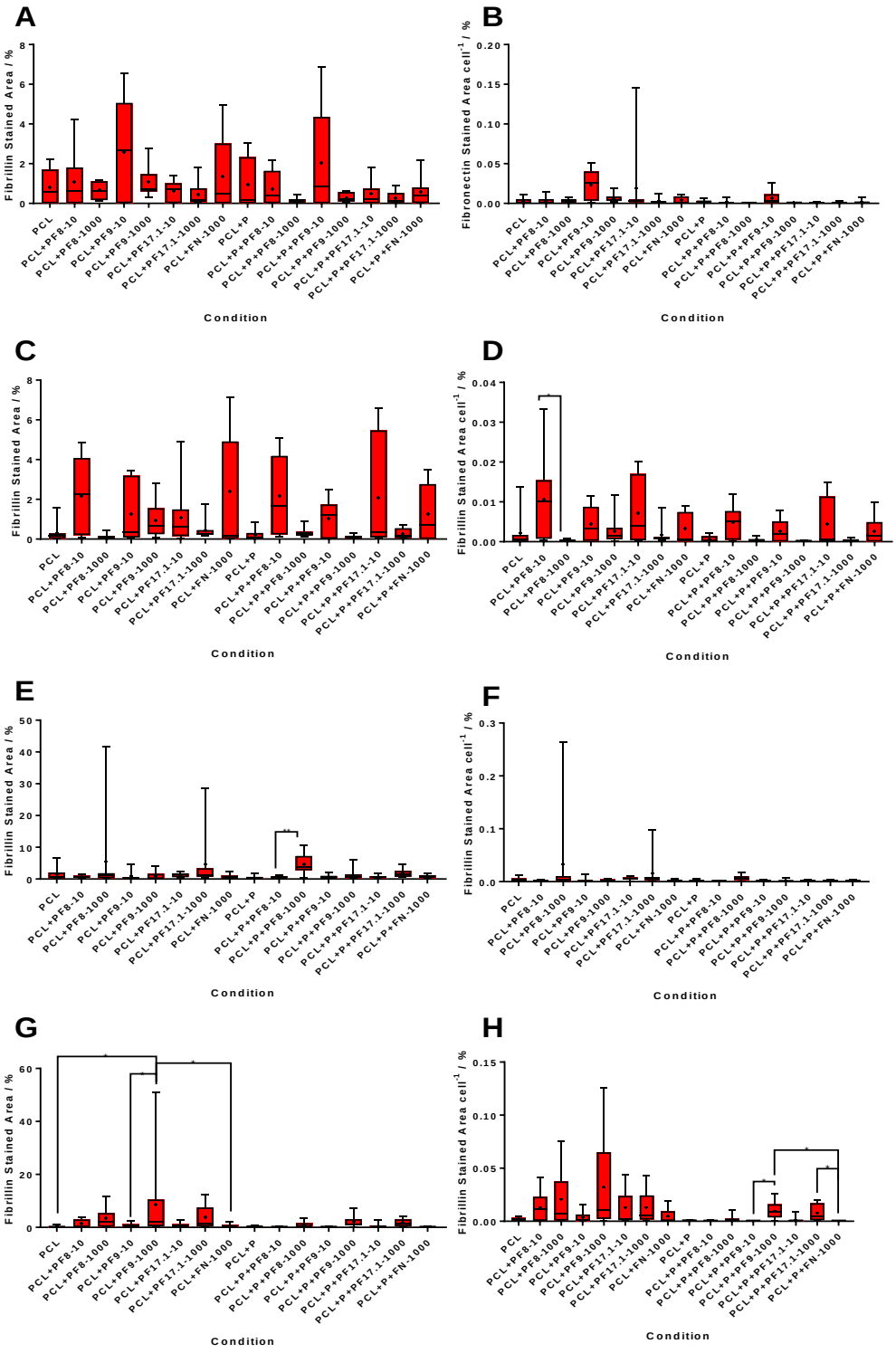

Figure 4-21 Graphs depicting the percentage area of fibrillin at 1 (A, B), 7 (C, D), 14 (E, F) and 28 (G, H) day time points. Graphs were produced that detail total % area of fibrillin (A, C, E, G) and % area when normalised to cell number (B, D, F, H). Box and whisker plats show the interquartile range, median and mean. Error bars

show ranges. Kruskal Wallis H test (with rank comparisons) was performed on all data sets. * $p<0.05$, ** $p<0.01$.

4.3.4.6 Intracellular Collagen type III Production

Collagen type III is an essential protein in the ACL ECM. It confers small amounts of elasticity in the ligament and will often occur in tissues that function under tensile stress. Cells were examined to determine whether the biofunctionalised scaffold could support the production of collagen type III and to ascertain the ligamentocytes' phenotype. Their ability to produce collagen type III ascertained that the cells were from the ACL midsubstance. Intracellular staining indicated the production of collagen type III within the cells on the conditions tested (Figure 4-22, Figure 4-23). This stain also elucidated on morphological changes of the cACL ligamentocytes between conditions. cACLs present on the plasma treated scaffolds and plasma treated-fibrillin-1 functionalised scaffolds appeared uniform in distribution and relatively elongated in morphology, compared to the untreated and corresponding fibrillin-1 functionalised scaffolds, where the scaffold appeared to facilitate cell clustering, and rounded cellular morphology on 10 ng conditions and slightly elongated cell masses of higher density in 1000 ng conditions.

Use of 10 ng of fibrillin-1 fragments PF8, PF9 and PF17.1 did not appear to have any profound effect on the ligamentocyte behaviour, compared to the negative control at any time point. Production of collagen type III appeared universal and cell shapes, with the exception of non-plasma treated PF17.1 at 14 days, displayed elongation along the fibre longitudinal axis. At earlier time points cells appeared to produce more collagen type III when exposed to the fragments. When observing the PCL samples, samples coated with the fragments did not have any discernible differences when compared against their negative controls. Image quality decreased when imaging cells on scaffolds treated with PF8 due to enhanced integration of cells into the scaffold. Interestingly, at later time points, cells on PF8 appeared less clustered on non-plasma treated scaffolds and more clustered on plasma treated ones than those on subjected to the PF9 or PF17.1 fragments.

Functionalisation with 1000 ng of fibrillin fragment proved to have a definitive effect on the ligamentocytes throughout all time points on non-plasma treated scaffolds. At 1 day post seeding, cells can be observed elongating along the fibres, with marked clustering still observable in the non-biofunctionalised controls. This effect was also observable at 7 days, where increasing coverage could be observed. At 14 days, PF8, PF17.1 and fibronectin appeared to perpetuate elongation of the ligamentocytes, whilst smaller but distinct clusters

could be observed on the non-biofunctionalised controls. PF9 displayed decreased cell density and subsequently, less collagen type III production. Plasma treated scaffolds maintained high degrees of anisotropic alignment of the scaffolds throughout all time points, though small amounts of clustering were observed on non-biofunctionalised controls at 1 and 7 days when compared to the fibrillin-1 fragment and fibronectin functionalised controls. Only small amounts of collagen type III appeared to be less obvious at 1 and 7 days, with more obvious staining present at day 14.

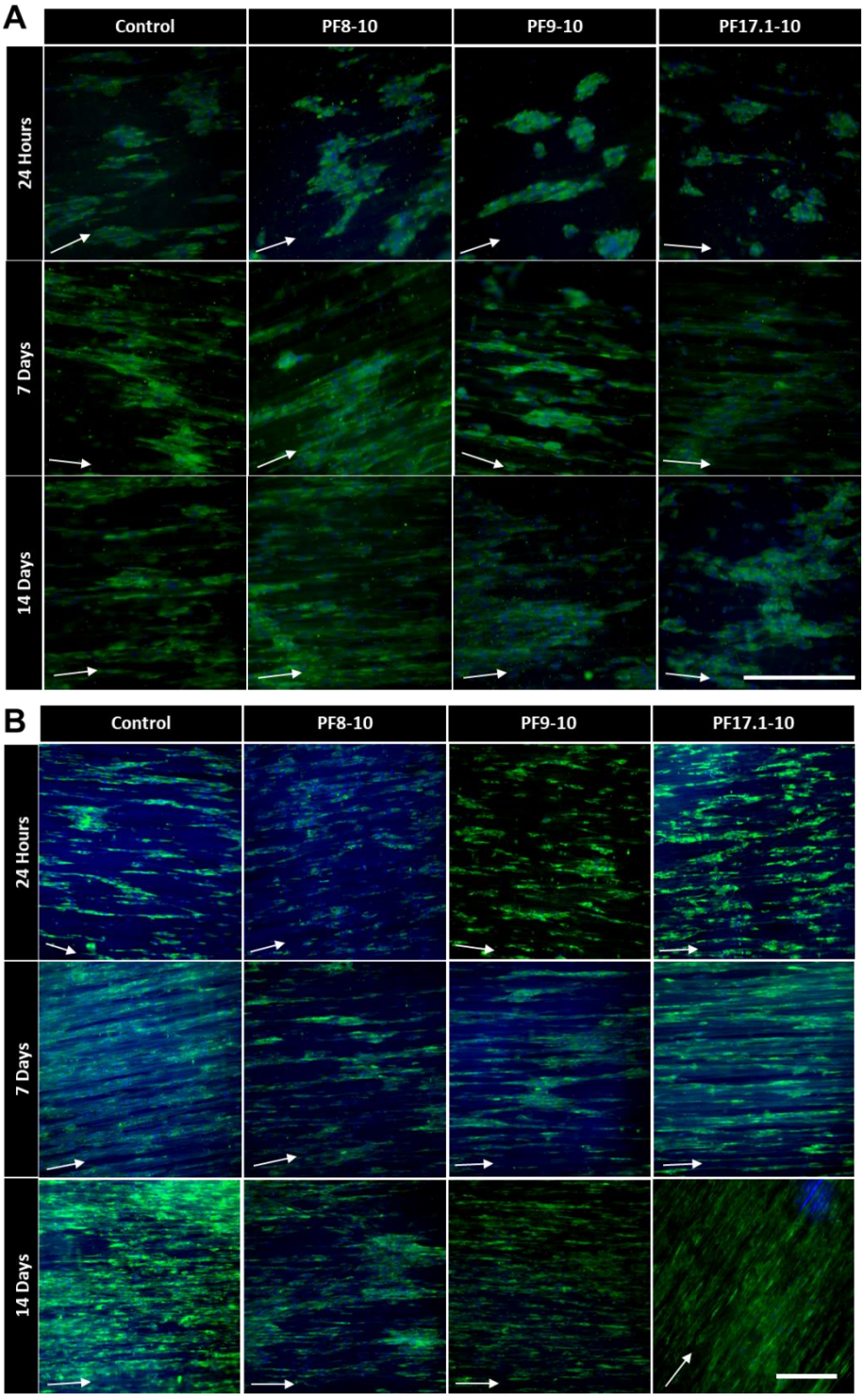

Figure 4-22 Intracellular collagen type III expression when primary canine ACL cells (cACLs) have been cultured on PCL scaffolds with 10 ng of different fibrillin-1 fragments for 1, 7 and 14 days (n=2) on non-plasma treated (**A**) and plasma treated (**B**) scaffolds. White arrows indicate the direction of the fibres, scale bars on the images represent 250µm. Green staining shows the presence of cytoplasmic collagen type III, while blue DAPI staining enables visualisation of the cell nucleus. Negatives and staining blanks are available in Appendix 10. Though parameters could not be kept the same throughout the whole experiment due to cell integration with fibres, each set of images were kept at the same parameters for their conditions, i.e. all untreated PCL and all treated PCL. Experiment was performed once.

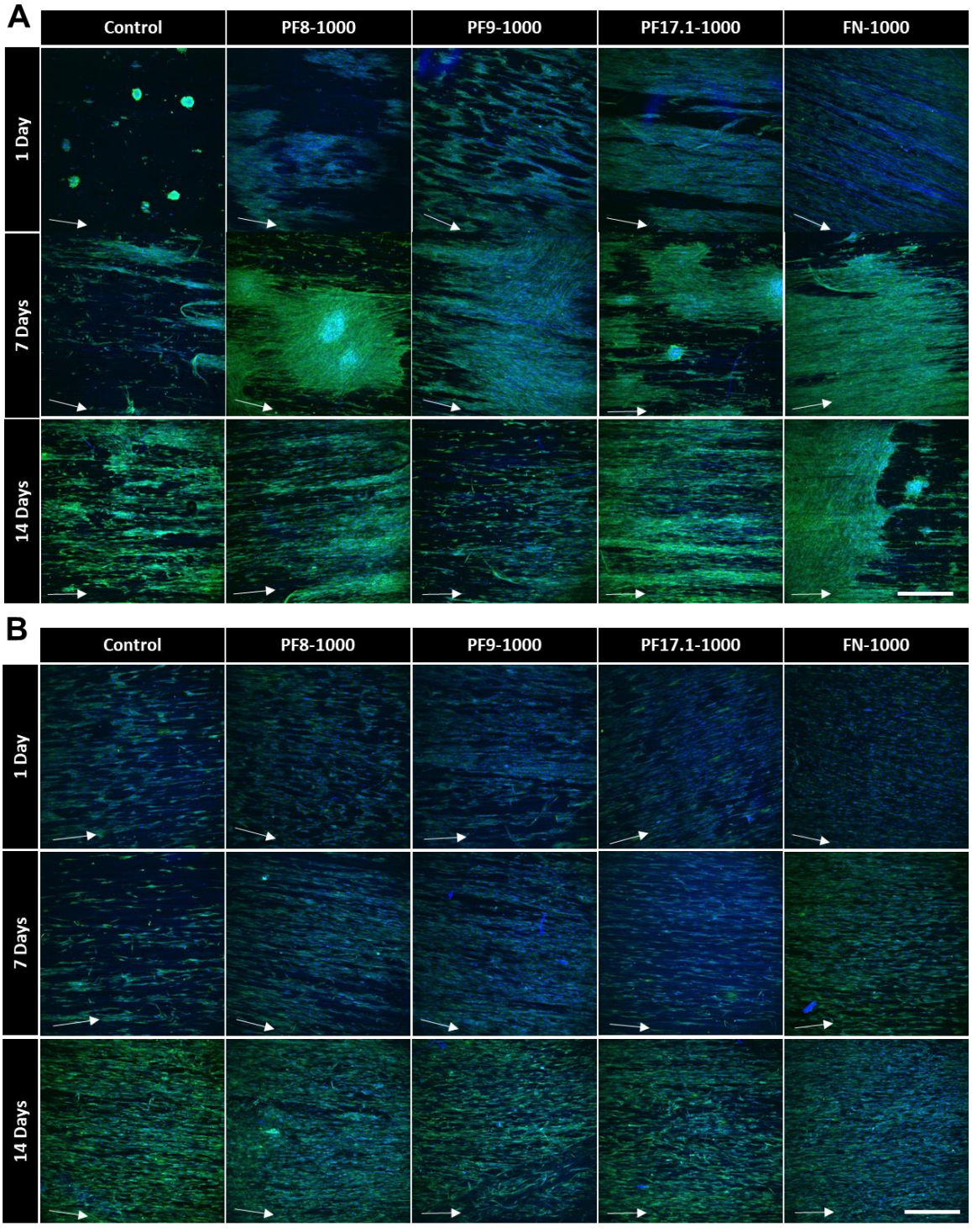

Figure 4-23 Collagen type III immunofluorescent micrographs on 1000 ng fibrillin-1 fragment biofunctionalised scaffolds (n=3). Cellular scaffolds were immunostained for collagen type III (green) and counterstained with DAPI (blue) at 1, 7 and 14 days on non-plasma treated (**A**) and plasma treated (**B**) scaffolds. 'Control' samples are non-biofunctionalised and FN samples are functionalised with fibronectin. Imaging parameters were kept consistent between all samples. White arrows indicate fibre direction and scale bars represent 500 µm. Negatives are available in Appendix 10.

4.3.5 Early Stage Orientation of cACLs on Fibrillin-1 Functionalised Scaffolds

To quantifiably assess the orientation of the cACLs on the scaffolds at early time points (1 day post seeding), a plug in for FIJI ImageJ – 'OrientationJ' was used. Figure 4-24 displays details of the distributions of those calculated orientations, and the variations in the standard deviations of those distributions. Curves for non-plasma treated scaffolds (Figure 4-24A) and plasma treated scaffolds (Figure 4-24C), show Gaussian distributions of the orientation angles determined by the software. Taller, narrower curves imply higher degrees of alignment along the fibres. It appeared from the data presented, that 1000 ng conditions were more capable of supporting good uniaxial alignment of cells along the fibres at early time points. Figure 4-24B shows that on non-plasma treated scaffolds, PF9-10 had the broadest range of orientations (40.06°), which was significantly higher ($p<0.01$) than FN-1000, which showed the narrowest range (12.30°), closely followed by PF8-1000 and PF17.1-1000 (12.35° and 12.88° respectively). Figure 4-24D displays PF17.10 as having the broadest orientation angle at 12.08°, which was significantly different ($p<0.05$) to the narrowest orientation angle spread in PF9-1000 (9.017°), closely followed by PF8-1000 (9.393°).

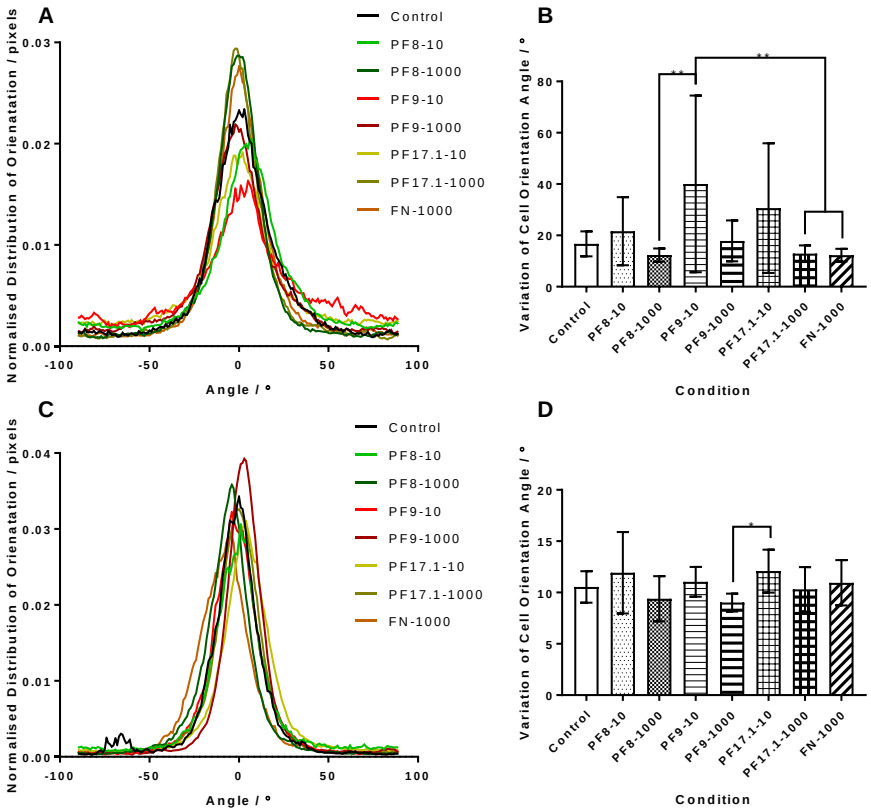

Figure 4-24 Orientation analysis of cACLs on fibrillin-1 functionalised scaffolds using intracellular collagen type I immunofluorescent staining at day 1. Normalised (to total counts) distributions of orientation of the

cACLs on non-plasma treated (**A**) and plasma treated (**C**) scaffolds. Variation of the spread of orientation, calculated from the SDs of each repeat measure (n=9 per condition) are shown for non-plasma treated (**B**) and plasma treated conditions (**D**). Kruskal Wallis H tests were performed with rank comparisons. *$p<0.05$, **$p<0.01$. Performed once.

4.4 Discussion

Initial (1 hr) attachment assessments showed that between the fibrillin-1 fragments, 1000 ng of PF8 and PF17.1 facilitated the highest cell attachment, with cells producing a significantly lower attachment response to PF9 than either PF8 ($p<0.05$) or PF17.1 ($p<0.001$). A possible explanation for this may be that the PF9 lacks the synergy site, which has been shown to be essential for cell-RGD binding in fibronectin. In fibrillin-1, the synergy site occurs as the upstream cbEGF domains 19-21, which has previously been determined to mediate RGD-cell interactions with human dermal fibroblasts via the $\alpha_v\beta_3$ integrin[310, 311]. Though in cACLs, results appear to imply that the synergy region has an enhancing effect only and attachment to the RGD site is not dependent upon its presence, as observed in PF9.

The attachment study was corroborated with both LIVE/DEAD and Alamarblue assays. For this reason, it is justifiable to assume that Alamarblue can be used as an indicator of cell number/attachment at these time points. Alamarblue is widely used as an indicator of attachment, proliferation, and cell number (though reportedly leads to an overestimation of cell number[401]). Enhanced attachment and cell number was observed with using 1000 ng of PF8 and PF17.1 at early time points on glass and untreated PCL with Alamarblue, however, this trend did not extend to the plasma treated scaffolds; large variation in donor ligamentocyte response determined that metabolic response of the cACLs on the plasma treated scaffolds were inconsistent. This may have also been due to the strong attachment mechanisms of hydrogen bonding between the cells and the plasma treated fibres, due to the surface not being saturated with fibrillin-1 fragment. Cheng *et al.* (2013)[402] have previously shown that plasma treatment alone can enhance cell attachment properties in the short term, resulting in enhanced cell attachment. LIVE/DEAD and metabolic activity from Alamarblue appeared to show a general trend at early time points, indicating higher attachment (and subsequently cell number) up to 24 hrs. Interestingly, 1000 ng fibrillin-1 fragments PF8 and PF17.1 encouraged elongation along the longitudinal axis of the fibres, comparable with fibronectin, evidencing the fragment's promise in supporting ACL cells in their native conformation. Cells are required to have native morphology in order to regulate tissue and

function-specific genes/proteins[167, 168] and ECM alignment is highly dependent on the alignment of the cells on the scaffold. PF8 and PF17.1 have shown that at early time points, they have the potential to support cells in their native morphology and distribution, equal to that of fibronectin. Though LIVE/DEAD can be quantified using a fluorescent plate reader, this was not performed. It was determined that due to the auto-fluorescence of the PCL fibres at $\sim\lambda_{exc}$490nm[403], and the non-specific adsorption of the ethidium homodimer label to the plasma treated fibres, the readings would be skewed. LIVE/DEAD was selected for use due to its ability to deliver multiple sets of information about cell-material interactions. Cell morphology of the live cells can be observed, as well as the live to dead cell ratio. The latter however, can be highly inaccurate. Adhesion-dependent cell death results in detachment from the substrate and consequently, cells are often washed away during the LIVE/DEAD assay-washing step, revealing live to dead ratios that are incorrect. Data presented does appear to show that 10 ng has little effect on the attachment or conformation of the cells, in contrast to results shown by Sakamoto *et al.* (1999)[309] upon which the justification for using this amount of fibrillin-1 fragment was based. It is important to note that the cells used by Sakamoto *et al.* were fibroblasts from the ligamentum nuchae, a tissue which has an unusually high elastic fibre content (associated with fibrillin-1) compared to most ligaments[404]. The second cell type used (chondroblasts) were from a matrix where elastin is sparse, and required higher amounts of fibrillin-1 for optimal attachment[309]. Use of 1000 ng was justified using a publication by Hajian *et al.* (2014)[315], where the order of magnitude required for effective cell response was determined. Though the study by Hajian *et al.* was performed with endothelial cells (cell type from elastin-rich tissues), data acquired in this thesis appears to agree that enhanced attachment and response can be observed at this magnitude of fibrillin-1 fragment. From the data gathered it appears that different cell types may require differing fibrillin-1 fragment concentration thresholds in order to elicit a positive response.

Confirmation of attachment through $\alpha_v\beta_3$ and $\alpha_5\beta_1$ integrins to the RGD motifs present in the fibrillin-1 fragments[30] was performed with both integrin blocking and integrin staining. Of the fibrillin-1 fragments, PF8 fragment was selected, due to the inclusion of the RGD synergy site within the fragment[311]. Cells seeded on both fibronectin and PF8 showed clear, positive staining for $\alpha_v\beta_3$ and clear presence of integrin expression at the cell membrane. Blocking of the $\alpha_v\beta_3$ integrin appeared to have a significant impact on the cell morphology, with cells seeded on both PF8 and fibronectin samples forming spherical conformations and

failing to spread. Rounded morphology is often indicative of a lack of attachment in adherent cell populations and was used as a positive marker of integrin inhibition[395]. For PF8, this was perpetuated during $\alpha_5\beta_1$ integrin blocking, along with bright intracellular/perinuclear staining. On the other hand, blocking of the $\alpha_5\beta_1$ for fibronectin did not prevent cell spreading at 1 hr time points and much weaker intensity of staining was observed. It has previously been reported that different cells will favour different integrins when interacting with the same proteins[30]. Considering the data presented, it is a possibility that ACL fibroblasts may use $\alpha_v\beta_3$ preferentially when interacting with the fibronectin, possibly due in part to the integrin $\alpha_v\beta_3$ being mechanically sensitive[264] and fibronectin's dependence on mechanical loading of the ACL ECM[97]. This may also explain why the blocking of $\alpha_5\beta_1$ appeared to have no impact on ACL cells attachment to fibronectin. Though it may be possible to imply these explanations from the data gathered, repeating of this experiment would be required to enable a more robust conclusion. Differences in canine cell response compared to reported literature may also have been due to the fragment being of human origin, and potential inter-species differences in fibrillin-1 amino acid conformation. It has been determined however, that fibrillin-1 is well conserved between mammals, and the TB4 domain, which all three of the fibrillin-1 fragments contain, is identical between canine and human fibrillin-1, limiting this theory[307].

Due to the ligamentocytes' trilineage differentiation capacity[69], and reports of fibrillin-1 fragment's ability to support differentiation (to chondrocytes) in stem cells[389], it was necessary to ensure that the cACLs were not differentiating into osteogenic lineages on the treated scaffolds. An ALP assay was performed to verify this. The results displayed provided evidence against the potential formation of calcium deposits in the neo-ECM, and determined that ligament regeneration with canine primary cells could be successful. It would also be prudent to determine whether the functionalised scaffold supports chondrocyte differentiation. As GAGs and small amounts of aggrecan are native to the midsubstance of the ACL[51], an alternative protein should be selected for detection, such as collagen type II.

For area (%) semi-quantification, it was determined that fibrillin-1 fragments contribute to the enhancement of the neo-matrix. Total ECM, collagen type I and fibronectin production were all shown to be enhanced by 1000 ng fibrillin-1 fragments at 1 (fibronectin), 7 and 14 days (collagen type I, total ECM). However, this may be an effect of the increased cell number supported by the biofunctionalisation with PF8, PF9 and PF17.1, as shown by the nuclear counts performed, using DAPI. To account for this, ECM protein production was

also normalised to cell number and analysed. PF8 and PF17.1 supported higher ECM production per cell at various time points with increased total ECM, collagen type I, and fibronectin. Both fragments displayed superior neo-fibrillin production per cell when compared to the fibronectin-functionalised controls, following 28 days of culture. The reason for this latter enhancement perhaps lies in the way in which the neo-fibronectin functions in the ECM. Fibronectin assembly is essential for the deposition of fibrillin[34] and forms a 'template' for its deposition. This is could be the reason for the steady increase in fibrillin, in line with fibronectin. At the 28 day time point, however, fibronectin content can be seen to decrease in total area for the 1000 ng fibrillin-1 fragments, with fibrillin total area also dropping slightly. At this time point however, micrographs displayed the formation of microfibrillar fibrillin, evidencing the cells exportation of this protein into the ECM. Interestingly, the exportation of fibrillar fibrillin on 10 ng functionalised, non-plasma treated scaffolds, may have something to do with the clustering of cells enabling them to form dense fibronectin networks that might aid in the deposition and organisation of fibrillin fibrils. This does not explain however, the lack of fibrillin microfibrils present on the non-functionalised controls. This exportation of fibrillar proteins could be interpreted as a change from an immature to mature ECM, although, the use of fibronectin as a functionalisation protein did not enhance fibrillin deposition. Fibronectin has also been implicated in the formation of collagen type I fibrillar structures[58], with collagen type I localising with relaxed fibronectin fibrils. Collagen type I total area appears to decrease at day 28, along with fibronectin (and cell number) which could be due to the lack of mechanical stimulation and therefore lack of further upregulation of collagen type I[405].

The collagen type III immunocytochemical staining was performed for qualitative analysis, to observe the performance of cells with regards to their collagen type III production, a collagen which accounts for 10% of the overall collagen present in the ACL[5]. The collagen type III present in this study serves a dual purpose; determination of collagen type III production and also characterisation of the cell phenotype. It was apparent that all cells were capable of producing collagen type III on the scaffolds, in disagreement with some reports of collagen type III immunofluorescent staining, where it has not been observed in human or porcine ACL fibroblasts[67, 406] alone. Although there have been reports of co-cultured ACL fibroblast-BM-MSC populations expressing collagen type III, it was determined that it was most likely the BM-MSCs expressing the protein[67].. However, it should be acknowledged that the donor ligaments for the cells in these studies were either from older

(>40 years) ligaments or from ligaments of a different species. Liu *et al.* (2019) however, have shown marked collagen type III staining in human ACL fibroblasts at time points up to 14 days, though the ligamentocytes used were from young adult patients (mean age ~23 years) and all of whom presented with ACL ruptures[407]. There may be inter-species differences between cells which influence the production of collagen type III, where canine ligament is reportedly more comparable to human ligament from young donors[73]. Another explanation is based on the fact that the fibres of the scaffold produced were strained to tension when mounted, to prevent fibre laxity. As collagen type III is associated with tissues that undergo stretching and are extensible (collagen type III is often detected in conjunction with elastic fibres)[408, 409], the mechanical stimulation may have induced collagen type III production via stretching and tension exertion on the fibres by the cells. For further investigation, in order to determine whether the scaffold can support native collagen type I:III production, western blotting could be utilised and would be an adequate method of determining the ratios of these two collagens.

It is important to note here that the two concentrations (10 ng and 1000 ng) are not directly comparable due to differing experimental conditions and separate control samples and negatives have been included for comparison with each set of conditions.

Orientation of the cells on the functionalised scaffolds, 24 hours following seeding determined that the 1000 ng sample^{-1} concentration of fibrillin-1 fragment had a superior effect on cell alignment, when compared with 10 ng concentrations. Although this was non-significant in most cases, it was apparent both on the LIVE/DEAD and collagen type I/fibrillin fluorescent micrographs. The presence of the RGD cell attachment motif is likely the cause of this outcome, with RGD functionalised materials previously reporting benefits of enhanced alignment at early time points[248]. Fibrillin-1 fragment interaction with individual fibres may have enhanced cell-fibre interaction, therefore increasing the uniaxial orientation of the cells.

4.5 Chapter Conclusions

The aim of this chapter was to characterise the response of canine ACL ligamentocytes to fibrillin-1 fragment functionalised scaffolds. In order to assess whether a fibrillin-1 mediated method of biofunctionalisation has the potential to enhance and support ACL tissue engineering, a number of methods have been employed. The main indicators of such are: whether fibrillin-1 can encourage and support native morphology and cell dispersion along

the scaffold fibres, its ability to facilitate attachment, and its effect on the cells' ability to produce a mature and aligned ECM on aligned fibre scaffolds.

Overall the results suggest that when seeding with canine cells, 1000 ng of fibrillin-1 fragment, rather than 10 ng, supports cell directionality, higher metabolic activity and an increased ECM production. It was noted however, that the indication of alignment from early-time point LIVE/DEAD imaging, later orientation analysis showed no notable differences between negative controls and functionalised conditions (non. sig.). Of the three fragments tested, PF8 and PF17.1 supported increased cell attachment (26.64 and 36.35% higher respectively, $p<0.05$) and higher metabolic activity (no significant increase within 24 hrs of seeding, compared to negative controls) over PF9, possibly due to the lack of synergy site at EGF domains 19-21[393]. Fragment effect on metabolic activity however was mainly only noted on glass substrates, and was attributed to variation introduced by changes in surface area on fibrous scaffolds. Ligamentocytes were confirmed to interact with RGD domains using $\alpha_v\beta_3$ and $\alpha_5\beta_1$ integrins, though blocking of $\alpha_5\beta_1$ had little effect on fibronectin RGD binding, which could be explained by a cell type preference for the use of mechanosensitive $\alpha_v\beta_3$ on mechanically dependent fibronectin[97] in an environment predominantly under cyclic tension. Interestingly, though 1000 ng of fibrillin fragment increased total ECM, collagen type I and fibronectin at various time points between 1 and 14 days, this effect disappeared at 28 days, possibly due to the lack of mechanical stimulation on the scaffold (and subsequently the cells). Despite this, extracellular fibrillin fibrils were evident at 14 days (plasma treated, 1000 ng fibrillin-1 fragment samples) and at 28 days (10 ng fragments, no plasma treatment; 1000 ng fragments, plasma treated).

To conclude, the potential for 1000 ng of fibrillin-1 fragment-mediated biofunctionalisation of aligned fibre scaffolds to perform a regenerative function of the ACL could hold potential, especially when considering the effect of the fragments on neo-ECM production. Further investigation into fragment concentration and culture environment (i.e. mechanical stimulation) however, would enable the determination of cell-fibrillin-1 fragment interaction in a more physiologically relevant environment, and would benefit the overall approach.

CHAPTER 5 HISTOCHEMICAL DONOR TO DONOR CHARACTERISATION OF EXTRACELLULAR MATRIX IN DEGENERATIVE HUMAN MALE ANTERIOR CRUCIATE LIGAMENTS

5.1 Overview

5.1.1 Introduction

There have been multiple examinations of the ACL ECM in aging and degenerative ligament, focusing largely on: collagen[50, 410], tissue integrity[410, 411], and ECM components that point to positive chondrogenically-associated (i.e. chondroid metaplasia, increases in aggrecan, collagen type II, etc.) or inflammatory (i.e. hypervascularisation) changes[412]. These studies aim to give an overview of multiple donors do not determine the differences between sex-specific donor ligaments that are characterised as 'degenerative'.

The most popular cell sources for ACL tissue engineering appear to be either BM-MSCs or primary ACL ligamentocytes. In order to acquire human primary ligamentocytes, tissue from surgical procedures has to be digested to isolate the cells. However, due to the nature of the operation required for tissue acquisition, tissue from younger patients is often scarce or unavailable. Factors such as age, medications, comorbidities and the nature of the ailment that requires the surgery, mean that available ACLs have often been exposed to rapidly degenerating environments, and are themselves degenerative (e.g. osteoarthritis), or have age-related changes (e.g. collagen fibre orientation, calcium deposition[411]). These changes can indicate alternations in cell phenotype and subsequent ECM production, and could elucidate on whether there might be significant inter-donor variation in cell response (when in culture) and ECM production.

5.1.2 Statement of Novelty

There has been no work presented in the literature (as far as is known) that examines the structure and quantifies the area of ECM proteins, of the male-specific degenerative ACL midsubstance between donors. This study aims to provide a full understanding of these ACLs, and how their protein structures are affected by degenerative changes in the knee joint.

5.1.3 Hypothesis

Donor variation is a significant issue in all biological materials derived from primary sources[413-415]. As such, it is expected that there will be significant (semi-quantifiable) differences in ECM content between donors and that some of these differences (e.g. elastin

content, and therefore fibrillin content also, due to their role in elastic fibre formation) will show differences with relation to donor age and clinical assessment of degeneration (Oxford knee and WOMAC scoring)[416].

5.1.4 Aims & Objectives

- Characterisation of the position, density and approximate quantity of integral ACL ECM proteins in the male degenerative ACL
- Alcian blue staining at pH 1 and pH 2.5 to observe highly sulphated and weakly sulphated GAGs.
- PSR to observe collagen type I to collagen type III position and co-localisation.
- H&E for tissue structure.
- von Kossa to identify calcium deposits.
- Immunohistochemical staining to identify the structure and location of integral ECM proteins (collagen types I & III, elastin, fibrillin, fibronectin, decorin and tenascin-c).
- Determination of the severity of degeneration in each donor ligament concerning cell quantity and shape, ECM integrity and vascularisation.
- Semi-quantification of ECM integrity by using a previously published scoring system[51].
- Determination of cell alignment, morphology and distribution between the degenerative ligaments, by use of the above scoring protocol.
- Determination of the vascularity of each donor to indicate extreme degeneration.
- Analysis of the many ACL ligament-associated proteins and determine the severity of variation between donors.
- Use of FIJI ImageJ to quantify % area of immunohistochemical stains to determine donor-donor variation.
- Determine structural position of proteins in the ligament by means of observation.

5.2 Materials & Methods

5.2.1 Materials

5.2.1.1 Chemicals

10% Neutral buffered formalin (HT501128, Sigma Aldrich UK), DPX mountant (06522, Sigma Aldrich UK), haematoxylin (A12431, Alfa Aesar UK), Potassium alum (aluminium potassium sulphate, CHE1114, Scientific Laboratory Supplies UK), sodium iodate (10286970, Acros Organics UK), glacial acetic acid (A/0360/PB17, Fisher Chemical UK), xylene (X/0250/17, Fisher Chemical UK), eosin Y (1% aqueous, HS250, TCS Biosciences UK), glycerol (G7757, Sigma Aldrich UK), ethanol (E/0650DF/17, Fisher Scientific UK), Alcian Blue powder (J60122, Alfa Aesar UK), hydrochloric acid (~37%, H/1200/PB15, Fisher Chemical UK), neutral red (HS555-250, TCS Biosciences UK), PSR stain kit (24901, Polysciences USA), silver nitrate (A13854, Alfa Aesar UK), sodium thiosulphate (27910.260, VWR Chemicals UK), hydrogen peroxide (H1009-500ML, Sigma Aldrich UK), methanol (M/4000/PC17, Fisher Scientific UK), Proteinase K (17916, Thermo Scientific UK), ethylenediaminetetraacetic acid (EDTA, E6758, Sigma Aldrich UK), triton-x-100 (T8787, Sigma Aldrich UK), tris-base (M02623, Fluorochem UK), Normal horse serum (2.5%; S-2012, Vector USA), normal antibody diluent (980641, MP UK), ABC reagent (Elite, PK-6100, Vector USA), DAB (with nickel, SK-4100, Vector USA), Nuclear Fast Red (2 mins; H-3403, Vector USA).

5.2.1.2 Antibodies

Mouse anti-elastin ([BA-4], ab9519, Abcam UK), mouse anti-fibrillin (MAB1919, Millipore UK), goat anti-collagen type I (1310-1, Southern Biotech USA), rabbit anti-tenascin-c (ab88280, Abcam UK), goat anti-decorin (ab189364, Abcam UK), rabbit anti-collagen type III (ab7778, Abcam UK), rabbit anti-fibronectin (F3648, Sigma Aldrich UK), IMMPRESS horse anti-mouse IgG polymer kit peroxidase (MP-7402, Vector USA), , biotinylated horse anti-goat secondary antibody (BA9500, Vector USA), IMMPRESS horse anti-rabbit IgG polymer kit peroxidase (MP-7401, Vector USA).

5.2.2 Tissue Collected from Donor Patients

The tissue was supplied by the Liverpool Musculoskeletal Biobank at Liverpool University from 9 donors (inclusion criteria and donor details below) and was recovered in PBS (2% A/A). Inclusion criteria and donor information are detailed in Table 5-1 and Table 5-2

respectively. In this chapter donors will be referred to as 'Donor 1, 2, etc.' and will correspond with the assigned number following the ACL-prefix (e.g. ACL01 becomes Donor 1).

Table 5-1 Selection criteria for supplied ACL donor ligaments.

Medical History	Age	Sex	Operation Performed	Medications
No connective tissue disorders, no previous ligament injury.	55-85	Male	Total Knee Replacement	No rapamycin

Table 5-2 Specific details of donors from whom the ligaments were donated, with relation to Table 5-1. OKS score – Oxford knee score and WOMAC score – Western Ontario and McMaster Universities Arthritis Index score.

Donor ID	Age	OK Score	WOMAC Score
ACL01	82	22 (45.83% function)	46.88% difficulty
ACL02	73	18 (37.50% function)	60.42% difficulty
ACL03	71	21 (43.75% function)	61.46% difficulty
ACL04	59	6 (12.50% function)	88.54% difficulty
ACL05	66	23 (47.92% function)	51.04% difficulty
ACL06	59	15 (31.25% function)	75.00% difficulty
ACL07	66	18 (37.50% function)	67.71% difficulty
ACL08	56	12 (25.00% function)	68.75% difficulty
ACL09	65	19 (39.58% function)	55.21% difficulty

5.2.2.1 Ethical Approval and Considerations

Ethical approval for the remit of this project was conferred by the Liverpool Musculoskeletal Biobank at Liverpool University (15/NW/0661). Approval was subject to the submission of project outline and protocol, risk assessments and COSHH/BioCOSHH forms, Human Tissue Authority (HTA)/Medical Research Council (MRC) Certificate of assessment for 'Research and Human Tissue Legislation', a material transfer agreement (MTA) and university project support and approval.

All patients had given full, generalised consent for the use of their tissue in research, and patients were aware that they could rescind their consent at any time.

All cell and tissue stocks were recorded thoroughly, as per HTA requirements.

5.2.3 Histochemical Staining of Human ACL Tissue

After formalin fixation (10% Neutral buffered formalin, ≥72 hrs), tissue from 9 individual donors (ACL01 to ACL09, as described in Table 5-2) were embedded in paraffin wax before being cut into sections (5 µm thickness). Wax removal was performed using xylene and tissue was rehydrated by moving through decreasing concentrations of ethanol into deionised water. After staining, all sections were dehydrated using sequentially increasing concentrations of ethanol and cleared in xylene, before being mounted with glass coverslips using DPX mountant. All staining was performed at room temperature unless otherwise stated. All images were taken using a Leica DM2700 M microscope with a Leica MC190 HD camera using LAS V4 1.1 software.

5.2.3.1 Haematoxylin & Eosin

Haematoxylin & Eosin (H&E) staining is widely used to observe the morphology of the tissue and cells. The nuclei are stained purple-black whilst the rest of the tissue is shown in pink.

Haematoxylin solution was made by adding 1 g of haematoxylin to 1 L distilled water using gentle heat. Potassium alum (50 g) was added and dissolved using gentle heat. Solution was cooled, 0.2 g sodium iodate was added, and shaken well. The final solution was filtered and glacial acetic acid (20 ml) was added. To produce Eosin solution; 50 ml eosin (1%) was added to 390 ml of 95% ethanol and 2 ml glacial acetic acid.

Sections were stained in Mayer's haematoxylin (5 mins) and blued in running water. Eosin staining was performed (2 mins) before dehydration in 95% ethanol (thrice, 1 min), and thrice rapidly in 100% ethanol.

Tissue and cell morphology was graded using a system previously published by Kharaz *et al.* (2018)[51], adapted from the original by Stoll *et al.* (2011)[417]. For cell morphology, x20 and x10 images were used (n=3/magnification), and for ECM organisation, cell distribution, alignment and tissue vascularity, x5 and x10 images were used (n=3/magnification).

Kendell's W coefficient of variance was used to determine intra- and inter-observer agreement[51] using an available online tool[418].

For cell counting, particle analysis on FIJI ImageJ was employed, using 3 images (x20 magnification) per donor.

5.2.3.2 Alcian Blue

Alcian blue is a bright blue stain that is often used to detect sulphated GAGs. The more acidic the stain, the higher the specificity for highly sulphated GAGs. If the pH is increased, the stain will also highlight carboxylated acid groups, found on neutral/weakly sulphated GAGs and proteoglycans. For this reason, this stain was performed at pH 1.0 (sulphated GAGs) and pH 2.5 (acidic weakly sulphated GAGs, mucins, hyaluronic acid and sialomucins)[419].

Alcian Blue powder (1 g) was mixed with 90 ml deionised water and 10 ml 1 N hydrochloric acid ($HCl_{(aq)}$) (pH 1.0) or 97 ml deionised water and 3 ml glacial acetic acid ($CH_3COOH_{(l)}$) (pH 2.5). Solutions were sterile filtered using filter paper (Whatman, UK) before use. Sections were covered in Alcian Blue solution for 30 mins and blotted dry (pH 1.0), or 15 mins (pH 2.5) before rinsing with deionised water. Sections were counterstained with 1% neutral red for 30 secs (pH 1.0) or 1 min (pH 2.5) before rapid dehydration in 95% ethanol (pH 1.0)/100% ethanol (pH 2.5).

5.2.3.3 Picrosirius Red (PSR)

PSR is a stain that under white light will determine total collagen by staining pink. However, under polarised light, the stain can specifically differentiate between collagen type I (orange) and collagen type III (green) content within tissues. For this staining procedure, a PSR stain kit was used.

Sections were submerged in Weigert's haematoxylin solution (1:1 ratio of solutions A and B, 8 mins), before removal to distilled water. Sections were then placed in Phosphomolybdic acid solution (Solution A, 2 mins) before being washed with distilled water and submerged in Picrosirius Red F3BA stain (Solution B, 1 hr). Sections were then immediately taken to 1 N Hydrochoride acid solution (Solution C, 2 mins) and dehydrated using 70% ethanol.

5.2.3.4 von Kossa

Von Kossa is a stain that determines the presence of mineralisation (calcification). Any calcified nodules will appear black/brown under the microscope, whilst tissue will appear pink.

Tissue was submerged in a 5% silver nitrate solution for 15 mins under bright light. Following this, sections were washed thrice with deionised water (with a 2 min soak between each wash). Thiosulphate solution (5%) was added to the sections for 5 mins and the aforementioned washing steps were repeated. Sections were rapidly stained with 1% neutral red (1 min, as above) before washing in deionised water and blotting dry.

5.2.4 ECM Protein Immunohistological Staining

Sections were stained for collagen type 1A1, collagen type III, fibronectin, fibrillin, elastin, decorin and tenascin-c. All procedures were performed at room temperature unless otherwise stated. Negatives for samples and positive control sections can be found in Appendix 10.

An endogenous block was performed to remove any residual peroxidase using 6 ml hydrogen peroxide ($H_2O_{2(l)}$) in 360 ml of methanol and incubated for 30 mins. Sections were then removed to deionised water ($dH_2O_{(l)}$) for a further 5 mins. Antigen retrieval was performed using the Proteinase K retrieval method. Proteinase K stock solution (0.008 g Proteinase K, 10 ml TE buffer, 10 ml glycerol) was diluted 1:20 in TE buffer (6.10 g tris base, 0.37 g EDTA, 5 ml triton-X-100 per 1000 ml $dH_2O_{(l)}$) and incubated (10 mins, 37ºC). Post soaking, the solution was left to cool for a further 10 mins. All sections were then washed in $dH_2O_{(l)}$ (5 mins).

Sections were placed in a rack on a Sequenza and PBS washed for 5 mins. Normal horse serum (2.5%) was added (2 drops) and left to block (30 mins) before the addition of 100 µl of the primary antibodies (mouse anti-elastin [BA-4], 1:100; mouse anti-fibrillin, 1:200; goat anti-collagen type I, 1:100; rabbit anti-tenascin-c, 1:50; goat anti-decorin, 1:250; rabbit anti-collagen type III, 1:100; rabbit anti-fibronectin, 1:400) in normal antibody diluent). Sections were incubated overnight at 4ºC.

Following incubation, sections were washed with PBS. For mouse and rabbit antibodies, IMMPRESS kits were used (IMMPRESS horse anti-mouse IgG polymer kit peroxidase, IMMPRESS horse anti-rabbit IgG polymer kit peroxidase) and 2 drops were added to the

sections (incubated for 30 mins). For the goat antibodies, a biotinylated horse anti-goat secondary antibody was used for 30 mins followed by a 5 min PBS wash. ABC reagent was added to biotinylated anti-goat stained sections (30 mins) before being washed with PBS (5 mins). DAB (100 µl, with nickel) was added for a further 5 mins. Sections were then washed in $dH_2O_{(l)}$ (5 mins) and counterstained with Nuclear Fast Red (2 mins) before being rinsed with water and sequentially dehydrated with graduated ethanol before mounting with DPX. Sections were rested in xylene to clear for 5 mins.

Each stain was performed using a negative control sections for each donor. Each section was imaged 3 times per slide for FIJI ImageJ analysis. Each donor ligament was thresholded to its own negative control for analysis.

5.2.5 Statistical Analysis

Statistical tests for ligament protein % area, and differences between ligament scores, were performed as in Chapter 3, section 3.2.13.2. All donor % area measurements are based on 3 images per donor, 'total' bars on graphs are the result of n=9 ligaments (each with n=3 images/ligament).

Scoring was performed by two independent observers (MOB, ZLS), twice. Each scoring analysis was completed a minimum of 2 weeks apart and Kendall's W Coordinance of Variance was used to analyse both inter- and intra-observer agreement[51] (Appendix 13). Scoring results are calculated using all scoring sets.

Agreements between two tested variables are shown using a correlation analysis with linear fit on Graphpad Prism V7, and R^2 value determined 'goodness of fit' of the expected linear model. Significance of that agreement was determined by Pearson's r (parametric) or Spearman Rho (non-parametric) tests.

5.3 Results

5.3.1 Tissue and Ligamentocyte Organisation

Interestingly, donor cell counts varied, but non-significantly in many cases. Higher cell number is usually indicative of degeneration, which was displayed by donors 2, 3, 4 and 6 in Figure 5-1A. This theory was loosely confirmed by the weak negative correlation between mean ECM organisation scores and nuclear counts ($R^2 = 0.421$) in Figure 5-1B.

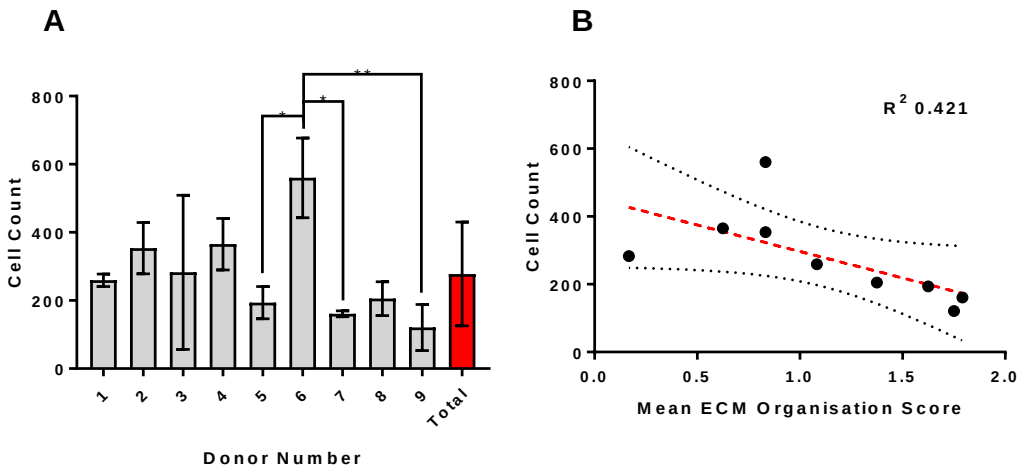

Figure 5-1 Cell numbers for each donor were counted using nuclear staining on FIJI ImageJ (**A**). All bars show means and SDs. *p<0.05, **p<0.01. Nuclear count and ECM organisation score were compared for a correlation in order to confirm whether increased cell number was indicative of ACL tissue degeneration (**B**). Red dashed line indicates linear predicted model of the relationship between the above parameters and black dotted lines indicate the 95% confidence interval of the linear model.

Histological scoring was performed using the scoring criteria developed by Kharaz *et al.* (2018)[51] and was used to assess the severity of degeneration in the donor ligament. Kendall's W was calculated to confirm observer agreement and resulted in averages of 'almost perfect' (0.8202) intra-observer agreement and 'substantial' (0.7238) inter-observer agreement[420] (see Appendix 13).

Micrographs present in Figure 5-2 show the various conformations of collagen fibre alignment in the degenerative male ACLs. Most ACLs had at least partial linear organisation of collagen fibres present, with some donors (3, 4, 6) having large areas of reduced density, with highly disorganised collagen. It was determined that donors 2, 3, 4 and 6 showed significantly less ECM organisation than donors 5, 7 and 9 ($p<0.01$), with donors 7 and 9 achieving an almost 'normal' ECM organisation score.

All donors showed the presence of both elongated fibroblastic-type cells and ovoid fibrochondral cells, with cell chains of the latter type present in multiple donors (as seen on the image inserts in Figure 5-2, donors 1, 5 and 9). Variation in cell shape (and therefore phenotype) was present, with donors 3, 5 and 9 showing significantly more fibrochondral/ovoid cells than those observed in donor 8 ($p<0.01$). As shown in Figure 5-3D, donor 3 showed the least amount of cell alignment, (which positively correlated with ECM organisation, $R^2 = 0.8223$, data not shown), and along with donors 2 and 6, displayed significantly less cell alignment than donors 5, 7, 8 and 9 ($p<0.05$). Cell clustering and cell chain formation was evident in both donor 6 and 9, resulting in significantly lower distribution scores than donor 5 ($p<0.05$).

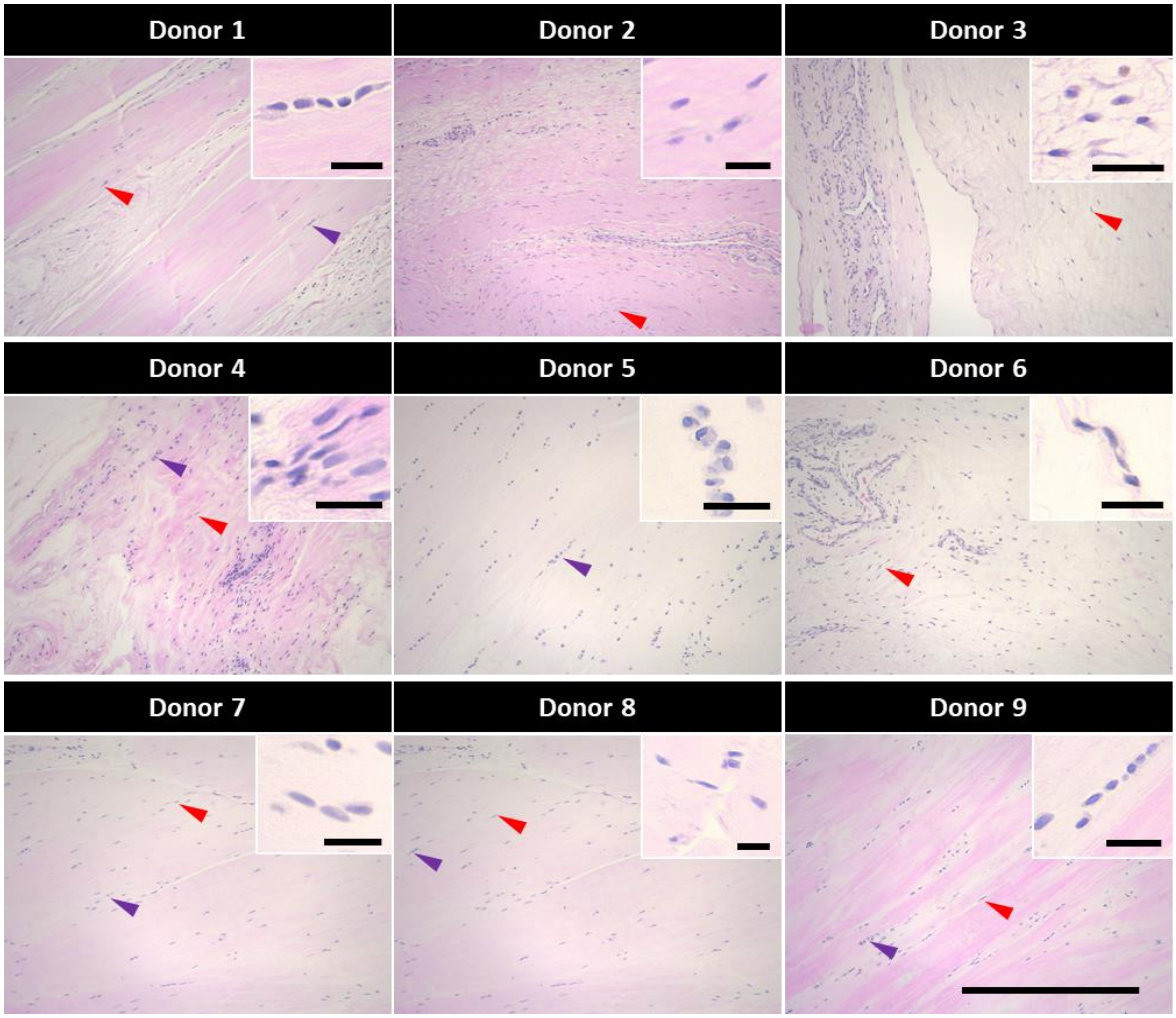

Figure 5-2 Haematoxylin and eosin staining of degenerative male human ACL tissue (n=1 section per donor). Purple arrowheads indicate ovoid fibrochondral cells often found near the insertion sites of the ACL, whilst red arrowheads indicate fibroblastic cells, often found in the ACL midsubstance of healthy ligament tissue. Images of cells in the smaller windows represent the majority of morphologies observed within that donor. Scale bar of larger images represents 500 µm, and on the smaller images, 50 µm.

Hypervascularity in the ACL is considered one of the hallmarks of degeneration and in other tissues, is often associated with osteoarthritis progression[421]. Variations in vascularity scores between the ligaments was determined to be significant, with donors 2, 3 and 6 displaying hypervascularisation throughout the ligament. All ligaments, bar 5 and 9, showed some evidence of hypervascularity, as seen in Figure 5-3E.

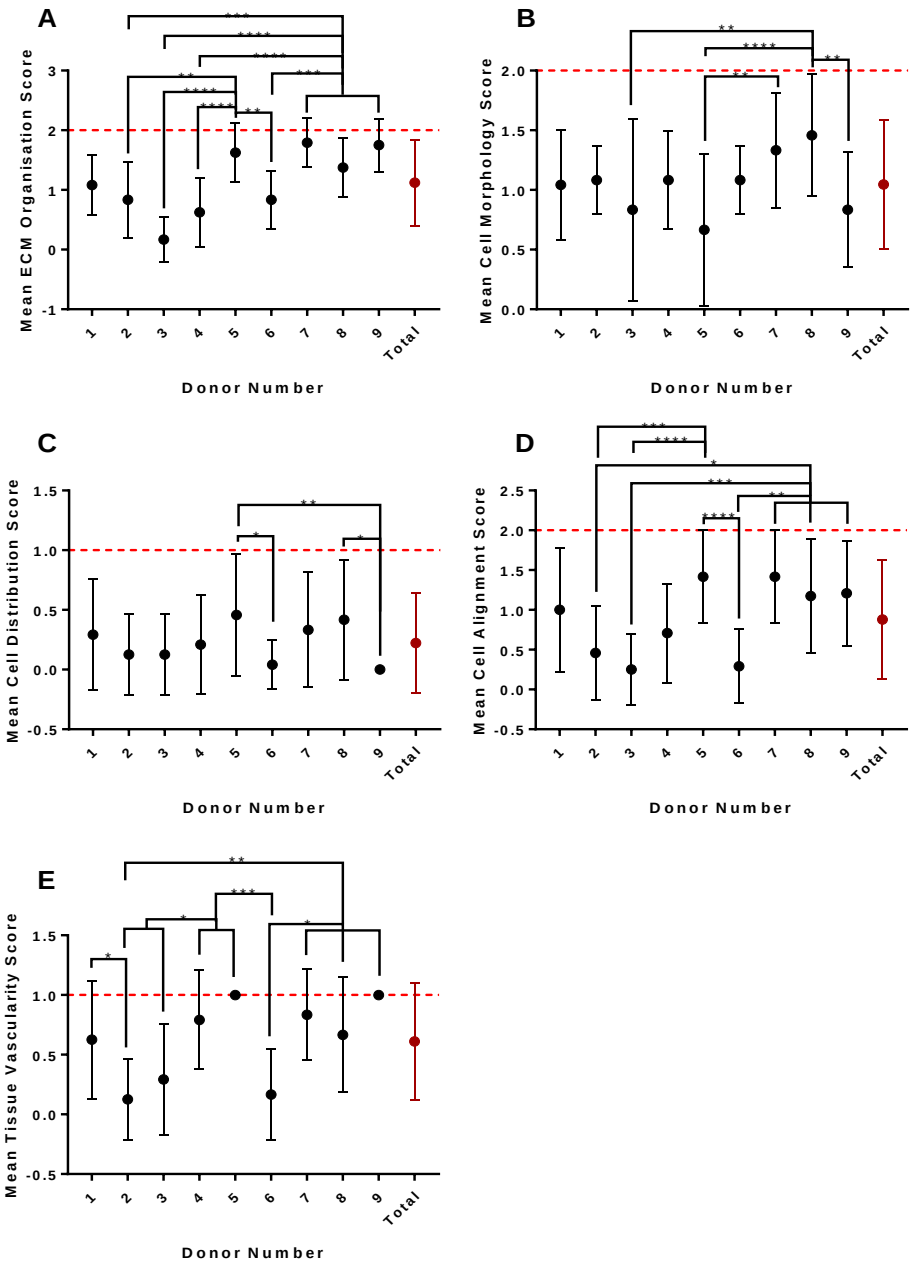

Figure 5-3 Scoring results of 9 individual donors from H&E stained images, performed by 2 independent observers. Graphs show ECM organisation (**A**), cell morphology (**B**), cell distribution (**C**), cell alignment (**D**)

and tissue vascularity (**E**). Red lines on graphs denote a 'normal' ACL score. Means ± SDs are shown. All statistical analyses were performed using Kruskal Wallis H test for non-parametric data and subsequent rank comparisons. *p<0.05, **p<0.01, ***p<0.001, ****p<0.0001.

5.3.2 Fibrous ECM Content

5.3.2.1 Collagen type I

As the ACL consists primarily of collagen type I, immunohistochemical staining in Figure 5-4A and B showed widespread presence and density across all donors, in agreement with Hasegawa *et al.* (2013)[50] and Kharaz *et al.* (2018)[51]. Significant donor variation was observed in Figure 5-4C, with donors 8 showing significantly less collagen type I area than donor 4 ($p<0.05$) and donor 9 showing significantly less collagen type I than donors 4 ($p<0.001$), 5 ($p<0.01$) and 1 ($p<0.01$).

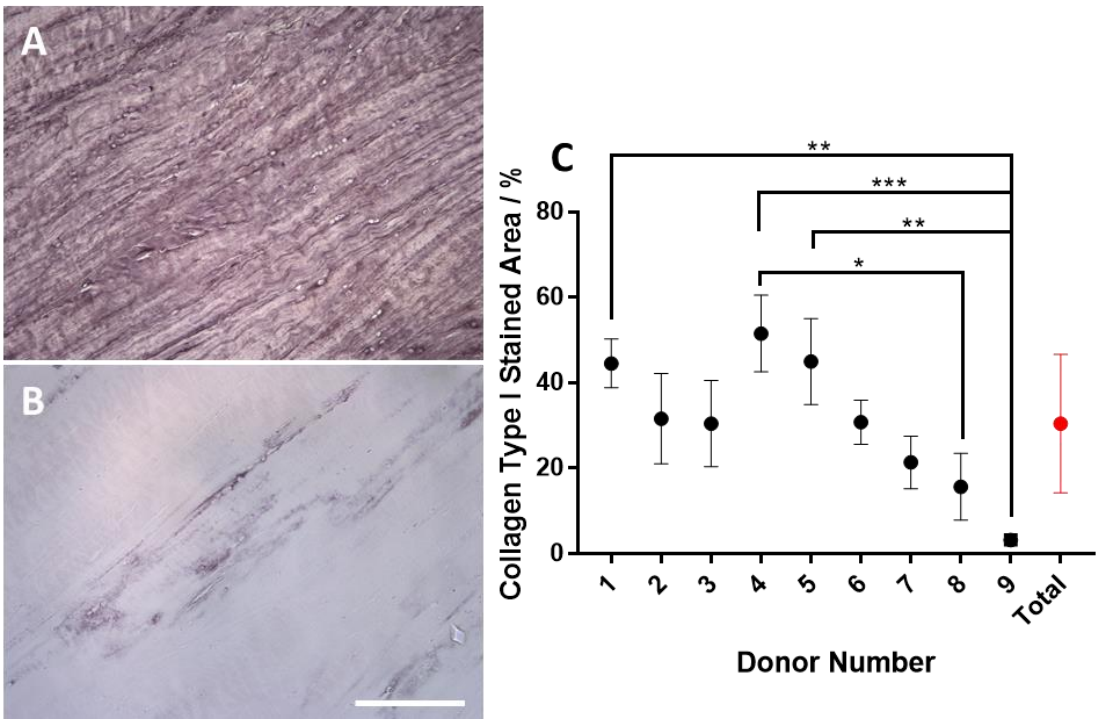

Figure 5-4 Immunohistochemical staining for collagen type I in degenerative ACL ligaments. Positive staining can be observed by the presence of DAB stained tissue, nuclei was stained using Fast red (n=1 section per donor). Most tissue showed complete coverage with staining of collagen type I (**A**), with the exception of one donor (**B**). Scale bars represent 500 µm. Collagen type I % area between donors is displayed (**C**). Means ± SDs are displayed. To determine statistical significances, a one-way ANOVA was performed with Tukey's multiple comparisons. *p<0.05, **p<0.01, ***p<0.001.

5.3.2.2 Collagen type III

Collagen type III is a major constituent of the ACL ECM, contributing to the small amounts of elasticity in the tissue and it accounts for 10% of all collagen present[43]. Collagen III has shown to be present within the interfascicular regions of the ACL in younger, healthy ACLs[50] and will often occur within the walls of blood vessels[422].

Collagen type III in the donor ligaments appeared to be more evenly distributed throughout the tissue in the degenerative ligaments (as shown in Figure 5-5A and B), in agreement with Hasegawa *et al.* (2013)[50]. Also noted were strong collagen type III staining both intracellularly or in the pericellular regions of the ligament. Content of collagen type III, as displayed in Figure 5-5C, showed no significant differences between any of the degenerative ligaments.

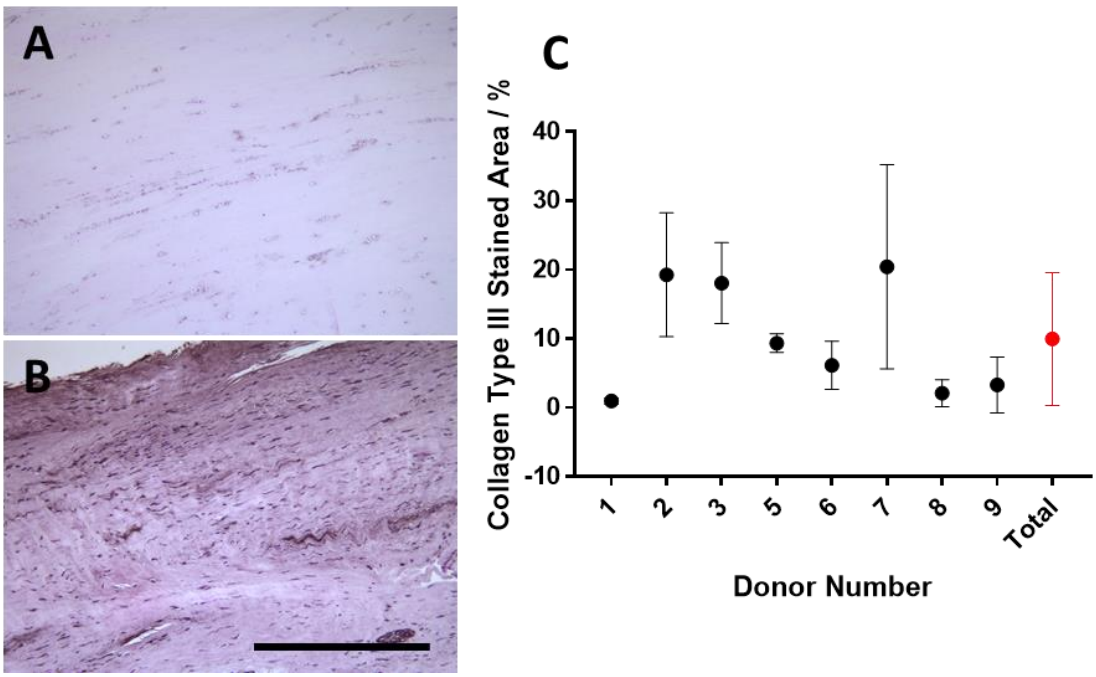

Figure 5-5 Collagen type III staining is displayed across 9 independent donors. Images show discrepancy in staining patterns in the ligament. Some samples displayed minimal staining (**A**), whilst others, showed large amounts of collagen type III staining (**B**) (n=1 section per donor). Scale bar represents 500 µm. Semi-quantification of stained area was performed to determine any significant differences between donors (**C**). N=1 section per donor was performed, 3 images were taken to semi-quantify. One-way ANOVA was performed with Tukey's host hoc tests. No significant differences were identified.

5.3.2.3 Collagen I:III Ratio

PSR staining, through the use of polarised light, enables the observation of both collagen type I (orange staining) and collagen type III (green staining) in the tissue. PSR staining showed larger amounts of collagen type III running longitudinally along the collagen type I fascicles, in the interfascicular regions (Figure 5-6A and B). Donor 3 showed dense collagen type III staining within the disorganised matrix, whilst donor 2 showed intense clustering of collagen type III around the vessels. Donors 1, 5, 7 and 8 showed highly aligned type III collagen, with intense collagen type I staining. Donor 4 displayed high levels of collagen I staining and type III could only be observed around the vessel structures. As displayed in Figure 5-6C and D below, donor 8 appeared to have the most 'normal' collagen ratio, which was in agreement with good ECM organisation scores.

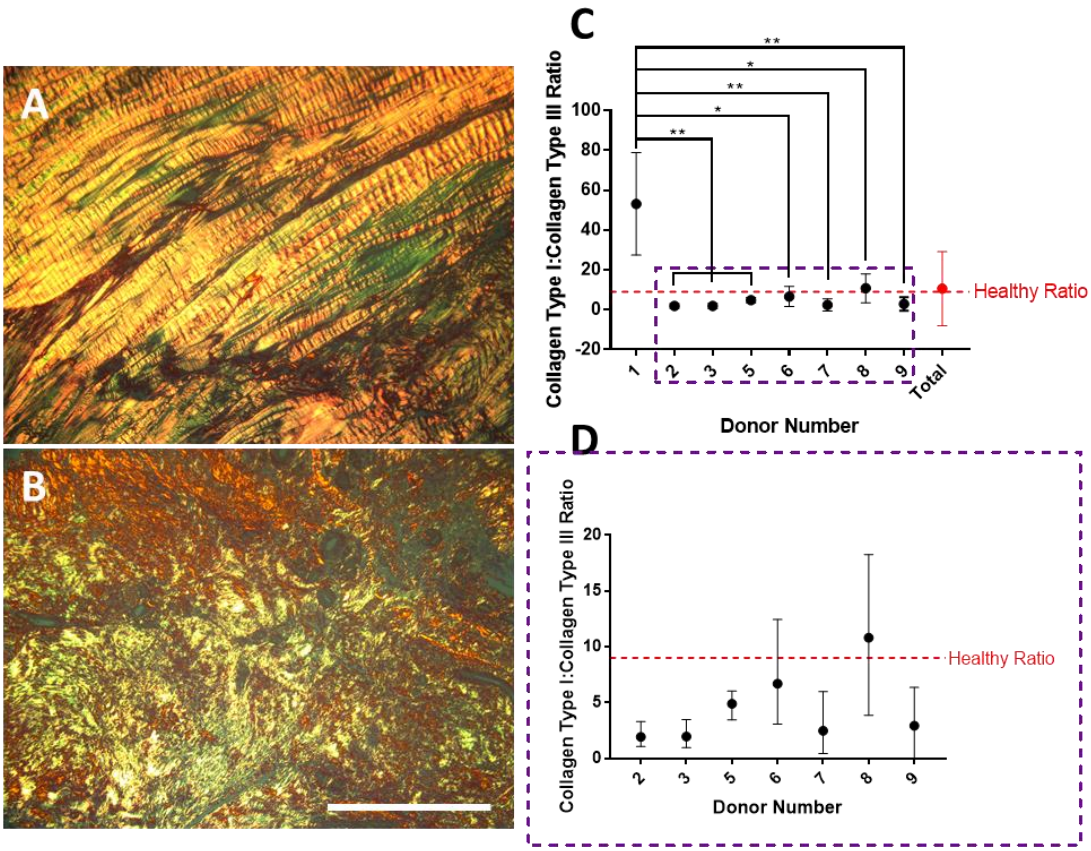

Figure 5-6 PSR staining (**A** and **B**) for visualisation of collagen type I and collagen type III in the degenerative ACL) (n=1 section per donor). Orange colouring indicates on image **A** the presence of collagen type I and green (which was more abundant on image **B**), that of collagen type III. Images were all taken under polarised light. Scale bar represents 250 µm. Graphs (**C** and **D**) presented display collagen type I:collagen type III ratios for all donors analysed (**C**). Donor 4 is absent, due to tissue no longer being available. Collagen type I to collagen type III ratio was calculated using percentage stained areas of immunohistochemical staining. Larger

ratios indicate a higher quantity of collagen type I to collagen type III. 'Healthy ratio' indicated on the graphs above was determined from the literature where a ratio of collagen type I to III of 9 is frequently referenced. The graph surrounded by a purple box shows donors 2 to 9 (**D**). Means ± SDs are shown. One-way ANOVA test was performed with Tuckey HSD post hoc test. *p<0.05, ** p<0.01, *** p<0.001.

5.3.3 Glycosaminoglycan and Proteoglycan Content

To determine the presence of GAGs in the degenerative ligament, Alcian blue staining and both pH 2.5 and pH 1.0 were performed. Increasing the pH of alcian blue will alter the specificity with which the stain binds to highly sulphated GAGs, staining those which are more weakly sulphated, including carboxylic acid groups. Staining at pH 2.5 confirmed the presence of sulphated GAGs in the degenerative ACLs. GAGs are a common feature in ACLs of all conditions, with them being responsible for the hydration of the tissue. Images in Figure 5-7C represented almost half of the donors (1, 5, 7 and 9), which displayed clear presence of GAGs with positive alcian blue staining. Some of the donors however (2, 3, 4, 6 and 8, represented by Figure 5-7D) displayed very weak staining throughout the ECM, only displaying mainly peri- or intra-cellular positive staining (indicated by purple arrowheads) that were observed in most of the donors. Interestingly, most strong staining observed was due to vascularisation of the ACL. However, donor 5 displayed the possible presence of mucoid degeneration (indicated by red arrowhead in Figure 5-7C).

In order to determine whether the degeneration of the donor ligaments was associated with chondrogenesis of the cells, a lower pH of alcian blue was used to stain sulphated GAGs (Figure 5-7A and B). Donors 3, 6, 7 and 8 appeared negative for sulphated GAG staining, indicating little or no chondrogenic degeneration of the ligament (as represented in Figure 5-7B). Donors 2 and 4 stained weakly around the ovoid fibrocartilage cells, indicating the possible presence of cartilage-associated GAGs, whilst donors 1, 5 and 9 had areas of strong staining (as in Figure 5-7A) which was observed primarily in the pericellular space around clusters of fibro-cartilaginous cells. Both showed broad interfascicular staining, with areas of mucoid degeneration and obvious cystic changes (indicated by red arrowheads).

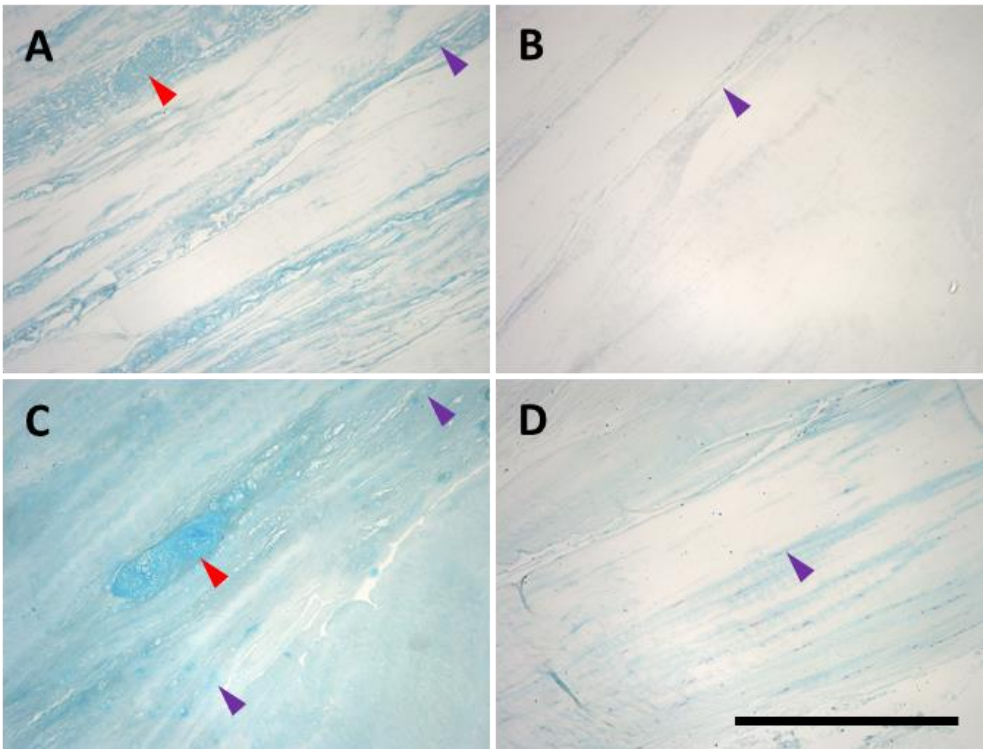

Figure 5-7 Alcian blue staining at pH 1.0 on degenerative ACL ligament to detect strongly sulphated GAGs (n=1 section per donor). Image **A** displays a ligament with positive strongly sulphated GAG staining, whilst image **B** shows that of a ligament which was mostly negative for strongly sulphated GAGs. Alcian blue staining at pH 2.5 was used to detect the weakly sulphated GAGs present in the degenerative ACL (n=1 section per donor). Image **C** displays the widespread presence of GAG content in the ligament ECM, with cystic changes present. Image **D** shows minimal GAG staining in degenerative ligament. Red arrowheads indicates pockets of strong staining present due to vasculature or possible mucoid degeneration and purple arrowheads indicate strong staining in the pericellular spaces of fibrochondral cells Scale bars represent 500 µm.

5.3.4 Calcification

Calcification of ligament situated in the intra-articular region is reported to be an indicator of severe degeneration[421]. To determine whether the ligaments contained any calcification or osseous nodules, due to their degeneration, and potential differentiation of ACL cells into the osteocyte lineage, a von Kossa stain was performed (Figure 5-8). Despite knee degeneration, only one of the donor ligaments (donor 1) presented with minor indications of calcification.

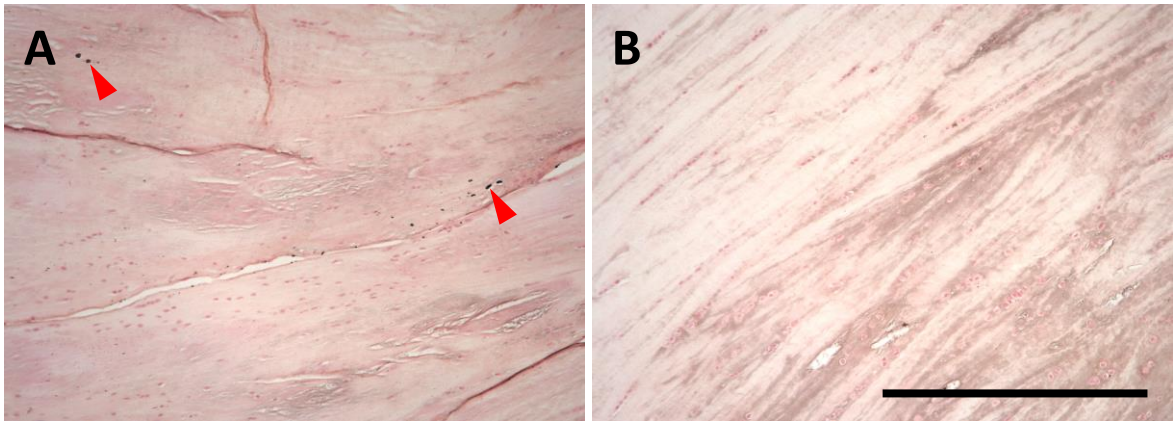

Figure 5-8 von Kossa staining was performed to detect any calcification in the degenerative human ACLs (n=1 section per donor). Red arrowheads indicates positive staining for calcification. Image **A** depicts the presence of calcification within the ligament, whilst image **B** displays a more 'normal' appearance of ligament. Scale bars represent 500µm.

5.3.5 Glycoproteins and Elastic Fibre Associated Proteins

5.3.5.1 Fibronectin

Fibronectin is an essential ECM protein that has multiple roles in cell-ECM attachment and matrix assembly[34, 58, 301]. All donors appeared to show similar % area coverage of fibronectin (Figure 5-9B), with the exception of donor 3, which retained significantly higher fibronectin expression when compared to donors 5 and 8 ($p<0.05$). Fibronectin staining, as shown in Figure 5-9A, appeared to be widespread, covering the entire matrix and closely following the staining patterns of collagen type I.

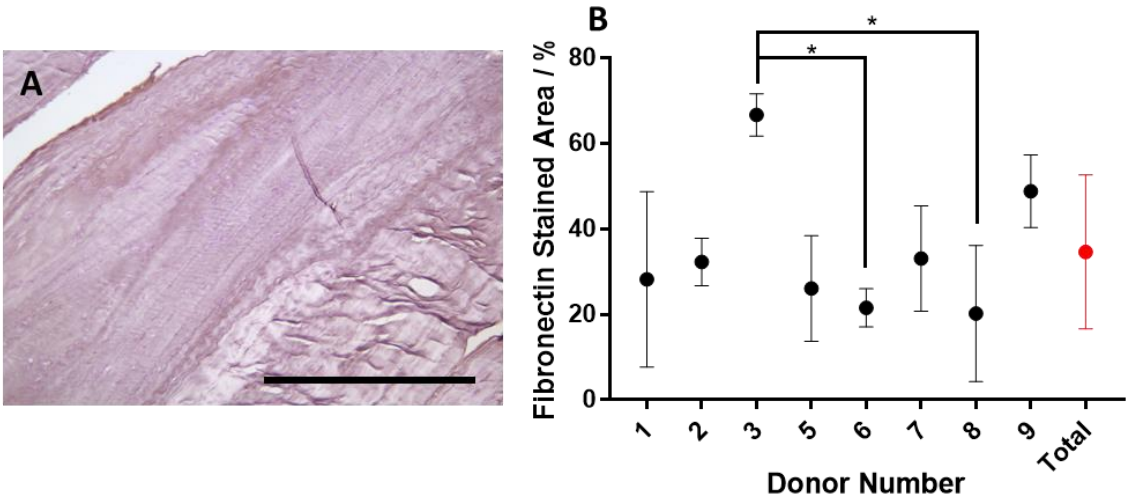

Figure 5-9 Immunohistochemical staining for fibronectin. Staining appeared consistant across all 9 donors (**A**) (n=1 section per donor). All scale bars represent 500 µm. Fibronectin % area of degenerative ACL ligament

tissue was analysed (**B**). Means ± SDs are displayed. One-way ANOVA with Tukey HSD post hoc was performed. * $p<0.05$.

5.3.5.2 Tenascin-C

Tenascin-C is a highly ligament-specific protein and has been found to be strongly linked to the perpetuation of inflammation in joints[57]. Tenascin-c appeared to be present on all donors as depicted in Figure 5-10A. All donors appeared to exhibit similar % areas of tenascin-c (Figure 5-10B), with positive staining observed mainly in the peri- and intra-cellular regions. No significant differences were observed between the different donors.

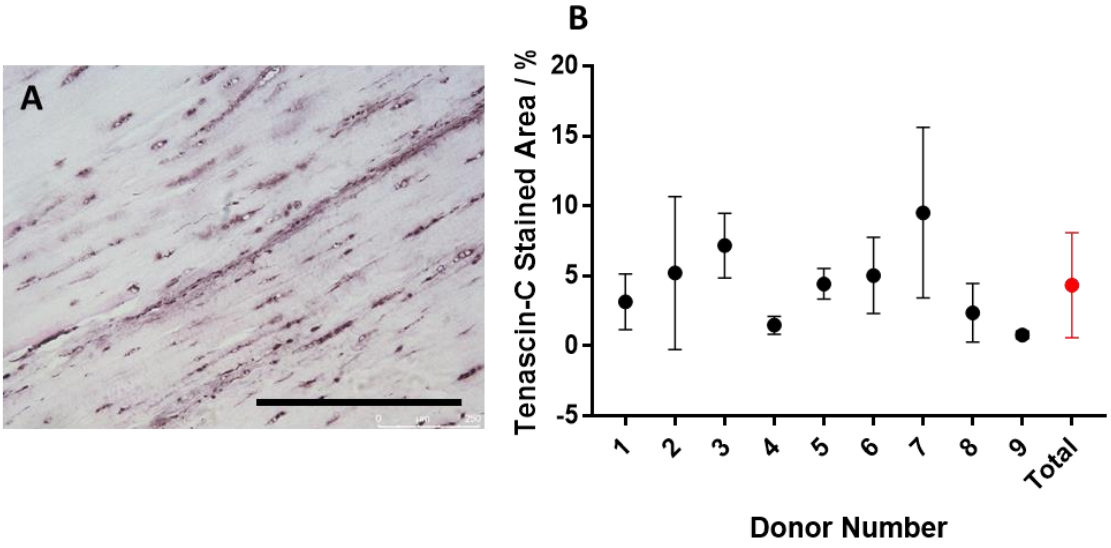

Figure 5-10 Tenascin-C immunohistochemical staining with DAB in the human degenerative ACL, representative of 9 individual donors (**A**). Scale bar represents 500 µm. Percentage area staining for tenascin-c showed no significant differences between donors, as determined by a One-way ANOVA with Tukey's post hoc tests (**B**). Means are displayed ± SDs.

5.3.5.3 Fibrillin

Fibrillin was stained, as it a major component of elastic fibre assembly. Staining for fibrillin in Figure 5-11A and B, displayed varying % areas across all donors. Largely increased areas of fibrillin were observed in donor 6. As shown in Figure 5-11C and D, all other donors displayed % areas of under 1.5%, with donor 9 having the lowest at 0.0043%. Often, the

fibrillin was observed to be pericellular or formed in linear fibrils, which extended parallel to the collagenous fibres of the ACL matrix.

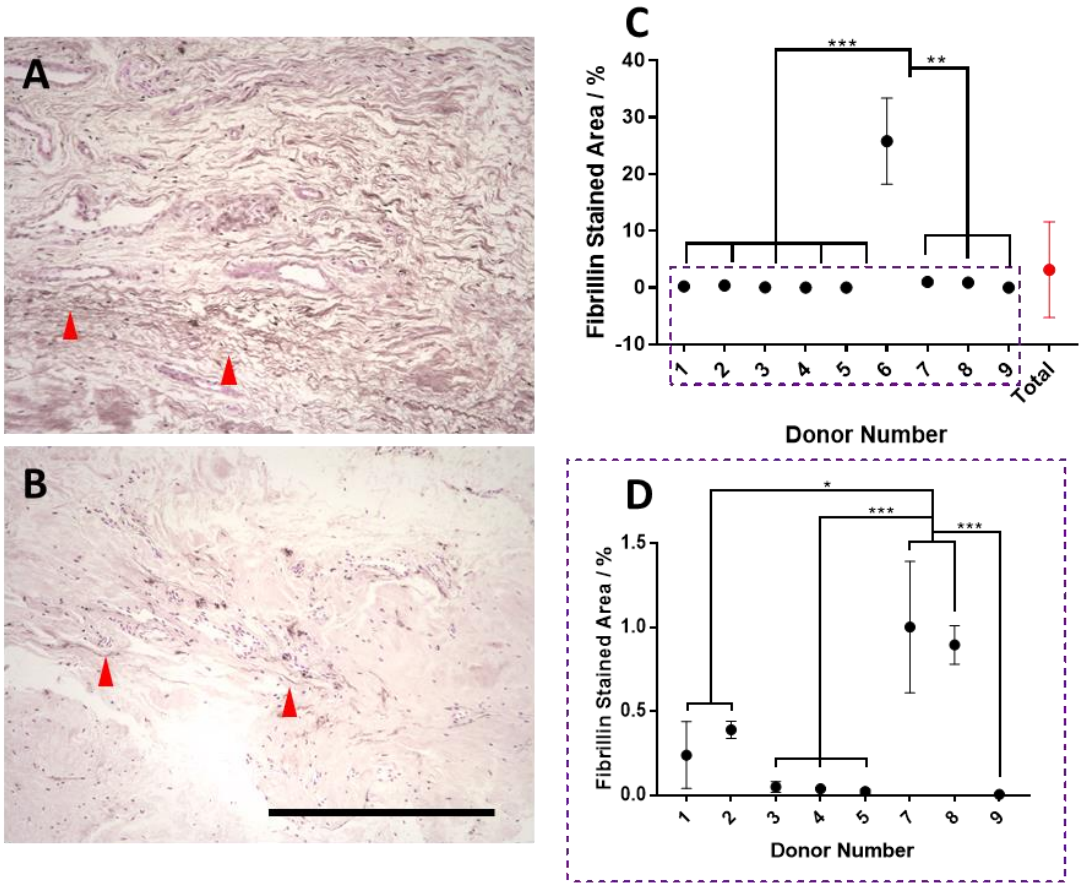

Figure 5-11 Immunohistochemical staining with DAB for fibrillin in degenerative ACL ligaments representative of 9 donors. Red arrows indicate the presence of fibrillin fibrils. Very rarely dense, wavy fibrils were observed (**A**), more often disorganised and fragmented fibrillin fibrils were present (**B**). Scale bars represent 500 µm. Percentage area of positive staining shows all donors (**C**) and donors 1-5 and 7-9 (**B**). Means ± SDs are displayed. One-way ANOVA was performed with Tukey's multiple comparisons post hoc tests. *p<0.05, **p<0.01, ***p<0.001.

5.3.5.4 Decorin

Decorin is a highly important proteoglycan in the ACL, facilitating the association of collagen type I and elastin and providing structural integrity to the ligament. Imaging in Figure 5-12A showed more enhanced staining closer to the pericellular space. For some donors (1, 6, 7 and 8) however, the decorin staining appeared to be present throughout the fibrillar ECM of the ACL, with the staining pattern being structurally similar to that of

collagen type I. Results appeared to be consistent with those reported of the canine cruciate ligament by Kharaz *et al.* (2018)[51], and in the human cruciate ligament by Zhu *et al.* (2012)[423]. Graphs in Figure 5-12B and C, show donor 7 displayed significantly increased presence of decorin compared to all other donors ($p<.0.001$). Only donor 8 was determined to be significantly higher in decorin content than donor 9, following the exclusion of donor 7 ($p<0.05$).

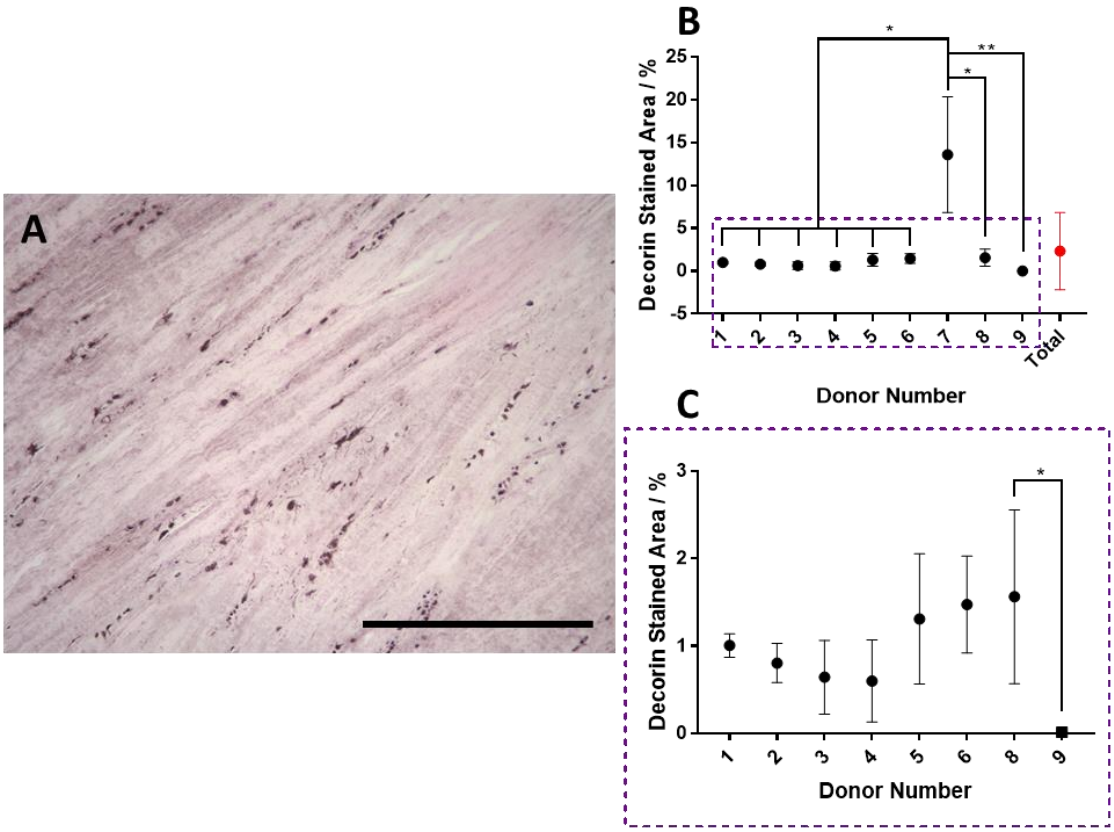

Figure 5-12 Immunohistochemical staining for decorin in degenerative ACL (n=1 per donor, 3 images per donor) (**A).** All scale bars represent 500 µm Graph shows the means and standard deviations for donors 1-9 (**B**) and 1-6, 8 and 9 (**C**). One-way ANOVA was performed with Tukey post hoc tests. *** $p<0.001$.

5.3.5.5 Elastin

Elastin is an integral part of the mature ACL, providing the tissue with the vast majority of elasticity it requires to undergo repeated cyclic loading. Despite the stability of elastin, it has previously reported and that elastin content decreases with age[424]. Elastin fibrils depicted in Figure 5-13A and B, appeared to align themselves anisotropically along the midsubstance of the ligament, running parallel to the collagen fascicles, as also shown in canine ligament by Kharaz *et al.* (2018)[51]. Due to marked degeneration and fragmentation of elastin in the majority of the ACL ECMs, it was not clear whether the elastin resided primarily in the inter-fascicular regions as previously reported[51], although donors 1 and 7 did appear to show indication of such. The % area was used to determine an approximate and semi-quantitative measure of elastin content within the ligament. As shown in Figure 5-13C and D, variation between donors was present, with donor 6 showing significantly higher content of elastin fibres when compared with other donors ($p<0.01$). Additionally, donor 1 displayed significantly elevated content of elastin compared to donors 2, 5 and 7 ($p<0.05$).

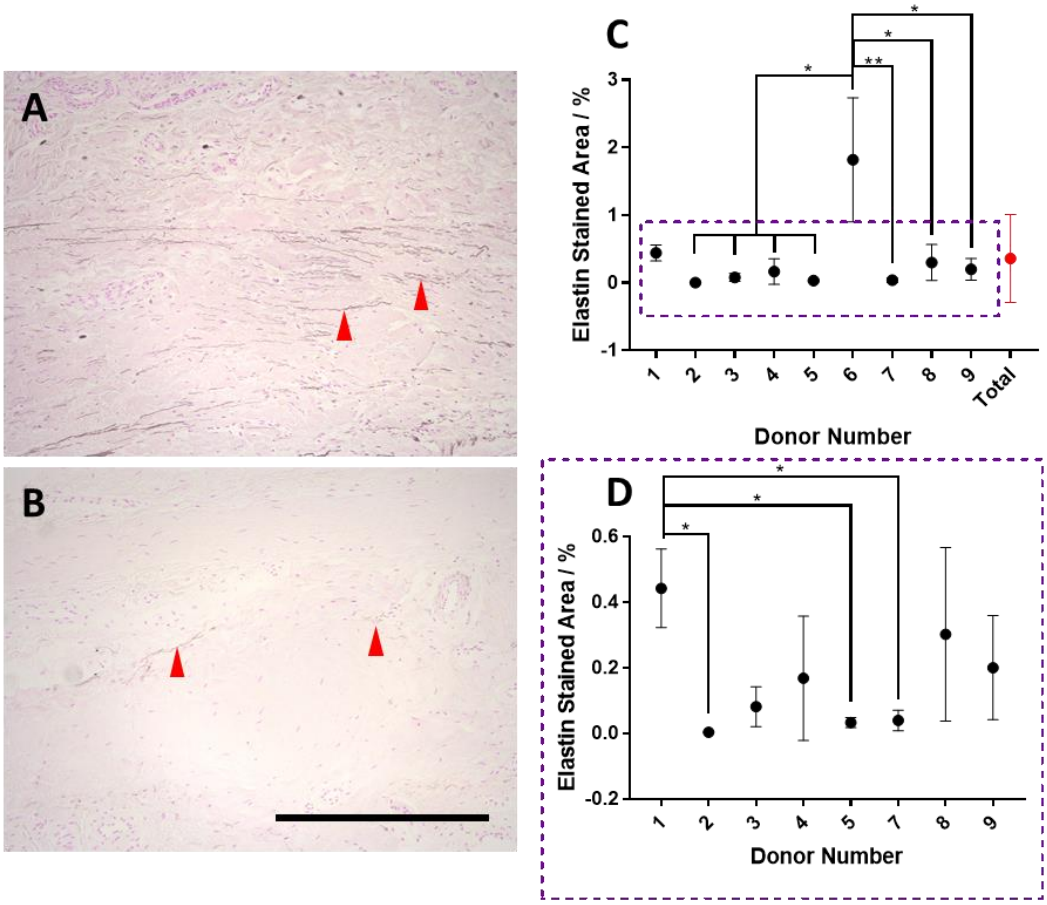

Figure 5-13 Micrographs of elastin fibrils present in the degenerative ACL ECM. Human donors (n=1 per donor, 3 images per donor) are displayed in representative images (red arrowheads indicate elastin fibre presence in midsubstance) (**A, B**). Scale bars represent 500 µm. Differences in % area elastin, quantified for each donor, with significances were determined by a one-way ANOVA with Tukey HSD post hoc tests (**C, D**) Symbols show means ± SDs. *p<0.05, **p<0.01.

5.3.6 Correlations between Immunostained Protein Area, in Comparison to Age, WOMAC Scores and Oxford Knee Scores

All stained samples were correlated with age, WOMAC scores and OKS scores to determine any significant relationship between the % stained area and the above listed variables. This was performed by determining the significance of each correlation (Pearson's r or Spearman's Rho) and the R^2 value for each correlation. Of all the correlations determined in , , and , only collagen type III vs. age was determined to be significant after the removal of a suspected abnormal result. Donor 4 is not included due to unavailability of tissue. R^2 value of displayed a moderate positive correlation between collagen type III area and age. This data was analysed with Pearson's r test and revealed a significance of $p<0.05$.

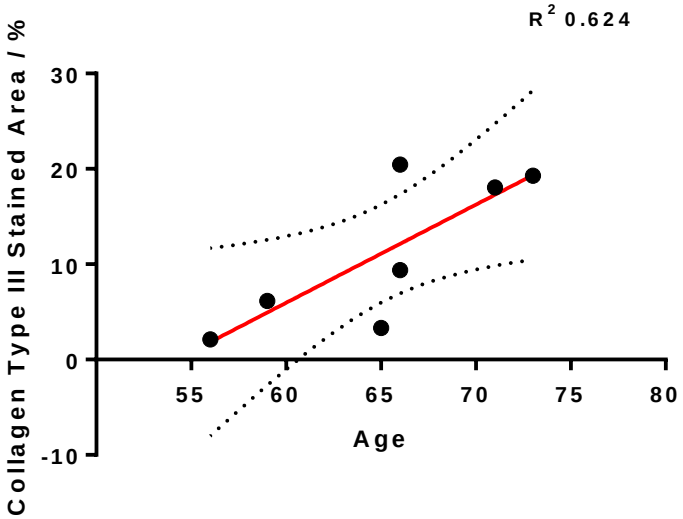

Figure 5-14 Correlation of Collagen type III stained area and age. Donor 1 was removed due to very low collagen type III scoring and Donor 4 was not available to be stained with collagen type III, but is shown in the corresponding graph in B. Pearson's r statistical test was performed to determine significances. R^2 value denotes strength of the correlations. Confidence interval (95%) bands are displayed on the graph.

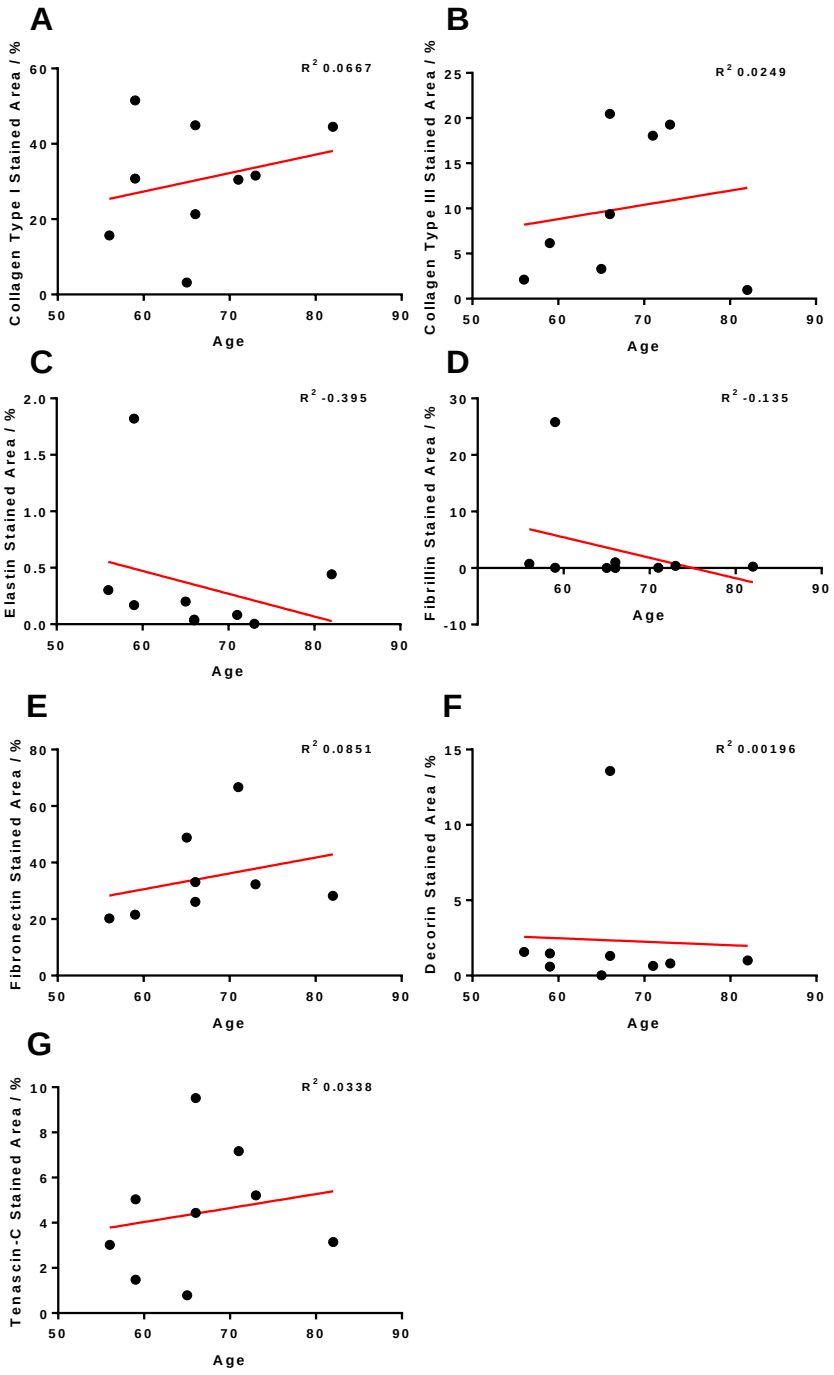

Figure 5-15 Correlations of % area measurements to the ages of the donors. R^2 scores show 'goodness of fit' to a linear association, i.e. the amount of variance in the dependent variable that can be attributed to the independent variable (linear fits where: 1 is strong positive, 0 is none and -1 is strong negative. All graphs are

plotted against age, where **A** shows collagen type I, **B** shows collagen type III, **C** displays elastin, **D** fibrillin, **E** fibronectin, **F** decorin, and **G** tenascin-c.

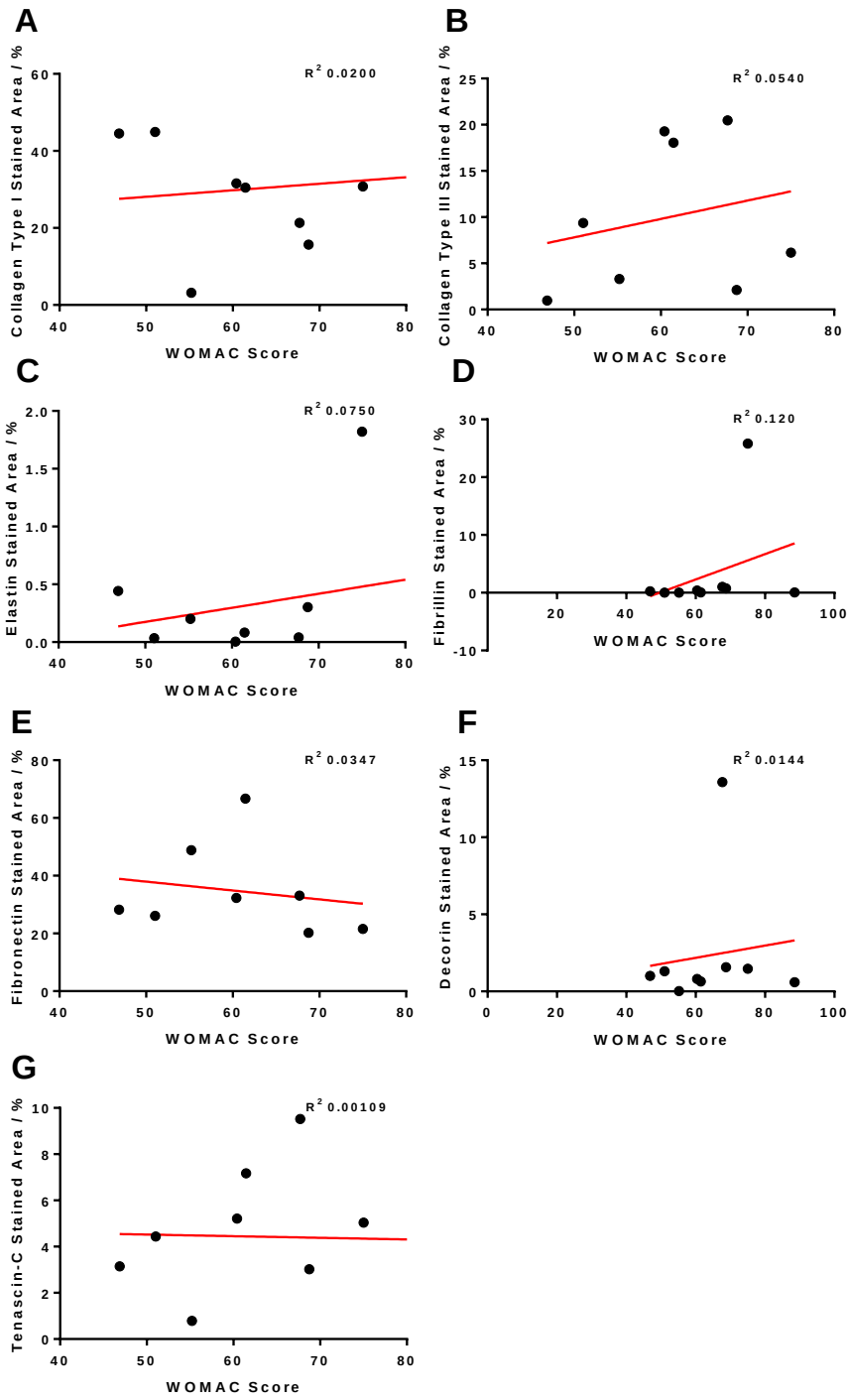

Figure 5-16 Correlations of % stained area to WOMAC scores. R^2 scores show 'goodness of fit' to a linear association, i.e. the amount of variance in the dependent variable that can be attributed to the independent variable (linear fits where: 1 is strong positive, 0 is none and -1 is strong negative). All graphs are plotted

against WOMAC score, where **A** shows collagen type I, **B** shows collagen type III, **C** displays elastin, **D** fibrillin, **E** fibronectin, **F** decorin, and **G** tenascin-c.

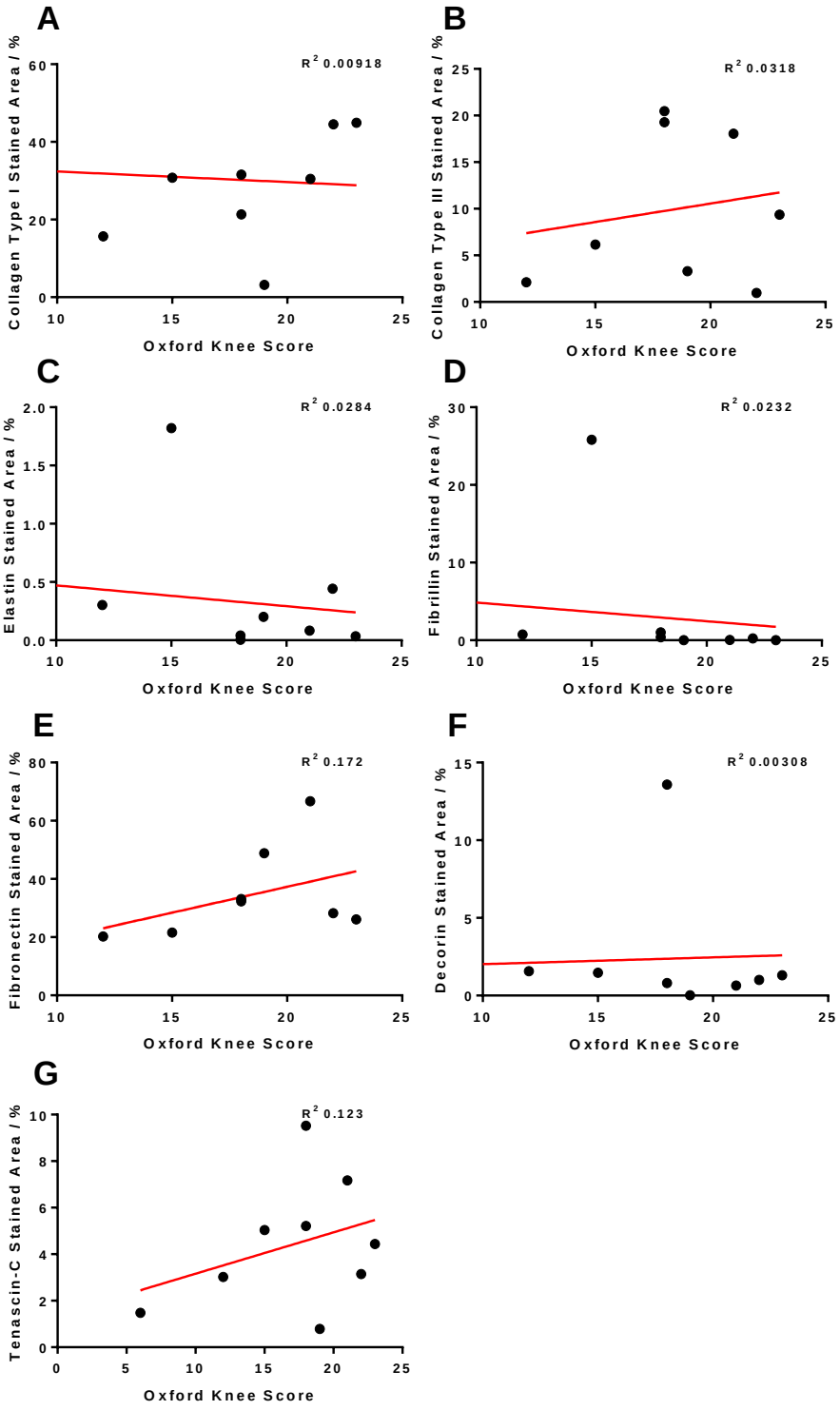

Figure 5-17 Correlations of % stained area to OKS scores. R^2 scores show 'goodness of fit' to a linear association, i.e. the amount of variance in the dependent variable that can be attributed to the independent variable (linear fits where: 1 is strong positive, 0 is none and -1 is strong negative). All graphs are plotted

against OKS, where **A** shows collagen type I, **B** shows collagen type III, **C** displays elastin, **D** fibrillin, **E** fibronectin, **F** decorin, and **G** tenascin-c.

5.3.7 Collagen Type I and Tenascin-C Correlation

Interestingly, it can be observed in Figure 5-18, that the linear relationship between collagen type I and tenascin-c had a strong negative correlation (r^2 = 0.866). N=8 donors were included in the analysis. Donor 9 was omitted due to highly irregular collagen type I content (<1%). Almost all donors fell on or within the 95% confidence interval bounds, giving added strength to the linear model.

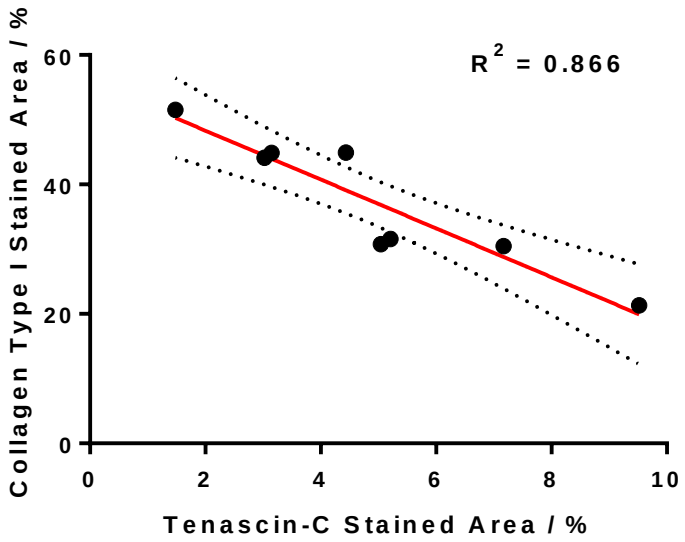

Figure 5-18 Correlation between collagen type I and tenascin-c content of the degenerative male ACL ligament. Red line shows the linear model and the dotted black lines, the 95% CI. Correlation was statistically analysed using Pearson's r test and was found to be stastistically significant ($p<0.001$).

5.4 Discussion

Immunohistochemical and histochemical characterisation was performed on 9 human donor ligaments (collagen type III and fibronectin being the exceptions), in order to observe and semi-quantify ECM protein expression and presence during ACL degeneration. It is to be noted that donor 4 is not included with the collagen type III and fibronectin stains due to the ligament sections no longer being available however, the donor was included with the remaining analysis. This method was selected in order to visualise the conformation and structure of the proteins within the ligament tissue. It was noted however, that multiple other assays would have provided more accurate and quantifiable methods of assessing protein composition, without giving structural information. Assays such as hydroxyproline (total collagen), Fastin (elastin, Bicolor UK), Blyscan (Bicolor UK)/DMMB (GAGs) and Bradford (total protein) assays, as well as protein-specific ELISAs would have provided this quantifiable information on major ACL ECM components. Semi-quantification by % area was selected due to the non-stoichiometric nature of DAB. The logarithmic relationship between protein concentration and staining intensity, means that it is highly sensitive to small changes in measured intensity[425]. Values that fall under the logarithmic/saturated section of the curve can increase disproportionately to those which fall within the curve's linear region. This can result in inaccurate data and false statistical comparisons. Whilst this method of analysis might be acceptable for comparing staining which shows only small or negligible differences, large differences can easily be overestimated.

In order to control for added variation that could be due to sex, male ligaments only were selected. Differences in protein concentration between males and female in the ACL has been previously reported, with higher matrix metalloproteinase 3 (MMP-3), serum albumin, complement component 9, alcohol dehydrogenase 1B (metabolises harmful alcohol-related by-products which have been shown to contribute to enhanced stiffness in tendon[426])[103]. Elastin expression was also found to be increased in women, whilst on average, women displayed lower collagen content than men, which continued to decrease with age[416]. Moreover, there have been differences noted in leukocyte presence within the synovium between males and females, in those presenting with osteoarthritis. Females have been determined to have a higher macrophage count than males[92]. This could potentially alter the presence of proteins such as tenascin-c, which are associated with inflammation and can perpetuate macrophage response[57].

Controls using younger ligaments were not procured for the determination of elastin content in relation to age. This was primarily due to the difficulty of acquisition. Rarely do younger people necessitate the need for total knee replacements, and those that have had this procedure often present with ligament damage from previous rupture, reconstruction or injury. Expected differences in elastin and elastic-fibre associated protein (fibrillin) content with relation to age were not observable. These differences may not be observable over such a small range of ages and may have required much younger (<30 years) ligament in order to observe marked differences. Interestingly, there appeared to be no correlations in any of the % area results to age, with the exception of collagen type III (once donor 1 had been removed due to suspected abnormal collagen type III content). None of the protein areas calculated aligned with either WOMAC or OKS scores. This could be due to the subjectivity of the scoring system (patient performed)[427, 428], or the lack of precision in a semi-quantitative method such as % area staining calculations.

Significantly higher levels of fibronectin staining were observed in donor 3 when compared to other donors ($p<0.05$) with the exception of donor 7. The increase in fibronectin area appeared to correspond with a decrease in ECM integrity score and a slight increase in tenascin-c expression. The occurrence of these factors imply severe degeneration of the ligament, due to both fibronectin's role in tissue remodelling and tenascin's function in perpetuating chronic inflammatory patterns[57].

Association of tenascin-c in inflammation may explain the relationship observed with collagen type I content, as shown in Figure 5-18. The data displayed a strong negative correlation between increasing tenascin-c and a reduction in collagen type I, which is often caused by degeneration[429]. Hasegawa *et al.* (2013) noted that less collagen type I is observed around chondrocyte-like cell clusters which appear to occur only in degenerative ligaments (and not in normal, ageing ones) and instead the pericellular sequestration of aggrecan and collagen type II can be observed[50]. Moreover, the degeneration of collagen is also associated with mucoid changes in the ligament, with increasing amounts of GAGs replacing the collagen[430]. In response to the secretion of pro-inflammatory cytokines (in osteoarthritic conditions) by synoviocytes in the joint capsule, chondrocytes can overexpress tenascin-c[431]. Tenascin-c reportedly perpetuates the pro-inflammatory cytokine production in macrophages and synoviocytes[57], which again interact with chondrocytes, and have been shown to upregulate the production of collagenase[432]. This may explain the correlation observed between ligament degeneration and tenascin-c content increase. To the author's

knowledge, though this effect has been mentioned in relation to cartilage tissue[57, 96], it had yet to be highlighted in anterior cruciate ligament. Considering the aforementioned, increases in tenascin-c content may prove to be a reliable indicator of ACL degeneration.

Mucoid degeneration is a benign, rare (up to ~9% occurrence[433]), but well-defined hallmark of degeneration in ligament that presents mainly in the middle aged[434]. Cystic changes were observed in donor 5 that appeared consistent with histological evaluations of mucoid degeneration, with lack of collagenous substance and intense alcian blue staining at pH2.5. It was theorised that this could be due to the accumulation of mucoid substances within the cyst[434]. Though this ligament generally retained good scores during the histology scoring (and OKS and WOMAC scores were relatively average compared to the group), it was noted that the majority of the cells present appeared to be fibrochondral in morphology, evidenced by the low cell morphology score. This could explain the presence of excess GAGs generally, but not that of the cystic changes, of which the cause are at present unestablished[433].

Donor 6 was found to have an unusually high elastin content (Figure 5-13C), as well as unusually high fibrillin content (Figure 5-11C). Considering that elastin degrades with age (by various elastases) and also due to chronic inflammation[435], the low vascularity score assigned to donor 6, coincides with osteoarthritic degeneration. Interestingly, these elastic and fibrillin structures do not all co-localise with the vessels present in the ligament. Elastin fibres in donor 6 appear to run longitudinally, parallel to the collagen fascicles (Figure 5-13A), which is where they are usually present in the ligaments of young and healthy donors[59, 404, 416].

Decorin is a glycoprotein which moderates the collagen-elastin interactions within the ECM. Interestingly, decorin appeared to align with collagen type I staining patterns more than that of elastin or fibrillin. This may be due to the major role of its GAG side chains in collagen fibre assembly[436].

The main weakness of this work is that it was based entirely upon qualitative and semi-quantitative data. Although an analysis software (FIJI ImageJ) was employed to performed % area experiments, the use of scoring systems is subjective. RNA/gene expression characterisation would be useful for determining the molecular function of the cells within these donor tissues and, determine whether the gene expression correlated with staining area of the tissue. Though histological staining was selected in order to observe the structure and

morphology of the tissue, previously mentioned biochemical assays would be useful for determining actual protein content and donor tissue variations therein.

5.5 Chapter Conclusions

This chapter aimed to determine the extracellular matrix content of human male degenerative ACLs and compare this between donors. Image analysis of immunohistochemical staining was employed to measure ECM content and donor variation.

The hypothesis that there will be significant variation between donors has been accepted for most proteins measured. Observable and semi-quantifiable differences in ECM content and ligament/cell integrity were confirmed for the majority of ECM proteins between numerous donors ($p<0.05$). However, it was found that elastin and fibrillin content did not correlate with age as was expected (r^2 -0.395 and -0.135 respectively), and might be attributed to the severity of degeneration within the knee joint, though the content of neither of these proteins correlated with WOMAC or OKS degeneration scores (r^2 0.075/0.0284 and 0.12/0.0232 for elastin and fibrillin respectively). Increasing tenascin-c and fibronectin content has been previously reported in association with wound healing and inflammation[57], and confirmation of this could be achieved with additional samples of normal ligament. Tenascin-c content was found to correlate strongly with collagen type I content, perhaps explained by increased tenascin-c mediated inflammation and collagen type I degradation by subsequent upregulation of collagenase[432]. Interestingly, neither tenascin-c nor collagen type III varied significantly between donors, which may indicate that the reduction of collagen type I to III ratios observed were due to a reduction of collagen type I, not an increase in collagen type III within the ACL. None of the protein contents examined correlated with either age, WOMAC or OKS scores, indicating there was no linearity between protein content and age (with the exception of collagen type III after the removal of a potentially erroneous result), or severity of degeneration.

CHAPTER 6 RESPONSE OF HUMAN ANTERIOR CRUCIATE LIGAMENT CELLS TO FIBRILLIN-1 FRAGMENT BIOFUNCTIONALISED CONSTRUCTS

6.1 Overview

6.1.1 Introduction

In order to translate any technology, and discern its appropriateness for human use, it should first be tested on human cells. Primary human cells are an excellent method of determining preliminary response to a material preceding *in vivo* translation, if indeed the application is for human medicine. Although donor to donor variation is known and acknowledged, it is imperative to determine whether a technology has the same, or indeed a similar impact on multiple donors, therefore validating its' generalised use.

Chapter 4 determined that RGD-containing fibrillin-1 fragments had significant effects on primary canine cruciate ligamentocytes that were more far-reaching than enhancement of early-stage attachment previously reported by Bax *et al.* (2007)[310], and that these enhancements were indicative of successful ACL regeneration.

In order to determine whether human cells respond in a similar manner, human ACL ligamentocytes were isolated in-house and characterised for their response. Due to the previous success of higher quantities of fibrillin-1 fragment (1000 ng), only these were taken forward for use with human cells.

6.1.2 Statement of Novelty

To date, the author understands that there is no known record of human ACL ligamentocytes being tested for their response on fibrillin-1 fragment (RGD containing) functionalised aligned fibrous scaffolds with the purpose of assessing their capability for ACL TE.

6.1.3 Hypothesis

With this work, it is expected that human ACL cells will exhibit higher levels of attachment to the scaffolds functionalised with fibrillin-1 fragments and will show higher cell number than the controls at early time points ($\leq$ 24 hrs). Cells will display native morphologies and exhibit good proliferative and regenerative capacity. It is also hypothesised that the cells will produce increased amounts of ECM proteins, which include sGAGs on samples functionalised with fibrillin-1 fragments.

6.1.4 Aims & Objectives

- Successfully isolate human ACL cells from ligament tissue.

- Perform flow cytometry for known human ACL cell markers CD44, CD73, CD90 and CD105.
- Determination the cells regenerative capacity and overall morphology once in culture.
- Colony forming assays with crystal violet will be performed at 10 days post seeding to determine whether the cells are capable of forming colonies.
- Confirm fibrillin-1 fragment-cell attachment efficacy
- Use dsDNA assay (QuantIT picogreen, Thermo Scientific UK) to determine cell attachment to the fragments using non-functionalised TCP as a positive control.
- Ascertain whether the functionalisation with fibrillin increases dispersion of cells and supports native 'spindle-like' morphology.
- LIVE/DEAD labelling assay to visualise the cell morphology and dispersion at early time points.
- Determination whether the functionalisation of the scaffolds has any effect on the overall viability of the cells.
- LIVE/DEAD assay to visualise cell survival versus cell death.
- Metabolic activity measured using the resazurin reduction assay will give information on attachment.
- Quantification of dsDNA to determine the scaffold's ability to support cell attachment and proliferation.
- Determination of the functionalised scaffolds effect ECM production.
- Immunochemical fluorescent staining of neo-collagen type I, fibronectin, and fibrillin on the scaffold.
- Calculate % area of the neo-ECM proteins using FIJI ImageJ for semi-quantitative analysis.
- Determine the effect of the functionalised scaffolds on GAG production.
- DMMB colourimetric assay to calculate the concentration of sGAGs associated with the neo-ECM following papain digestion of the cells on the scaffold.

6.2 Materials & Methods

6.2.1 Materials

6.2.1.1 General Cell Culture

Trypsin/EDTA solution (0.05% trypsin, 0.02% EDTA in Hanks' balanced salt solution, 59417C, Sigma Aldrich UK), bovine serum albumin (BSA; A7906, Sigma Aldrich UK), Dulbecco's phosphate buffered saline (PBS, D8537, Sigma Aldrich UK), Dulbecco's Modified Eagles Media (DMEM, high glucose, D5976, 4500 mg L^{-1} glucose, 584 mg L^{-1} L-glutamine, 3700 mg L^{-1} sodium bicarbonate, D5796, Sigma Aldrich UK), fetal bovine serum (FBS; F9665, Sigma Aldrich UK), antibiotic-antimycotic (A/A; 10,000 U penicillin, 10 mg streptomycin, 25 µg amphotericin B ml^{-1} A5955, Sigma Aldrich UK), low serum growth factor (LSGS; basic fibroblastic growth factor (0.3 µg ml^{-1}), epidermal growth factor (1 µg ml^{-1}), heparin (1 mg ml^{-1}) and hydrocortisone (0.1 mg ml^{-1}), FBS (0.004% v/v), S00310, Gibco UK), 2% gelatin solution (G1393, Sigma Aldrich UK), Accutase® (A6964, Sigma Aldrich USA).

6.2.1.2 Chemicals

10% neutral buffered formalin (HT501128, Sigma Aldrich Germany), gelatin from cold water fish (G7041, Sigma Aldrich, UK), glycine (G8898, Sigma Aldrich UK), Triton-X-100 (X100, Sigma Aldrich UK), ProLong™ Diamond Antifade Mountant (P36970, Invitrogen UK), Resazurin salt (R7017, Sigma Aldrich UK), collagenase type I (from clostridium histolyticum, C0130, Sigma Aldrich USA), crystal violet (C3886, Sigma Aldrich UK), DMSO (dimethyl sulphoxide, D4540, Sigma Aldrich UK), papain (papaya latex, P4762, Sigma Aldrich UK), $HCl_{(aq)}$ (H/1200/PB15, Fisher Chemicals UK), L-cystine (30200, Sigma Aldrich UK), sodium acetate (241245, Sigma Aldrich USA), DMMB powder (1, 9-dimethyl methylene blue, 341088, Sigma Aldrich UK), formic acid, (F0507, Sigma Aldrich UK) sodium formate (094820, Fluorochem UK), shark chondroitin sulphate (C64384, Sigma Aldrich UK), sodium hydroxide (10192863, Fisher Scientific UK), DMSO (dimethyl sulphoxide, D4540, Sigma Aldrich UK) methanol (M/4000/PC17, Fisher Scientific UK), ethylenediaminetetraacetic acid (EDTA, E6758, Sigma Aldrich UK).

6.2.1.3 Assays

Quant-IT™ PicoGreen™ dsDNA Assay Kit (P7589, Thermo Fisher UK), LIVE/DEAD solution (LIVE/DEAD Viability kit, L3224, Life Technologies Ltd. UK), BD Human MSC Analysis kit (562245, BD Biosciences, USA).

6.2.1.4 Antibodies

DAPI (D1306, Thermo Fisher Scientific UK), mouse anti-fibrillin (MAB1919, Millipore UK), rabbit anti-fibronectin (F3648, Sigma Aldrich UK), goat anti-type I collagen (UNLB, 1310-01, Southern Biotech USA), donkey anti- mouse IgG Alexa Fluor 633nm conjugate (SAB4600131, Sigma Aldrich UK), donkey anti-rabbit IgG (H+L) Alexa Fluor 594 nm (A31572, Thermo Fisher Scientific UK), donkey anti-goat IgG (H+L) Alexa Fluor 488 nm (A11055, Thermo Fisher Scientific UK).

6.2.2 Acquisition of Human Anterior Cruciate Ligament Cells

Information on tissue acquisition and inclusion criteria is detailed in Chapter 5, section 5.2.1.

6.2.2.1 Ethical Approval and Considerations

Ethical approval information is documented in Chapter 5, section 5.2.2.1.

6.2.3 Tissue Digestion

Tissue was divided into three parts. One section of the ligament was halved and snap frozen in liquid nitrogen and stored at -80°C. Another was fixed for histological analysis (see Chapter 5, section 5.2.3). The remainder was minced into ~0.5-1 mm^3 sections and washed thrice with 10 ml sterile PBS. Tissue sections were placed in sterile centrifuge tubes with 10 ml sterile filtered (0.22 µm pore filter, MillexGP PES membrane, SLGP033RS, Fisher Scientific UK) 0.1% collagenase type I w/v in hgDMEM (1% A/A, serum free), for between 6 and 20 hrs, depending on tissue quantity. Tissue was incubated on a sample shaker to facilitate digestion (37°C, 50 rpm)[61]. Cells were passed through a 100 µm pore strainer to remove any debris/residual tissue before being centrifuged at 300 g for 4 mins and resuspended in fully supplemented media (hgDMEM, 10% FBS, 1% A/A, 0.2% LSGS). Cells were plated on 0.1% gelatin coated (15 mins, 37°C) T75 flasks at an initial density of ~1 x 10^4 cells cm^{-2} and labelled as P0. Media was changed after 4-7 days to allow for attachment of adherent cells. A diagrammatic representation of the protocol is displayed below in Figure 6-1.

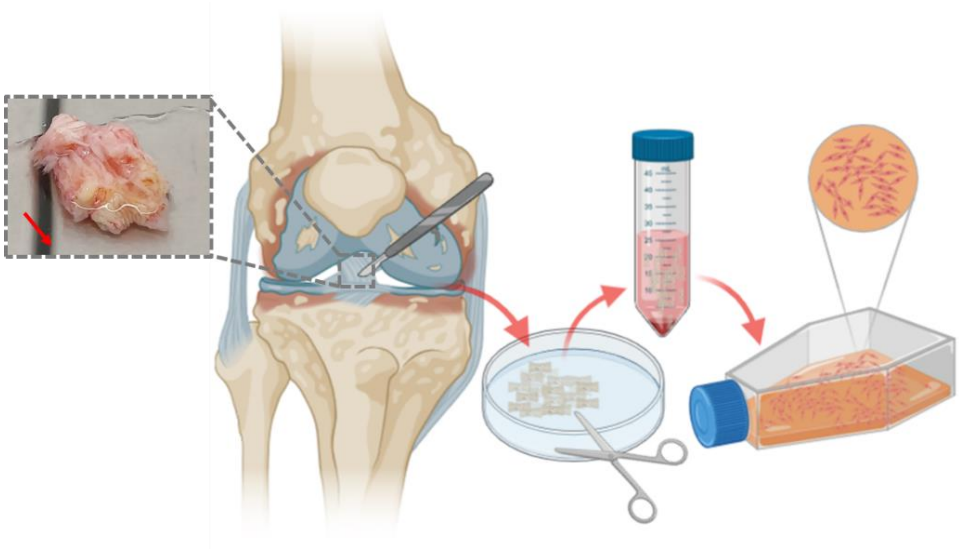

Figure 6-1 Depiction of human ACL ligament extraction and digestion technique. Red arrow indicates direction of fibrous collagen matrix. Ends of the ligament were trimmed to remove as much of the bone integration sites at the proximal and distal ends as possible. The remaining midsubstance of the ligament was then sectioned as described in below.

6.2.4 Culture and Maintenance of hACLs

6.2.4.1 Maintenance of hACLs

hACLs were maintained in CellStar T75 flasks with hgDMEM media (supplemented with 10% FBS and 1% A/A). LSGS (0.2%) containing; Basic Fibroblastic Growth Factor (0.3 µg ml^{-1}), Epidermal Growth Factor (1 µg ml^{-1}), Heparin (1 mg ml^{-1}) and Hydrocortisone (0.1 mg ml^{-1}), FBS (0.004% v/v) was added to the media to encourage cell proliferation. The cells were replenished with 10 ml of fresh medium every 3-4 days as required. Confluences of 90-95% were reached before passaging (1:3).

6.2.4.2 Seeding and Culture of hACLs on Scaffolds

Cells at passages 3 -5 were used in all experiments. Various donors described in Table 6-1 were used in scaffold-seeded, attachment (TCP) and clonogenic (TCP) experiments. hACLs were detached from flasks using trypsin-EDTA (2 ml, 3-4 mins, 37°C, 5% CO2, 95% humidity) and centrifuged at 300 g for 4 mins. Cells were seeded onto the scaffolds using the 'drop method' at a density of 6 x 10^4 cm^{-2}[179] using 100 µl drops for all scaffold culture experiments. Drops were suspended on the scaffolds for a further 2 hrs in standard incubation (37°C, 5% CO2, 95% humidity) to enable attachment, before the wells were flooded with 2 ml standard media (hgDMEM with 10% FBS, 1% A/A).

Table 6-1 Specific details of donors used for viability experiments.

Donor ID	Age	Oxford Knee Score	WOMAC Score
ACL02	73	18 (37.50% function)	60.42% difficulty
ACL04	59	6 (12.50% function)	88.54% difficulty
ACL07	66	18 (37.50% function)	67.71% difficulty
ACL09	65	19 (39.58% function)	55.21% difficulty

6.2.5 Flow Cytometry for Donor Cell Characterisation using ACL Markers

Table 6-2 Information relating to the specific donor ligaments used for flow cytometry hACL cell marker analysis.

Donor ID	Age	Oxford Knee Score	WOMAC Score
ACL04	59	6 (12.50% function)	88.54% difficulty
ACL06	59	15 (31.25% function)	75.00% difficulty
ACL07	66	18 (37.50% function)	67.71% difficulty
ACL09	65	19 (39.58% function)	55.21% difficulty

Flow cytometry was used to perform cell characterisation on donors described in Table 6-2, by detection of previously reported ACL cell surface markers CD44, CD73 and CD90, CD105, using the BD Human MSC Analysis kit. A negative control cocktail containing CD19, CD34, CD11b, CD45 and HLA-DR were used to determine levels of population homogeneity. Isotype controls were used for all staining cocktails. These were used to ascertain the homogeneity of the cultured cell population isolated from the ligaments, to be used in experiments. Flow cytometry experiments were performed with passage 4 cells.

Media was removed from a single flask of each donor and cells were washed once with pre-cooled PBS (4°C, 5 ml). Accutase® solution (5 ml) was applied to the cultures (5 mins, 37°C) before washing again with PBS and mixing well to achieve a single cell suspension. Cells were transferred to a 50 ml centrifuge tube and centrifuged (400 g, 5 mins). Cells were resuspended in stain buffer (10 mg ml^{-1} BSA in PBS, 10 ml, 4°C) and counted. Cells were split into equal numbers in 2 ml micro-centrifuge tubes and centrifuged (500g, 5 mins, 4°C). Supernatant was removed and cells were resuspended in stain buffer (600 µl, 4°C) at a

concentration of 1.5 – 2.25 x 10^6 cells ml^{-1}. Single target antibodies (FITC Mouse anti-Human CD90, PE Mouse anti-Human CD44, APC Mouse anti-Human CD73, PerCP-Cy5.5 Mouse anti-Human CD105 and PE Mouse IgG2b κ isotype control) were added at a dilution of 1:600 and cocktail antibodies (PE hMSC Negative Cocktail, PE hMSC Isotype Control Negative Cocktail, hMSC Positive Cocktail, hMSC Isotype Control Positive Cocktail) were added at 1:150 and were incubated on ice (45 mins). Cells were then centrifuged (500 g, 5 mins, 4°C) and resuspended in stain buffer (500 µl, 4°C) twice before being resuspended in 350 µl stain buffer for analysis.

Measurements were taken using a BD FACS Diva, with 10,000 events measured per suspension. Spectra were analysed using FlowJo v10.7.

6.2.6 hACL Response to Fibrillin-1 Fragment-Functionalised Scaffolds

6.2.6.1 Regenerative Potential and Cell Morphology

To determine the regenerative potential of the human donor cells, a colony forming unit (CFU) assay was performed for 3 individual donors. Cells were seeded in 6 well plates at a density of 200 cells cm^{-2} and cultured for 10 days (n=6)[240]. Fixation was performed using 10% neutral buffered formalin (2 ml, 20 mins, room temperature) and washed with PBS, before the addition of 0.5% crystal violet in methanol (2 ml $well^{-1}$, 5 mins, room temperature). Excess stain was removed, and plates were washed (x5) with deionised water before imaging on an EVOS LV light microscope to visualise colonies.

6.2.6.2 Confirmation of Attachment to Fragments

Fragments were adsorbed to 96 well plates (overnight, 4°C) as described previously. Excess solution was removed and 200 µl of sterile filtered 10 mg ml^{-1} BSA (in PBS) was incubated in the wells for 1 hr (37°C). Cells were seeded in 100 µl aliquots at a density of 1.5 x 10^4 cells $well^{-1}$ using serum free media. Media was removed at 1 hr time point. Cells were washed with PBS and suspended in lysis buffer (200 µl, 1% triton-X-100 in X1 TE buffer, 20 mins). To analyse, 50 µl per well of suspension was added to 50 µl of X1 TE buffer in a 96 well plate in duplicate (n=4). Analysis protocol on the fluorescent plate reader was performed as in Chapter 4, section 4.2.5.

6.2.6.3 Cytotoxicity, Cell Distribution and Morphology on Functionalised Scaffolds

Protocol was as performed in Chapter 3, section 3.2.14.3.

Cells were imaged on a Yokogawa CQ1 cell imaging system with a 5µm step size. All imaging parameters were kept consistent throughout imaging.

6.2.6.4 Metabolic Activity

Protocol was performed as in Chapter 3, section 3.2.14.4.

6.2.6.5 Proliferation and Cell Number

Samples were cultured to 4 hrs (0 days), 1 day, 7 days and 14 days before being washed with PBS and digested in 500 µl of a 10 U ml^{-1} buffered papain solution (60°C, overnight). Resulting suspension was pipetted (50 µl) in duplicate with 50 µl X1 TE buffer (1 mM EDTA, 10 mM Tris-base) in sterile filtered deionised water) into a 96 well plate for measurement. Analysis protocol is described in Chapter 4, section 4.2.5; standard curve used is displayed in Appendix 17A.

6.2.6.6 Extracellular Matrix and sGAG Production

6.2.6.6.1 Immunofluorescent Detection of ECM Production

Protocol performed as in Chapter 4, section 4.2.7.1.

6.2.6.6.2 Orientation of Cells

Analysis performed as in Chapter 4, section 4.2.8.

6.2.6.6.3 ECM-Associated sGAG Production

This method was adapted from Kharaz (2015)[388], using the method first published by Farndale *et al.* (1986)[437].

Cells were cultured until 1, 7 and 14 day time points before being digested in 500 µl of a buffered papain solution (10 U ml^{-1} papain, 5 mM Na_2EDTA; 2.4 mM L-cystine; 0.1 M sodium acetate; corrected with 6 M $HCl_{(aq)}$ to pH 6) overnight at 55-60°C (100 rpm). Suspensions were stored at -80°C until analysis.

To analyse, 250 µl of DMMB solution (16 mg 1, 9-dimethyl methylene blue, 2 ml formic acid,; 2 g sodium formate, 998 ml deionised H_2O, pH 3.0) was added to 40 µl of sample suspension in duplicate. Absorbance maximum at 520 nm was read immediately on a Labsystems Multiskan Ascent plate reader.

Shark chondroitin sulphate was used to create a standard curve (Appendix 17B) from 0 to 25 µg ml^{-1} from which sGAG concentrations were calculated. sGAG concentration was reported as both µg ml^{-1} and µg µg $dsDNA^{-1}$ ml^{-1}.

6.2.7 Statistical Analyses

All statistical analyses were performed using Graphpad Prism V7. Gaussian distributions of results were verified using D'Augstino-Pearson normality test. A one or two-way ANOVA (with Tukey's post hoc tests) was performed if normal distribution assumption was satisfied. A Geisser-Greenhouse correction (non-homogeneity of variances) was applied as standard. Non-normally distributed data was subject to a non-parametric Kruskal Wallis H test with Dunn's rank comparison post hoc (lack of normal distribution). N number for experimental data represents sample repeats within the experiment. All data shown is based on a minimum of two experimental repeats unless otherwise stated.

6.3 Results

6.3.1 Characterisation of ACL Ligamentocyte Marker Expression

In order to determine homogeneity of the individual donor populations of cultured cells, and to ascertain cell phenotype, four donors were randomly selected to determine the expression of widely reported ACL-related CD markers. Of the markers tested, CD73 was highly expressed in all donor populations (>99%) with very little variation between donors (see Figure 6-2)**.** CD90 appeared to be stably expressed, and was positively identified in approximately 50% of each donor population, whilst CD105, though stably expressed in ACL06, ACL07 and ACL09 at approximately 40%, showed very low expression (1.23%) in ACL04. Similarly with CD44, where ACL06 only positively displayed expression in 67.8% of the population, compared to the other donors (94.5-96.7%). As seen in Figure 6-2, under 1% of cells from all donors (with the exception of ACL07, of which approximately 2% of all cells displayed positive expression) expressed negative control markers, implying lack of "contamination" in the cell populations with haemocyte and immunoprotective cell types.

A

Marker	Expression
CD44	++
CD73	+++
CD90	++
CD105	+
CD11b	-
CD19	-
CD34	-
CD45	-
HLA-DR	-

B

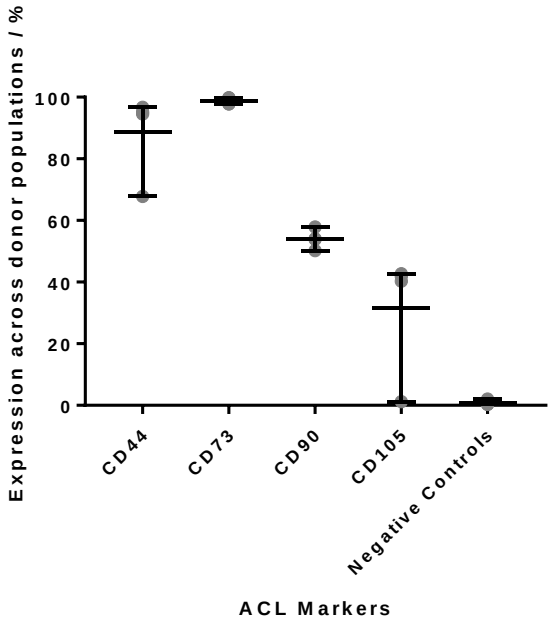

Figure 6-2 Average CD marker expression of ACL cells from 4 independent donors, characterised by flow cytometry. **A -** Expected positive (CD44, CD73, CD90, CD105) and negative (CD11b, CD19, CD34, CD45, HLA-DR) markers are shown. Symbols indicate % positive expression within the characterised population;

+++ >90%, ++ >50-90%, + >5-50%, - ≤1%. **B** – A graph to show the variation in expression of expected positive and negative (CD11b, CD19, CD34, CD45, HLA-DR) markers between the characterised donors (n=4). Aligned dot plots show a more detailed range of expression, to complement the data presented in **A** and elucidate on data spread. Grey points show individual donor percentage expression, mid-lines represent means and error bars show data range.

6.3.2 Clonogenic Potential and Cell Morphology

In order to assess the regenerative potential of the cell used in the subsequent experiments, a colony-forming unit (CFU) assay was performed. As opposed to seeing the formation of tight and distinctly stained colonies, the ACL04 cells appeared to be mostly uniformly disperse, coating the bottoms of the wells or in loosely formed, small colonies. Narrow fibroblastic shaped cells, which formed small, elongated networks, were seen to be interspersed with wider cell morphologies (Figure 6-3B). Similarly in ACL02, where cells formed very few colonies and cells displayed a mix of elongated, smaller cell and highly spread, larger morphologies (Figure 6-3C) ACL09 however, formed multiple dense and tightly packed colonies after 10 days of culture (Figure 6-3A), with cells retaining their elongated, fibroblastic shape, indicating higher regenerative potential than that of ACL04.

All images were displayed due to the high degree of variation in clonogenic response of the donor cells.

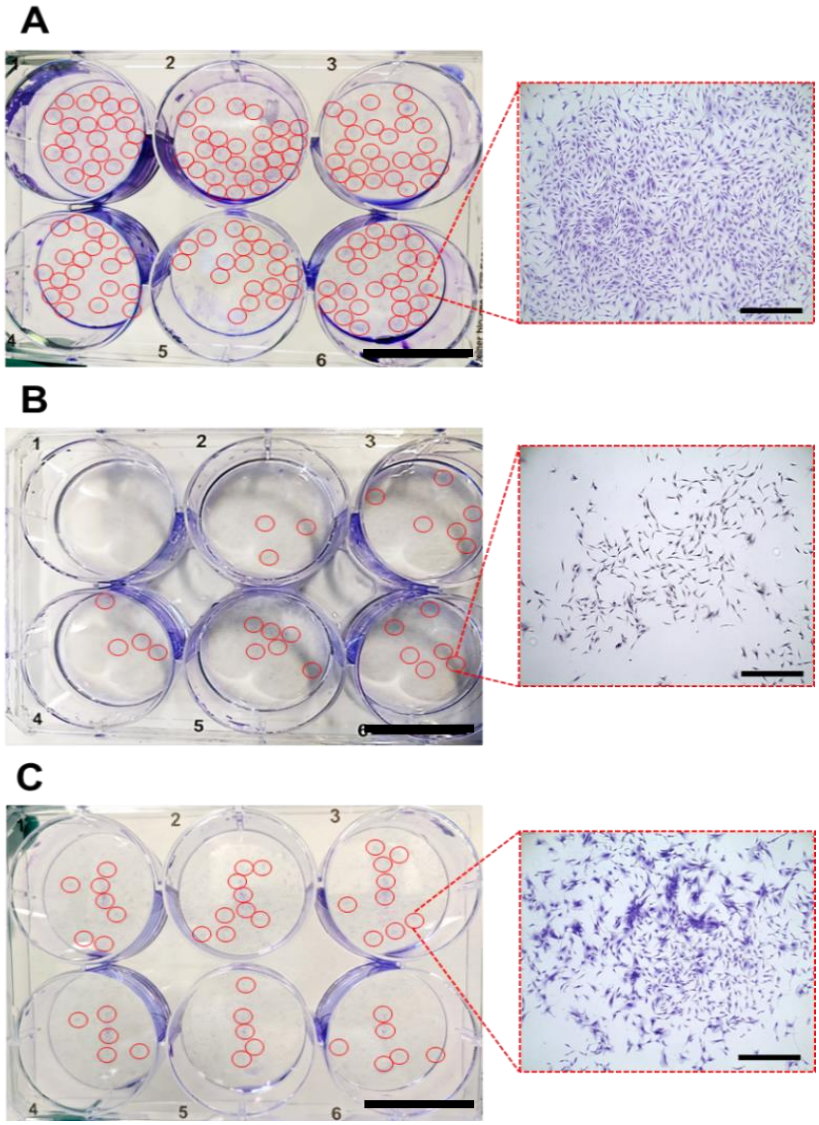

Figure 6-3 Colony forming assay of ACL09 (**A**), ACL04 (**B**) and ACL02 (**C**), performed to show the regenerative potential of isolated human anterior cruciate ligament cells. Brightness was enhanced across the whole image uniformly for easier visualisation. Images show overall staining in the plate and brightfield images of 0.5% crystal violet stained cells. Scale bars are equivalent to 30 mm (plate view) and 1 mm (microscope view) respectively. Red circles indicate areas of colony formation.

6.3.3 hACL Attachment to the Fibrillin-1 Fragments

hACLs were seeded on (relatively) non-variable substrates (TCP) to determine preferential attachment between fragments (Figure 6-4). As TCP is a widely used substrate for cell attachment, it was used as the 100% control from which % attachment was calculated. Pervious to this, non-specific cell attachment was normalised to the BSA control. hACLs

were found to attach most strongly to fragments PF8 and PF17.1 with 114.9 and 109% attachment respectively when compared to the positive TCP control. Cells also displayed a strong preference for fibronectin (as expected, due to use as a positive control cell adhesion protein[315]) with 114.2% attachment compared to the TCP control. PF9 supported the lowest levels of attachment ($p<0.0001$), with on 68.27% attachment when normalised to TCP.

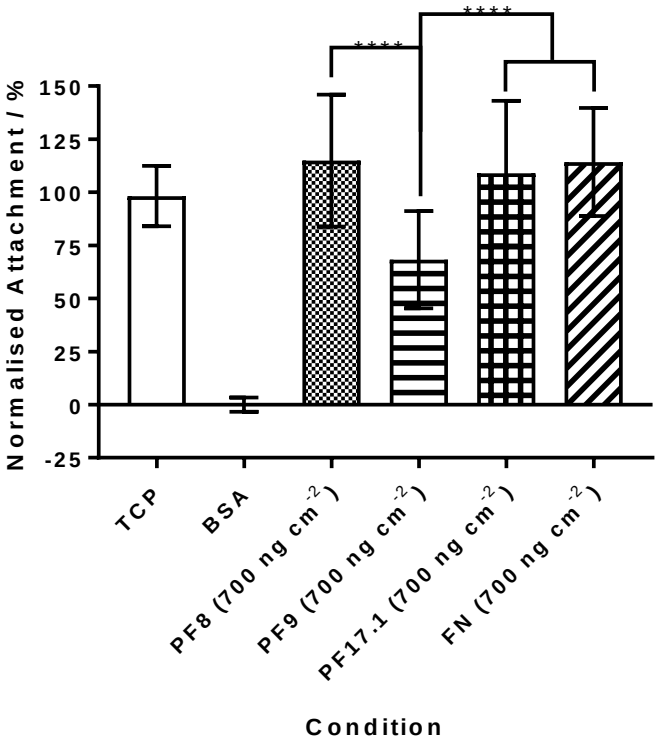

Figure 6-4 Attachment of human ACL cells to fibrillin-1 fragments at 1 hr post seeding on a non-variable substrate (TCP, n=4). Surfaces were normalised to BSA attachment (adsorbed 1 hr, 37°C), and TCP control was used for reference as 100% attachment. Data shown in pooled from 3 experimental repeats (includes 2 independent donors). One way ANOVA with Tukey post hoc tests were performed. Bars show means ± SDs. ****$p<0.0001$.

6.3.4 Viability of hACLs on Functionalised Scaffolds

6.3.4.1 Morphology, Dispersion and Cytocompatibility

Depicted in Figure 6-5A, B and C, at 4 hours post seeding, cell morphology and dispersion appeared uniform across all conditions within each donor (with the exception of ACL09). However, at 24 hrs, it became apparent that PF8 and PF17.1 displayed cell morphology and attachment that mimicked native morphology more closely than the other conditions, and comparable to the fibronectin positive controls. However, though the negative controls and PF9 appeared to support very early time point attachment (with the exception of ACL09), at

24 hrs they appeared to display lower cell densities and organisation compared to PF8, PF17.1 and fibronectin.

Interestingly, ACL04 and ACL07 showed agreement with regards to preference in fragment, with PF8 retaining both the highest density of ligamentocytes and appearing to support the highest degree of cellular alignment and dispersion 24 hours following seeding. This degree of orientation appeared to be of equal performance with the fibronectin control, where cells displayed extremely high degrees of directionality as described by Missirlis *et al.* (2017)[301].

Interestingly, with ACL09, there were more dead cells observed than on either ACL04 or ACL07 where they were rarely detected.

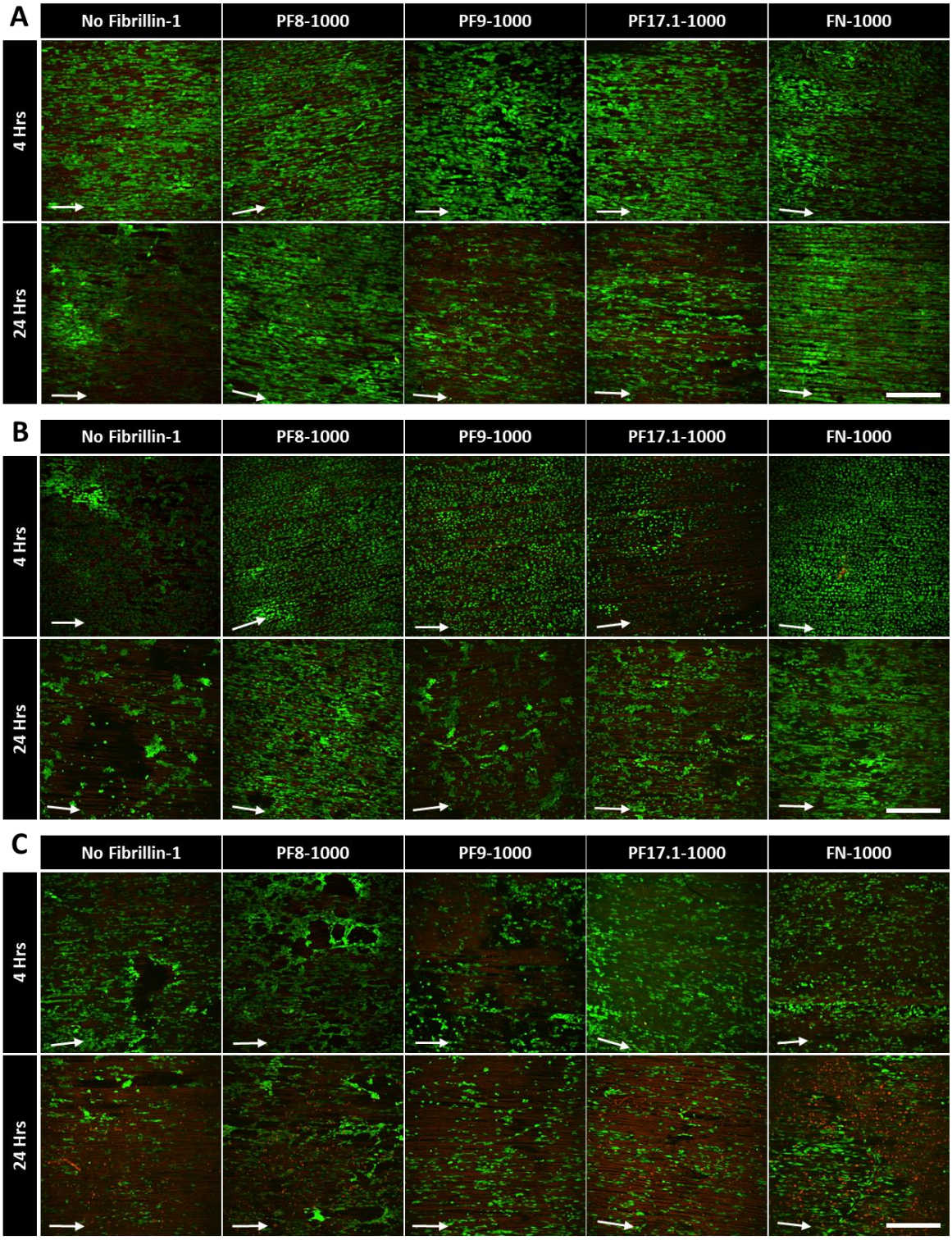

Figure 6-5 LIVE/DEAD assay montages of cell populations from the ACLs of 3 independent human donors (ACL04 – **A**, ACL07 – **B**, ACL09 – **C**) on fibrillin-1 fragment, fibronectin or non-biofunctionalised plasma treated scaffolds. In these micrographs, live cells are shown in green and dead cells in red. Scale bars represent 500 µm and the white arrows indicate fibre direction.

6.3.4.2 Metabolic Activity

Metabolic activity analyses were performed on two donors of hACLs. Inter-donor variation in response was noted between both donors. Significant differences in response between functionalisation conditions occurred at both early and later time points for ACL09 and ACL04 respectively and differences in trend of response were observed. Graphs shown in Figure 6-6A and B, revealed that ACL09 ligamentocytes seeded on PF8 and PF17.1 functionalised scaffolds maintained a higher metabolic activity than those cultured on PF9-functionalised scaffolds (non-significant) and the non-functionalised controls ($p<0.05$, $p<0.01$ respectively). This trend was maintained until 24 hours, and at 7 days, responses of all substrates became almost equal. Meanwhile, ACL04 began to show significantly greater responses to the fibrillin-1 fragments at later time points. At 24 hrs however, the responses to the fibrillin-1 fragments were reduced compared to that of fibronectin or the non-functionalised controls ($p<0.0001$). At 7 days, both PF8 and PF9 induce significantly enhanced responses with the ligamentocytes ($p<0.0001$ and $p<0.01$ respectively), perpetuating this response until 14 days where enhanced hACL response to PF17.1 was also observed ($p<0.0001$). Conversely, ACL09 ligamentocytes began to reduce their metabolic

activity on PF8 and PF9-fucntionalised scaffolds ($p<0.05$, $p<0.0001$ respectively) compared to the control scaffolds.

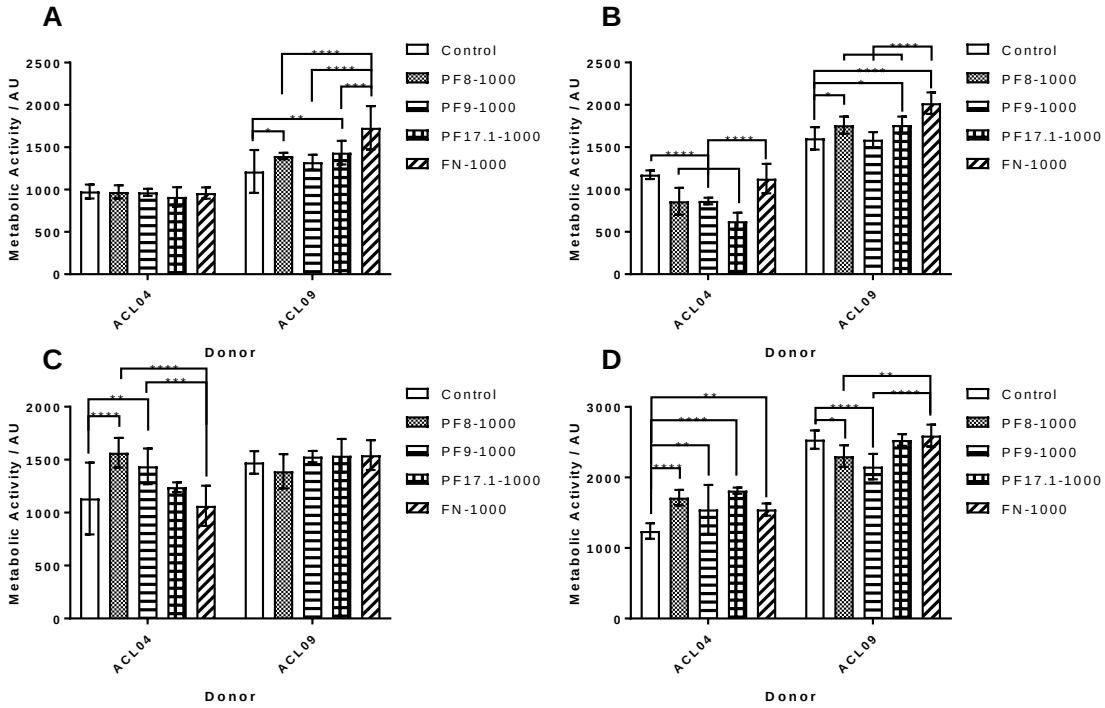

Figure 6-6 Metabolic activity of functionalised scaffolds with 2 independent donors (n=3). Bar chart shows metabolic activity as a comparison between conditions at day 0 (4 hrs, **A**), day 1 (**B**), day 7 (**C**) and day 14 (**D**). Means ± SDs are displayed. Donors are shown separately due to variation in response. Experimental repeats for ACL04 and ACL09 are 1 and each donor was analysed separately due to differences in cell response. Two-way ANOVAs were performed with Tukey's post hoc tests to identify individual significances. *p<0.05, **p<0.01, ***p<0.001, ****p<0.0001.

6.3.4.3 Proliferative Response and DNA Content

Double stranded DNA (dsDNA) concentration is a popular and quantitative method for inferring the cellular content of the material present in a sample.

As shown in Figure 6-7A, at following initial seeding (4 hrs/0 days), ACL04 appeared to have a lower dsDNA concentration on the fibrillin-1 functionalised scaffolds than either the non-functionalised or fibronectin-functionalised scaffolds. This trend was perpetuated for all time points up to 7 days, with the exception to 0 days where neither were significantly different to PF17.1 (4 hrs/0 days $p<0.01$, 1 day $p<0.0001$ and 7 days $p<0.0001$). Fibronectin remained significantly higher in dsDNA concentration than all fibrillin-1 fragment functionalised scaffolds from day 1 to day 14 ($p<0.0001$)and significantly different to non-

functionalised controls at 7 and 14 days ($p<0.0001$). Non-functionalised scaffolds retained a significantly higher dsDNA concentration to PF8 and PF9-functioanlised scaffolds at 14 days also, but did not display significantly higher cell content than PF17.1 scaffolds at 14 days. The content of cellular material on non-functionalised controls remained somewhat consistent (with small fluctuations) throughout the experiment, though fibronectin-functionalised scaffolds appeared to support a maximum cell number at 7 days, where dsDNA concentration appeared to stabilise. A small reduction in dsDNA concentration is displayed for PF17.1 scaffolds at day 1 (possibly due to the washing step before papain digestion at 4 hours), though fragments remained consistent in cell concentration until 14 days where a small increase could be observed.

ACL09 (displayed in Figure 6-7B) however, shows an elevated dsDNA concentration at 4 hours compared to the non-functionalised controls on both PF8 and PF9 functionalised scaffolds ($p<0.05$). A decrease in dsDNA concentration at 7 days appears to suggest cell confluence on the scaffolds, with the concentration of cellular material slowly increasing at day 14. Fibronectin-functionalised samples showed significantly greater dsDNA concentration when compared to all other scaffolds from 7 days onwards ($p<0.01$) and this concentration steadily increased over the entire 14 day period.

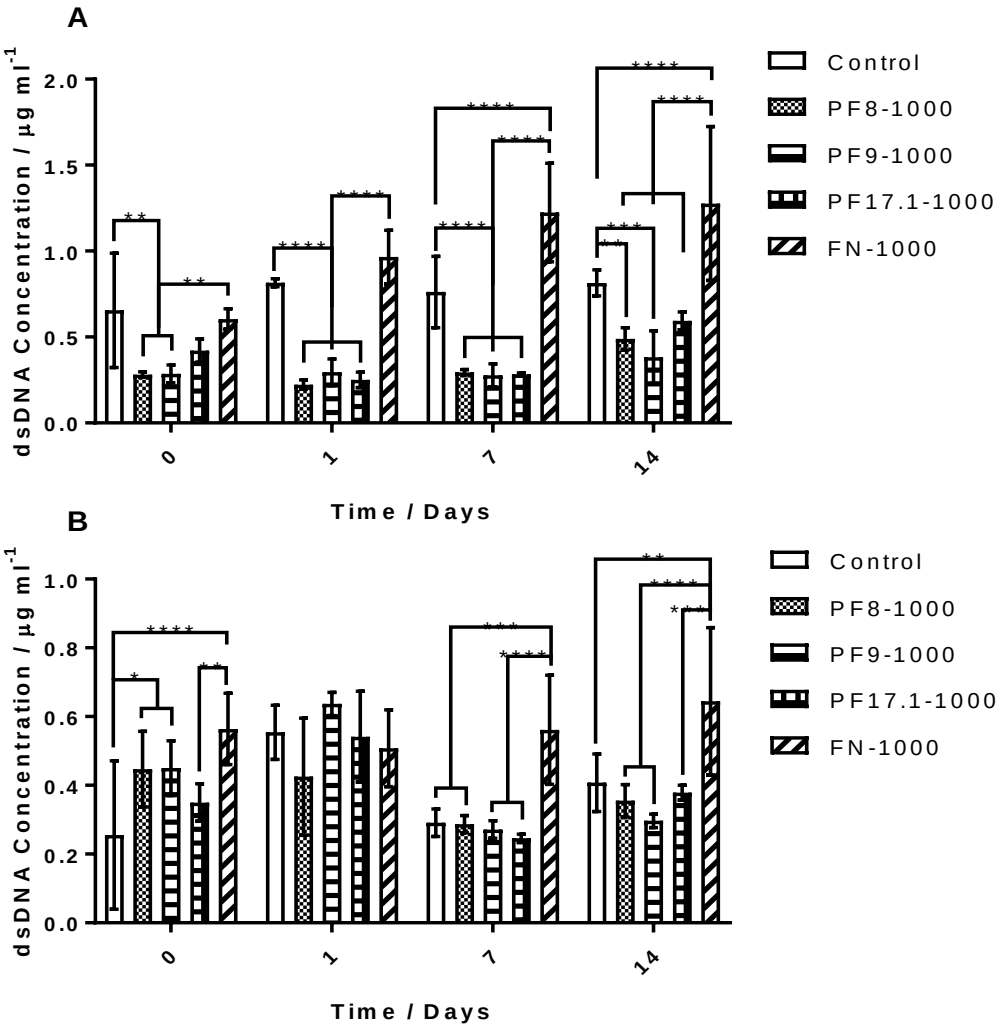

Figure 6-7 Total hACL DNA concentration present on the fibrillin-1 biofunctionalised scaffolds using donors ACL04 (**A**) and ACL09 (**B**), at 0 (4 hrs post seeding), 1, 7 and 14 days. Means ± SDs are displayed for both graphs. A two-way ANOVA test was performed with Tukey's multiple comparisons test. Data shown and analysed is from 1 experiment per donor. Means ± SDs are shown. *p<0.05, **p<0.01, ***p<0.001, ****p<0.0001.

6.3.5 hACL ECM Production and Deposition

6.3.5.1 Total ECM Content

Immunofluorescent micrographs of hACLs (Figure 6-8) were semi-quantified for % area of total ECM protein in collagen type I, fibronectin and fibrillin (Figure 6-9). All conditions showed strongly anisotropic ECM protein production and cell orientation. Though PF9 performed well, increasing total ECM content per cell at day 1, this effect was lost at day 7. PF8 however, was determined to have increased ECM proteins per cell at day 7 and all fragments and the non-functionalised controls were shown to have significantly higher total ECM than that of fibronectin-functionalised scaffolds (negative control $p<0.01$, PF8 and PF9 $p<0.05$, PF17.1 $p<0.001$). At day 14, it appeared that PF8 had enhanced total protein content significantly, when compared to both negative controls and fibronectin ($p<0.05$ and $p<0.01$ respectively). The comparison with fibronectin also translated to total ECM production per cell at day 14, where fragments PF8 and PF17.1 were shown to have significantly higher ECM production than that of fibronectin ($p<0.001$, $p<0.01$ respectively). At 28 days, both total ECM coverage of the scaffolds and total ECM production per cell appeared to stabilise amongst the conditions, where PF8 showed only a slight increase in total ECM coverage that was significant to fibronectin ($p<0.05$).

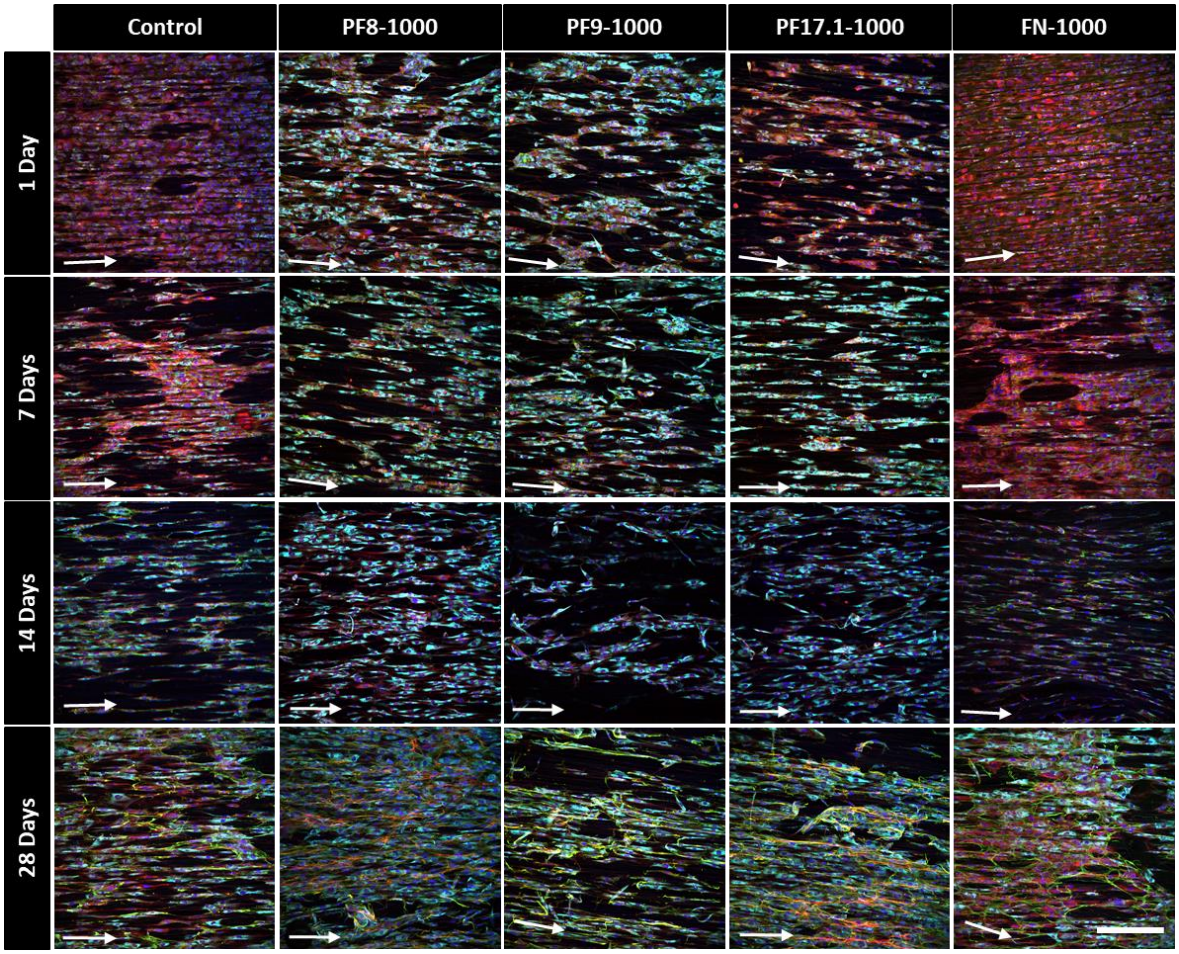

Figure 6-8 Immunofluorescent imaging of hACLs on fibrillin-1 fragment functionalised plasma-treated scaffolds and controls. These images display the representative cell numbers (cell nuclei, blue), collagen type I (cyan), fibronectin (green) and fibrillin (red) production over 28 days in culture. White arrows indicate fibre direction and the scale bar (bottom right) represents 250 µm.

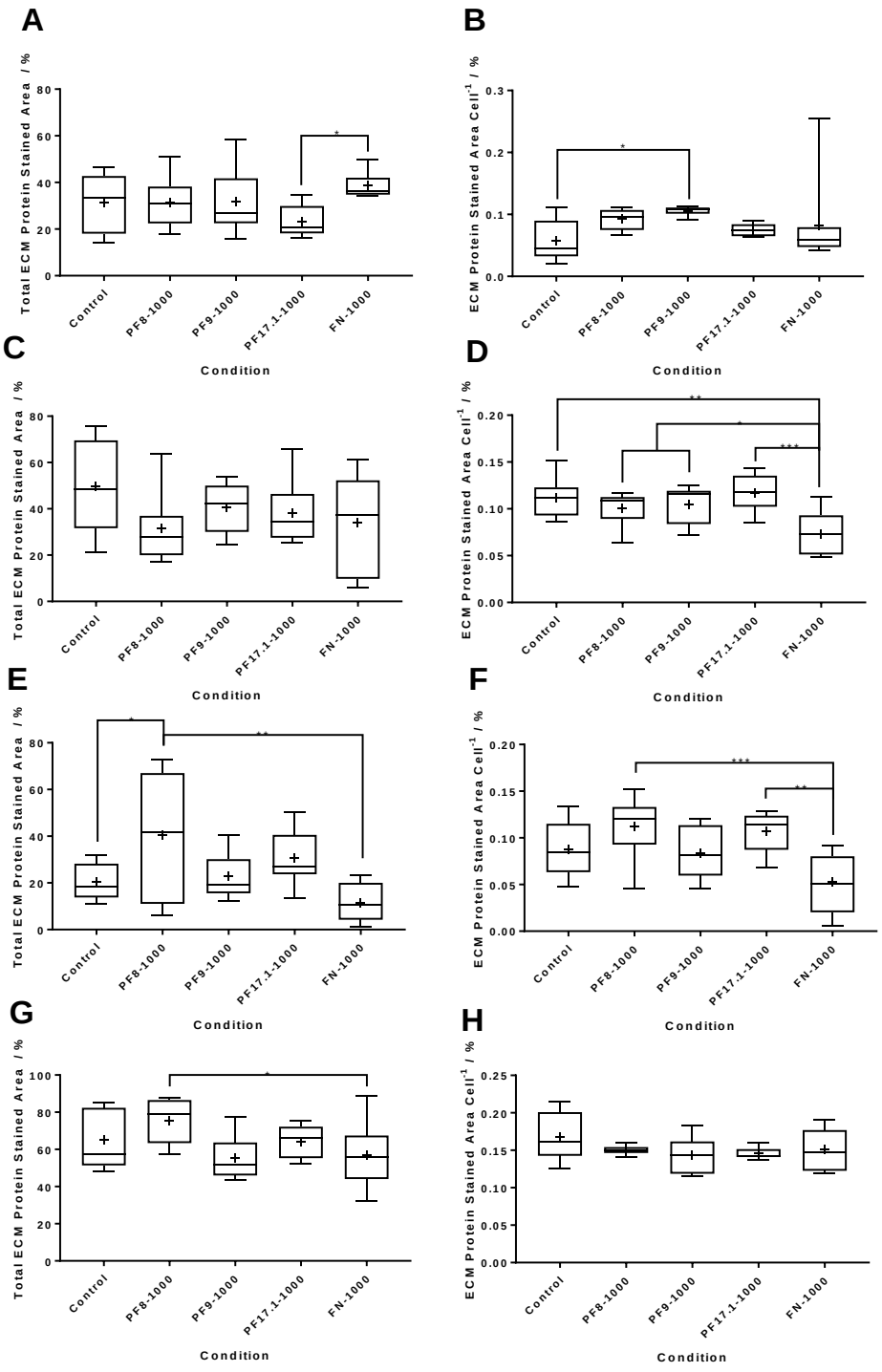

Figure 6-9 Total ECM proteins displayed on the fluorescent micrographs (n=3) at 1 (**A**, **B**), 7 (**C**, **D**), 14 (**E**, **F**) and 28 (**G**, **H)** days. Total % area is shown in the left column (**A**, **C**, **E**, **G**) and % area per cell is shown in the right (**B**, **D**, **F**, **H**), One-way ANOVA with Tukey's HSD post hoc tests and Geisser-Greenhouse corrections were used. Box and whisker plots show median (midline), interquartile ranges (box bounds), min and max range (error bars). The mean is denoted as '+'. Experiment performed once. *p<0.05, **p<0.01, ***p<0.001.

6.3.5.2 Nuclear Count for Cell Number Approximation

hACL number present on the scaffolds was approximated by FIJI ImageJ particle analysis of DAPI stained cell nuclei. As shown on Figure 6-10A, at day 1, nuclear counts displayed elevated numbers of cell nuclei present on both non-biofunctionalised and fibronectin-functionalised scaffolds in comparison to the ones functionalised with fibrillin-1 fragments ($p<0.0001$). Presented on Figure 6-10B, PF8 appeared to stabilise the cell population on the scaffolds over 14 days of culture, before increasing at 28 days ($p<0.05$). PF17.1 appeared to provide greater support to preventing a decrease in ligamentocyte number compared to PF9 and fibronectin/non-functionalised controls at 14 days, however there was a small, but observable decrease present (non-significant to nuclear counts at 1 and 7 days). This is shown in contrast to both the non-functionalised and fibronectin-functionalised scaffolds which showed large decreases in cell number from 1 to 14 days ($p<0.0001$), elevating slightly again at 28 days ($p<0.05$).

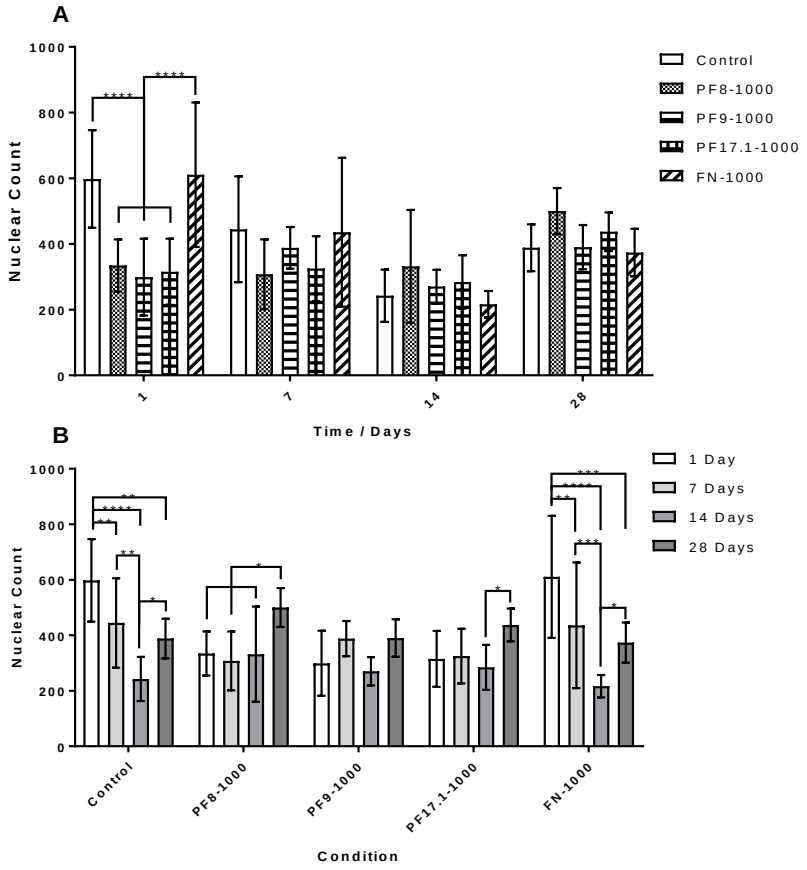

Figure 6-10 Image analysis of DAPI staining from micrographs taken of ACL04 hACLs on functionalised scaffolds. Nulear count was shown between conditions within time points (**A**) and within conditions between time points (**B**). Approximate cell number was counted using particle analyser for cell nuclei. Data was

analysed using a two-way ANOVA (corrected using Giesser-Greenhouse) and significances identified using Tukey's multiple comparisons test. Means ± SDs are displayed. *p<0.05, **p<0.01, ***p<0.001, **** p<0.0001.

6.3.5.3 Collagen Type I Production

Collagen matrix, as shown in Figure 6-11, that was produced by the hACLs, appeared mainly intracellular and did not show evidence of being exported into the ECM. Cell alignment was mostly retained on all scaffolds. By using % area calculations (FIJI ImageJ), and normalising to cell count (displayed in Figure 6-12), it became apparent that cells on PF9 were producing the most collagen type I compared to the negative controls ($p<0.01$). Interestingly, hACLs on both PF9 and PF8 functionalised scaffolds produced more collagen type I that those seeded onto fibronectin functionalised scaffolds ($p<0.0001$ and $p<0.05$ respectively). This remained true after 7 days, where all scaffolds functionalised with fibrillin-1 fragments were determined to be producing more collagen type I per cell that the fibronectin positive controls (PF17.1 $p<0.001$, PF9 $p<0.001$, PF8 $p<0.05$). However, there was no notable increase in hACL collagen production between fragment functionalisation and no functionalisation. At day 14, it appeared that the quantity of collagen type I present decreased. PF8 functionalised scaffolds were capable of supporting the stability of more total collagen type I and more collagen type I per cell than the negative controls ($p<0.01$ and $p<0.05$ respectively), whilst PF9 and PF17.1 displayed more collagen production per cell that the fibronectin controls. At day 28, production of collagen appeared to stabilise across all scaffolds, showing no notable distinctions between the fragments nor their controls.

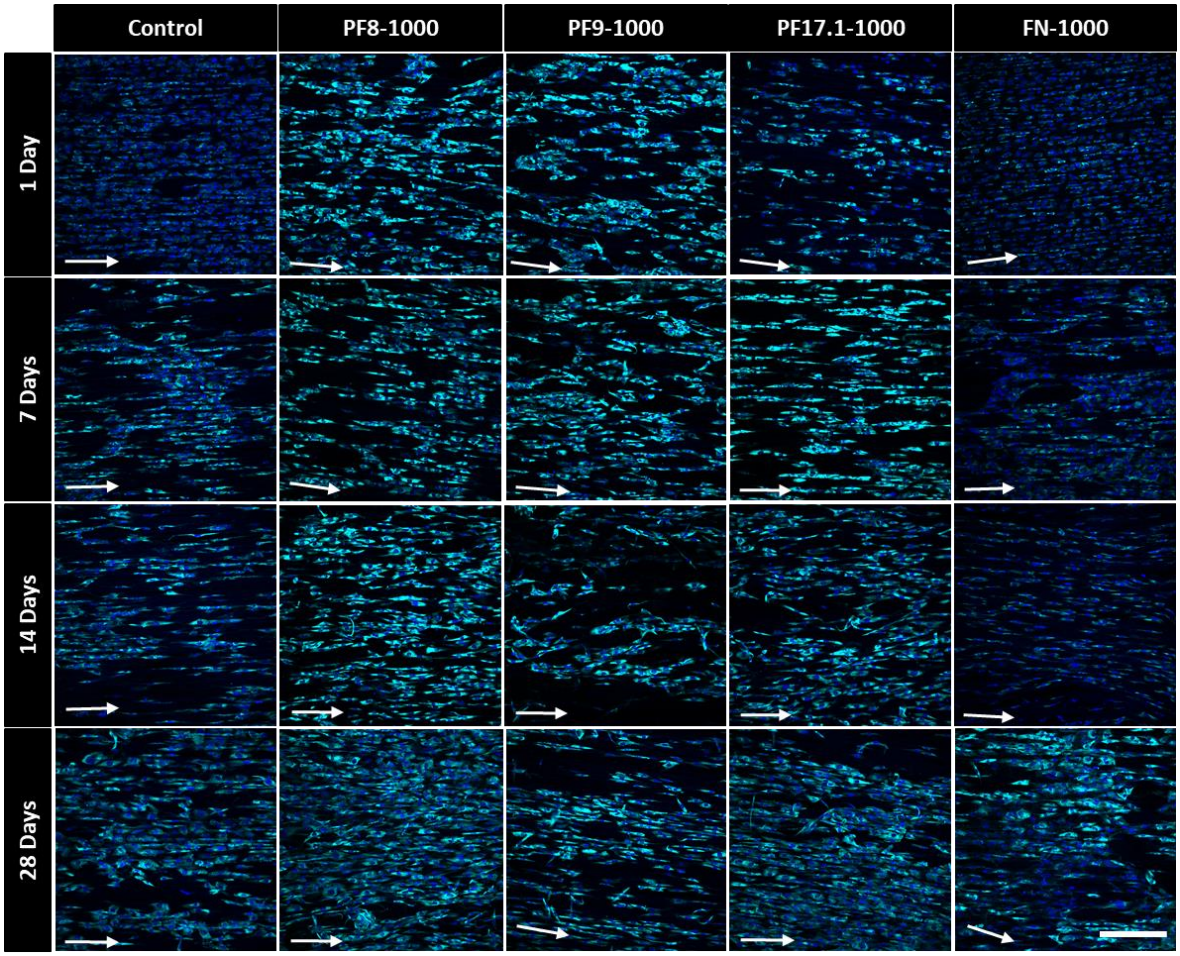

Figure 6-11 Human donor hACLs collagen type I production (cyan), counterstained with DAPI (blue) over 28 days on fibrillin-1 fragment functionalised plasma treated aligned fibre scaffolds. Control images represent samples that were not treated with any FBN1 fragments. White arrows indicate direction of fibre alignment and scale bar represents 250 µm.

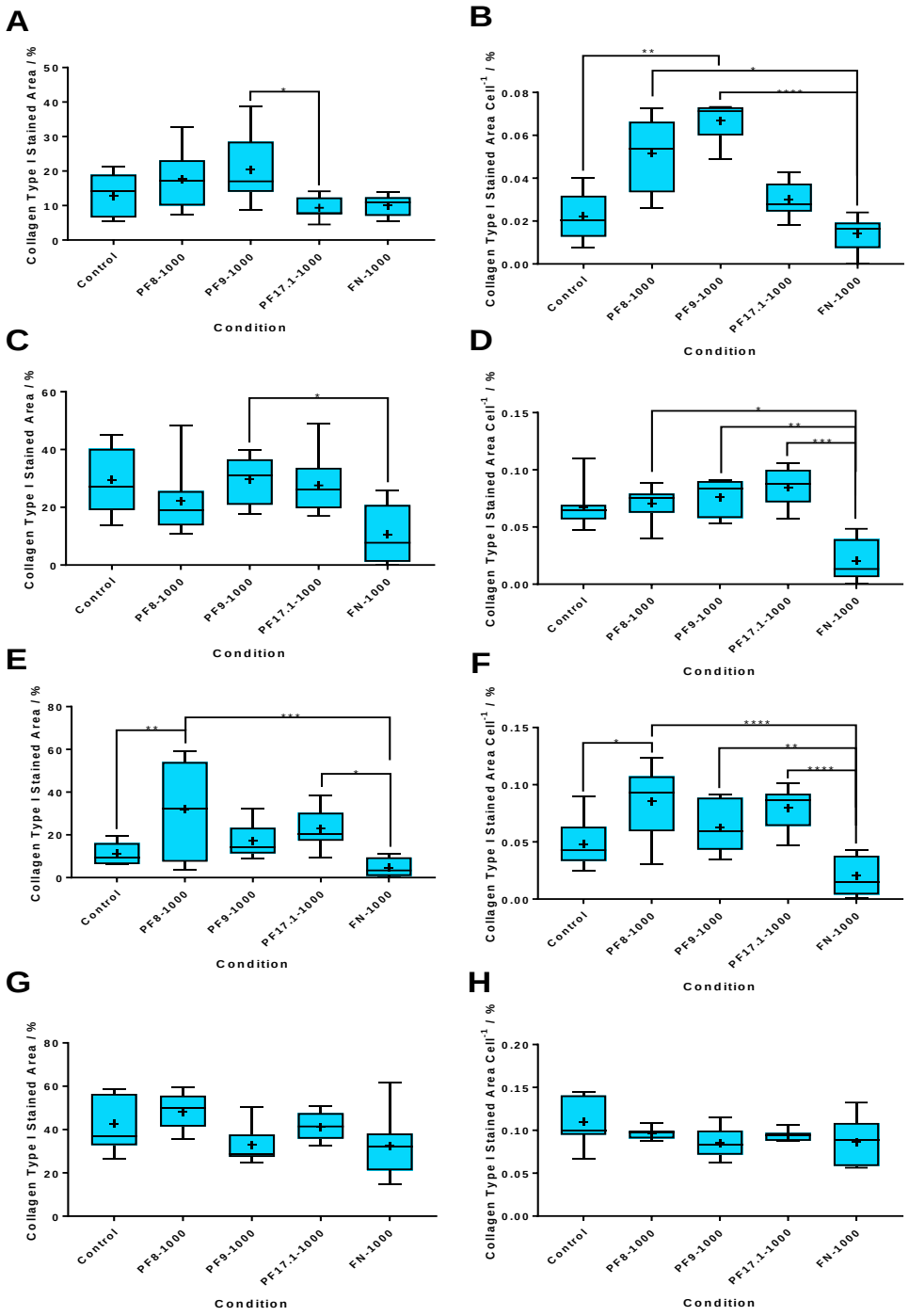

Figure 6-12 Collagen type I production in one hACL donor. Graphs **A**, **C**, **E**, **G** show total % area of COL1 produced at 1 (**A**, **B**), 7 (**C**, **D**), 14 (**E**, **F**) and 28 (**G**, **H**) days respectively. Graphs **B**, **D**, **F**, **H** show COL1 production normalised to cell number at 1, 7, 14 and 28 days respectively. One-way ANOVA with Tukey's HSD Post Hoc comparisons were performed. Box and whisker plots show median, interquartile ranges and means. Error bars represent minimum and maximum values. * $p<0.05$, ** $p<0.01$, *** $p<0.001$, **** $p<0.0001$.

6.3.5.4 Fibronectin Production

Fibronectin plays an integral role in the human ACL, providing an ECM template for the deposition of collagen and fibrillin, and is upregulated in wound healing. Presented in Figure 6-14, fibrillin-1 fragments PF8 and PF9 were found to support an increase in total fibronectin, compared to non-biofunctionalised controls ($p<0.05$). The enhanced production of fibronectin by cells at day 1 ($p<0.0001$) was shown to be supported by all fibrillin-1 fragments, and PF17.1 appeared to perpetuate this trend at day 7. It was determined however, that at day 14, fibronectin content of neo-ECM began to degrade. No-biofunctionalised scaffolds appeared to better support the conservation of lower quantities of fibronectin both in terms of total ECM and ECM per cell at day 14. Degradation of the fibronectin matrix can be observed in Figure 6-13 from 14 days, although it appears to increase once more at 28 days, forming fibrillar structures throughout the neo-ECM (yellow arrowheads). In this instance, PF8 appeared to support higher quantities of total fibronectin that the fibronectin-functionalised controls ($p<0.05$).

It was also observed that fibronectin coatings were slightly visible during the immunofluorescence staining, and as they had the same intensity as the neo-matrix, could not be removed for image quantification and may have increased the % area (as seen at 1 day in Figure 6-13, background image comparison available in Appendix 10).

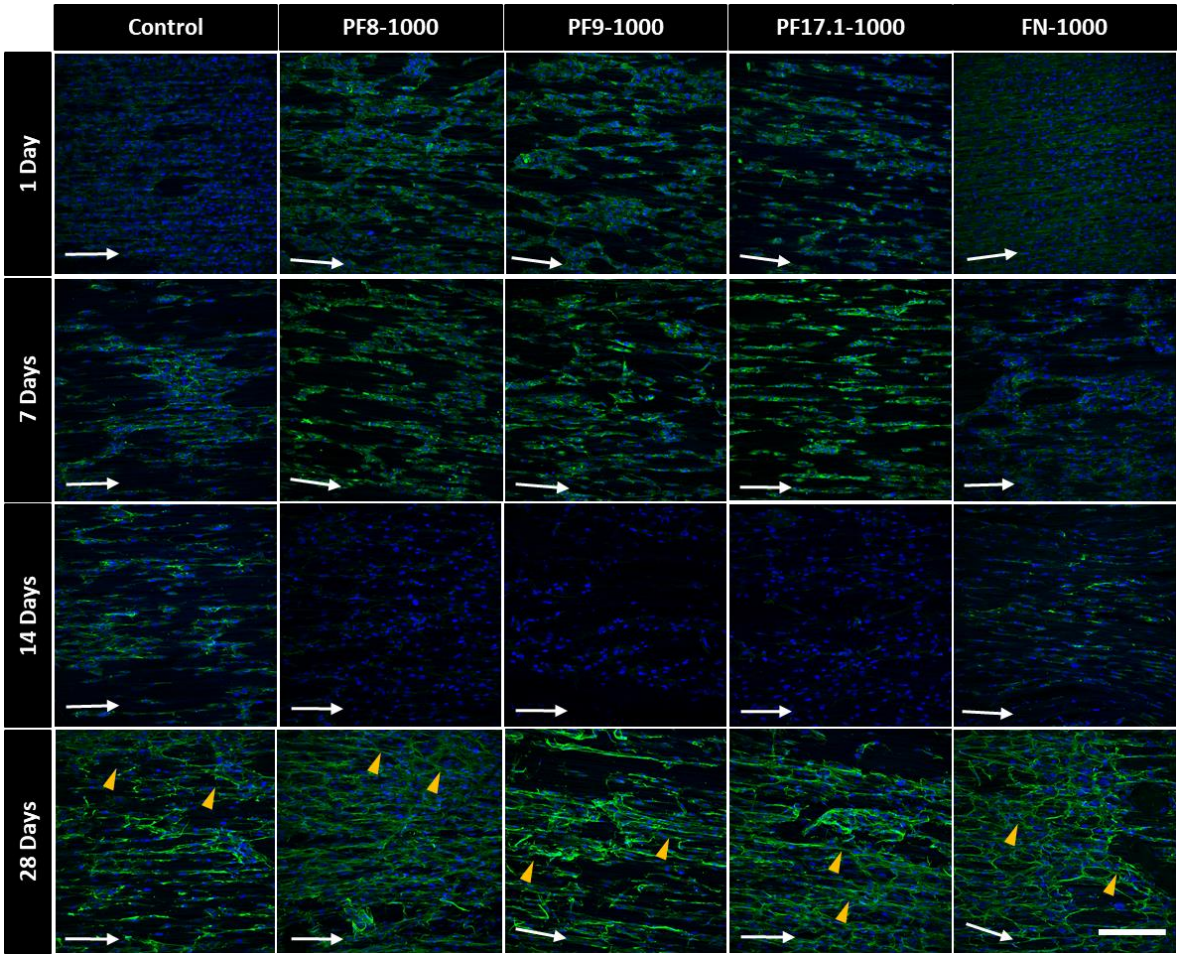

Figure 6-13 Human donor hACLs fibronectin production (green), counterstained with DAPI (blue) over 28 days on fibrillin-1 fragment functionalised plasma treated aligned fibre scaffolds. Control images represent samples that were not biofunctionalised. White arrows indicate direction of fibre orientation and yellow arrowheads show extracellular fibronectin networks. Scale bars represent 250 µm.

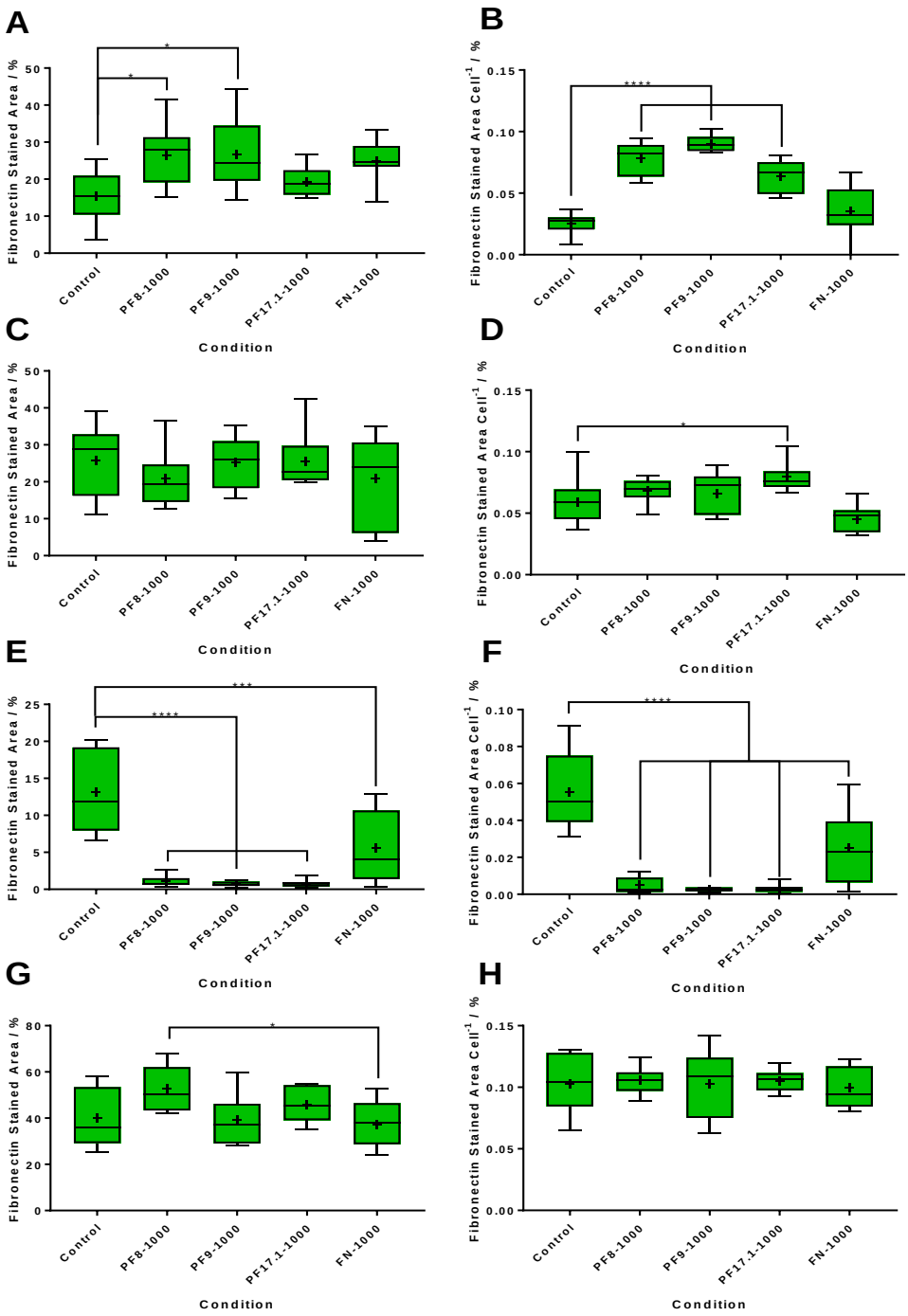

Figure 6-14 Area (%) covered by fibronectin, produced by one hACL donor, present in the fluorescent micrographs above, at 1 (**A**, **B**), 7 (**C**, **D**), 14 (**E**, **F**) and 28 (**G**, **H**) days. Graphs **A**, **C**, **E** and **G** show the total amount of fibronectin and graphs **B**, **D**, **F** and **H** show the amount area of fibronectin produced, averaged to nuclear count. One-way ANOVAs with Tukey's post hoc tests were performed for each graph. Box and whiskers show median, interquartile ranges and error bars show min. max. values. The '+' present indicates the mean. *p<0.05, ***p<0.001, ****p<0.0001.

6.3.5.5 Fibrillin Production

Fibrillin plays an important role in the ACL ECM, providing a template for elastin deposition, and supporting and stabilising the elastic fibre structures in the ACL, integral for stretching and recovery[306]. hACLs appeared to produce cell-surface associated fibrillin[312] up to day 28 in all conditions. As depicted by Figure 6-15, it was determined that the use of fibrillin-1 fragments encouraged the hACLs to export fibrillin into the extracellular matrix, though this was more noticeable in PF8 and PF17.1 than with PF9. Here the fibrillin was remodelled into fibrils, which were aligned along the PCL fibres, and can be observed after 28 days in culture (yellow arrowheads).

Total fibrillin production, depicted in Figure 6-16, was significantly greater in PF17.1 ($p<0.05$). The negative controls after only 1 day in culture remained stable between conditions, until 28 days, where significantly more fibrillin was produced on the PF8 and PF17.1 functionalised scaffolds than either the negative ($p<0.05$, $p<0.001$ respectively) or the fibronectin-functionalised controls ($p<0.001$, $p<0.0001$ respectively). This increase also directly translated to an increase in production per cell, where significances remained as above.

Though fibrillin-1 fragments appeared to support higher quantities of fibrillin-1 production at day 1 (non-significant), this effect was not observed at the 7 day time point. After 28 days in culture, the fragment PF17.1 was found to have produced significantly more fibrillin than either the positive or negative controls ($p<0.05$).

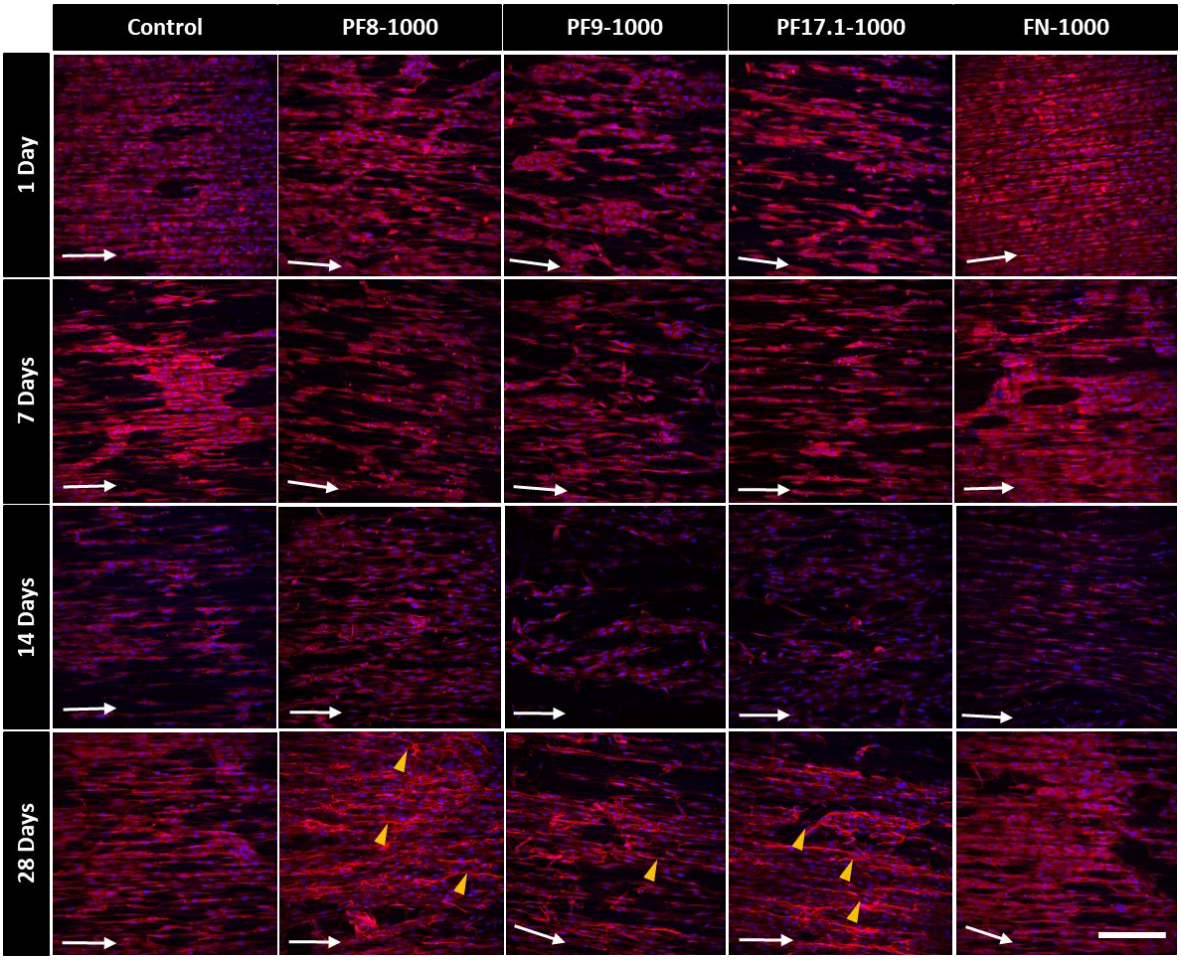

Figure 6-15 Human donor hACLs fibrillin production (red), counterstained with DAPI (blue) over 28 days, on fibrillin-1 fragment functionalised plasma treated aligned fibre scaffolds. Control images represent samples that were not treated with any FBN1 fragments. White arrows indicate direction of fibre orientation and small yellow arrowheads indicate extracellular fibrillin fibrils. Scale bar represents 250 µm.

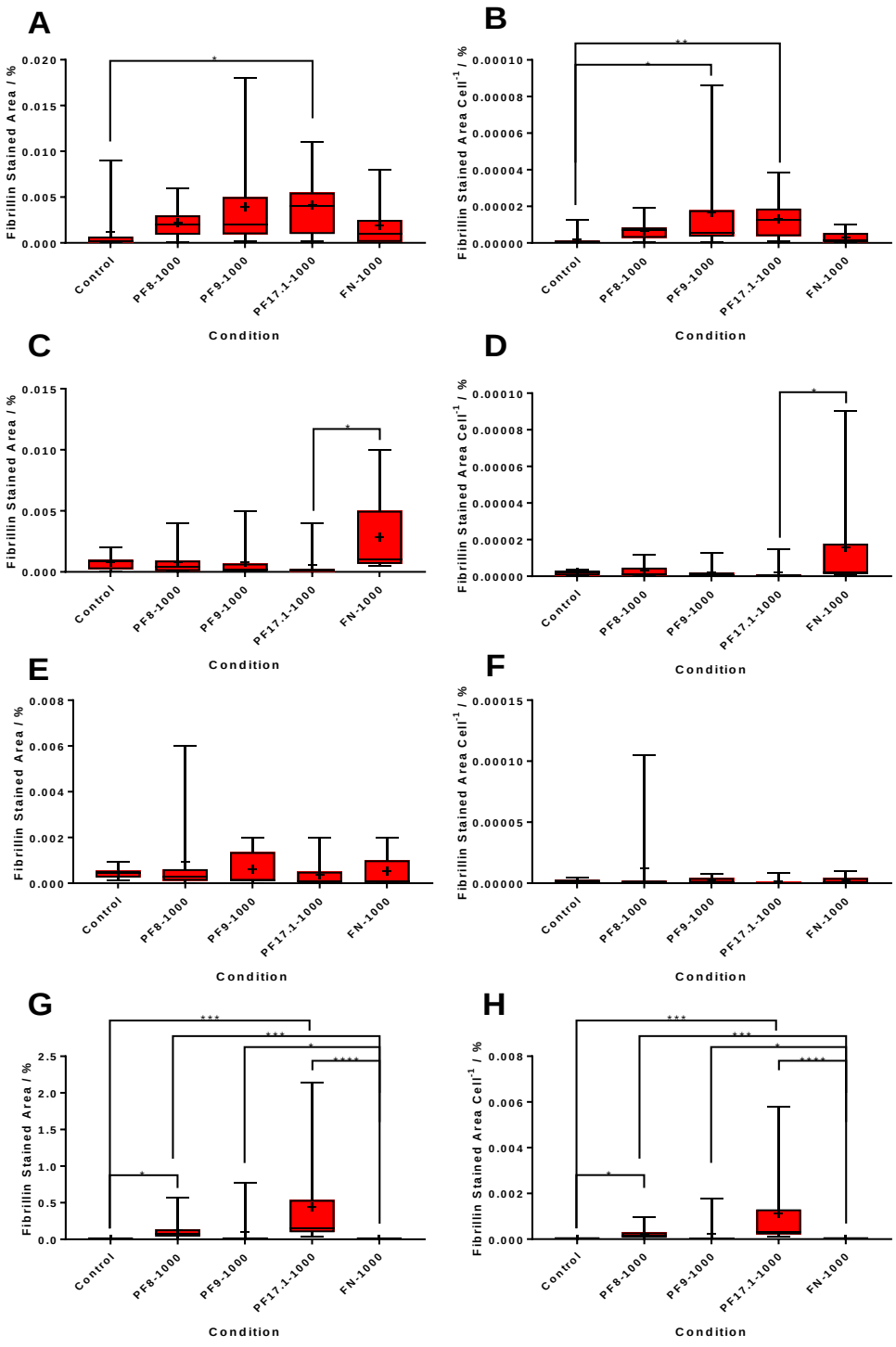

Figure 6-16 Fibrillin production (% area) by hACLs (ACL04) on fibrillin-1 functionalised scaffolds and controls at 1(**A**, **B**), 7 (**C**, **D**), 14 (**E**, **F**) and 28 (**G**, **H**) days. Total % area of proteins (**A**, **C**, **E**, **G**) and % area per cell (**B**, **D**, **F**, **H**) are displayed.. Box and whisker plots show medians (centre line), interquartile ranges (box bounds) and min-max value range. '+' inside the box denotes the mean. Kruskal Wallis H tests for non-parametric data, with rank comparisons, was performed. *p<0.05, **p<0.01, ***p<0.001, ****p<0.0001.

6.3.5.6 Initial Cell Orientation

Cell orientation was analysed using the collagen type I images at the day 1 time point. These images proved the most accurate for judging cell orientation due to the large amounts of intracellular collagen present at this time point that had not yet been exported into the ECM. For these analyses, the higher and narrower the curve, the larger the number of cells following the scaffold fibre orientation.

Interestingly, higher concentrations of fibrillin-1 fragments PF8 and PF9 appeared to support more unidirectional organisation (Figure 6-17A), however, though these conditions showed high pixel counts, the angle range was larger than some of the conditions with lower counts. Normalisation per group to total count enabled comparison of the different fragments over a set angle range (Figure 6-17B). This showed that the condition exhibiting the highest levels of anisotropic orientation was the 1000 ng of fibronectin (FN-1000), closely followed by the negative (no protein fragment) condition.

Interestingly, the PF17.1 condition appeared to display the largest range of orientation, even after normalisation.

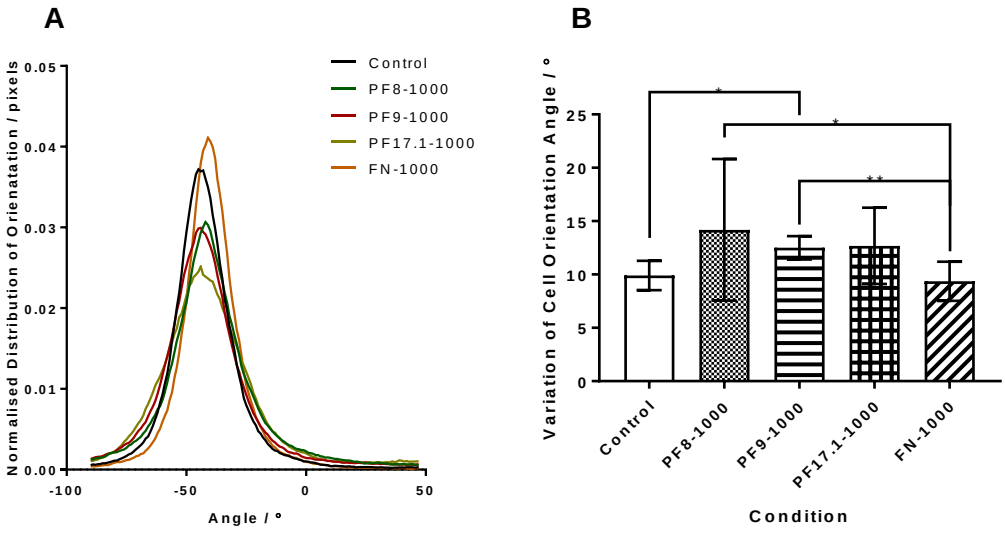

Figure 6-17 Histograms of the distribution of neo-ECM anisotropic orientation on the scaffolds at 1 day post seeding using the collagen type I micrographs. Histograms were generated using OrientationJ (FIJI ImageJ plugin), and show the normalised distribution of pixel orientation in the image (**A**) and the width of the normalised distribution curves to show how spread the data was over multiple angles (n=8, the higher the value, the larger the data spread) (**B**). Distribution calculations for every pixel on the image are based on the structure

tensor, width of distribution is defined as 'the number of degrees by which the curve deviates from its mean value'. Performed once.

6.3.5.7 ECM-Associated GAG Content

Glycosaminoglycans, associated with the neo-ECM and removed by papain digestion, were quantified by using the DMMB assay. Two independent hACL donors were used in order to quantify sulphated GAG expression and incorporation into the ECM. Donor GAG production was found to be highly variable, with ACL04 showing very low concentrations of ECM-associated GAGs (Figure 6-18A and C), whilst ACL09 produced much higher quantities (Figure 6-18B and D). Due to the extreme variation within the samples of ACL04, no significances could be identified. However, in ACL09, it appeared that PF9, PF17.1 and fibronectin-functionalised scaffolds supported the production of much higher concentrations of ECM-associated GAGs; approximately 7, 8 and 8 µg ml^{-1} higher in concentration than the non-biofunctionalised controls. Concentration magnitudes at early time points for ACL09 (for cells from aging human donors) were found to be in agreement with Prager *et al.* (2018)[240].

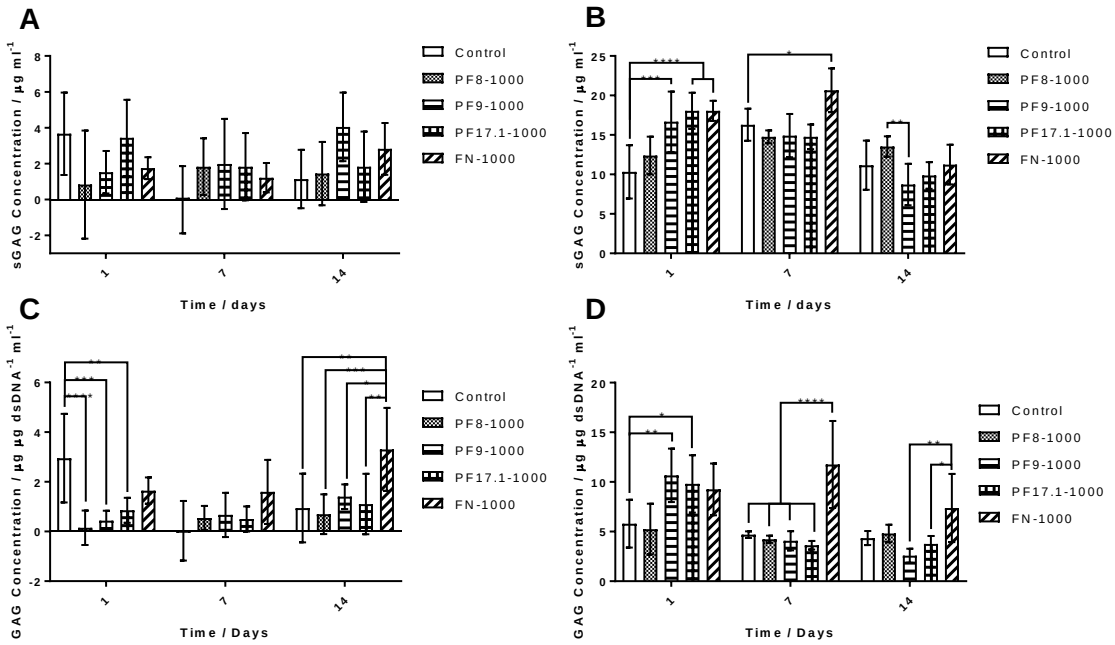

Figure 6-18 Digestion of scaffolds and subsequent DMMB assay for ECM-associated sulphated GAGs produced results from two donors of hACLs (n=3). Total GAG concentration measured from ACL04 (**A**) and ACL09 (**B**) and µg GAGs per µg dsDNA ml^{-1} is expressed for ACL04 (**C**) and ACL09 (**D**) due to extreme variation between donors. Statistical analysis was performed using two-way ANOVAs with Tukey's multiple

comparisons. Bars show means and error bars signify standard deviations. *p<0.05, **p<0.01, ***p<0.001, ****p<0.0001.

6.4 Discussion

Donor tissue from which the cells were digested, was collected from patients undergoing total knee arthroscopy surgery (ages 59-73). Knee ligaments from which to isolate the cells of young donors could not be procured with regularity. Ruptured ligaments were considered for this project, however they are often preserved and the stumps are left in place for optimal integration of nerves and vasculature into the autograft[243]. Parameters were set as to which inclusion criteria would be suitable for cell experiments. Due to ligaments of younger, healthier patients without concurrent comorbidities not being available, ligaments from donors undergoing total knee replacement surgeries were selected. Though it is important to note that all patients presented with osteoarthritic knees (so should be taken into consideration when assigning research impact), it has been determined that degenerative ligaments possess higher cellularity and have a higher proportion of progenitor cells[50]. Age alone was not deemed a significant issue as evidence suggests that there are no differences between proliferative capabilities between old and young donor cells[240]. It was considered however, that this characteristic of the cells may have been altered by the presence of comorbidities.

As mentioned previously, medications were considered, including rapamycin, a medication which disrupts decorin-mediated fibrillin synthesis. Though literary evidence speaks mainly of this mainly effecting the kidneys, inhibition of the mammalian target of rapamycin (mTOR) can decrease insulin growth factor signalling, which has been shown to upregulate fibrillin synthesis[35] and to which ACL ligamentocytes have been shown to respond[438]. As this study determines hACL production of fibrillin as a marker of successful neo-ECM formation, and rapamycin-medicated patients could be easily omitted without significantly reducing donor availability, rapamycin was added to the exclusion criteria. Numerous other medications which reduce protein production, such as NSAIDs with collagen[439], could not be controlled due to the likelihood of donor patient comorbidities.

Markers for ACL characterisation were determined from the literature. Negative markers were analysed to determine any contamination of blood-related cells, or inflammatory cell infiltration into the ligament. The latter was especially important to determine, due to the

osteoarthritic condition of the ligaments received. Ligamentocytes were characterised following four passages in culture, as it was determined that the analysis would be more representative of the cultured population, rather than that of the population acquired immediately upon digestion, and would identify cell types present during further experimentation. Though there were none present in the flow cytometry analysis, CD34+ stem cells have been reported by Mufine *et al.* (2012)[76] to be present in the ligament, and have shown to be beneficial to bone-tunnel region healing, where CD34+ cells increase osteo- and angiogenesis of the ligament. Due to this project focusing on the midsubstance of the ACL, these cells may have hindered regeneration, and if present, would have had to be excluded using fluorescent activated cell sorting (FACS).

The markers used for flow cytometry in this study are further validated for use from the literature by Steinert *et al.* (2011), who reported that isolated ACL fibroblasts were determined to be positive for all CD90, CD44, CD73 and CD105, and negative for CD34 and CD45[68]. In agreement with the degree of expression in human ligamentocytes isolated in this thesis, strongly CD44+, CD73+ and CD90+ cells have been widely reported at multiple different passages, and between ligamentocyte populations from donors of differing age[61, 68, 79, 407, 440]. Proportion of ligamentocytes with stem cell character were also found to not differ over increasing passage[440].

It was also noted that there were no discernible differences between collagenase digested and explanted cells (allowed to migrate out of the tissue into the culture flask), further validating the digestion method for cell isolation, which was used in this thesis. Many ligamentocytes analysed in the literature appeared to have a much higher expression of CD105 than reported in this study (>95% in comparison with <50%)[68]. Reduced CD105 expression in human BM-MSCs has been reported to associate with serum free cultures, though this was not the case with the ligamentocytes in this study, which were all cultured with 10% FBS. It was noted that reported instances of low to moderate levels of expression, were from cells that had been initially digested in serum free media (which was used to isolate the human ligamentocytes in this thesis)[61, 79], while those which retained strongly positive CD105 were digested or explanted in serum-containing solutions[68, 240]. Considering the similarities between BM-MSCs and ACL ligamentocytes, this could be a possible explanation as to the decrease in CD105 expression was observed. This may serve to confirm that this evidence for BM-MSCs might translate to hACLs.

hACLs were shown to have a highly variable degree of clonogenic potential at relatively early passage numbers (3-4). It was possible that this was affected by initial seeding density during the isolation protocol. hACLs were found to also have highly variable levels of attachment to TCP following collagenase digestion, irrespective of coating with gelatin, a widely accepted, and cost effective method of facilitating initial cell attachment[441]. Cells that sparsely attached were occasionally observed to maintain an increase in surface area (as depicted in Appendix 16), and possess reduced proliferative ability.

Interestingly, it has been previously determined that there were no differences observed between ACL ligamentocytes from young and old donors in terms of differentiation and proliferative capability, yet these cells differ in gene expression of many important cell cytoskeletal genes including stress fibre and focal adhesion formation. Ligamentocytes from younger donors were found to have higher expression of all cytoskeletal genes identified, compared to older donors[240]. Cell-mediated stress on the ECM is essential for the formation and organisation of mature collagen fibrils, through interactions with fibronectin fibre networks[58]. The effect of downregulated cytoskeletal mechanostimulatory processes (compared to younger donors), may have contributed to the lack of collagen fibrils formed (as shown in Figure 6-11).

hACLs were seeded onto equivalent amounts of fragment on a 96 well plate. As expected, ligamentocytes attached more strongly to PF8 and PF17.1 fragments than PF9. This is likely due to the presence of the synergy site in cbEGF domains 19-21[393]. This domain regulates cells attachment via the RGD motif through integrins $\alpha_v\beta_3$, $\alpha_v\beta_6$ and $\alpha_5\beta_1$[30]. As PF9 does not contain the synergistic site, this may hamper cell attachment to the RGD motif. Observation of this result suggests that this interaction is independent of cell type, with human endothelial cells[315] and human dermal fibroblasts[310] both showing favourable responses to PF8.

To assess the morphology, dispersion and viability of cells on the scaffolds, LIVE/DEAD labelling was performed on three independent donors. ACL04 and ACL07 appeared to respond favourably to two of the fibrillin-1 fragments, in terms of both supporting cell density and alignment, equal to that of fibronectin at 24 hours: PF8 and PF17.1. ACL09 however, appeared to only respond to PF8 and fibronectin. The results inferred the ability of PF8 and PF17.1 to support increased hACL attachment at early time points and guide alignment along the scaffold topography. This displays a role beyond enhancing the attachment of hACLs, as it also appears to have the ability to guide hACL alignment. It is

possible that this high degree of ligamentocyte elongation and orientation could be an indicator of the ability of fibrillin-1 fragments PF8 and PF17.1 to support and enhance cellular migration along the fibres. Cells are found to polarise during migration, an in the instance of cellular unidirectional elongation, are caused by the organisation of long, direction bundles of actin filaments along the longitudinal axis of the cell. This leads to the establishment of a 'leading edge' by which they determine the direction of migration[301, 442]. In order to establish whether this is the case, further investigation using live microscopy and cell tracking would need to be performed.

Orientation of the cells at 1 day post seeding (using collagen type I images as an indicator of cell alignment due to the intracellular-only production) was performed. Cells oriented most strongly on the fibronectin controls. Work produced by Missirlis *et al.* (2017) determined that both the heparan binding site and the RGD binding site in fibronectin are essential for the high directional alignment observed on fibronectin-functionalised scaffolds[301]. Interestingly, though PF17.1 also possesses both these binding sites within the fragment, it displayed the lower cell directionality than fibronectin or the control. It should be noted however, that small variations in alignment of the images and small variations in fibre alignment (or fibre breaks) could have severely affected the result of this experiment.

The ability of PF8 and PF7.1 to encourage cell alignment is further confirmed by the ECM immunofluorescent staining. At 7 days, fibrillin-1 fragment functionalised scaffolds appear to support a higher degree of alignment than that of either non-biofunctionalised or fibronectin controls. However, this effect is lost with time, presumably due to the adsorption of serum proteins onto the fibres. Though this initial effect may be lost, it does appear that there may be a longer-lasting effect of the fragments, with PF8 and PF17.1 supporting the production and exportation of more mature fibrillin fibrils at 28 days than PF9 or either of the controls (no biofunctionalisation or fibronectin-functionalised). Alamarblue of ACL09 supported this trend at early time points, showing significantly higher metabolic activity at early time points (4 hrs, 24 hrs), inferring higher levels of attachment to the scaffolds functionalised with PF8, PF17.1 and fibronectin.

Metabolic activity of both ACL04 and ACL09 was found to be different at each time point. ACL09 expressed increased metabolic activity of PF8 and PF17.1 at early time points (4 hrs, 24 hrs), in line with observations in the attachment and LIVE/DEAD assays. However, ACL04 appeared to show significant differences later in the culture period. A general

decrease in metabolic activity was observed at day 14 in ACL04, which agreed with results observed for fibronectin immunostained area and DAPI-stained nuclear counts at the same time point. For the dsDNA concentration, this effect was observed at 7 days post seeding for both ACL04 and ACL09. This decrease would otherwise indicate the cells reaching confluence on the scaffolds around the 7 day time point, however, ECM immunofluorescent images do not display ligamentocyte confluence at the same time point. This could be due to cells in the various experiments reaching confluency at slightly differing time points. If confluency was achieved between day 7 and day 14 for the ECM experiment, it is unlikely that the micrographs would display this, as the cells may have already detached from the scaffold. If this was indeed the case, the cells appeared to recover the fibronectin density, with cells covering approximately 50% of the total measureable area at day 28. The decrease in fibronectin at day 14, though corroborated with nuclear counts and GAG quantification (for ACL09), may have an alternative explanation. Breakdown of fibronectin in the ECM can occur in stress-deprived ligaments[443], potentially causing a reduction in cell number due to preliminary matrix breakdown. Though, it is important to note that these changes were reported at much later time points. If this is indeed the case, exposing cells to cyclic tensile strain in a bioreactor set-up may prevent the decrease in fibronectin observed in this chapter. This trend can also be observed at 14 days in total GAG concentration results for ACL09, where PF8 appeared to support stable GAG production, while other conditions experienced a decrease in ECM-associated GAG concentrations.

GAG production was markedly different between donors; hence, both are shown, as such variable trends are not conducive to data pooling. Though ACL04 displayed extremely variable results that were highly irregular, ACL09 appeared to display results where the concentrations detected were found to be in agreement with the literature[240]. ACL04 results however, could not be used for drawing any conclusions, due to all sGAG concentration values being under the accurate assay detection limit for the assay (approximately 5 µg/ml according to the standard curve in Appendix 17B). When normalised to dsDNA concentration (and indeed before normalisation) it was clearly displayed that GAG sequestration occurred on most significantly on the PF9, PF17.1 and fibronectin functionalised samples. One explanation for this could be the presence of heparan binding sites in the TB5 domain, which is absent in PF8 (hence GAG sequestration on the ECM was similar to the negative control both with raw concentration data and following normalisation). The heparan sulphate-containing proteoglycan, perlecan, is known to

associate with elastic fibre constituents in the ACL to assist in the coacervation of tropoelastin with fibrillin-1 to form elastic fibre assemblies[52].

Due to the absence of the TB5 heparan sulphate-binding domain in PF8[31], more GAGs may have been exported into the media at early time points (before the formation of a neo-ECM), instead of coacervating with the fibrillin-1 fragments. To examine this theory, experiments to determine the GAG concentration in the media, at shorter, but regular intervals (i.e. every 48 hours) could be performed.

6.5 Chapter Conclusions

Human ACL cells showed donor-donor variation and therefore unequal responses in the assays used to assess their response to the biofunctionalised scaffolds. The ligamentocytes did however, show the correct expression markers, confirming their phenotype[68, 240], though donor-to-donor differences in expression were observed in CD44 (28.9% range in expression) and CD105 (41.47% range in expression). Though lower CD105 has previously been linked to serum free culture[61, 79], it was determined that it was unlikely to explain differences in expression due to all donors undergoing the same treatment. Ligamentocytes showed variable clonogenic potential, with ACL09 forming multiple colonies but ACL02/ACL04 forming very few small, sparse colonies, possibly due to initial seeding density following isolation, and the resulting time in culture. This may infer the possible requirement for added growth factor stimulation in the media (for future experiments).

As there was equivalent donor response to the fibrillin-1 fragments on TCP, the results from three donors were compiled. Human ligamentocytes showed a preference for PF8 and PF17.1 over PF9 ($p<0.0001$, possibly due to PF9's lack of synergistic site[393]), and it was observed that PF8 maintained cell density over 24 hrs in ACL04 and ACL07. ACL09 also showed an increase in metabolic activity when using PF8 and PF17.1 functionalised scaffolds over 24 hrs. It was noted however, that though donors showed indication of enhanced response on each experiment, the results between experiments and within donors, did not appear to corroborate (e.g. ACL09 increased metabolic activity, observed reduced cell density during LIVE/DEAD labelling). It was noted that the added variation of the scaffold substrate (differences in surface roughness and surface area, and the introduction of plasma treatment, as well as differences in protein adsorption onto the scaffold, characterised in Chapter 3, section 3.3) may have altered expected ligamentocyte responses.

The hypothesis that ECM proteins would be enhanced overall can be somewhat accepted. Though ligamentocytes display increased fibrillin production and showed presence of extracellular fibrils, compared to the negative controls at 28 days ($p<0.05$, using PF8 and PF17.1), and increased ECM overall when using PF8 fragments at 7 days ($p<0.05$), increased responses using fibrillin-1 fragments were often not significant. Interestingly, a decrease was observed with fibronectin at 14 days, perhaps due to stress deprivation on the cells and the ECM[97].

Though fibrillin-1 fragment functionalised scaffolds appear to have promise, it is clear that more analysis is required to determine whether fibrillin-1 has any significant effect on the protein output and overall response of human ligamentocytes. Repeats with additional donors will verify responses and allow identification of erroneous/abnormal response to fibrillin-1 functionalised scaffolds.

CHAPTER 7 GENERAL DISCUSSION AND PROJECT LIMITATIONS

7.1 General Discussion

For achieving the overall aims of this thesis, electrospun fibres were selected as the optimal method for production of an aligned substrate. This was in part due to the ability to retain control over topographical properties, such as fibre diameter and alignment, but also due to this technique being able to mimic the fascicular bundles between which the cells reside in the native ACL tissue[51, 262]. Variation presented substantial hurdles throughout the work performed in this thesis; both with physical and mechanical properties of the scaffolds and with inter- and intra-donor variations in the primary cells responses. This is because large variations (as evidenced by the standard deviations displayed) make it difficult to attribute significance to data, and hence the outcomes of experiments become vague.

Fibrous mats yielded scaffolds with a surface roughness that accounted for ~12% of the overall scaffold thickness and introduced much variation into the scaffold properties (evidenced by the standard deviations). This was presumably the cause of variable wettability at the surface (12° angle range) and was exaggerated following plasma treatment, resulting in a 47.53° contact angle range between batch means. Yet, despite increased variability due to plasma treatment, no significant differences in protein adsorption could be detected. Though not measured, it is possible that plasma treatment may have introduced variability into the cell culture experiments, as evidenced by large standard deviations on the negative control samples.

Another notable source of variation in this work came from the cells. It has been reported that whilst 80% of observable variation can be attributed to inter-donor variability, the remaining 20% occurs within a single donor population[415]. Difficulty in maintaining consistency with cells can introduce variation at any point, further confounded by use of primary cells in experimentation. The added variable of the patient or cell source, the health of the tissue from which cells are isolated, the conditions in which the tissue is transported, and the method used to isolate the cells, can further introduce variability[415]. Despite this, as the overall goal of this work (as detailed in Chapter 1, section 1.2) is to use cells from the patient to populate the scaffold, primary cell work was still conducted. Primary cells often provide a more accurate portrayal of native cell response to the scaffold compared with continuous cell lines. This choice was further validated by the lack of ACL-related available cell lines for use (though efforts have been made regarding this[406]). Inequivalent responses were noted, especially between human ACL donor populations. Variations in both increased

metabolic activity (discrepancy between time point effects) and sGAG production (non-measurable concentrations and small concentrations of GAGs) suggests the requirement for a larger sample of donor cell populations.

Variation in the scaffolds may also have contributed to variation in the cell response. When the cell response was measured on non-variable substrates (relative to the scaffolds i.e. TCP or glass), the variation was reduced. This suggests that not all the observed variability can be attributed to primary cells, and that physical and chemical variation within the scaffolds (characterised in Chapter 3) may have had an effect on cell response. It has already been noted that the plasma treatment may have influenced the cell culture experiments, and further experiments should be undertaken to investigate this.

Some elements of the experimental protocols used in this work may have masked the effects of fibrillin-1 on the cell response. For example, plasma treatment might have provided a suitably 'moderate' hydrophilic surface for cell attachment[209] (see Figure 4-5). Provisional early time point experiments performed in Appendix 7 detail the results of a method that involved the hydrophobic recovery of the scaffolds following protein adsorption. This method would have removed any major contributions of the plasma treatment on cell metabolic response. Despite plasma treatment interfering with cell metabolic activity, it did merit some notable success in maintaining native elongated morphologies of the ACL ligamentocytes. Another example was the use of serum-supplemented media during cell culture. Though a standard culture technique, using this method may have introduced serum proteins onto the surface of the scaffold, further confounding the ability to observe the effects of fibrillin-1 fragments alone. Further work should involve the removal of serum from the media (or involve the use of a low concentration, e.g. 1%) to prevent substantial serum protein-mediated cell attachment in the culture set-up.

The impact of this work, with regards to the overall goal of a functional ACL TE construct, is that fibrillin-1 functionalised scaffolds have been shown to support and encourage native elongated cell morphology (Figure 4-3, Figure 4-4, Figure 6-5) and have shown to increase the production of protein components essential to the ligament ECM (Figure 4-12). The use of primary cells in this work has been instrumental in the discovery of how ACL ligamentocytes (taken directly from a patient) may respond to the scaffold in an *in vitro* environment. Discovery of the ligamentocyte response will inform on future progression and optimisation of this technology. With regards to impact within the literature, this work is the

first to demonstrate the interaction of primary ACL ligamentocytes of both canine and human origin with fibrillin-1, and specifically with the isolated fragments detailed in this thesis. Work performed has also given the indication that canine and human ACL ligamentocytes do not display the same requirement for the cbEGF 19-21 synergy site and have shown higher levels of attachment to PF9 than has been reported in the literature[310]. Also concerning attachment, it has been observed that canine ligamentocytes demonstrate a preference for the use of $\alpha_5\beta_1$ integrins when attaching to fibronectin, evidenced by the lack of effect $\alpha_5\beta_1$ blocking has upon early stage cell attachment. Moreover, the analysis performed in Chapter 5 is the first to report on elastic fibre (elastin, fibrillin) constituent content in male specific degenerative ACLs.

7.2 Methodological Limitations of the Project

For electrospinning, a fume-cupboard enclosed set-up was used to produce aligned microfibre scaffolds, where temperature and humidity could not be controlled. An increase in relative humidity can cause a reduction in fibre diameter[218], with alterations in mechanical properties (increase in fibre diameter = decreasing Young's modulus)[444]. Increasing temperature can also cause a reduction in fibre diameter due to increasing speed of solvent evaporation[445]. To overcome this, a fully enclosed instrument with temperature and humidity control could have been used as an alternative option. For synthetic polymers however (as used in this thesis), the protocol often requires hazardous solvents, e.g. chloroform, dichloromethane, or dimethylformamide[229, 253, 257, 261] known to have detrimental effects during cell culture experiments[377]. To remove this risk factor melt electrospinning could have been used.

SEM is a standard technique used for determining fibre diameter and orientation[209, 446, 447], though analysis of pore size on aligned fibres could have been better performed with µCT. In comparison to SEM images, which image only a single z plane, and therefore inability to fully observe the pores, µCT enables a fully 3D render. This could have been used to more accurately quantify scaffold pore sizes and may have also resulted in the quantification of surface area, a parameter that would have proven useful for determining any surface area-mediated effects of the scaffold on protein adsorption and cell response. µCT could have also been used to determine porosity instead of gravimetric analysis. Though gravimetric analysis is commonly used in the literature[176, 257, 347], when measuring thin and lightweight fibres such as the ones produced in this work, sensitive measuring equipment is required for

which incorrect calibration can introduce large errors. XPS is primarily used to determine the chemical character of the material surface. This method has relatively low spatial resolution (with XPS being the lowest) compared to methods such as time of flight secondary ion mass spectrometry (ToF-SIMS). To fully determine whether there was variation in surface chemistry of the scaffold following plasma treatment, and form a conclusion regarding the sources of scaffold variation, detailed mapping of the chemical by Tof-SIMS would have been useful[448].

In order to quantify protein adsorption characteristics of the scaffold, indirect ELISAs were used. Due to the fragment being a sequence of amino acids that no known antibody had been produced for, and only having one tagged region, the capture-detection antibody method of a standard sandwich ELISA was not possible. Other methods, such as NanoOrange™ were considered, yet were determined to have a peptide size-based detection limit which hindered fibrillin-1 fragment detection[386]. The disadvantage of using the indirect ELISA, was that a material with a consistently higher adsorption capacity than plasma treatment was required to produce a standard curve for measurement, and was not found. Other methods for concentration determination could have included; the BCA protein assay (though would have required a much higher initial fragment concentration and required protein desorption), ToF-SIMS (could also map the protein adsorption patterns on the scaffold[448]), or XPS, (can only been used to derive presence, not quantify fragment concentration). Immunocytochemistry/immunofluorescence (ICC/IF) was used to determine collagen type I, fibronectin and fibrillin-1 production. Whilst immunostaining is useful for determining intracellular distributions of expression and production of the target molecule[67], quantification can be challenging, and is usually considered semi-quantifiable. These arguments stand equally for the use of immunohistochemistry (IHC)[422], though this measure is more difficult to quantify staining, due to the non-stoichiometric character of DAB, a widely used developing agent for IHC[425]. As such, scoring methods (similar to the ones used in Chapter 5) are often employed for feature quantification[51, 411]. Though for both of these methods, more accurate methods, such as sandwich ELISAs, or colorimetric quantitative assays (e.g. hydroxyproline, Blyscan or Fastin – all produced by Bicolor UK) could have instead been used. Staining was utilised however, as it enabled the determination of the structure of the ECM present, especially with regards to the neo-ECM immunofluorescent staining, where visualisation of neo-ECM alignment was imperative for determining the success of the fibrillin-1 fragment functionalised scaffolds.

Though LIVE/DEAD assays also use fluorescence for visualisation of the cells, this labelling method does not use antibodies. Though used primarily to determine cytotoxicity, it can also be used to visualise the morphology. Determination of cytotoxicity however, can be inaccurate. As mentioned in sections 3.4 and 4.4, live to dead ratios of anchorage-dependent cells can be misrepresented, due to removal of dead cells during the final stages of the assay. Overcoming this by visualising live cells requires knowledge of initial cell number and could be better measured using quantitative DNA-binding assays, such as Quant-IT Picogreen. The resazurin reduction assay, also known as Alamarblue, is a popular method of determining metabolic activity of a cell population/per cell and can supposedly inform environmental cytotoxicity. As mentioned in section 3.4, this assumption does not hold for all cell types, with some appearing to be resistant to reductions in metabolic activity in the presence of cytotoxic agonists[381]. It has also been previously reported as a method of cell number quantification, but has been reported to result in overestimated data[401]. Despite this, resazurin reduction assays are simple, non-destructive assays which can give clear and quantitative information regarding cell behaviour on a material. For cytotoxicity, methods such as lactose dehydrogenase assays, attachment assays using Quant-IT Picogreen, or annexin staining using flow cytometry[128] are alternative methods available, with Quant-IT Picogreen a suitable measure for cell number estimations.

To estimate the concentration of GAGs present, a DMMB assay was used. Originally developed in the 1980s by Farndale *et al.*[437], this colorimetric assay has been a popular method[51] for GAG estimation, and provides the ability to quantify, in contrast to histological staining methods such as alcian blue or safranin O. It has previously been determined however, that though this assay has a wide detection range, it is sensitive to DNA present in the sample (though this can be negated by use of proteinase K preceding the complexation step)[449]. More refined methods, such as the Blyscan assay (produced by Bicolor UK), appear to offer increased sensitivity for GAG detection at lower concentrations, which would have been more appropriate for the work in this thesis. Alternatively, more specific detection methods, such as high performance liquid chromatography would have presented as viable alternatives[450].

CHAPTER 8 CONCLUSIONS AND FUTURE WORK

8.1 Concluding Remarks

The original aim of this thesis was to determine whether fibrillin-1 fragment (RGD-containing) functionalised scaffolds could be used as a platform for the enhancement of ligamentocyte response, for ACL tissue engineering. This response was determined by attachment, metabolic activity, morphology, distribution, cell alignment and neo-ECM production. Fibrillin-1 interacts with multiple other proteins in the mature ECM, including (but not limited to); perlecan[36], fibronectin[34], tropoelastin/elastin[37], TGFβ1 and associated LTBPs[32], fibulin-5[33] and decorin[35], and as such, it was hypothesised that this may lead to an increase in both ECM content and ECM maturity due to these ECM protein interactions.

To the knowledge of the author, this is the first instance of fibrillin-1 peptide fragment biofunctionalised microfibre scaffolds have being utilised as a regeneration strategy for the anterior cruciate ligament. To date, the specific fragments used in this thesis have only shown response enhancement of endothelial cell[315] and dermal fibroblast attachment[310] and the supporting of embryonic stem cell differentiation into chondrocytes[389].

Microfibre scaffolds were shown to display variability in: surface roughness, wettability, porosity, fibre diameter and mechanical properties (ultimate tensile strength, strain at failure, limit of elastic strain/stress) and during cell culture, which was more pronounced upon hydrophilisation of the surface by air plasma treatment. This was determined to be due to increased available surface area conferred by the fibrous morphology and variable surface roughness. Plasma treatment showed superior performance in: increasing the scaffold surface wettability ($p<0.0001$), alignment of the cells and cell metabolic activity when compared to untreated samples up to 7 days ($p<0.05$), and displayed the second highest protein adsorption ability (after sodium hydroxide treated samples).

Considering the data acquired using canine and human primary ACL fibroblasts, it is likely that the majority of promise with fibrillin-1 fragment functionalised scaffolds lies within their early time point (≤ 24 hrs) effect and interactions with cells, as evidenced by LIVE/DEAD labelling of cell morphology and density, and increased metabolic activity. In order to validate these conclusions however, especially in human ligamentocytes, an increased number of donors would be required. Is it imperative to note, that the physical and chemical variability (outlined above) may have affected cell response due to increased

hydrophilic surface area following plasma treatment. It was also noted that human and canine cells responded differently to the functionalised fibres. Interestingly, it was observed that 1000 ng of fibrillin-1 fragments promoted canine cell elongation, where overall, human cells (between donors) did not appear to alter in morphology compared to the non-functionalised control. Similarly, whilst fragments (namely PF8 and PF17.1 at ≤ 24 hrs for ACL09, $p<0.05$; PF8/9 at 7 days and all fragments at 14 days for ACL04, $p<0.01$) increased metabolic activity of human ligamentocytes on fragment-functionalised, plasma treated scaffolds, compared to the non-biofunctionalised controls, this was not the case for canine ligamentocytes. Effects on the ECM however, have shown positive responses at later time points (≥ 14 days) with fibrillin-1 fragments being shown to encourage and support the formation of extracellular fibrils from fibronectin, collagen type I and fibrillin in both species. Earlier time point effects (≤ 14 days) appeared much more evident with canine cells than with human where greater differences in total ECM protein content were observed between scaffolds functionalised with 1000 ng of fibrillin-1 fragments and the non-biofunctionalised controls between 1 and 14 days ($p<0.05$). Though these differences were not observed at 28 days in canine cells (with the exception of fibrillin content, after using 1000 ng PF9 on non-plasma treated scaffolds), possibly due to the lack of tensile stress on the scaffolds required for maintaining and upregulating integral ECM components[97, 405].

Donor-to-donor variation was observable in almost all experiments when using human ligamentocytes, and was also present in the ligaments they were isolated from. ECM content (with the exception of tenascin-c and collagen type III) was found to be highly variable between donors (which did not correlate linearly with age, nor degeneration scores), may have been indicative of the variation in cell response. Interestingly, collagen type I and tenascin-c were found to correlate, possibly due to increased levels of tenascin-c resulting in production of the collagen-degrading enzyme collagenase[432], and positively indicated degeneration of the ACL.

To conclude, it appears that the use of fibrillin-1 fragment functionalised scaffolds show promise as ACL tissue engineering scaffolds, despite variability in both the cells and the microfibre platforms used. To fully determine their potential however, further research (at both longer time points and perhaps at increased fragment concentration) is required.

8.2 Future Work

As the development and use of the PCL fibre scaffold was only as a platform, further optimisation would be required in order to use this as a tissue engineering graft for *in vivo* experimentation. Currently, the mechanical properties (shown in Chapter 3, section 3.3.3) are inferior to that of a suitable graft and could not withstand any potential load in the knee joint. The option of knitting or braiding individual fibre strips has shown promise[24, 302] and may provide mechanical stability to the scaffold, which would enable it to perform as a biodegradable TE graft in further testing (i.e. in bioreactors or *in vivo*). This modification would also serve to provide cells with a 3D structure, where the architecture would more closely mimic the native ACL. This would also be highly beneficial for enhancing the cellular response, as ACL cells have been shown to respond favourably to 3D environments[42].

The next, step would be to explore increased concentrations of fibrillin-1 fragments to determine whether the ECM production response can be enhanced further. It would also be beneficial to determine whether different fragments of fibrillin work more effectively, as N-terminal fragments produced (termed PF10 and PF11) have been shown to regulate the bioavailability of TGFβ1, though receptor-moderated Smad2 signalling[32]. Fibrillin-1 fragments that coacervate with tropoelastin and fibulin-5 (another elastic fibre-associated protein which contains an RGD site)[33] may also prove useful in further enhancing the neo-ACL ECM. A combination effect of using fibrillin-1 fragments with other proteins such as fibulin-5, or collagen type I/III, or the exploration of other combinations of relevant ACL ECM proteins, may further serve to enhance cell response.

Although ACL fibroblasts are often used for ACL TE as one of the main cell sources (to the knowledge of the author at present, a suitable cell line for ACL cells does not exist), bone marrow MSCs also have been used widely in this field[20, 177, 233, 337, 451]. Determining their response to differing concentrations of fibrillin-1 fragment may validate the suitability of these fragments for use in ACL TE, especially when co-cultures of ACL ligamentocytes and MSCs have been found to produce the most native-like ACL ECM[67]. In addition to the use of ligamentocytes from osteoarthritic patients (as in this thesis), it may prove beneficial to assess the response of ligamentocytes from donors with ruptured ligament (which have been shown to be highly proliferative in culture[452]) to the biofunctionalised scaffold. As one of the goals of tissue engineering is to provide personalised therapies, using cells from the

patient's own ruptured ligament to produce the graft would be highly beneficial to the patient, reducing the likelihood of immunogenic responses.

Three main parameters could be explored to replicate the native environment of the ACL *in vitro*. The ACL exists in an environment that contains very limited vasculature, and little blood supply, especially to the midsubstance. Due to the hypoxic environment of the ligament, it has previously been suggested that ACL cells should be cultured in conditions that replicate this. Kowalski *et al.* (2016)[453] have determined that ACL cells cultured in hypoxia increase gene expression of collagen and display increased metabolic activity. To increase the physiological relevance of ACL cell behaviour on the graft, hypoxic chambers could be used, which may demonstrate the response of ACL cells to the graft in physiologically relevant conditions.

It has also been reported that both the maintenance of the ACL fibroblast phenotype and subsequently, the ligament neo-ECM proteins (such as collagen types I and III), rely on tensile stretch being applied to the cells[405]. Bioreactors are useful tools in providing stimuli to cells, which they feel through the material tension and relaxation, and in turn, make the culture conditions of the cells more physiologically valid. In order to replicate human movement, bioreactors that provide mechanical stimulation in the form of uniaxial strain can be used in tandem with biofunctionalisation of scaffolds in order to achieve a mature neo-ECM.

The final proposal is based on the cell types present in the ligament. Whilst fibroblasts mainly inhabit the midsubstance of the ACL, the proximal and distal ends are populated by fibrochondral-like cells. ACL cells are known to have trilineage differentiation capacity and therefore can be induced to pursue a chondrocyte lineage[69]. These cells, along with the elongated fibroblastic cells could be seeded in specific places on the grafts, relevant to their native positions within the ACL. They could then be assessed to determine whether they are producing the correct matrix for their area and whether that matrix has integrated. Fibrillin-1 fragments, which have already been shown to support chondrogenesis *in vitro*[389], could be used to enhance attachment and neo-ECM production in co-cultured cells.

As the ultimate aim in tissue engineering is to recapitulate the existing tissue as closely as possible, it would be beneficial to determine the mechanical properties of the graft following long-term culture, both with and without environment-mimicking set-ups to discover which individual, or combination environment is best suited to directing the cellular production of

a native-like ECM. Assessment of this *in vivo* would provide information on the graft success in a systemic environment, and provide information as to the cells' regenerative capacity inside the joint capsule, especially in the presence of inhibitory synovial fluid[6].

Fibrillin-1 is widespread throughout the body, yet is especially concentrated in highly elastic tissues. Many of these tissues are also collagenous, and may benefit from topographical guidance cues, provided by electrospun fibres. Therapies for oesophageal, skeletal muscle, dermal wound and major vessel TE may provide other relevant focuses for which this biofunctionalised scaffold could be applied.

REFERENCES

1. Zinser L (2008) Minutes in, Brady's season is in jeopardy. in *NFL*, ed Archibald R (The New York Times, https://www.nytimes.com/2008/09/08/sports/football/08patriots.html).
2. ESPN (2008) Brady had procedure to clear out infection in knee. in *NFL*, ed ESPN (ESPN, https://www.espn.co.uk/nfl/news/story?id=3648586).
3. Phillips M (The Financial Impact of Tom Brady's Injury. Newsweek.
4. Amis A & Dawkins G (1991) Functional anatomy of the anterior cruciate ligament. Fibre bundle actions related to ligament replacements and injuries. *The Journal of Bone and Joint Surgery* 73-B(2):260-267.
5. Lyon R, *et al.* (1991) Ultrastructural differences between the cells of the medial collateral and the anterior cruciate ligament. *Clinical Orthapaedics and Related Research* 272:279-286.
6. Zigang G, Goh J, & Lee E (2005) Selection of cell source for ligament tissue engineering *Cell Transplantation* 14(8):573-583.
7. Ma J, *et al.* (2012) Three-dimensional engineered bone-ligament-bone constructs for anterior cruciate ligament replacement. *Tissue Engineering Part A* 18(1-2):103-116.
8. Butler D, *et al.* (1995) Location-dependent variations in the material properties of the anterior cruciate ligament. *Journal of Biomechanics* 25(5):511-518.
9. Joseph A, *et al.* (2013) A multisport epidemiologic comparison of anterior cruciate ligament injuries in high school athletics. *Journal of Athletic Training* 48(6):810-817.
10. Mather RI, *et al.* (2013) Societal and economic impact of anterior cruciate ligament tears. *The Journal of Bone and Joint Surgery* 95(19):1751-1759.
11. Csintalan R, Inacio M, & Funahashi T (2008) Incidence rate of anterior cruciate ligament reconstructions. *The Permanente Journal* 13(3):17-21.
12. Nicholls M, Aspelund T, Ingvarsson T, & Briem K (2018) Nationwide study highlights a second peak in ACL tears for women in their early forties. *Knee Surgery, Sport Traumatology, Arthroscopy* 26(2):648-654.
13. Su M, *et al.* (2021) Medium-term (least 5 years) comparative outcomes in anterior cruciate ligament reconstruction using 4SHG, allograft, and LARS ligament. *Clinical Journal of Sport Medicine* 31(2):e101-e110.
14. Iliadis D, Bourlos D, Mastrokalos D, Chronopoulos E, & Babis G (2016) LARS artificial ligament versus ABC purely polyester ligament for anterior cruciate ligament reconstruction. *Orthopaedic Journal of Sports Medicine* 4(6):2325967116653359.
15. Guirea M, Zorilla P, Amis A, & Aichroth P (1999) Comparative pull-out and cyclic-loading strength tests of anchorage of hamstring tendon grafts in anterior cruciate ligament reconstruction. *Amercian Journal of Sports Medicine* 27(5):621-625.
16. Amiel D, Frank C, Harwood F, Fronek J, & Akeson W (1984) Tendons and ligaments: a morphological and biochemical comparison. *Journal of Orthopaedic Research* 1:257–265
17. Hanson A & Bentley J (1983) Quanitation of type I to type III collagen ratios in small samples of human tendon, blood vessels and atherosclerotic plaque. *Analytical Biochemistry* 130:32-40.
18. Chen K, *et al.* (2012) A hybrid silk/RADA-based fibrous scaffold with triple hierarchy for ligament regeneration. *Tissue Engineering Part A* 18(13-14):1399-1409.
19. Chen X, *et al.* (2008) Ligament regeneration using a knitted silk scaffold combined with collagen matrix. *Biomaterials* 29(27):3683-3692.
20. Figueroa D, *et al.* (2014) Anterior cruciate ligament regeneration using mesenchymal stem cells and collagen type I scaffold in a rabbit model. *Knee Surgery, Sports Traumatology, Arthroscopy* 22(5):1196-1202.
21. Kimura Y, Hokugo A, Takamoto T, Tabata Y, & Kurosawa H (2008) Regeneration of anterior cruciate ligament by biodegradable scaffold combined with local controlled release of basic fibroblast growth factor and collagen wrapping. *Tissue Engineering Part C* 14(1):47-57.

22. Leong N, *et al.* (2015) Evaluation of polycaprolactone scaffold with basic fibroblast growth factor and fibroblasts in an athymic rat model for anterior cruciate ligament reconstruction. *Tissue Engineering Part A* 21(11-12):1859-1868.
23. Liu H, Fan H, Toh S, & Goh J (2008) A comparison of rabbit mesenchymal stem cells and anterior cruciate ligament fibroblasts responses on combined silk scaffolds. *Biomaterials* 29:1443-1453.
24. Ruan D, *et al.* (2019) Knitted silk-collagen scaffold incorporated with ligament stem/progenitor cells sheet for anterior cruciate ligament reconstruction and osteoarthritis prevention. *ACS Biomaterials Science & Engineering* 5:5412-5421.
25. Leong N, *et al.* (2014) In vitro and in vivo evaluation of heparin mediated growth factor release from tissue engineered constructs for anterior cruciate ligament reconstruction. *Journal of Orthopaedic Research* 33(2):229-236.
26. Yu X, Mengsteab P, Narayanan G, Nair L, & Laurencin C (2020) Enhancing the surface properties of a bioengineered anterior cruciate ligament matrix for use with point-of-care stem cell therapy. *Engineering* 7(2):153-161.
27. Chen J, *et al.* (2003) Human bone marrow stromal cell and ligament fibroblast responses on RGD-modified silk fibers. *Journal of Biomedical Materials Research Part A* 67A(2):559-570.
28. Tao T, *et al.* (2018) Fibronectin enhances cartilage repair by activating progenitor cells through integrin α5β1 receptor. *Tissue Engineering Part A* 24(13-14):1112-1124.
29. Vélez C, Babeito C, & Koncurat M (2018) αvβ3 integrin and fibronectin expressions and their relation to estrogen and progesterone during placentation in swine. *Biotechnic & Histochemistry* 93(1):15-24.
30. Bax D, *et al.* (2003) Cell adhesion to Fibrillin-1 molecules and microfibrils is mediated by a5B1 and avB3 integrin. *Journal of Biological Chemistry* 278:34605-34616.
31. Cain S, *et al.* (2005) Fibrillin-1 interactions with heparin. *The Journal of Biological Chemistry* 280(34):30526 –30537.
32. Chaudhry S, *et al.* (2007) Fibrillin-1 regulates the bioavailability of TGFβ1. *Journal of Cell Biology* 176(3):355-367.
33. Freeman L, *et al.* (2005) Fibulin-5 interacts with fibrillin-1 molecules and microfibrils. *Biochemical Journal* 388:1-5.
34. Kinsey R, *et al.* (2008) Fibrillin-1 microfibril deposition is dependent on fibronectin assembly. *Journal of Cell Science* 121(16):2696-2704.
35. Schaefer L, *et al.* (2007) Decorin-mediated regulation of fibrillin-1 in the kidney involves the insulin-like growth factor-I receptor and mammalian target of rapamycin. *The American Journal of Pathology* 170(1):301-315.
36. Tiedemann K, *et al.* (2005) Microfibrils at basement membrane zones interact with perlecan via fibrillin-1. *Journal of Biological Chemistry* 280(12):11404-11412.
37. Clarke A, Wise S, Cain S, Kielty C, & Weiss A (2005) Coacervation is promoted by molecular interactions between the PF2 segment of fibrillin-1 and the domain 4 region of tropoelastin. *Biochemistry* 44(30):10271-10281.
38. Zantop T, Herbort M, Raschke M, Fu F, & Petersen W (2007) The role of the anteromedial and posterolateral bundles of the anterior cruciate ligament in anterior tibial translation and internal rotation. *American Journal of Sports Medicine* 35(2):223-227.
39. Giuliani J, Kilcoyne K, & Rue J (2009) Anterior cruciate ligament anatomy: a review of the anteromedial and posterolateral bundles. *Journal of Knee Surgery* 22:148–154.
40. Li G, DeFrate LE, Sun H, & Gill TJ (2004) In vivo elongation of the anterior cruciate ligament and posterior cruciate ligament during knee flexion. *American Journal of Sports Medicine* 32(6):1415-1420.
41. Ristaniemi A, Tanska P, Stenroth L, Finnilä M, & Korhonen R (2021) Comparison of material models for anterior cruciate ligament in tension: from poroelastic to a novel fibril-reinforced nonlinear composite model. *Journal of Biomechanics* 114:110141.
42. Gögele C, *et al.* (2020) Enhanced growth of lapine anterior cruciate ligament-derived fibroblasts on scaffolds embroidered from poly(L-lactide-co-e-caprolactone) and polylactic

acid threads functionalized by fluorination and hexamethylene diisocyanate cross-linked collagen foams. *International Journal of Molecular Sciences* 21(3):1132-1154.
43. Petersen W & Tillmann B (1999) Structure and vascularization of the cruciate ligaments of the human knee joint. *Anatomy and Embryology (Berlin)* 200(3):325-334.
44. Meaney Murray M, Bennett R, Zhang X, & Spector M (2002) Cell outgrowth from human ACL in vitro: regional variation and response to TGF-B1. *Journal of Orthopaedic Research* 20:875-880.
45. Toy B, Yeasting R, Morse D, & McCann P (1995) Arterial supply to the Human Anterior Cruciate Ligament. *Journal of Athletic Training* 30(2):149-152.
46. Pappa AGL, *et al.* (2001) The presence of proprioceptive mechanoreceptors in the remnants of the ruptured ACL as a possible source of re-innervation of the ACL autograft. *Knee Surgery, Sports Traumatology, Arthroscopy* 9(6):364-368.
47. Shutte M, Dabezies E, Zimney M, & Happel L (1987) Neural anatomy of the human anterior cruciate ligament. *Journal of Bone and Joint Surgery (America)* 69:243–247
48. Weiss J & Gardiner J (2001) Computational Modeling of Ligament Mechanics. *Critical Reviews in Biomedical Engineering* 29(4):1-70.
49. Kastelic J, Palley I, & Baer E (1978) The multicomposite ultrastructure of tendon. *Connective Tissue Research* 6:11-23.
50. Hasegawa A, *et al.* (2013) Cellular and extracellular matrix changes in anterior cruciate ligaments during human knee ageing and osteoarthritis. *Arthritis Research & Therapy* 15(1):R29.
51. Kharaz Y, Canty-Laird E, Tew S, & Comerford E (2018) Variations in the internal structure, composition and protein distribution between intra- and extra- articular knee ligaments and tendons. *J. Anat.* 232(6):943-955.
52. Hayes A, *et al.* (2011) Colocalization in vivo and association in vitro of perlecan and elastin. *Histochemistry and Cell Biology* 136:437-454.
53. Reinboth B, Hanssen E, Cleary E, & Gibson M (2002) Molecular interactions of biglycan and decorin with elastic fiber componants: biglycan forms a ternary complex with tropoelastin and microfibril-associated glycoprotein-1. *Journal of Biological Chemistry* 277:3950-3957.
54. Robinson K, *et al.* (2017) Decorin and biglycan are necessary for maintaining collagen fibril structure, fiber realignment, and mechanical properties of mature tendons. *Matrix Biology* 64:81-93.
55. Shukunami C, *et al.* (2018) Scleraxis is a transcriptional activator that regulates the expresion of tenomodulin, a marker of mature tenocytes and ligamentocytes. *Scientific Reports* 8:3155.
56. Komiyama Y, *et al.* (2013) Tenomodulin expression in the peridontal ligament enhances cellular adhesion. *PLOS ONE* 8(4):e60203.
57. Midwood K, *et al.* (2009) Tenascin-c is an endogenous activator of toll-like receptor 4 that is essential for maintaining inflammation in arthritic joint disease. *Nature Medicine* 15(7):774-780.
58. Kubow K, *et al.* (2015) Mechanical forces regulate the interactons of fibronectin and collagen I in extracellular matrix. *Nature Communications* 6:8026.
59. Smith KD, *et al.* (2011) The organisation of elastin and fibrillins 1 and 2 in the cruciate ligament complex. *J. Anat.* 218(6):600-607.
60. Zantop T, Petersen W, & Fu F (2005) Anatomy of the anterior cruciate ligament. *Operative Techniques in Orthopaedics* 15(1):20-28.
61. Lee J, *et al.* (2020) Anterior cruciate ligament remnant cells have different potentials for cell differentiation based on their location. *Scientific Reports* 10:3097.
62. Amiel D, Billings E, & Akeson W (1989) Ligament structure, chemistry and physiology. *Knee Ligaments: structure, injury and repair*, ed Daniel D ea (Raven Press, New York), p 34.
63. Murray M & Spector M (1999) Fibroblast distribution in the anteromedial bundle of the human anterior cruciate ligament: the presence of α-smooth muscle actin-positive cells. *Journal of Orthopaedic Research* 17:18-27.

64. Noyes F, DeLucas J, & Torvik P (1974) Biomechanics of anterior cruciate ligament failure: an analysis of strain-rate sensitivity and mechanisms of failure in primates. . *Journal of Bone and Joint Surgery (America)* 56(2):236-253.
65. Taylor K, *et al.* (2013) In vivo measurement of ACL length and relative strain during walking. *Journal of Biomechanics* 46(3):478-483.
66. Beynnon B, *et al.* (1995) Anterior cruciate ligament strain behaviour during rehabiliation exeercises in-vivo. *American Journal of Sports Medicine* 23(1):24-34.
67. Canseco J, *et al.* (2012) Effect on ligament marker expression by direct-contact co-culture of mesenchymal stem cells and anterior cruciate ligament cells. *Tissue Engineering: Part A* 18(23 & 24):2549-2558.
68. Steinert A, *et al.* (2011) Mesenchymal stem cells characteristics of human anterior cruciate ligament outgrowth cells. *Tissue Engineering Part A* 17(9-10):1375-1388.
69. Lee K, Comerford E, Simpson D, Clegg P, & Canty-Laird E (2019) Identification and characterisation of canine ligament progenitor cells and their extracellular matrix niche. *Journal of Proteome Research* 18(3):1328-1339.
70. Alsook M, *et al.* (2015) Tissues from equine cadaver ligaments up to 72 hours of post-mortem: a promising resevior of stem cells. *Stem Cell Research & Therapy* 6:253.
71. Furumatsu T, *et al.* (2010) Anterior cruciate ligament-derived cells have high chondrogenic potential. *Biochemical and Biophysical Research Communications* 391:1142-1147.
72. Lee K, Clegg P, Comerford E, & Canty-Laird E (2017) Ligament-derived stem cells: identification, characterisation and therapeutic application. *Stem Cells International* 2017:1919845.
73. Murray M, Weiler A, & Spindler K (2004) Interspecies variation in the fibroblast distribution of the anterior cruciate ligament. *The American Journal of Sports Medicine* 32(6):1484-1491.
74. Lee I, Wang J, Lee Y, & Young T (2007) Development of a useful technique to discriminate anterior cruciate ligament cells and mesenchymal stem cells - the application of cell electrophoresis. *Journal of Biomedical Materials Research Part A* 82(1):230-237.
75. van Vijven M, *et al.* (2020) Identifying potential patient-specific predictors for anterior cruciate ligament reconstruction outcome - a diagnostic in vitro tissue remodeling platform. *Journal of Experimental Orthopaedics* 7:48.
76. Mifune Y, *et al.* (2012) Therapeutic potential of anterior cruciate ligament-derived stem cells for anterior cruciate ligament reconstruction. *Cell Transplantation* 21(8):1651-1665.
77. Wetzel A, *et al.* (2004) Human thy-1 (CD90) on activated endothelial cells is a counterreceptor for the leukocyte integrin mac-1 (CD11b/CD18). *The Journal of Immunology* 172(6):3850-3859.
78. Dreyer E, *et al.* (1995) An astrocytic binding site for neuronal thy-1 and its effect on neurite outgrowth. *Proceedings of the National Academy of Science USA* 92(24):11195-11199.
79. Ogata Y, *et al.* (2018) Anterior cruciate ligament-derived mesenchymal stromal cells have a propensity to differentiate into the ligament lineage. *Regenerative Therapy* 8:20-28.
80. Zhang J, Pan T, Im H, Fu F, & Wang J (2011) Differential properties of human ACL and MCL stem cells may be responsible for their differential healing capacity. *BMC Medicine* 9.
81. Cheng M, Lui C, Chen T, & Lee O (2014) Optimization of culture conditions for stem cells derived from human anterior cruciate ligament and bone marrow. *Cell Transplantation* 23(7):791-803.
82. Airas L, *et al.* (1995) CD73 is involved in lymphocyte binding to the endothelium: characterization of lymphocyte-vascular adhesion protein 2 identifies it as CD73. *Journal of Experimental Medicine* 182(5):1603-1608.
83. Goswami S, *et al.* (2020) Immune profiling of human tumors identifies CD73 as a combinatorial target in glioblastoma. *Nature Medicine* 26(1):39-46.
84. Togarrati P, Dinglasan N, Desai S, Ryan W, & Muench M (2018) CD29 is highly expressed on epithelial, myoepithelial and mesenchymal stromal cells of human salivary glands. *Oral Diseases* 24(4):561-572.
85. Woodard G, *et al.* (2014) Characterization of discrete subpopulations of progenitor cells in traumatic human extremity wounds. *PLOS ONE* 9(12):e114318.

86. Suzuki A, *et al.* (2000) Flow-cytometric separation and enrichment of hepatic progenitor cells in te developing mouse liver. *Hepatology* 32(6):1230-1239.
87. Vetrano M, *et al.* (2019) Hyaluronic acid (HA), platelet-rich plasm and extracorporeal shock wave therapy (ESWT) promote human chondrocyte regeneration *in vitro* and SWT-mediated increase of CD44 expression enhances their susceptibility to HA treatmet. *PLOS ONE* 14(6):e0218740.
88. Liu Y, *et al.* (2017) $CD44^{+}$ fibroblasts increases breast cancer cell survival and drug resistance *via* IGF2BP3-CD44-IGF2 signalling. *Journal of Cellular and Molecular Medicine* 21(9):1979-1988.
89. Cheifetz S, *et al.* (1992) Endoglin is a component of the transforming growth factor-beta receptor system in human endothelial cells. *Journal of Biological Chemistry* 267(27):19027-19030.
90. Schmidt-Weber C, *et al.* (2005) TGF-β signaling of human T cells is modulated by the ancillary TGF-β receptor endoglin. *International Immunology* 17(7):921-930.
91. Sándor N, *et al.* (2016) CD11c/CD18 dominates adhesion of human monocytes, macrophages and dendritic cells over CD11b/CD18. *PLoS ONE* 11(9):e0163120.
92. Kriegova E, *et al.* (2018) Gender-related differences observed among immune cells in synoval fluid in knee osteoarthritis. *Osteoarthritis and Cartilage* 26(9):1247-1256.
93. Comerford E, Tarlton J, Avery N, Bailey A, & Innes J (2006) Distal femoral intercondylar notch dimensions and their relationship to composition and metabolism of the canine cruciate ligament. *Osteoarthritis and Cartilage* 14(3):273-278.
94. Herchenhan A, *et al.* (2015) Lysyl oxidase activity is required for ordered collagen fibrillogenesis by tendon cells. *Journal of Biological Chemistry* 290(26):16440-16450.
95. Smith K, Clegg P, Innes J, & Comerford E (2014) Elastin content is high in the canine cruciate ligament and is associated with degeneration. *The Veterinary Journal* 199(1):169-174.
96. Chockalingam P, Glasson S, & Lohmander L (2013) Tenascin-C levels in synovial fluid are elevated after injury to the human and canine joint and correlate with markers of inflammation and matrix degradation. *Osteoarthritis and Cartilage* 21(2):339-345.
97. AbiEzzi SF, RA, Harwood F, Akeson W, & Amiel D (1997) Decrease in fibronectin occurs coincident with increased expression of its integrin receptor alpha5beta1 in stress-deprived ligaments. *The Iowa Orthopoedic Journal* 17:102-109.
98. Valiyaveettil M, Mort J, & McDevitt C (2005) The connection, gene expression, and spatial distribution of aggrecan in canine articular cartilage, meniscus, and anterior and posterior cruciate ligaments: a new molecular distinction between hyaline cartilage and fibrocartilage in the knee joint. *Connective Tissue Research* 46(2):83-91.
99. Cain SB, AK, *et al.* (2008) Heparan sulfate regulates fibrillin-1 N- and C-terminal interactions. *Journal of Biological Chemistry* 283(40):27017-27027.
100. Hua R, *et al.* (2020) Biglycan and chondroitin sulfate play pivotal roles in bone toughness via retaining bound water in bone mineral matrix. *Matrix Biology* 94(95-109).
101. Roberts J, Elder R, Neumann A, Jayaraman A, & Bryant S (2014) Interaction of hyaluronan binding peptides with glycosaminoglycans in poly(ethylene glycol) hydrogels. *Biomacromolecules* 15(4):1132-1141.
102. Kram V, Kilts T, Bhattacharyya N, Li L, & Young M (2017) Small leucine rich proteoglycans, a novel link to osteoclastogenesis. *Scientific Reports* 7(1):12627.
103. Little D, *et al.* (2014) Proteomic differences between male and female anterior cruciate ligament and patellar tendon. *PLOS ONE* 9(5):e96526.
104. Engebretsen K, *et al.* (2013) Decorin, lumican and their GAG chain-synthesizing enzymes are regulated in myocardial remodeling and reverse remodeling in the mouse. *Journal of Applied Physiology* 114(8):988-997.
105. Harten I, *et al.* (2020) The synthesis and secretion of versican isoform V3 by mammalian cells: a role for N-linked glycosylation. *Matrix Biology* 89:27-42.
106. Doege K, Sasaki M, Kimura T, & Yamada Y (1991) Complete coding sequence and deduced primary structure of the human cartilage large aggregating proteoglycan, aggrecan. *The Journal of Biological Chemistry* 266(2):894-902.

107. Oldberg A, Antonsson P, Lindblom K, & Heinegård D (1989) A collagen-binding 59-kd protein (fibromodulin) is structuarally related to the small interstitial proteoglycans PG-S1 and PG-S2 (decorin). *The EMBO Journal* 8(9):2601-2604.
108. Yazdanshenas H, Madadi F, Washington E, Jones K, & Shamie A (2015) Patellar tendon donor-site healing during six and twelve months after Anterior Cruciate Ligament Reconstruction. *Journal of Orthopaedics* 12(4):179-183.
109. Ristić V, Srđan N, Vladimir H, & Miroslav M (2010) Causes of anterior cruciate ligament injuries. *Medicinski pregled (Serbian)* 63(7-8):541-545.
110. Anderson D, Madigan M, & Nussbaum M (2007) Maximum voluntary joint torque as a function of joint angle and angular velocity: Model development and application to the lower limb. *Journal of Biomechanics* 40(14):3105-3113.
111. Markolf K, Gorek J, Kabo J, & Shapiro M (1990) Direct measurement of resultant forces in the anterior cruciate ligament. *The Journal of Bone and Joint Surgery* 72-A(4):557-567.
112. Markolf K, *et al.* (1995) Combined knee loading states that generate high anterior cruciate ligament forces. *Journal of Orthopaedic Research* 13(6):930-935.
113. Murray M, *et al.* (2007) Advanced histologic repair in a central wound in the anterior cruciate ligament with a collagen-platelet-rich plasma scaffold. *Journal of Orthopaedic Research* 25(8):1007-1017.
114. Cone S, Piedrahita J, Spang J, & Fisher M (2019) In situ joint stiffness increases during skeletal growth but decreases following partial and complete anterior cruciate ligament injury. *Journal of Biomechanical Engineering* 141(12):121001-121008.
115. Ralles S, Agel J, Obermeier M, & Tompkins M (2015) Incidence of Secondary Intra-articular Injuries With Time to Anterior Cruciate Ligament Reconstruction. *American Journal of Sports Medicine* 43(6):1373-1379.
116. Magnussen R, Reinke E, & Huston L (2016) Factors Associated with High Grade Lachman, Pivot Shift and Anterior Drawer at the Time of Anterior Cruciate Ligament Reconstruction. *Arthroscopy: Journal of Arthroscopic and Related Research* 32(6):1080-1085.
117. Dejour D, Ntagiopoulos P, Saggin P, & Panisset J (2013) The Diagnostic Value of Clinical Tests, Magnetic Resonance Imaging and Instrumented Laxity in the Differentiation of Complete vs Partial Anterior Cruciate Ligament Tears. *Arthroscopy: Journal of Arthroscopic and Related Surgery* 29(3):491-499.
118. Noyes F, Bassett R, Grood E, & Butler D (1980) Arthroscopy in acute traumatic hemarthrosis of the knee. Incidence of anterior cruciate tears and other injuries. *Journal of Bone and Joint Surgery America* 62(5):687-695.
119. Brophy R, Sandell L, Wright R, & Rai M (2015) Transcriptomic signatures of mensical tears and articular cartlidge from knees undergoing arthroscopic partial meniscectomy show evidence for early osteoarthritis. *Orthopaedic Journal of Sports Medicine* 3(7):Supp. 2.
120. Maffulli N, Binfield P, & King J (2003) Articular lesions in the symptomatic anterior cruicate ligament-deficient knee. *Arthroscopy* 19(7):685-690.
121. Meunier A, Odensten M, & Good L (2006) Long-term results after primary repair or non-surgical treatment of anterior cruciate ligament rupture: a randomized study with a 15-year follow-up. *Scandinavian Journal of Medicine and Science in Sports* 17(3):230-237.
122. Claes S, Hermie L, Verdonk R, Bellemans J, & Verdonk P (2013) Is osteoarthritis an inevitable consequence of anterior cruciate ligament reconstruction? A meta-analysis. *Knee Surgery, Sports Traumatology, Arthroscopy* 21(9).
123. Maerz T, *et al.* (2014) Increased risk of osteoarthritis after anterior cruciate ligament reconstruction. A 14 year follow-up study of a randomized controlled trial. *Amercian Journal of Sports Medicine* 42(5):1049-1057.
124. Stevens A, Wishnok J, White F, Grodzinsky A, & Tannenbaum S (2009) Mechanical injury and cytokines cause loss of cartidge integrity and upregulate proteins associated with catabolism, immunity, inflammation, and repair. *Molecular Cell Proteomics* 8(7):1475-1489.
125. Chauffier K, *et al.* (2012) Induction of the chemokine IL-8/Kc by the articular cartilage: possible influence on oesteoarthritis. *Joint Bone Spine* 79(6):604-609.

126. Moradi B, *et al.* (2015) Unicompartmental and bicompartmental knee osteoarthritis show different patterns of mononuclear cell infiltration and cytokine release in the affected joints. *Clinical & Experimental Immunology* 180(1):143-154.
127. Lee W, *et al.* (2014) Synergy between Piezo1 and Piezo2 channels confers high-strain mechanosensitivity to articular cartilage. *Proceedings of the National Academy of Sciences of the United States of America* 111(47):E5114-E5122.
128. Lawrence K, *et al.* (2017) Chondroprotection by urocortin involves blockade of the mechanosensitive ion channel Piezo1. *Scientific Reports* 7(1):5147.
129. Ventura A, Terzaghi C, Legnani C, Borgo E, & Albisetti W (2010) Synthetic grafts for anterior cruciate ligament rupture: 19 year outcome study. *The Knee* 17(2):108-113.
130. Maletius W & Gillquist J (1997) Long-term results of anterior cruciate ligament reconstruction with a Dacron prosthesis: The frequency of osteoarthritis after seven to eleven years. *American Journal of Sports Medicine* 25(3):288-293.
131. Olsen E, *et al.* (1988) The biochemical and histological effects of artifical ligament wear particles: in vitro and in vivo studies. *The American Journal of Sports Medicine* 16(6):558-570.
132. Bray R, Leonard C, & Salo P (2002) Vascular physiology and long-term healing of partial ligament tears. *Journal of Orthopaedic Research* 20(5):984-989.
133. Adachi N, *et al.* (2002) Mechanoreceptors in the anterior cruciate ligament contribute to the joint position sense. *Acta Orthopaedica Scandanavia* 73(3):330-334.
134. Almqvist K, Willaert P, De Brabandere S, Criel K, & Verdonk R (2009) A long-term study of anterior cruciate ligament allograft reconstruction. *Knee Surgery, Sport Traumatology, Arthroscopy* 17(7):818-822.
135. Tibor L, *et al.* (2016) Surgical technique trends in primary ACL reconstruction from 2007 to 2014. *The Journal of Bone and Joint Surgery* 98(13):1079-1089.
136. Foster T, Wolfe B, Ryan S, Silvestri L, & Kaye E (2010) Does the graft source really matter in the outcome of patients undergoing anterior cruciate ligament reconstruction? An evaluation of autograft verus allograft reconstruction results: a systemic review. *American Journal of Sports Medicine* 38(1):189-199.
137. Singhal M, Gardiner J, & Johnson D (2007) Failure of primary anterior cruciate ligament surgery using anterior tibialis allograft. *Arthroscopy* 23:469-475.
138. Crawford D, *et al.* (2013) Post-operative complication following primary ACL reconstruction using allogenic and autogenic soft tissue grafts: Increased relative morbidity risk is associated with increased graft diameter. *The Knee* 20(6):520-525.
139. Persson A, *et al.* (2014) Increased risk of revision with hamstring tendon grafts compared with patellar tendon grafts after anterior cruciate ligament reconstruction. *American Journal of Sports Medicine* 42(2):285-291.
140. Biau D, *et al.* (2009) Patellar tendon verus hamstring tendon autografts for reconstructing the anterior cruciate ligament: a meta-analysis based on individual patient data. *American Journal of Sports Medicine* 37(12):2470-2478.
141. Pinczewski L, *et al.* (2007) A 10 year comparison of anterior cruciate ligament reconstructions with hamstring tendon and patellar tend autografts: a controlled, perspective trial. in *American Journal of Sports Medicine*, pp 564-574.
142. Achtnich A, *et al.* (2013) Tunnel widening after anatomic double bundle and mid-position single bundle anterior cruciate ligament reconstruction. *Arthroscopy* 29(9):1514-1524.
143. Järvelä T, Moisala A, Paakkala T, & Paakkala A (2008) Tunnel enlarement after double-bundle anterior cruciate ligament reconstruction: a prospective, randomised study. *Arthroscopy* 24(12):1349-1357.
144. Friendlaender G, Strong D, & Sell K (1984) Studies on the antigenicity of bone. II. Donor-specific c anti-HLA antibodes in human reipients of freeze-dried allografts. *Journal of Joint and Bone Surgery America* 66:107-112.
145. Hsu R, Himeno S, & Coventry M (1988) Transactions of the 34th annual meeting of the orthopedic research society (Orthopedic Research Society).

146. Dowdy P, Miniaci A, Arnockzy S, Fowler P, & Boughner D (1995) The effect of cast immobilization on meniscal healing. An experimental study in the dog. *American Journal of Sports Medicine* 23:721-728.
147. Gordon M & Bullough P (1982) Synovial and osseous inflammation in failed silicone-rubber prosthesis. *Journal of Bone and Joint Surgery* 64A:574-580.
148. Levy L, Lipscomb C, & McDonald H (1954) Complications of Judet arthroplasty due to foreign-body reaction to nylon prosthesis. *Journal of Bone and Joint Surgery* 36A:1175-1180.
149. Paulos L, Rosenberg T, Grewe S, Tearse D, & Beck C (1992) The GORE-TEX anterior cruciate ligament prosthesis: a long-term follow-up. *American Journal of Sports Medicine* 20(3):245-252.
150. Trieb K, Blahovec H, Brand G, & Kotz R (2004) In vivo and in vitro cellular ingrowth into a new generation of artificial ligaments. *European Surgical Research* 36(3):148-151.
151. Gillquist J & Odensten M (1993) Reconstruction of old anterior cruciate ligament tears with a Dacron prosthesis: a prospective study. *American Journal of Sports Medicine* 21:358-366
152. Glousman R, *et al.* (1988) Gore-Rex prosthetic ligament in anterior cruciate deficient knees. *American Journal of Sports Medicine* 16(4):321-326.
153. Batty L, *et al.* (2015) Synthetic devices for reconstructive surgery of the cruciate ligaments: a systematic review. *Arthroscopy* 31(5):957-968.
154. Huang J, Wang Q, Shen F, Wang Z, & Kang Y (2010) Cruciate ligament construction using LARS artificial ligament under arthroscopy: 81 cases report. *Chinese Medical Journal (England)* 123(2):160-164.
155. Machotka Z, Scarborough I, Duncan W, Kumar S, & Perraton L (2010) Anterior cruciate ligament repair with LARS (ligament advanced reinforcement system): a systematic review. *Sports Medicine, Arthroscopy, Rehabilitation, Therapy & Technology* 2(1):29.
156. Muren O, Dahlstedt L, Brosjö E, Dahlborn M, & Dalén N (2005) Gross osteolytic tibia tunnel widening with the use of Gore-Tex anterior cruciate ligament prosethesis. *Acta Orthopaedica* 76(2):270-274.
157. Escamilla R, MacLeod T, Wilk K, Paulos L, & Andrews J (2012) Anterior Cruciate Ligament strain and tensile forces for weight-bearing and non-weight bearing exercises: a guide to exercise selection. *Journal of Orthopaedic & Sports Physical Therapy* 42(3):208-220.
158. Gao K, *et al.* (2010) Anterior cruciate ligament reconstruction with LARS artificial ligament: A multicenter study with 3- to 5- year follow-up. *Journal of Arthroscopic & Related Surgery* 24 (4):515-523
159. Murray A & Macnicol M (2004) 10-16 year results of Leeds-Keio anterior cruciate ligament reconstruction. *Knee* 11:9-14.
160. Barrett G, Line L, Shelton W, Manning J, & Phelps R (1993) The Dacron ligament prosthesis in anterior cruciate ligament reconstruction: a four- year review *American Journal of Spots Medicine* 21:367-373
161. Langer R & Vacanti J (1993) Tissue engineering. *Science* 260(5110):920-926.
162. Deepthi S, Jeevitha K, Niveditha Sundaram M, Chennazhi K, & Jayakumar R (2015) Chitosan-hyaluronic acid coated poly (caprolactone) multiscale bilayer scaffold for ligament regeneration. *Chemical Engineering Journal* 260:478-485.
163. Sanders T, *et al.* (2016) Incidence of anterior cruciate ligament tears and reconstruction: a 21-year population-based study. *The American Journal of Sports Medicine* 44(6):1502-1507.
164. Bax D, McKenzie D, Weiss A, & Bilek M (2009) Linker-free covelant attachment of the extracellular matrix protein tropoelastin to a polymer surface for directed cell spreading. *Acta Biomaterialia* 5:3371-3381.
165. Beynnon B, *et al.* (1997) The strain behaviour of the anterior cruciate ligament during squatting and active flexion-extension. A comparison of an open and a closed kinetic chain exercise. *The American Journal of Sports Medicine* 25(6):823-829.
166. Thomlinson R & Gray L (1955) The histological structure of some human lung cancers and the possible implcations for radiotherapy. *British Journal of Cancer* 9(4):539-549.

167. Shao H, Lee Y, Chen C, Wang J, & Young T (2010) Modulation of gene expression and collagen production of anterior cruciate ligament cells through cell shape changes on polycaprolactone/chitosan blends. *Biomaterials* 31(17):4695-4705.
168. Gögele C, *et al.* (2021) Cyclically stretched ACL fibroblasts emigrating from spheroids adapt their cytoskeleton and ligament-related expression profile. *Cell and Tissue Research* 384:675-690.
169. Petrigliano F, *et al.* (2015) In Vivo Evaluation of Electrospun Polycaprolactone Graft for Anterior Cruciate Ligament Engineering. *Tissue Engineering Part A* 21(7-8):1228-1236.
170. Sahoo S, Ouyang H, Goh J, Tay T, & Soh S (2006) Characterization of a Novel Polymeric Scaffold for Potential Application in Tendon/Ligament Tissue Engineering. *Tissue Engineering* 12(1):91-99.
171. Jeong L, Lee K, & Park W (2007) Effect of solvent on the characteristics of electrospun regenerated silk fibroin nanofibers. *Key Engineering Materials* 342-343:813-816.
172. Luo C, Stride E, & Edirisinghe M (2012) Mapping the influence of solubility and dielectric constant on electrospinning polycaprolactone solutions. *Macromolecules* 45(11):4669-4680.
173. Wannatong L, Sirivat A, & Supaphol P (2004) Effects of solvents on electrospun polymeric fibers: preliminary study on polystyrene. *Polymer International* 53(11):1851-1859.
174. Sun Z, Deitzel J, Knopf J, Chen X, & Gillespie J (2012) The effect of solvent dielectric properties on the collection of oriented electrospun fibers. *Journal of Applied Polymer Science* 125(4):2585-2594.
175. Beachley V & Wen X (2009) Effect of electrospinning parameters on the nanofiber diameter and length. *Materials Science and Engineering: C: Materials for Biological Applications* 29(3):663-668.
176. Olvera D, Schipani R, Sathy B, & Kelly D (2019) Electrospinning of highly porous yet mechanically functional microfibrillar scaffolds at the human scale for ligament and tendon tissue engineering. *Biomedical Materials* 14(3):035016.
177. Gwiazda M, Kumar S, Świeszkowski W, Ivanovski S, & Vaquette C (2020) The effect of melt electrospun writing fiber orientation onto cellular organization and mechanical properties for application in anterior cruciate ligament tissue engineering. *Materials* 104:103631.
178. Leong N, *et al.* (2015) Use of ultra-high molecular weight polycaprolactone scaffolds for ACL reconstruction. *Journal of Orthopaedic Research* 34(5):828-835.
179. Lee C, *et al.* (2005) Nanofiber alignment and direction of mechanical strain affect the ECM production of human ACL fibroblast. *Biomaterials* 26(11):1261-1270.
180. Gentleman EL, AN, Dickerson D, Nauman E, Livesay G, & Dee K (2003) Mechanical characterization of collagen fibres and scaffolds for tissue engineering. *Biomaterials* 24(21):3805-3813.
181. Conway J, *et al.* (2017) Three-dimensional organotypic matrices from alternative collagen sources as pre-clinical models for cell biology. *Scientific Reports* 7:16887.
182. Ueda H, *et al.* (2002) Use of collagen sponge incorporating transforming growth factor-B1 to promote bone repair in skull defects in rabbits. *Biomaterials* 23(4):1003-1010.
183. Lee H, *et al.* (2019) Evaluation of a novel collagen hemostatic matrix in a porcine heart and cardiac vessel injury model. *Journal of Thoracic Disease* 11(7):2722-2729.
184. Raz P, Brosh T, Ronen G, & Tal H (2019) Tensile properties of three selected collagen membranes. *BioMed Research International* 2019:5163603.
185. Hu Y, Zhang Q, You R, L W, & Li M (2012) The Relationship between Secondary Structure and Biodegradation Behavior of Silk Fibroin Scaffolds. *Advances in Materials Science and Engineering* 2012:5 pages.
186. Altman G, *et al.* (2002) Silk matrix for tissue engineered anterior cruciate ligaments. *Biomaterials* 23(20):4131-4141.
187. Teh T, Toh S, & Goh J (2011) Aligned hybrid silk scaffold for enhanced differentiaton of mesenchymal stem cells into ligament fibroblasts. *Tissue Engineering Part C* 17(6):687-703.
188. Ran J, *et al.* (2017) Ectopic tissue engineered ligament with silk collagen scaffold for ACL regeneration: A preliminary study. *Acta Biomaterialia* 53:307-317.

189. Taşkin A, *et al.* (2013) The hemostatic effect of calcium alginate in experimental splenic injury model. *Turkish Journal of Trauma & Emergency Surgery* 19(3):195-199.
190. Bhattarai N, Li Z, Edmondson D, & Zhang M (2006) Alginate-based nanofiborous scaffolds: structural, mechanical and biological properties. *Advanced Materials* 18(11):1463-1467.
191. Kong H, Kaigler D, Kim K, & Mooney D (2004) Controlling rigidity and degredation of alginate hydrogels via molecular weight distribution. *Biomacromolecules* 5(1720-1727).
192. Zhang L, *et al.* (2018) A fiber-optic refractive index sensor detects the isoelectric point of gelatin. *Cogent Chemistry* 4(1):271-275.
193. Oz M, Rondinone J, & Shargill N (2003) Floseal matrix: new generation topical hemostatic sealant. *Journal of Cardiac Surgery* 18(6):486-493.
194. Ma Z, He W, Yong T, & Ramakrishna S (2005) Grafting of gelatin on electrospun poly(caprolactone) nanofibers to improve endothelial cell spreading and proliferation and to control cell orientation. *Tissue Engineering* 11(7-8):1149-1158.
195. Sisson K, Zhang C, Farach-Carson M, Chase D, & Rabolt J (2009) Evaluation of cross-linking methods for electrospun gelatin on cell growth and viability. *Biomacromolecules* 10(7):1675-1680.
196. Labay C, *et al.* (2020) Enhanced generation of reactive species by cold plasma in gelatin solutions for selective cancer cell death. *ACS Applied Materials & Interfaces* 12(42):47256-47269.
197. Huang Z, Zhang Y, Ramakrishna S, & Lim C (2004) Electrospinning and mechanical characterization of gelatin nanofibers. *Polymer* 45(15):5361-5368.
198. Onishi H & Machida Y (1999) Biodegradation and distribution of water soluble chitosan in mice. *Biomaterials* 20:175-182.
199. Chan M, Brooks H, Moratti S, Hanton L, & Cabral J (2015) Reducing the oxidation level of dextran aldehyde in a chitosan/dextran-based surgical hydrogel increases biocompatibility and decreases antimicrobial efficacy. *International Journal of Molecular Sciences* 16(6):13798-13814.
200. Aldana A & Abraham G (2017) Current advances in electrospun gelatin-based scaffolds for tissue engineering applications. *International Journal of Pharamceutics* 523(2):441-453.
201. Lee C, Singla A, & Lee Y (2001) Biomedical applications of collagen. *International Journal of Pharmaceutics* 221:1-22.
202. Fratzl P, *et al.* (1998) Fibrilliar structure and mechanical properties of collagen. *Journal of Structural Biology* 122(1-2):119-122.
203. Carrasco F, Pagès P, Gámez-Pérez J, Santana O, & Maspoch M (2010) Processing of poly(lactic acid): characterization of chemical structure, thermal stability and mechanical properties. *Polymer Degredation and Stability* 95(2):116-125.
204. Murray M, *et al.* (2007) Enhanced histologic repair in a central wound in the anterior cruciate ligament with a collagen-platelet rich plasma scaffold. *Journal of Orthopaedic Research* 25(8):1007-1017.
205. Jha B, *et al.* (2011) Electrospun collagen: A tissue engineering scaffold with unique functional properties in a wide variety of applications. *Journal of Nanomaterials* 2011:1-15.
206. Ottani V, Raspanti M, & Ruggeri A (2001) Collagen structure and functional implications. *Micron* 32(3):251-260.
207. Friess W (1998) Collagen - biomaterial for drug delivery. *European Journal for Pharmaceutics and Biopharmaceutics* 45:113-136.
208. Crispim J, *et al.* (2017) TGF-β1 activation in human hamstring cells through growth factor binding peptides on polycaprolactone surfaces. *Acta Biomaterialia* 53:165-178.
209. Kumbar S, Nukavarapu S, James R, Nair L, & Laurencin C (2008) Electrospun poly(lactic acid-*co*-glycolic acid) scaffolds for skin tissue engineering. *Biomaterials* 29(30):4100-4107.
210. Ganjalinia A, Akbari S, & Solouk A (2017) PLLA scaffolds surface-engineered via poly (propylene imine) dendrimers for improvement on its biocompatibility/controlled pH biodegredability. *Applied Surface Science* 394:446-456.
211. Yu D, Li Q, Mu X, Chang T, & Xiong Z (2008) Bone regeneration of critical calvarial defect in goat model by PLGA/TCP/rhBMP-2 scaffolds prepared by low-temperature rapid-

prototyping technology. *International Journal of Oral and Maxillofacial Surgery* 37(10):929-934.
212. Nguyen T & Lee B (2012) The effect of cross-linking on the microstructure, mechanical properties and biocompatibility of electrospin polycaprolactone-gelatin/PLGA-gelatin/PLGA-chitosan hybrid composite. *Science and Technology of Advanced Materials* 13(3):035002.
213. Rouxhet L, Duhoux F, Borecky O, Legras R, & Schneider Y (1998) Adsorption of albumin, collagen, and fibronectin on the surface of poly(hydroxybutyrate-hydroxyvalerate) (PHB/HV) and of poly(e-caprolactone) (PCL) films modified by an alkaline hydrolysis and of poly(ethylene terephtalate) (PET) track-etched membranes. *Journal of Biomaterials Science. Polymer Edition* 9(12):1279-1304.
214. Gurlek A, Sevinc B, Bayrak E, & Erisken C (2017) Synthesis and characterization of polycaprolactone for anterior cruciate ligament regeneration. *Materials Science and Engineering: C* 71:820-826.
215. Asadian M, *et al.* (2018) Plasma functionalization of PCL nanofibers changes protein interactions with cells resulting in increased cell viability. *Interfaces* 10(49):41962-41977.
216. Chan S, Yang H, Ko F, Ayranci C, & Basu S (2012) Tensile Stress-Strain Response of Small-diameter Electrospun Fibers. *Application Note.*
217. Vaquette C, *et al.* (2010) Aligned poly(L-lactic-co-e-caprolactone) electrospun microfibres and knitted structure: a novel scaffold for ligament tissue engineering. *Journal of Biomedical Materials Research, Part A* 94A(4):1270-1282.
218. Ghobeira R, *et al.* (2018) Wide-ranging diameter scale of random and highly aligned PCL fibers electrospun using controlled working parameters. *Polymer* 157:19-31.
219. Sun H, Mei L, Song C, Cui X, & Wang P (2006) The in vivo degredation, absorption and excretion of PCL-based implant. *Biomaterials* 27(9):1735-1740.
220. Pinese C, *et al.* (2017) *In vivo* evaluation of hybrid patches composed of PLA based copolymers and collagen/chrondrotin sulfate for ligament tissue engineering. *Journal of Biomaterials Research, Part B: APPLIED BIOMATERIALS* 105(7):1778-1788.
221. Lim H, Raku T, & Tokiwa Y (2005) Hydrolysis of polyesters by serine proteases. *Biotechnology Letters* 27:459-464.
222. Byun Y, *et al.* (2012) The effect of solvent mixture on the properties of solvent cast polylactic acid (PLA) film. *Journal of Applied Polymer Science* 124(5):3577-3582.
223. Montes de Oca H, Farrar D, & Ward I (2011) Degredation studies on highly oriented poly(glycolic acid) fibres with different lamellar structures. *Acta Biomaterialia* 7(4):1535-1541.
224. Sanko V, Sahin I, Sezer U, & Sezer S (2019) A versatile method for the synthesis of poly(glycolic acid): high solubility and tunable molecular weights. *Polymer Journal* 51:637-647.
225. Vainionpää S, *et al.* (1987) Strength and strength retention $_{vitro,}$ of absorbable, self-reinforced polyglycolide (PGA) rods for fracture fixation. *Biomaterials* 8(1):46-48.
226. Miller R, Brady J, & Cutright D (1977) Degradation rates of oral resorbable implants (polylactates and polyglycolates): rate modification with changes in PLA/PGA copolymer ratios. *Journal of Biomedical Materials Research* 11(5):711-719.
227. Wang B, Zhang P, Song W, Zhao L, & He C (2016) Modification of polyglycolic acid and poly lactic-co-glycolic acid fibers by ultrasonic treatment for enhancing hydrophilicity and cytocompatibility. *Journal of Industrial Textiles* 45(4):516-530.
228. Weiler A, Helling H, Kirch U, Zirbes T, & Rehm K (1996) Foreign-body reaction and the course of osteolysis after polyglycolide implants for fracture fixation. *The Journal of Bone and Joint Surgery* 78(3):369-376.
229. Bashur C, Dahlgren L, & Goldstein A (2006) Effect of fiber diameter and orientation on fibroblast morphology and proliferation on electrospun poly(D, L-lactic-*co*-glycolic acid) meshes. *Biomaterials* 27(33):5681-5688.
230. Ma C, *et al.* (2018) Comparison of the degredation behavior of PLGA scaffolds in micro-channel, shaking, and static conditions. *Biomicrofluidics* 12(3):034105.

231. Xin X, Hussain M, & Mao J (2007) Continuing differentiation of human mesenchymal stem cells and induced chondrogenic and osteogenic lineages in electrospun PLGA nanofiber scaffolds. *Biomaterials* 28(2):316-325.
232. Zhu H, *et al.* (2015) Mesenchymal stem cells attenuated PLGA-induced inflammatory responses by inhibiting host DC maturaton and function. *Biomaterials* 53:688-698.
233. van Eijk F, *et al.* (2004) Tissue engineering of ligaments: a comparison of bone marrow stromal cells, anterior cruciate ligament, and skin fibroblasts as cell source. *Tissue Engineering* 10(5-6):893-903.
234. Jang K, Lim H, Jung W, Moon S, & Wang J (2015) Efficacy and safety of human umbilical cord blood-derived mesenchymal stem cells in anterior cruciate ligament reconstruction of a rabbit model: new strategy to enhance tendon graft healing. *Arthroscopy: The Journal of Arthroscopic & Related Surgery* 31(8):1530-1539.
235. Li Y, *et al.* (2017) Differentiation of human amniotic mesenchymal stem cells into human anterior cruciate ligament fibroblast cells by in vitro coculture. in *BioMed Research International* (Hindawi, https://www.hindawi.com/journals/bmri/2017/7360354/), p 15.
236. Nakanishi Y, *et al.* (2019) Histological evaluation of tendon formation using a scaffold-free three-dimensional-bioprinted construct of human dermal fibroblasts under *in vitro* static tensile culture. *Regenerative Therapy* 11(47-55).
237. Wakitani S, *et al.* (2003) Embryonic stem cells injected into the mouse knee joint form teratomas and subsequently destroy the joint. *Rheumatology* 42(1):162-165.
238. Kouroupis D, *et al.* (2016) Generation of stem cell-based bioartificial anterior cruciate ligament (ACL) grafts for effective ACL rupture repair *Stem Cell Research* 17(2):448-457.
239. Volarevic V, *et al.* (2018) Ethical and safety issues of stem cell-based therapy. *International Journal of Medical Sciences* 15(1):36-45.
240. Prager P, *et al.* (2018) Mesenchymal stem cells isolated from the anterior cruciate ligament: characterisation and comparison of cells from old and young donors. *Knee Surgery and Related Research* 30(3):193-205.
241. Brune T, *et al.* (2007) *In vitro* comparison of human fibroblasts from intact and ruptured ACL for use in tissue engineering. *European Cells and Materials* 14:78-91.
242. Matsumoto T, *et al.* (2012) Isolation and characterisation of human anterior cruciate ligament-derived vascular stem cells. *Stem Cells and Development* 21(6):859-872.
243. Reda W & Khedr A (2017) Stump incorporation for anterior cruciate ligament reconstruction: a step towards more anatomical reconstruction. *Arthroscopy Techniques* 6(4):e1303-e1307.
244. Ventre M, Natale C, Rianna C, & Netti P (2014) Topographic cell instructive patterns to control cell adhesion, polarization and migration. *Journal of the Royal Society Interface* 11(100):20140687.
245. Dalby M, *et al.* (2007) The control of human mesenchymal cell differentiation using nanoscale symmetry and disorder. *Nature Materials* 6:997-1003.
246. Li F, Jia H, & Yu C (2007) ACL reconstruction in a rabbit model using irradiated achilles allograft seeded with mesenchymal stem cells or PDGF-B gene-transfected mesechymal stem cells. *Knee Surgery Sports Traumatology Arthroscopy* 15(10):1219-1227.
247. Hughes L, Gaston J, McAlindon K, Woodhouse K, & Thibeault S (2015) Electrospun fiber constructs for vocal fold tissue engineering: effects of alignment and elastomeric polypeptide coating. *Acta Biomaterialia* 13:111-120.
248. Wang P, *et al.* (2013) Modulation of cell attachment and collagen production of anterior cruciate ligament cells via submicron grooves/ridges structures with different cell affinity. *Biotechnology and Bioengineering* 110(1):327-337.
249. Inititative USNN (2021) What is nanotechnology? in *Nano101: What it is and how it works*, ed Inititative USNN (United States National Nanotechnology Initiative, https://www.nano.gov/nanotech-101/what/definition).
250. Wolfenstine J, Campos S, Foster D, Read J, & Behl W (2002) Nano-scale Cu_5Sn_6 anodes. *Journal of Power Sources* 109(1):230-233.

251. Dodel M, *et al.* (2017) Electrical stimulation of somatic human stem cells mediated by composite containing conductive nanofibers for ligament regeneration. *Biologicals* 46:99-107.
252. Sooriyaarachchi D, Minière H, Maharubin S, & Tan G (2019) Hybrid additive microfabrication scaffold incorporated with highly aligned nanofibers for musculoskeletal tissues. *Tissue Engineering and Regenerative Medicine* 16(1):29-38.
253. Pauly H, *et al.* (2016) Mechanical properties and cellular response of novel electrospun nanofibers for ligament tissue engineering: effects of orientation and geometry. *Journal of the Mechanical Behaviour of Biomedical Materials* 61:258-270.
254. Abel S, Liverani L, Boccaccini A, & Abraham G (2019) Effect of benign solvents composition on poly(ε-caprolactone) electrospun fiber properties. *Materials Letters* 245:86-89.
255. Thapa A, Miller D, Webster T, & Haberstroh K (2003) Nano-structured polymers enhance bladder smooth muscle cell function. *Biomaterials* 24(17):2915-2926.
256. Saatcioglu E, *et al.* (2021) Design and fabrication of electrospun polycaprolactone/chitosan scaffolds for ligament regeneration. *European Polymer Journal* 148:110357.
257. Soliman S, *et al.* (2010) Multiscale three-dimensional scaffolds for soft tissue engineering via multimodal electrospinning. *Acta Biomaterialia* 6(4):1227-1237.
258. Cardwell R, Dahlgren L, & Goldstein A (2012) Electrospun fibre diameter, not alignment, affects mesenchymal stem cell differentiation into the tendon/ligament lineage. *Journal of Tissue Engineering and Regenerative Medicine* 8(12):937-945.
259. Wong S, Baji A, & Leng S (2008) Effect if fiber diameter on tensile properties of electrospun poly(ε−caprolactone). *Polymer* 49(21):4713-4722.
260. Barua B & Saha M (2015) Investigation on jet stability, fiber diameter, and tensile properties of electrospun polyacrylonitrile nanofibrous yarns. *Journal of Applied Polymer Science* 132(18):41918.
261. Morita Y, Sakamoto H, & Suye S (2017) Characterization of protein adsorption on stretched polyurethane nanofibers prepared by electrospinning. *RSC Advances* 7:56484-56488.
262. Silver F, Kato Y, Ohno M, & Wasserman A (1992) Analysis of mammalian connective tissue: relationship between hierachical structures and mechanical properties. *Journal of Long-term Effects of Medical Implants* 2(2-3):165-198.
263. Newman P, *et al.* (2016) Relatonship between nanotopographical alignment and stem cell fate with live imaging and shape analysis. *Scientific Reports* 6:37909.
264. Tetsunaga T, *et al.* (2009) Mechanical stretch stimulates integrin alphaVbeta3-mediated collagen expression in human anterior cruciate ligament cells. *Journal of Biomechanics* 42(13):2097-2103.
265. Checa S, Rausch M, Petersen A, Kuhl E, & Duda G (2015) The emergence of extracellular matrix mechanics and cell traction forces as important regulators of cellular self-organization. *Biomechanics and Modelling in Mechanobiology* 14(1):1-13.
266. Rens E & Merks R (2020) Cell shape and durotaxis explained from cell-extracellular matrix forces and focal adhesion dynamics. *iScience* 23(9):101488.
267. Wang J, Jia F, Gilbert T, & Woo S (2003) Cell orientation determines the alignment of cell-produced collagenous matrix. *Journal of Biomechanics* 36(1):97-102.
268. Wang W, *et al.* (2018) Extracellular matrix alignment dictates the organization of focal adhesions and directs uniaxial cell migration. *APL Bioengineering* 2(4):046107.
269. Doyle A, Wang F, Matsumoto K, & Yamada K (2009) One-dimensional topography underlies three-dimensional fibrillar cell migration. *Journal of Cell Biology* 184(4):481-190.
270. Yang F, Wolke J, & Jansen J (2008) Biomimetic calcium phosphate coating on electrospun poly (ε-caprolactone) scaffolds for bone tissue engineering. *Chemical Engineering Journal* 137(1):154-161.
271. Yu H, *et al.* (2008) Surface modification of polypropylene microporus membrane to improve its antifouling characteristics in an SMBR: air plasma treatment. *Journal of Membrane Science* 311(1-2):216-224.

272. Rani K, *et al.* (2018) Optimization and surface modification of silk fabric using DBD air plasma for improving wiking properties. *The Journal of The Textile Institute* 109(3):368-375.
273. Livadiotis G (2019) Collision frequency and mean free path for plasmas described by kappa distributions. *AIP Advances* 9(10):105307.
274. Fitzpatrick R (2011) Collisions. in *Plasma Physics*, ed Fitzpatrick R (University of Texas, Austin, Texas, USA).
275. Wypench G (2016) PGA Poly(Glycolid Acid). *Handbook of Polymers*, ed Wypench G (ChemTech Publishing, Toronto), Second Ed, pp 419-421.
276. Jokinen V, Suvanto P, & Franssila S (2012) Oxygen and nitrogen plasma hydrophilization and hydrophobic recovery of polymers. *Biomicrofluidics* 6(1):16501-165001-165010.
277. Wang Y, *et al.* (2019) Preparation of super-hydrophilic polyphenylsulfone nanofiber membranes for water treatment. *RSC Advances* 9:278-286.
278. Stallard C, McDonnell K, Onayemi O, O'Gara J, & Dowling D (2012) Evaluation of protein adsorption on atmospheric plasma deposited coatings exhibiting superhydrophilic to superhydrophobic properties. *Biointerfaces* 7(1-4):31.
279. Getnet M & Chavan R (2015) Catalyzation of alkaline hydrolysis of polyester by oxidising agents for surface modification. *International Journal of Sciences: Basic and Applied Research* 22:232-252.
280. Lee S, Khang G, Lee Y, & Lee H (2002) Interaction of human chondrocytes and NIH/3T3 fibroblasts on chloric acid-treated biodegradable polymer surfaces. *Journal of Biomaterials Science. Polymer Edition* 13(2):197-212.
281. Park J, *et al.* (2007) Surface hydrolysis of fibrous poly(-caprolactone) scaffolds for enhanced osteoblast adhesion and proliferation. *Macromolecular Research* 15(5):424-429.
282. Bosworth L, Hu W, Shi Y, & Cartmell S (2019) Enhancing biocompatibility without compromising material properties: an optimised NaOH treatment for electrospun polycaprolactone fibres. *Journal of Nanomaterials* 2019:11.
283. Bhaskaran A, Prasad T, Kumary T, & Kumar P (2019) Simple and efficient approach for improved cytocompatibility and faster degradation of electrospun polycaprolactone fibers. *Polymer Bullitin* 76(3):1333-1347.
284. Sadeghi A, *et al.* (2016) Surface modification of electrospun PLGA scaffold with collagen for bioengineered skin substitutes. *Materials Science and Engineering: C* 66:130-137.
285. Kowalczyk P, Trzaskowska P, Łojszczyk I, Podgórski R, & Ciach T (2019) Production of 3D printed polylactide scaffolds with surface grafted hydrogel coatings. *Colloids and Surfaces B: Biointerfaces* 179:136-142.
286. Jung J, Ree M, & Kim H (2006) Acid and base-catalyzed hydrolyses of aliphatic polycarbonates and polyesters. *Catalysis Todat* 115(1):283-287.
287. Peret B & Murphy W (2010) Controllable soluble protein concentration gradients in hydrogel networks. *Advanced Functional Materials* 18(21):3410-3417.
288. Tsermentseli S, Kontogiannopoulos K, Papageorgiou V, & Assimopoulou A (2018) Comparative study of PEGylated and conventional liposomes as carriers for shikonin. *Fluids* 3(2):36.
289. Meany Murray M, Rice K, Wright R, & Spector M (2003) The effect of selected growth factors on human anterior cruciate ligament cell interactions with a three-dimensional collagen-GAG scaffold. *Journal of Orthopaedic Research* 21(2):238-244.
290. Kalasin S & Santore M (2009) Non-specific adhesion on biomaterial surfaces driven by small amounts of protein adsorption. *Colloids and Surfaces B: Biointerfaces* 73(2):229-236.
291. Roach P, Farrar D, & Perry C (2005) Interpretation of protein adsorption: surface-induced conformational changes. *Journal of the American Chemical Society* 127(22):8168-8173.
292. Amdursky N & Stevens M (2015) Circular dichroism of amino acids: following the structural formation of phenylalanine. *ChemPhysChem* 16(13):2768-2774.
293. Welin-Klintström S, Askendal A, & Elwing H (1993) Surfactant and protein interactions on wettability gradient surfaces. *Journal of Colloid and Interface Science* 158(1):188-194.

294. Roach P, Farrar D, & Perry C (2006) Surface tailoring for controlled protein adsorption: effect of topography at the nanometer scale and chemistry. *Journal of the American Chemical Society* 128(12):3939-3945.
295. Jeon S & Andrade J (1991) Protein-surface interactions in the presence of polyethylene oxide: II. Effect of protein size. *Journal of Colloid and Interface Science* 142(159-166).
296. Denis F, *et al.* (2002) Protein adsorption on model surfaces with controlled nanotopography and chemistry. *Langmuir* 18(3):819-828.
297. Sigal G, Mrksich M, & Whitesides G (1998) Effect of surface wettability on the adsorption of proteins and detergents. *Journal of the American Chemical Society* 120(14):3464-3473.
298. Vroman L & Adams A (1986) Adsorption of proteins out of plasma and solutions in narrow spaces. *Journal of Colloid and Interface Science* 111(2):391-402.
299. Ye H, *et al.* (2017) Protein adsorption and desorption behavior of a pH-responsive membrane based on ethylene vinyl alcohol copolymer. *RSC Advances* 7:21398-21405.
300. Kobayashi J, *et al.* (2018) Effect of temperature changes on serum protein adsorption on thermoresponsive cell-culture surfaces monitored by a quartz crystal microbalance with dissipation. *International Journal of Molecular Sciences* 19(5):1516.
301. Missirlis D, Haraszti T, Kessler H, & Spatz J (2017) Fibronectin promotes directional persistence in fibroblast migration through inteactions with both its cell-binding and heparin-binding domains. *Scientific Reports* 7:3711.
302. Lu H, *et al.* (2005) Anterior cruciate ligament regeneration using braided biodegradable scaffolds: in vitro optimisation studies. *Biomaterials* 26(23):4805-4816.
303. Shen W, *et al.* (2014) Long-term effects of knitted silk-collagen sponge scaffold on anterior cruciate ligament reconstruction and osteoarthritis prevention. *Biomaterials* 35(28):8154-8163.
304. Yoshikawa T, *et al.* (2006) Effects of local administration of vascular endothelial growth factor on mechanical characteristics of the semitendinous tendon graft after anterior cruciate ligament reconstruction in sheep. *The American Journal of Sports Medicine* 34(12):1918-1925.
305. Pauly H, *et al.* (2017) Hierarchically structured electrospun scaffolds with chemically conjugated growth factor for ligament tissue engineering. *Tissue Engineering Part A* 23(15-16):823-836.
306. Lockheart-Cairns M, *et al.* (2020) Transglutaminase-mediated cross-linking of tropoelastin to fibrillin stabilises the elastin precursor prior to elastic fibre assembly. *Journal of Molecular Biology* 432(21):5736-5751.
307. Piha-Gossack A, Sossin W, & Reinhardt D (2012) The evolution of extracellular fibrillins and their functional domains. *PLoS ONE* 7(3):e33560.
308. Sabatier L, *et al.* (2011) Fibrillin-3 expression in human development. *Matrix Biology* 30(1):43-52.
309. Sakamoto H, *et al.* (1996) Cell-type Recognition of RGD- and Non-RGD-Containing Cell Binding Domains in Fibrillin-1. *The Journal of Biological Chemistry* 271:4916-4922.
310. Bax D, *et al.* (2007) Cell adhesion to fibrillin-1: identification of the Arg-Gly-Asp-dependent synergy and a heparin-binding site that regulates focal adhesion formation. *Journal of Cell Science* 120:1383-1392.
311. Zeyer K, RM Z, Kumra H, Hassan A, & Reinhardt D (2019) The fibrillin-1 RGD integrin binding site regulates gene expression and cell function through microRNAs. *Journal of Molecular Biology* 431(2):401-421.
312. Hubmacher D, Bergeron E, Fagotto-Kaufmann C, Sakai L, & Reinhardt D (2014) Early fibrillin-1 assembly monitroed through a modifiable recombinant cell approach. *Biomacromolecules* 15:1456-1468.
313. Sabatier L, *et al.* (2014) *Heparin/heparan sulfate controls fibrillin-1, -2 and -3 self-interactions in microfibril assembly* pp 2890-2897.
314. Mariko B, *et al.* (2010) Microfibrils and fibrillin-1 induce inegrin-mediaed signalling, proliferation and miration in human endothelial cells. *American Journal of Physiology: Cell Physiololgy* 299:C977-C987.

315. Hajian H, *et al.* (2014) Immobilisation of a Fibrillin-1 fragment enhances the biocompatibility of PTFE. *Colloids and Surfaces B: Biointerfaces* 116:544-552.
316. Maurer E, *et al.* (2015) Fibrillar cellular fibronectin supports efficient platelet aggregation and procoagulant activity. *Thrombosis and Haemostasis* 114(06):1175-1188.
317. Baldock C, *et al.* (2011) Shape of tropoelastin, the highly extensible protein that controls human tissue elasticity. *Proceedings of the National Academy of Science USA* 108(11):4322-4327.
318. Nakamura T, *et al.* (2002) Fibulin-5/DANCE is essential for elastogenesis *in vivo*. *Nature* 415:171-175.
319. Yanagisawa H, *et al.* (2002) Fibulin-5 is an elastin-binding protein essential for elastic fibre development *in vivo*. *Nature* 415:168-171.
320. Yin Y, *et al.* (2009) Covalent immobilisation of tropoelastin on a plasma deposited interface for enhancement of endotheialisation on metal surfaces. *Biomaterials* 30:1675-1681.
321. Wise S, *et al.* (2011) A multilayered synthetic human elastin/polycaprolactone hybrid vascular graft with tailored mechanical properties. *Acta Biomaterialia* 7(1):295-303.
322. Barenghi R, *et al.* (2014) Elastin-coated biodegradable photopolymer scaffolds for tissue engineering application. *BioMed Research International.* 2014:9.
323. Hirukawa M, *et al.* (2018) Development of a tissue-engineered artificial ligament: reconstruction of injured rabbit medial collateral ligament with elastin-collagen and ligament cell composite artifical ligament. *Artifical Organs* 42(7):736-745.
324. Lee P, Yeo G, & Weiss A (2017) A cell adhesive peptide from tropoelastin promotes sequential cell attachment and spreading via distinct receptors. *The FEBS Journal* 284:2216-2230.
325. McLaughlin P, *et al.* (2006) Targeted disruption of fibulin-4 abolishes elastogenesis and causes perinatal lethality in mice. *Molecular Cell Biology* 26:1700-1709.
326. Preis M, *et al.* (2016) Co-expression of fibulin-5 and VEGF165 increases long-term patency of synthetic vascular grafts seeded with autologous endothlial cells. *Gene Therapy* 23:237-246.
327. Lotz M, Burdsal C, Erikson H, & McClay D (1989) Cell adhesion to Fibronectin and Tenascin: Quantitative measurements of initial binding and subsequent strengthening response. *The Journal of Cell Biology* 109(4):1795-1805.
328. Tsuchiya K, Chen G, Ushida T, Matsuno T, & Tateishi T (2001) Effects of cell adhesion molecules on adhesion of chondrocytes, ligament cells and mesenchymal stem cells. *Materials Science and Engineering: C* 17(1-2):79-82.
329. Li H, Chen C, Ge Y, & Chen S (2014) Spray-painted human fibronectin coating as an effective strategy to enhance graft ligamentization of a polyethylene terephthalate artificial ligament. *Biotechnology Letters* 36(5):1079-1088.
330. Asgari M, Latifi N, Heris H, Vali H, & Mongeau L (2017) *In vitro* fibrillogenesis of tropocollagen type III in collagen type I affects its relative fibrillar topology and mechanics. *Science Letters* 7(1):1392.
331. Zhang P, *et al.* (2016) Local delivery of controlled-release simvastin to improve the biocompatibility of polyethylene terephthalate artificial ligaments for reonstruction of the anterior cruciate ligament. *International Journal of Nanomedicine* 11:465-478.
332. da Câmara P, *et al.* (2019) Novel cationic tannin/glycosaminoglycan-based polyelectrolyte multilaters promote stem cells adhesion and proliferation. *RSC Advances* 9:25836-25846.
333. Meade K, *et al.* (2013) Immobilization of heparan sulfate on electrospun meshes to support embryonic stem cell culture and differentiation. *Journal of Biological Chemistry* 288(8):5530-5538.
334. Agrawal P & Pramanik K (2019) Enhanced chondrogenic differentiation of human mesenchymal stem cells in silk fibroin/chitosan/glycosaminoglycan scaffolds under dynamic culture condition. *Differentiation* 110:36-48.
335. Honarpardaz A, Irani S, Pezeshki-Modaress M, Zandi M, & Sadeghi A (2018) Enhanced chondrogenic differentiation of bone marrow mesenchymal stem cells on gelatin/glycosaminoglycan electrospun nanofibers with different amount of glycosaminoglycan. *Journal of Biomaterials Research Part A* 107(1):38-48.

336. Meany Murray M & Spector M (2001) The migration of cells from the ruptured human anterior cruciate ligament in collagen-glycosaminoglycan regeneration templates in vitro. *Biomaterials* 22(17):2393-2402.
337. Gouveia P, *et al.* (2021) Development of collagen-poly(caprolactone)-based core-shell scaffolds supplemented with proteoglycans and glycosaminoglycans for ligament repair. *Materials Science and Engineering: C* 120:111657.
338. Kapp T, *et al.* (2017) A comprehensive evaluation of the activity and seleectivity profile of ligands for RGD-binding integrins. *Scientific Reports* 7:39805.
339. Hansson A, *et al.* (2012) *In vitro* evaluation of an RGD-functionalized chitosan derivative for enhanced cell adhesion. *Carbohydrate Polymers* 90(4):1494-1500.
340. D'Andrea P, Sciancalepore M, Veltruska K, Lorenzon P, & Bandiera A (2019) Epidermal growth factor-based adhesion substrates elicit myoblast scattering, proliferation, differentiation and promote satellite myogenic activation. *Biochimia et Biophysica Acta (BBA) - Molecular Cell Research* 1866(3):504-517.
341. Pham Q, Sharma U, & Mikos A (2006) Electrospun poly(e-caprolactone) microfiber and multilayer nanofiber/microfiber scaffolds: characterization of scaffolds and measurement of cellular infiltration. *Biomacromolecules* 7:2796-2805.
342. Sunami H, *et al.* (2018) Modulation of surface stiffness and cell patterning on polymer films using micropattersn. *Journal of Biomedical Materials Research* 106(3):976-985.
343. Pilipchuk S, *et al.* (2016) Integration of 3D printed and micropatterned polycaprolactone scaffolds for guidance of oriented collagenous tissue formation in vivo. *Advanced Healthcare Materials* 5(6):676-687.
344. Ramos Marques D (2016) ACL PROJECT - RESULTS. ed Smith Z, p 17.
345. Crichton G (2016) Novel electrospun polycaprolactone fibres for anterior cruciate ligament reconstruction. MEng Biomaterials Science and Tissue Engineering MEng (University of Manchester, Manchester).
346. Keyence (2021) Surface Roughness Parameters. in *What is line roughness?*, ed Keyence (Keyence, https://www.keyence.com/ss/products/microscope/roughness/line/parameters.jsp).
347. Kim M, *et al.* (2014) Highly porous 3D nanofibrous scaffolds processed with an electrospinning/laser process. *Current Applied Physics* 14(1):1-7.
348. Regis S, *et al.* (2013) Fibronectin adsorption on functionalized electrospun polycaprolactone scaffolds: Experimental and molecular dynamics studies. *Journal of Biomedical Materials Research: Part A* 102(6):1697-1706.
349. Tseng H, *et al.* (2014) Anisotropic poly(ethylene glycol)/polycaprolactone hygrogel-fiber composites for heart valve tissue engineering. *Tissue Engineering: Part A* 20(19-20):2634-2645.
350. Saha S, *et al.* (2012) Electrospun fiborous scaffolds promote breast cancer cell alignment and epithelial-mesenchymal transition. *Langmuir* 28(4):2028-2034.
351. Vaz C, van Tuijl S, Bouten C, & Baaijens F (2005) Design of scaffolds for blood vessel tissue engineering using a multi-layersing electrospinning technique. *Acta Biomaterialia* 1(5):575-582.
352. Hu M (2016) Evaluating Canine Cruciate Ligament Cell Response to Biofunctionalised Electrospun Scaffolds. MSc (University of Manchester, Manchester).
353. Vance R, Miller D, Thapa A, Haberstroh K, & Webster T (2004) Decreased fibroblast cell density on chemically degraded poly-lactic-co-glycolic acid, polyeurathane and polycaprolactone. *Biomaterials* 25(11):2095-2103.
354. Cyster L, Parker K, Parker T, & Grant D (2003) The effect of surface chemistry and nanotopography of titanium nitride (TiN) films on 3T3-L1 fibroblasts. *Journal of Biomedical Materials Research: Part A* 67A(1):138-147.
355. Alhadlaq A, *et al.* (2004) Adult stem cell driven genesis of human-shaped articular condyle. *Annals of Biomedical Engineering* 32:911-923.
356. Matsuura K, Wang W, Ching A, Chen Y, & Cheng C (2019) Paper-based resazurin assay of inhibitor-treated porcine sperm. *Micromachines* 10(8):495.

357. Subramanian A, Krishnan U, & Sethuraman S (2012) Fabrication, characterization and *in vitro* evaluation of aligned PLGA-PCL nanofibres for neural regeneration. *Annals of Biomedical Engineering* 40(10):2098-2110.
358. Semitela Â, *et al.* (2020) Electrospinning of bioactive polycaprolactone-gelatin nanofibres with increased pore size for cartilage tissue engineering applications. *Journal of Biomaterials Applications* 35(4-5):471-484.
359. Kai D, Prabhakaran M, Jin G, & Ramakrishna S (2011) Guided orientation of cardiomyocytes on electrospun aligned nanofibres for cardiac tissue engineering. *Journal of Biomedical Materials Research: Part B* 98B(2):379-386.
360. Jahani H, *et al.* (2012) The effect of aligned and random electrospun fiborous scaffolds on rat mesenchymal stem cell proliferation. *Cell Journal* 14(1):31-38.
361. Can-Herrera L, *et al.* (2016) Surface modification of electrospun polycaprolactone microfibres by air plasma treatment: Effect of plasma power and treatment time *European Polymer Journal* 84:502-513.
362. MERCK (2021) IR Spectrum Table & Chart. in *Technical Documents*, ed MERCK (MERCK, https://www.sigmaaldrich.com/technical-documents/articles/biology/ir-spectrum-table.html).
363. Wittenburg G, Lauer G, Oswald S, Labudde D, & Franz C (2013) Nanoscale topographic changes on sterilized glass surfaces affect cell adhesion and spreading. *Journal of Biomedical Materials Research Part A* 102(8):2755-2766.
364. Morent R, De Geyter N, Leys C, Gengembre L, & Payen E (2008) Comparison between XPS- and FTIR-analysis of plasma-treated polypropylene film surfaces. *Surface and Interface Analysis* 40(3-4):597-600.
365. de Valence S, *et al.* (2013) Plasma treatment for improving cell biocompatibility of a biodegradable polymer scaffold for vascular graft applications. *European Journal for Pharmaceutics and Biopharmaceutics* 85(1):78-86.
366. Song J, Kim J, Oh S, & Yun J (2019) Contamination particles and plasma etching behaviour of atmospheric plasma sprayed Y_2O_3 and YF_3 coatings under NF_3 plasma. *Coatings* 9(2):102.
367. Kuzminova A, *et al.* (2017) Etching of polymers, proteins and bacterial spores by atmospheric pressure DBD plasma in air. *Journal of Physics D: Applied Physics* 50(13):135201.
368. Puliyalil H & Cvelbar U (2016) Selective plasma etching of polymeric substrates for advanced applications. *Nanomaterials* 6(6):108.
369. Lin J, *et al.* (2021) Oriented and sustained protein expression on biomimicking electrospin fibers for evaluating functionality of cells. *Materials Science and Engineering: C* 118:111407.
370. Pauly H, *et al.* (2018) Mechanical properties of a hierarchical electrospun scaffold for ovine anterior cruciate ligament replacement. *Journal of Orthopaedic Research* 37(2):421-430.
371. Rnjak-Kovacina J, *et al.* (2011) Tailoring the porosity and pore size of electrospun synthetic human elastin scaffolds for dermal tissue engineering. *Biomaterials* 32(28):6729-6736.
372. Akay G, Birch M, & Bokhari M (2004) Microcellular polyHIPE polymer supports osteoblast growth and bone formation in vitro. *Biomaterials* 25(18):3991-4000.
373. Ghiasi M, Naghashzargar E, & Semnani D (2014) Silk fibroin nano-coated textured silk yarn by electrospinning method for tendon and ligament scaffold application. *Nano Hybrids* 7:35-51.
374. Accardi M, *et al.* (2013) Effects of fiber orientation on the frictional properties of regenerative articular cartilage surfaces. *Tissue Engineering Part A* 19(19-20):2300-2310.
375. Wittmer C, Hébraud A, Nedjari S, & Schlatter G (2014) Well-organized 3D nanofibrous composite constructs using cooperative effects between electrospinning and electrospraying. *Polymer* 55(22):5781-5787.
376. Reigada R & Sagués F (2015) Chloroform alters interleaflet coupling in lipid bilayers: an entropic mechanism. *Journal of the Royal Society Interface* 12(106):20150197.
377. Huq F (2006) Molecular modelling analysis of the metabolism of chloroform. *Journal of Pharmacology and Toxicology* 1:438-466.

378. Strocci R, *et al.* (1992) The human anterior cruciate ligament: histological and ultrastructural observations. *J. Anat.* 180(3):515-519.
379. Delaittre G, Greiner A, Pauloehrl T, Bastmeyer M, & Barner-Kowollik C (2012) Chemical approaches to synthetic polymer surface biofunctionalization for targeted cell adhesion using small binding motifs. *Soft Matter* 8:7323-7347.
380. Bean A & Tuan R (2015) Fiber diameter and seeding density influence chondrogenic differentiation of mesenchymal stem cells seeded on electrospun poly(e-caprolactone) scaffolds. *Biomedical Materials* 10(1):015018.
381. Bains O, *et al.* (2013) A correlation between cytotoxicity and reductase-mediated metabolism in cell lines treated with doxorubicin and daunorubicin. *The Journal of Pharmacology and Experimental Therapies* 347(2):375-387.
382. Mortazavi M & Nosonovsky M (2012) A model for diffusion-driven hydrophobic recovery in plasma treated polymers. *Applied Surface Science* 258(18):6876-6883.
383. Asadian M, *et al.* (2020) Fabrication and plasma modification of nanofibrous tissue engineering scaffolds. *Nanomaterials* 10(1):119.
384. Grinnell F & Feld M (1981) Adsorption characteristics of plasma fibronectin in relationship to biological activity. *Journal of Biomedical Materials Research* 15(3):363-381.
385. Jensen S, Corbett A, Knott V, Redfield C, & Handford P (2005) Ca^{2+} -dependent interface formation in fibrillin-1. *Journal of Biological Chemistry* 280(14):14076-14084.
386. Jones L, Haugland R, & Singer V (2018) Development and characterization of the NanoOrange protein quantitation assay: a fluorescence-based assay of proteins in solution. *BioTechniques* 34(4):850-861.
387. Lee K (2017) Tendon and ligament stem cells and their niche. PhD Traditional (University of Liverpool, Liverpool, UK).
388. Ashraf Kharaz Y (2015) The molecular and cellular differences between tendons and ligaments. PhD (University of Liverpool, Liverpool, U.K.).
389. Cheng A, *et al.* (2018) Recombinant extracellular matrix protein fragments support human embryonic stem cell chondrogenesis. *Tissue Engineering Part A* 24(11-12):968-978.
390. Rock M, *et al.* (2004) Molecular basis of elastic fibre formation critical interactions and a tropoelastin-fibrillin-1 crosslink. *Journal of Biological Chemistry* 279:23748-23758.
391. Marson A, *et al.* (2004) Homotypic fibrillin-1 interactions in microfibril assembly. *Journal of Biological Chemistry* 280:5013-5021.
392. Cain S, McGovern A, Baldwin A, Baldock C, & Kielty C (2012) Fibrillin-1 mutations causing Weill-Marchisani syndrome and acromicric and geleophysic dysplasias disrupt heparan sulfate interactions. *PLoS One* 7(11):e48634.
393. Lee S, *et al.* (2004) Structure of the Integrin Binding Fragment from Fibrillin-1 gives new insights into microfibril organisation. *Structure* 12(4):717-729.
394. Bax D, *et al.* (2014) Surface plasma modification and tropoelastin coating of a polyeurethane co-polymer for enhanced cell attachment and reduced thrombogenicity. *Biomaterials* 35:6797-6809.
395. Zhou M, *et al.* (2009) Self-assembled peptide hydrogels as scaffolds for achorage-dependent cells. *Biomaterials* 30(13):2523-2530.
396. Sage D (2018) OrientationJ (Biomedical Imaging Group, École polytechnique fédérale de Lausanne, Lausanne, Switzerland), OrientationJ_16.01.2018.
397. Rezakhaniha R, *et al.* (2012) Experimental investigation of collagen waviness and orientation in the arterial adventia using confocal laser scanning microscopy. *Biomechanics and Modelling in Mechanobiology*:461-473.
398. Zhang Z, Vuori K, Reed J, & Ruoslahti E (1995) The alpha 5 beta 1 integrin supports survival of cells on fibronectin and up-regulates Bcl-2 expression. *Proceedings of the National Academy of Science USA* 92(13):6161-6165.
399. Charo I, Nannizzi L, JW S, & Cheresh D (1990) The vitronectin receptor alpha v beta 3 binds fibronectin and acts in concert with alpha 5 beta 1 in promoting cellular attachement and spreading on fibronectin. *Journal of Cell Biology* 111(6):2795-2800.
400. di Blasio L, *et al.* (2015) PDK1 regulates focal adhesion disassembly by modulating endocytosis of αvβ3 integrin. *Journal of Cell Science* 128(5):863-877.

401. Rampersad S (2012) Multiple applications of alamar blue as an indicator of metabolic function and cellular health in viability assays. *Sensors (Basel)* 12(9):12347-12360.
402. Cheng Q, Lee B, Komvopoulos K, Yan Z, & Li S (2013) Plasma surface chemical treatment of electrospun poly(l-lactide) microfibrous scaffolds for enhanced cell adhesion, growth and inflitration. *Tissue Engineering Part A* 19(9-10):1188-1198.
403. Nam J, Johnson J, Lannutti J, & Agarwal S (2011) Modulation of embryonic mesenchymal progenitor cell differentiation via control over pure mechanical modulus in electrospin nanofibers. *Acta Biomaterialia* 7(4):1516-1524.
404. Henninger H, Ellis B, Scott S, & Weiss J (2019) Contributions of elastic fibers, collagen, and extracellular matrix to the multiaxial mechanics of ligament. *Journal of the Mechanical Behaviour of Biomedical Materials* 99:118-126.
405. Kim S, Akaike T, Sasagawa T, Atomi Y, & Kurosawa H (2002) Gene expression of type I and III collagen by mechanical stretch in anterior cruciate ligament cells. *Cell Structure and Function* 27(3):139-144.
406. Schulze-Tanzil G, *et al.* (2020) SV40 trasnfected human anterior cruciate ligament derived ligamentoctyes - suitable as a human in vitro model for ligament reconstruction? *International Journal of Molecular Sciences* 21(2):593.
407. Liu Z, *et al.* (2019) Enhancement of in vitro proliferation and bioactivity of human anterior cruciate ligament fibroblasts using an in situ tissue isolation method and basic fibroblast growth factor culture conditions a pilot analysis. *Medicine* 98(22):e15904.
408. Buckley M, *et al.* (2013) Distributions of types I, II and III collagen by region in the human supraspinatus tendon. *Connective Tissue Research* 54(6):374-379.
409. Wan C, Hao Z, Wen S, & Leng H (2014) A quantitative study of the relationship between the distibution of different types of collagen and the mechanical behaviour of rabbit medial collateral ligaments. *PLOS ONE* 9(7):e103363.
410. Kumagai K, *et al.* (2012) The extent of degeneration of cruciate ligament is associated with chondrogenic differentiation in patients with osteoarthritis of the knee. *Osteoarthritis and Cartilage* 20(11):1258-1267.
411. Hasegawa A, *et al.* (2012) Anterior cruciate ligament changes in the human knee joint in ageing and osteoarthritis. *Arthritis & Rheumatology* 64(3):696-704.
412. Komro J, *et al.* (2020) Fibrocartilaginous metaplasia and neovascularisation of the anterior cruciate ligament in patients with osteoarthritis. *Clinical Anatomy* 33(6):899-905.
413. Kim M, *et al.* (2018) Donor variation and optimization of human mesenchymal stem cell chondrogenesis in hyaluronic acid. *Tissue Engineering Part A* 24(21-22):1693-1703.
414. Kwon H, *et al.* (2017) Tissue engineering potential of human dermis-isolated adult stem cells from multiple anatomical locations. *PLoS ONE* 12(8):e0182531.
415. The National Academies of Sciences EaM (2019) Exploring sources of variability related to the clinical translation of regenerative engineering products: Proceedings of a workshop. (The National Academies Press, Washington DC, USA), pp 1-84.
416. Osakabe T, *et al.* (2001) Age- and gender-related changes in ligament components. *Annals of Clinical Biochemistry* 38:527-532.
417. Stoll C, *et al.* (2011) Healing parameters in a rabbit partial tendon defect following tenoctye/biomaterial implantation. *Biomaterials* 32(21):4806-4815.
418. StatsToDo (2020) StatsToDo: Kendall's W for Ranks Program. in *Agreement*, ed StatsToDo (StatsToDo, https://www.statstodo.com/KendallW_Pgm.php).
419. Lai M & Lü B (2012) 3.04 - Tissue preparation for microscopy and histology. *Comprehensive sampling and sample preparation: analytical techniques for scientists*, eds Pawliszyn J, Bayona J, Lord H, Le X, Mondello L, Li X, Lee H, & Dugo P (Elsevier, Amsterdam, The Netherlands; Oxford, UK; Burlington, Mass., USA), Vol 3, pp 73-74.
420. Landis J & Koch G (1977) The measurement of observer agreement for catagorical data. *Biometrics* 33(1):159-174.
421. Schulze-Tanzil G (2019) Intraarticular ligament degeneration is interrelated with cartilage and bone destruction in osteosrthritis. *Cells* 8(9):990-1010.
422. Georgiev G, *et al.* (2019) A comparative study of the epiligament of the medial collateral and the anterior cruciate ligament in the human knee. Immunohistochemical analysis of

collagen type I and V and procollagen type III. *Annals of Anatomy - Anatomischer Anzeiger* 224:88-96.
423. Zhu J, Zhang X, Ma Y, Zhou C, & Ao Y (2012) Ultrastructural and morphological characteristics of human anterior cruciate ligament and hamstring tendons. *The Anatomical Record* 295(9):1430-1436.
424. Zarkovic K, *et al.* (2015) Elastin aging and lipid oxidation products in the human aorta. *Redox Biology* 4:109-117.
425. van der Loos C (2008) Multiple immunoenzyme staining: methods and visualisation for the observation with spectral imaging. *Journal of Histochemistry & Cytochemistry* 56(4):313-328.
426. Reddy G, Stehno-Bittel L, & Enwemeka C (2002) Glycation-induced matrix stability in the rabbit achilles tendon. *Archives of Biochemistry and Biophysics* 399(2):174-183.
427. McConnell S, Kolopack P, & Davis A (2001) The Western Ontario and McMaster Universities Osteoarthritis Index (WOMAC): a review of its utility and measurement properties. *Arthritis Care & Research* 45(5):453-461.
428. Dawson J, Fitzpatrick R, Murray D, & Carr A (1998) Questionnaire on the perceptions of patients about total knee replacement. *The Journal of Bone and Joint Surgery* 80-B(1):63-69.
429. Schwartz S, *et al.* (2019) Migrating myofibroblastic iliotibial band-derived fibroblasts represent a promising cell source for ligament reconstruction. *International Journal of Molecular Science* 20(8):1972.
430. Levy Y, *et al.* (2013) Histopathological changes in the human posterior cruciate ligament during aging and osteoarthritis: correlations with ACL and cartilage changes. *Annals of the Rheumatic Diseases* 72(2):271-277.
431. Pfander D, Heinz N, Rothe P, Carl H, & Swoboda B (2004) Tenascin and aggrecan expression by articular chondrocytes is influences by interleukin 1beta: a possible explanation for the changes in matrix synthesis during osteoarthritis. *Annals of the Rheumatic Diseases* 63(3):240-244.
432. Dozin B, Malpeli M, Camardella L, Cancedda R, & Pietrangelo A (2002) Response of young, aged and osteoarthritic human articular chondrocytes to inflammatory cytokines: molecular and cellular aspects *Matrix Biology* 21:449-459.
433. Himpe N, Berger P, & Vandenneucker H (2020) Mucoid degeneration of the anterior cruciate ligament. Complete resection as equivalent treatment to partial resection. *Acta Orthopaedica Belgium* 86:272-279.
434. Motmans R & Verheyden F (2009) Mucoid degeneration of the anterior cruciate ligament. *Knee Surgery, Sports Traumatology, Arthroscopy* 17:737-740.
435. Labat-Robert J, Fourtanier A, Boyer-Lafargue B, & Robert L (2000) Age dependent increase of elastase type protease activity in mouse skin: effect of UV-radiation. *Journal of Photochemistry and Photobiology B: Biology* 57(2-3):113-118.
436. Daquinag A, Gao Z, Fussell C, Sun K, & Kolonin M (2020) Glycosaminoglycan modfication of decorin depends on MMP14 activity and regulates collagne assembly. *Cells* 9(12):2646.
437. Farndale R, Buttle D, & Barrett A (1986) Improved quantitation and discrimination of sulphated glycosaminoglycans by use of dimethylmethylene blue. *Biochimia et Biophysica Acta* 883(2):173-177.
438. Steinert A, *et al.* (2008) *In situ* IGF-1 gene delivery to cells emerging from the injured anterior cruciate ligament. *Biomaterials* 29(7):904-916.
439. Christensen B, Dandanell S, Kjaer M, & Langberg H (2011) Effect of anti-inflammatory medication on the running-induced rise in patella tendon collagen synthesis in humans. *Journal of Applied Physiology* 110(1):137-141.
440. Lee D, *et al.* (2015) Effect of donor age on the proportion of mesenchymal stem cells derived from anterior cruciate ligaments. *PLOS ONE* 10(3):e0117224.
441. Nishimura M, *et al.* (2019) Development and characterisation of novel clinical grade neonatal porcine bone marrow-derived mesenchymal stem cells. *Xenotransplantation* 26(3):e12501.

442. Bade N, Xu T, Kamien R, Assoian R, & Stebe K (2018) Gaussian curvature directs stress fiber orientation and cell migration. *Biophysical Journal* 114(6):1467-1476.
443. AbiEzzi S, Foulk R, Harwood F, Akeson W, & Amiel D (1997) Decrease in fibronectin occurs coincident with increased expression of its integrin receptor alpha5beta1 in stress-deprived ligaments. *The Iowa Orthopoedic Journal* 17:102-109.
444. Pelipenko J, Kristl J, Janković B, Baumgartner S, & Kocbek P (2013) The impact of relative humidity during electrospinning on the morphology and mechanical properties of nanofibers. *International Journal of Pharamceutics* 456(1):125-134.
445. Yang G, Li H, Yang J, Wan J, & Yu D (2017) Influence of working temperature on the formation of electrospun polymer nanofibers. *Nanoscale Research Letters* 12(1).
446. Ko J, *et al.* (2014) Fabrication of poly (ϵ-caprolactone) microfiber scaffolds with varying topography and mechanical properties for stem cell-based tissue engineering applications. *Journal of Biomaterials Science. Polymer Edition.* 25(1):1-17.
447. Zhong S, *et al.* (2006) An aligned nanofibrous collagen scaffold by electrospinning and its effects on *in vitro* fibroblast cell culture. *Journal of Biomedical Materials Research Part A* 79A(3):456-463.
448. Lee C, Harbers GG, DW, Gamble L, & Castner D (2008) Fluorescence, XPS and ToF-SIMS surface chemical state image analysis of DNA microarrays. *Journal of the American Chemical Society* 129(30):9429-9438.
449. Barbosa I, *et al.* (2003) Improved and simple micro assay for sulfated glycoasminoglycans quantification in biological extracts and its use in skin and muscle tissue studies. *Glycobiology* 13(9):647-653.
450. Volpi N, *et al.* (2013) Plasmatic dermatan sulfate and chondroitin sulfate determination in mucopolysaccharidoses. *Journal of Pharmaceutical and Biomedical Analysis* 85:40-45.
451. Chen B, *et al.* (2016) Enhancement of tendon to bone healing after anterior cruciate reconstruction using bone marrow-derived stem cells genetically modified with bFGF/BMP2. *Scientific Reports* 6:25940.
452. Barrow M, Tew S, Comerford E, McNicholas M, & Oldershaw R (2018) Characterisation of stem cell populations within normal and ruptured anterior cruciate ligaments. *Osteoarthritis and Cartilage* 26:S405-S406.
453. Kowalski T, *et al.* (2016) Hypoxic culture conditions induce increased metabolic rate and collagen gene expression in ACL-derived cells. *Journal of Orthopaedic Research* 34(6):985-994.
454. Biovision (2021) Alkaline phosphatase activity colorimetric assay kit. in *Metabolism Assays (A-Z)* (Biovision Inc., https://www.biovision.com/alkaline-phosphatase-activity-colorimetric-assay-kit.html).
455. Shapira L & Halabi A (2009) Behavior of osteoblast-like cell lines cultured on machined or rough titanium surfaces. *Clinical Oral Implants Research* 20(1):50-55.

APPENDICIES

Appendix 1 Previous Work Optimising Fibre Production

	ALIGNED	RANDOM
Flow Rate (ml/hr)	1.5	1.5
High Voltage (kV)	18 ± 0.1	18 ± 0.1
Mandrel Speed (RPM)	1400	200
Spinning Time (mins)	20	60
Collector Distance (mm)	200	200

Parameters for the electrospinning of random and aligned microfibres, optimised by Dr Douglas Ramos-Marques for cACL tissue engineering.

Experimental work performed by Dr Douglas Ramos Marques optimising and characterising random and aligned PCL fibres for comparison. Bright field images (**A**), orientation histograms (**B**), pore size histograms (**C**), fibre diameters (**D**) and contact angles (**E**) show fibre characteristics over the two differing orientations. PCL Res-A denotes aligned fibres, PCL Res-R, randomly oriented fibres. For these analyses, an α level of 0.025 was chosen to identify significances[344].

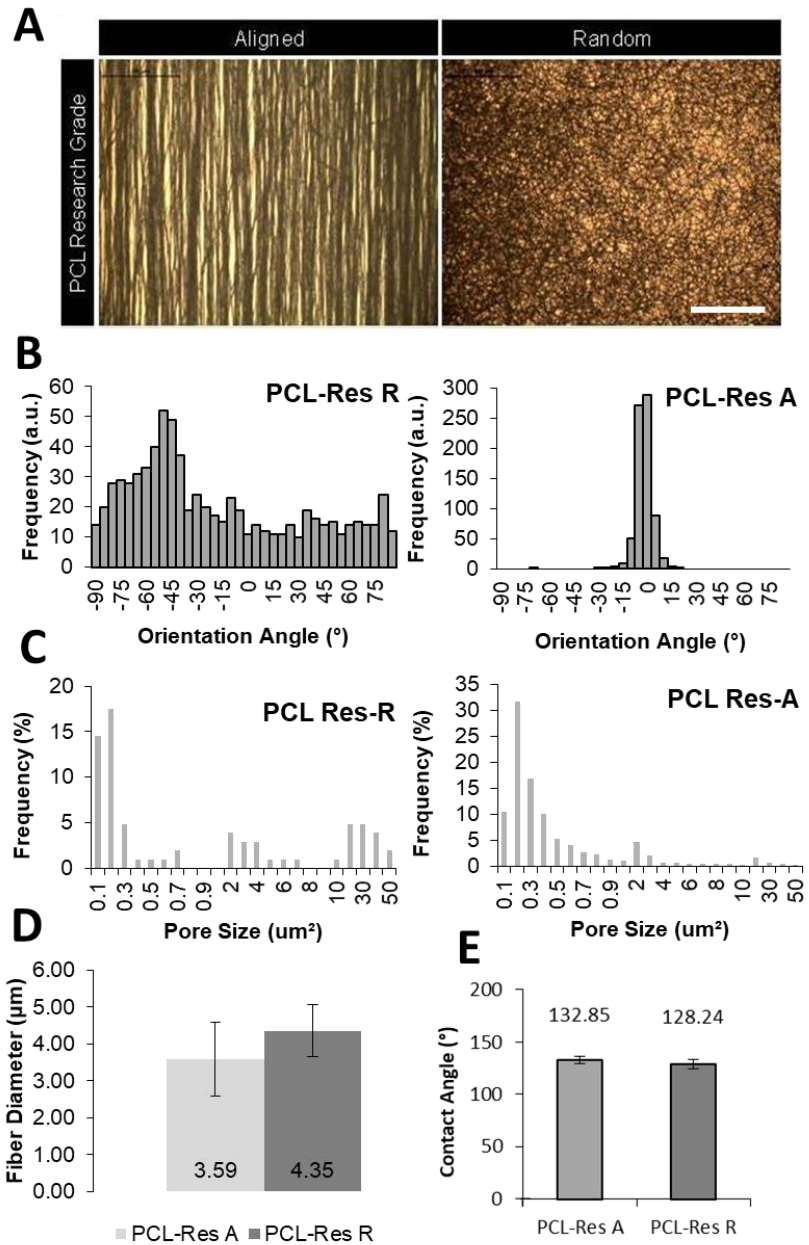

Appendix 2 Previous Work Optimising Scaffold Alignment for cACL Culture

LIVE/DEAD labelling images showed morphology, viability (**A**) and PSR histological staining showed collagen production (**B**) of cACLs on random and aligned electrospun fibrous scaffolds. As shown in the LIVE/DEAD images (**A**), cell adopted an aligned morphology on the unidirectional substrates, whilst those seeded onto the randomly oriented substrates showed a more random and spread morphologies. As evidenced by images of collagen staining (**B**), cells were producing highly aligned collagenous ECM at 7 days, as compared to random fibres where barely any collagen is observed. PCL Res-A denotes aligned fibres, whilst PCL Res-R denotes random fibre orientation. White arrows indicate fibre directions, scale bars on **A** and **B** represent 200 µm. Dr Douglas Ramos Marquez and Miss Georgia Crichton performed this work (unpublished undergraduate thesis, University

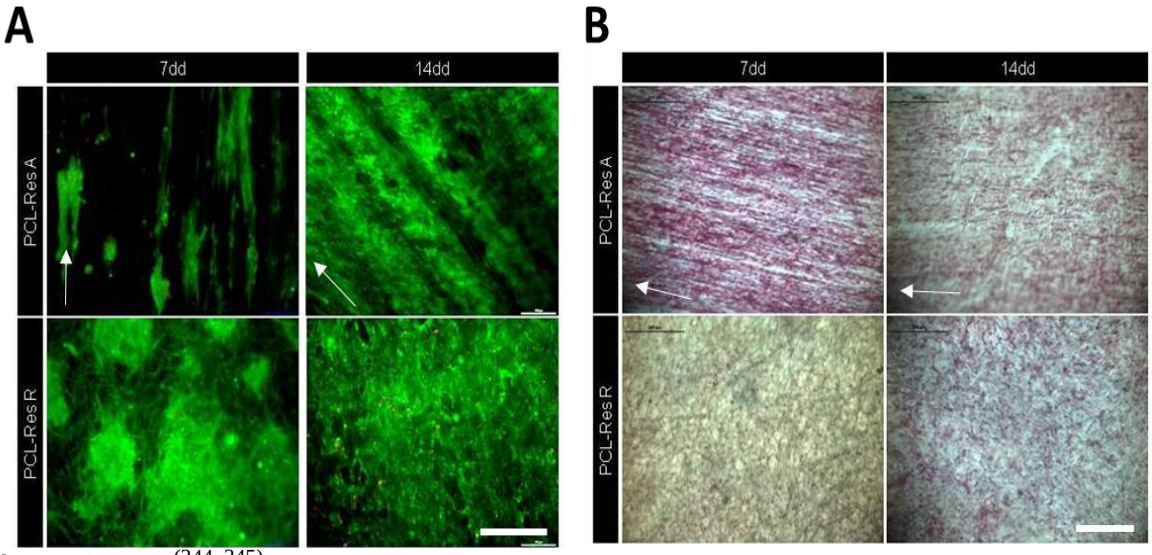

of Manchester)[344, 345].

Appendix 3 Limit of Elastic Strain for Recovery at Varying Strain Rates

The limit of elastic strain reached before plastic deformation began, across different strain rates. The strain rates used are detailed on the X axis. Dotted lines represent the following: 3% (red), 5% (green) and 7% (blue) strains at the tested scaffold length (25 mm).

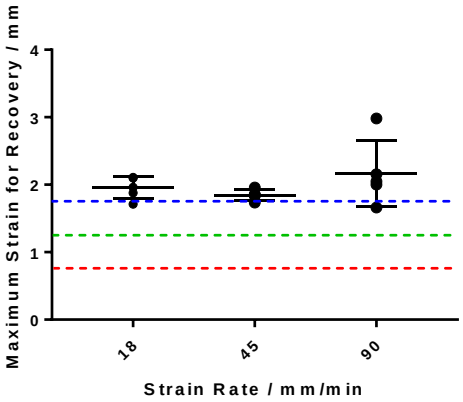

Appendix 4 Previous Work Testing Donor Variability in cACL Cells

LIVE/DEAD images showing morphological and cytotoxic responses and corresponding metabolic activity responses of three cACL donors on commercially acquired FBN1 (ab114345, Abcam UK; 10 ng sample-1, 60,000 cells sample^{-1}) functionalised substrates and their controls, performed by Miss Mingyue Hu (unpublished MSc thesis for MSc Biomedical Materials, University of Manchester). Data shows very little variation in the trends of cACL responses to the functionalised scaffolds. Arrows indicate fibre direction and scale bars represent 100 µm. For statistical analysis on metabolic activity graphs, Two way ANOVAs with Dunnet's post hoc comparisons were performed. Means ± SDs are displayed. * $p<0.05$, *** $p<0.001$, **** $p<0.0001$[352].

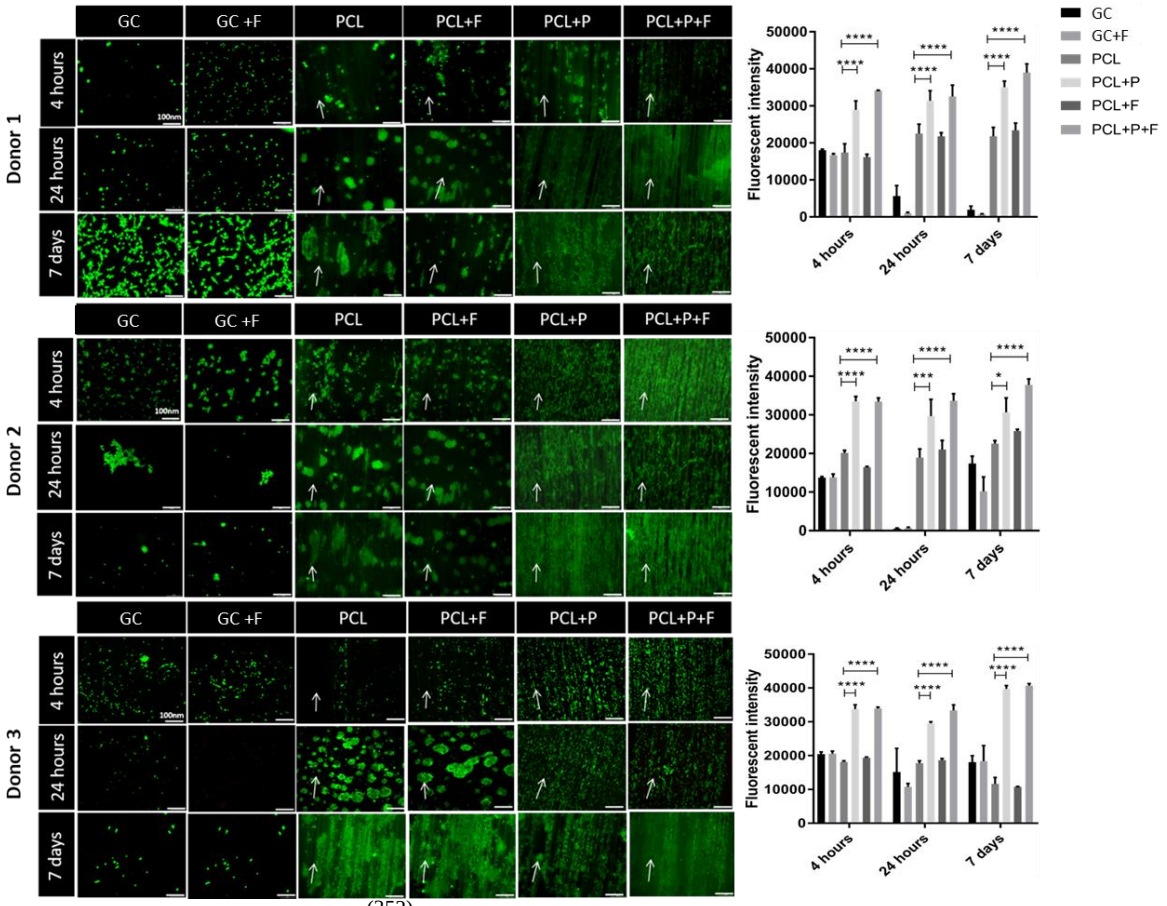

Appendix 5 FTIR Confirmation of Plasma Treatment

Samples were prepared as in section 3.2.9 and were allowed to dry for a period of one hour to prevent spectral saturation with O-H peak due to water. FTIR spectrophotometer Omic SmartOrbit software was used. For these samples, a diamond source (30,000 – 200 cm-1) was selected and background was read every 30 mins during experimentation. The instrument itself collected an average of 32 readings per analysis (total of 192 readings per condition).

Diagrams of the PCL chemical bonding before and after plasma treatment (**A**) (n=2) which shows the corresponding bonds labelled in the FTIR spectra (**B**). The spectra shows the continuity in chemical structure before and after electrospinning and the differences before and after air plasma treatment. Dotted lines indicate important chemical bonding, which is labelled above. Coloured arrows indicate which bonding corresponds which peak in the spectra. FTIR spectra below (**B**) shows the presence of the same peaks throughout different treatment conditions, bar the air plasma treated condition, which also exhibits a peak at a wavelength of ~3300 cm-1, indicative of an increase in O-H (carboxylic acid) bonds. Characteristic peaks at ~2900 cm-1, ~1700 cm-1 and ~1150 cm-1 indicate the presence of C-H, C=O and C-O bonds respectively. The absence of any C-Cl bonds at ~850 cm-1 indicate the suitability of chloroform for solubilising the PCL for electrospinning, as there appears to be no residual solvent. '**A'** indicates where in the chemical structure of PCL these bonds are positioned. Due to the now hydrophilic nature of the plasma treated samples, it was first considered that these bonds may be due to the presence of residual ethanol from the sterilisation protocol. This theory was rejected after this peak did not appear in the untreated PCL spectra. The increase of intensity in the peaks of the PCL pellet is likely to be due to closer contact of the material with the source. As the aligned fibres were mounted on glass coverslips, it was not possible to get them close to the source, unlike the pellets, which were much smaller and rounded in shape and dimension. Interestingly, the C=O peak (~1700 cm-1) in air plasma treated samples appears to decrease compared to non-plasma treated samples, perhaps due to destabilisation of the double bond.

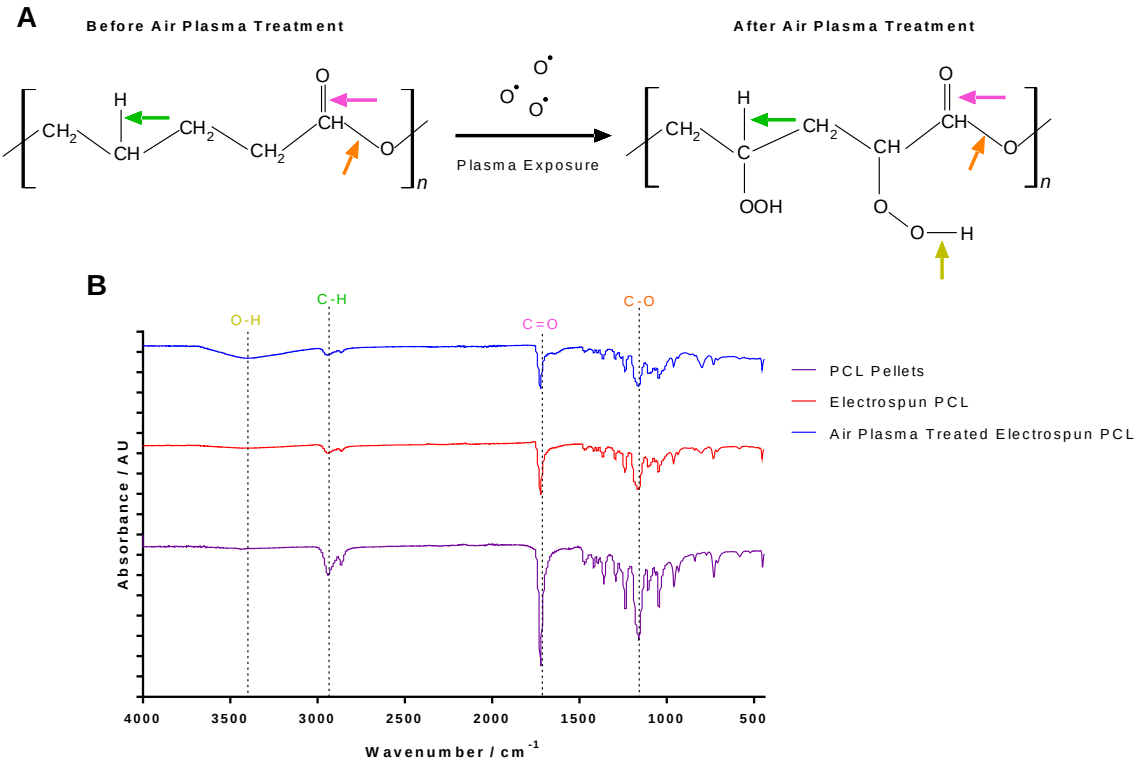

Appendix 6 SDS-PAGE to Ascertain Purity of Fibrillin-1 Fragments

To determine purity, conformation and approximate molecular weight of the in-house isolated protein fragments, an SDS-PAGE was performed. A solution of 2.5 µg of fibrillin-1 fragment was mixed with 5 µl of 4X LDS loading buffer. One sample of each fragment was reduced using 5 µl of 10X sample reducing agent before all samples were heated to denature (90ºC, 5 mins). A gradiented (4-12%) Bis-Tris gel in its cassette, was loaded into a chamber and covered with 1 L of 1X MOPS SDS running buffer. Samples were loaded into the gel, along with 10 µl of PrecisionPlus Protein AllBlue Standard at each end and run at 200 V (400 mA) for 1 hr. Gel was removed from chamber and cassette and covered with 20 ml of InstantBlue staining solution (2 hrs, room temperature) on a rocking plate at a speed of 10 RPM. Destaining was performed using reverse osmosis purified water for 30 mins and images were taken using an Epson scanner.

SDS-PAGE gel image detailing the size and purity of the in-house isolated fibrillin-1 fragments. 'NR' – non-reduced, 'R' - reduced. Reduction unwinds the disulphide bonds, breaking the protein tertiary structure. Ladders were run both to the left and right of the samples, indicating fragment size. Performed once due to prior validation of fragments. SDS-PAGE was run to confirm the purity of the fragments. Reduced and non-reduced

samples were run to observe upwards shift in the bands, which indicate characteristically high concentrations of disulphide bonding present in the cysteine-rich residues of the cbEGF-like and TB domains and can be observed in. This suggests that the fragment is correctly folded, with no dimerisation present and hence confirming the correct pairing of the disulphide bonds, and align with work previously published by Cheng *et al.* (2018)[389] for PF8, Bax *et al.* (2007)[310] for PF9 and Cain *et al.* (2012)[392] for PF17.1.

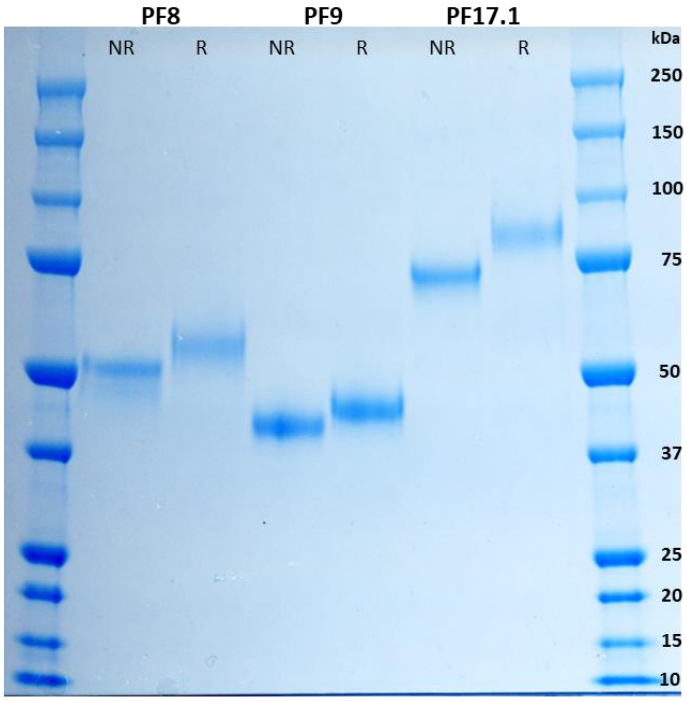

Appendix 7 cACL Metabolic Activity on Hydrophobically-Recovered Plasma Treated, Biofunctionalised Scaffolds

Metabolic activity of cACLs on hydrophobically-recovered scaffolds that have undergone fibrillin-1 fragment functionalisation immediately following plasma treatment and UV sterilisation. A proof-of-concept experiment at 4 hr time point was performed to determine whether plasma treatment was negating the effect of fibrillin-1 functionalisation (n=3, performed once). Scaffolds were dried following protein treatment and left to fully recover for a period of 2 weeks. Protein adsorption previously established, appeared to have stably adsorbed to the plasma treated surface. Freshly treated and non-plasma treated functionalised controls were performed alongside. Graph **A** shows that whilst 1000 ng of PF8/PF17.1 increased metabolic activity on untreated scaffolds, fragments universally increased the

metabolic response of cACLs on hydrophobically recovered ones. Freshly treated scaffolds appeared to lose any effect of fibrillin-1 functionalisation due to the cells adhering to the plasma-treated surface. Graph **B** demonstrates that metabolic viability of the cells was not lost due to hydrophobic recovery. Bars display means and error bars show standard deviations. Two-way ANOVA with Tukey's HSD post hoc test (A) and Sidak's multiple comparisons (B) was performed. **p<0.01, ***p<0.001, ****p<0.0001.

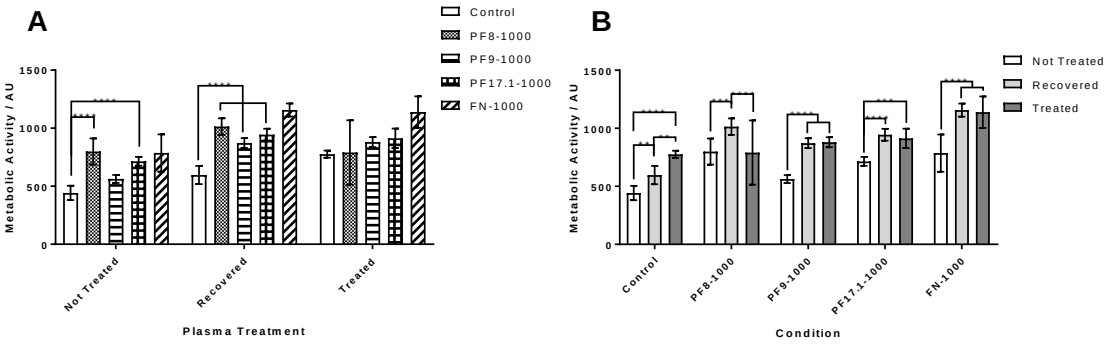

Appendix 8 ALP Activity of cACLs on the Functionalised Scaffolds

cACLs on scaffolds were checked for alkaline phosphatase (ALP) production to determine the probability of cells causing calcification in the ligament and to determine that the cells were not differentiating into osteoblast-like cell types. Saos-2 cells were used as a positive control and seeded at lower densities (in accordance with the literature) to account for increased proliferative capacity. Cells were cultured for 2 weeks in hgDMEM (cACLs) and McCoys 5A (Saos-2) medium (10% FBS, 1% A/A) and replenished every 2-3 days.

All cells were lysed in 400 µl of a 1% triton-X-100 solution in dH_2O and 80 µl of each sample (in triplicate) was pipetted into a clear 96 well plate. Two of the aliquots were used for measurement and one as a negative control. *p*Npp substrate (50 µl) was added to the aliquots and incubated (room temperature, 1 hr). To stop the reaction, 20 µl of 2 M $NaOH_{(aq)}$ was added. Negative controls had 2 M $NaOH_{(aq)}$ added before the *p*Npp substrate. Absorbance maximum was read at 412 nm due to constraints in instrument capability. Standard curves were generated using increasing concentrations of the *p*Npp substrate (0 – 80 µM, as above) diluted in assay buffer (total volume 120 µl) developed with ALP enzyme (10 µl). Reaction was stopped after 1 hr with $NaOH_{(aq)}$ (incubation conditions and $NaOH_{(aq)}$ molarity as above, 20 µl). pNpp concentration from cell lysates were determined using the

standard curve for ALP activity (U L^{-1}) was calculated using the below equation[454] and standard curve.

$$U\,L^{-1} = A/V/T$$

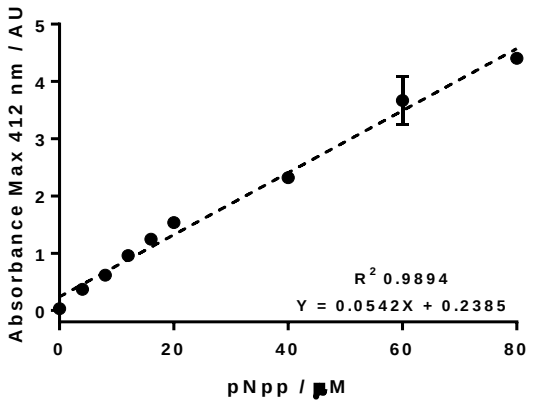

Due to the ability of ACL fibroblasts to differentiate into osteoblasts, it was imperative that the scaffold (with/without functionalisation) did not induce any osteoblastic changes. Increase in calcification could invalidate any produced tissue engineered ligament, compromising its structural and mechanical integrity. A known indicator of osteoblastic cell lineage, alkaline phosphatase (ALP), was determined for activity within the cells on functionalised scaffolds.

A preliminary experiment was performed to check ALP activity of functionalised cACL scaffolds over 14 day period, compared to a well-defined ALP-expressing cell source (Saos-2)[455]. As determined by the graph below, Saos-2 cells produced significantly more ALP than cACLs on the scaffolds after 2 weeks ($p<0.0001$), with minimal cACL production of ALP detected. Means ± SDs are displayed. A two-way ANOVA with Sidak's multiple comparisons was used to determine significances. Statistics are based on a single experiment. ****$p<0.0001$.

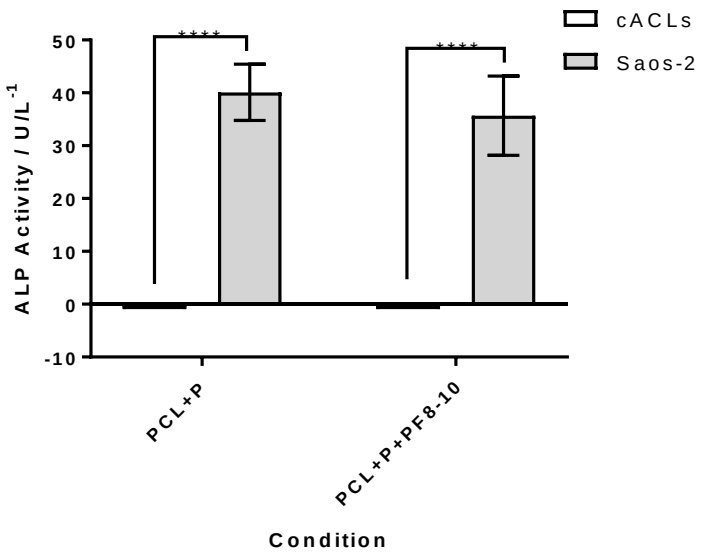

Appendix 9 Immunofluorescent Staining of Fibronectin-Adsorbed Fibres to Differentiate Neo-Matrix

Images showing the background staining of fibronectin-coated fibres detected by the rabbit anti-fibronectin antibody used in ECM staining. The difference between neo-ECM fibronectin produced by the cells and fibronectin adsorbed to the scaffolds is displayed, 1 day post seeding. White arrows indicate fibre alignment and scale bar represents 250 µm.

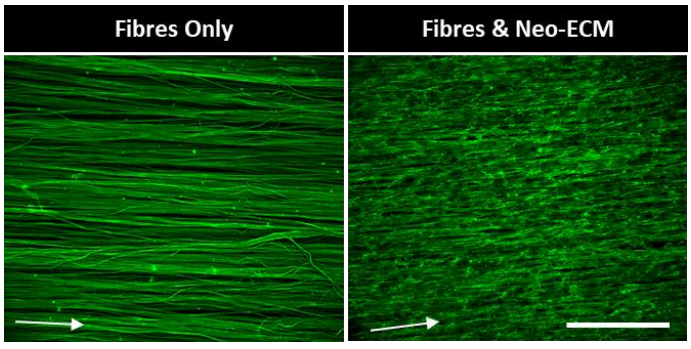

.

Appendix 10 Negatives for Immunofluorescent Staining in Chapter 4 and 6

Immunofluorescent negative control images for primary antibody specificity and background auto fluorescence. Negatives for: ACL ECM staining for human and dog cells (A, scale bar 250 µm), collagen type III fluorescent staining (B, scale bars 250 and 500 µm for 10 and 1000 ng respectively and 250 µm for the blank), 6His tag for protein adsorption (C, scale bar 500 µm) and the negatives for integrin staining and non-BSA blocked cell morphology/attachment controls (D, scale bars 50 and 500 µm respectively). White arrows show fibre direction.

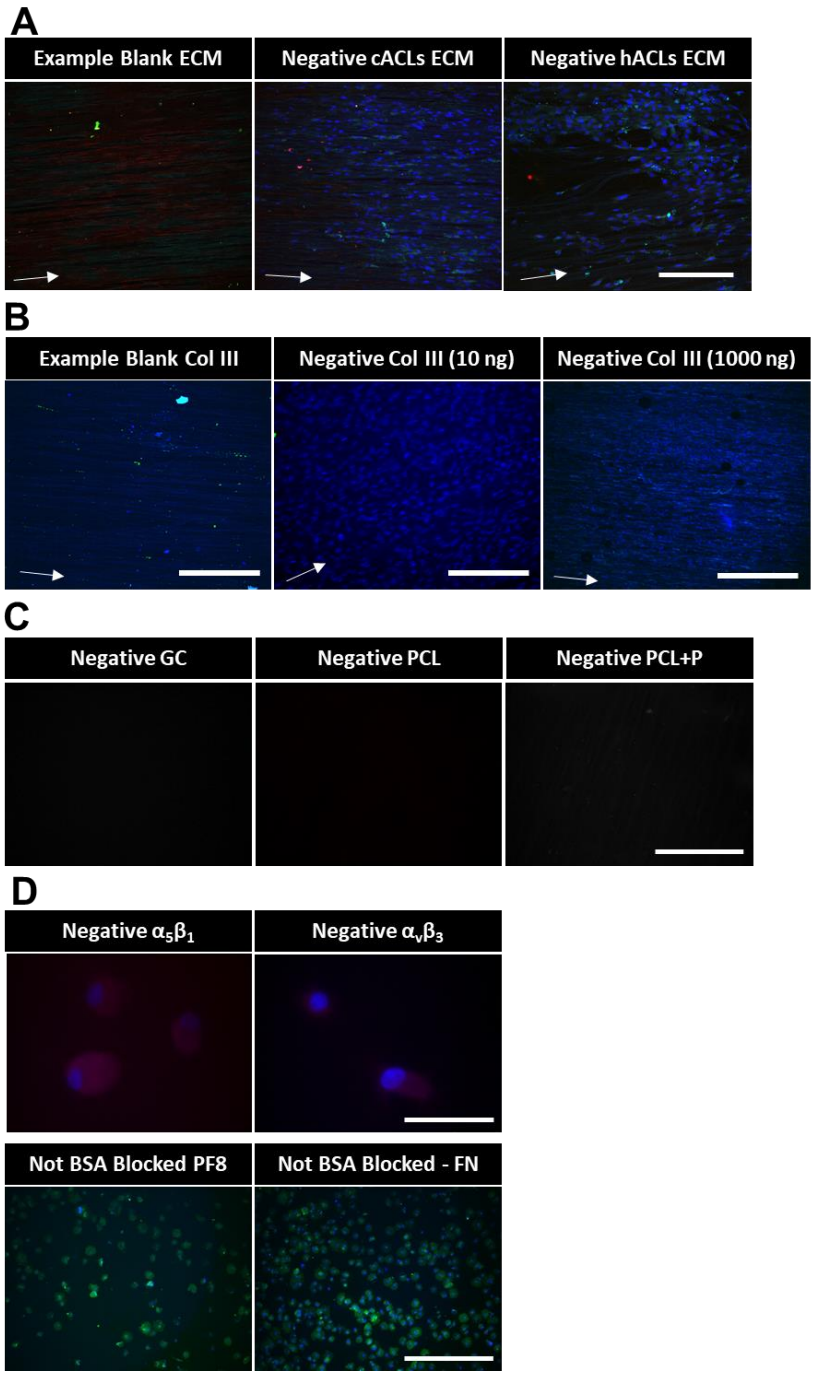

Appendix 11 Macros for FIJI ImageJ Analysis

Appendix 11.1 Nuclei Counting

Code for 'DAPICounterNew' macro written by Mr Wouter van Verre (on 05/08/2019, unpublished) to process and count nuclei in FIJI ImageJ. Images were imported into FIJI ImageJ, stacked and thresholded before the application of this macro.

```
//setAutoThreshold("Default dark no-reset");

N = nSlices
print("Found " + N + " Slices")

for (i = 1; i <= N; i++) {
	setSlice(i);
	run("Analyze Particles...", "size=25-450 exclude summarize");
}
```

Appendix 11.2 ECM % Area Analysis

Code for 'MeasureMacro' macro written by Mr Wouter van Verre (on 05/08/2019, unpublished) to analyse the % area of 16 bit TIFFs from immunofluorescent ECM staining images. Images of the same channel were imported into FIJI ImageJ, stacked and thresholded to negatives before the application of this macro.

```
setAutoThreshold("Default dark no-reset");

N = nSlices
print("Found " + N + " Slices")

for (i = 1; i <= N; i++) {
	setSlice(i);
	run("Measure");
	run("Next Slice [>]");
}
```

Appendix 11.3 Compiling Separate Greyscale TIFFs for Total % Area ECM Analysis

Code for 'ECMImageCompiler' macro written by Mr Wouter van Verre (on 06/04/2020, unpublished) for compiling independent image channels to enable the measuring of total ECM per image. This macro matched images from separate channels, stacked and performed z projections to show the final image for analysis. Images were then thresholded to a negative stack projection before applying the 'MeasureMacro', detailed in Appendix 9.2.

```
import sys
import os
import os.path

from ij import IJ, ImageStack, VirtualStack, ImagePlus
from ij.plugin import ZProjector
from ij.io import FileSaver

## https://forum.image.sc/t/max-intensity-projection-in-jython/10757/5
def getMIP(stackImp):
        """
        Create a maximum intensity projection (MIP) from an ImagePlus stack

        @return ImagePlus maximum projection
        """
        zp = ZProjector(stackImp)
        zp.setMethod(ZProjector.MAX_METHOD)
        zp.setStopSlice(stackImp.getNSlices())
        zp.doHyperStackProjection(False)
        return zp.getProjection()

basepath = r"/mnt/usb/Zara_ECM_Images_28d/"


files_collagen = os.listdir(os.path.join(basepath, "Collagen1A1"))
files_fibrillin = os.listdir(os.path.join(basepath, "Fibrillin"))
files_fibronectin = os.listdir(os.path.join(basepath, "Fibronectin"))
filecombos = list()

for file in files_collagen:
        base, end = file.split("W")

        files = [file]

        for otherfile in files_fibrillin:
                if otherfile.startswith(base):
                        break
        else:
                print("[E]  No  matching  file  found  in  Fibrillin  folder  for  base
".format(base))
                sys.exit()

        files.append(otherfile)

        for otherfile in files_fibronectin:
                if otherfile.startswith(base):
                        break
        else:
                print("[E]  No  matching  file  found  in  Fibronectin  folder  for
base".format(base))
                sys.exit()

        files.append(otherfile)
        filecombos.append(tuple(files))
```

```
ims = None
for combo in filecombos:
        base, end = combo[0].split("W")
        fpath = os.path.join(os.path.join(basepath, "Collagen1A1"), combo[0])

        imp = IJ.openImage(fpath)
        ims = ImageStack(imp.width, imp.height)
        ims.addSlice(imp.getProcessor())

        imp = IJ.openImage(os.path.join(os.path.join(basepath, "Fibrillin"), combo[1]))
        ims.addSlice(imp.getProcessor())

        imp = IJ.openImage(os.path.join(os.path.join(basepath, "Fibronectin"), combo[2]))
        ims.addSlice(imp.getProcessor())

        stackImp = ImagePlus(base, ims)
        projection = getMIP(stackImp)

        print(combo[0], base)
        fs = FileSaver(projection)
        fs.saveAsTiff(os.path.join(os.path.join(basepath,   "projections"),      base   +
".tif"))
```

Appendix 12 Aspect Ratio Measurements for cACLs on Biofunctionalised Scaffolds

Immunofluorescent images of collagen type I staining at day 1 were used to generate aspect ratio measurements. Images from all conditions were imported into FIJI ImageJ and compiled into a single stack and brightness and contrast were altered uniformly to enable clear visualisation of the entire cell body. Cell bodies were manually identified using the freehand tool and 25 cells per image were analysed for aspect ratio measurements (9 images per condition).

As observed below, **A** shows the functionalised conditions on non-plasma treated scaffolds, whereas **B** shows those on plasma treated ones. Interestingly, cells seeded onto plasma treated scaffolds, functionalised with 1000 ng of PF8, had higher aspect ratios than the negative (no biofunctionalisation, termed ‘Control’) and positive (fibronectin, termed ‘FN-1000’) controls, as well as the lower concentration (10 ng) of PF8 (all $p<0.0001$). Higher aspect ratios indicate elongation, and the higher the ratio, the more elongated the cell (aspect ratio of 1 = a perfect circle).

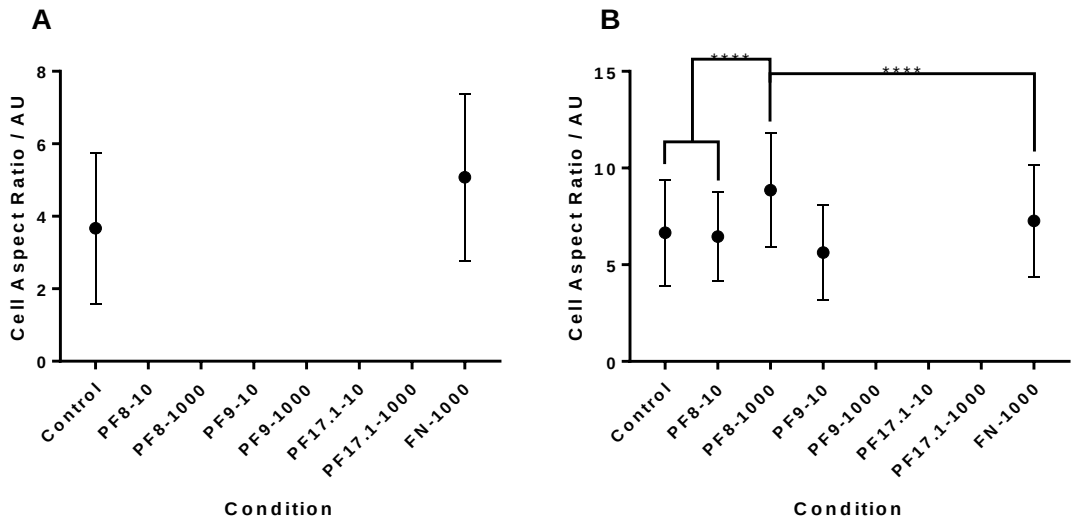

Appendix 13 Kendall's W for Coordinance of Variance Observer Outcomes

Coordinance of variance between two scoring observers was calculated. Each value shown below is the average of that category, taking into account the scores of both observers with both sets of scores. Average total scores of 0.82 and 0.72 confirm 'almost perfect' agreement within observer scoring and 'substantial' agreement between observer scoring (using the categories defined by Landis and Koch (1977)[420]).

Scoring Topic	Intra-Observer Agreement (mean)	Inter-Observer Agreement (mean)
ECM Organisation	0.855	0.8075
Cell Shape	0.7588	0.5351
Cell Distribution	0.7516	0.6331
Cell Alignment	0.8740	0.7848
Vascularity	0.8616	0.8587
AVERAGE	**0.8202**	**0.7238**

Appendix 14 Positive Controls for Histology

Positive controls were performed for special staining protocols on the human ligament tissue. Alcian blue pH 1.0 used porcine cartilage, alcian blue pH 2.5, ovine intestinal mucosa, PSR – rat lung and lastly, a Saos-2 cell pellet was used as the positive control for von Kossa. All black scale bars represent 250 µm, and the white scale bar, 500 µm.

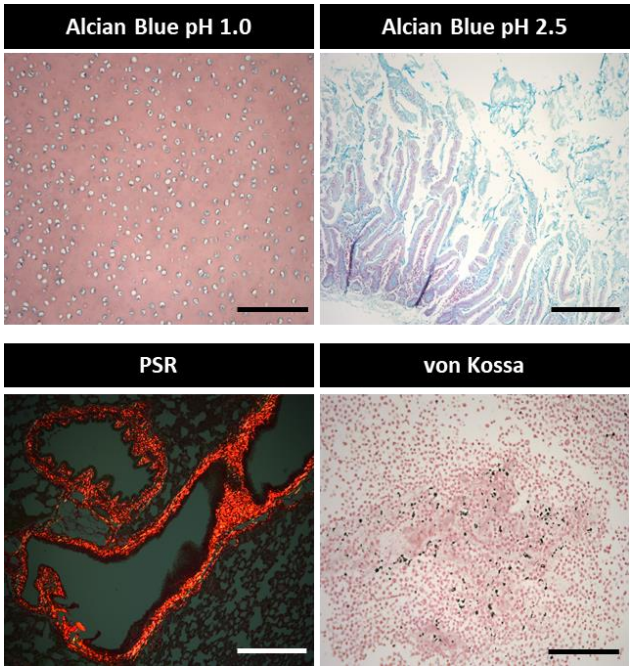

Appendix 15 Controls for Immunohistochemistry

Both the positive staining and negative/background controls for IHC staining in Chapter 5. To perform these positive controls, selected tissues, with known presence of target protein were stained. For the negatives (shown in the left column and the small inserts in the right-hand column), primary antibody was omitted and replaced by PBS to determine any artefacts due to endogenous reactions or non-specificity of the secondary antibodies for all donors and staining controls. COL1 – collagen type I (positive control – porcine skin), COL3 – collagen type 3 (positive control – rat intestine), TEN-C – tenascin-c (positive control – damaged ovine tendon), DEC – decorin (positive control – ovine tendon), FN – fibronectin (positive control – porcine skin), FBN – fibrillin (positive control – porcine ligament), ELN – elastin (positive control – porcine liver). Scale bars represent 500 µm.

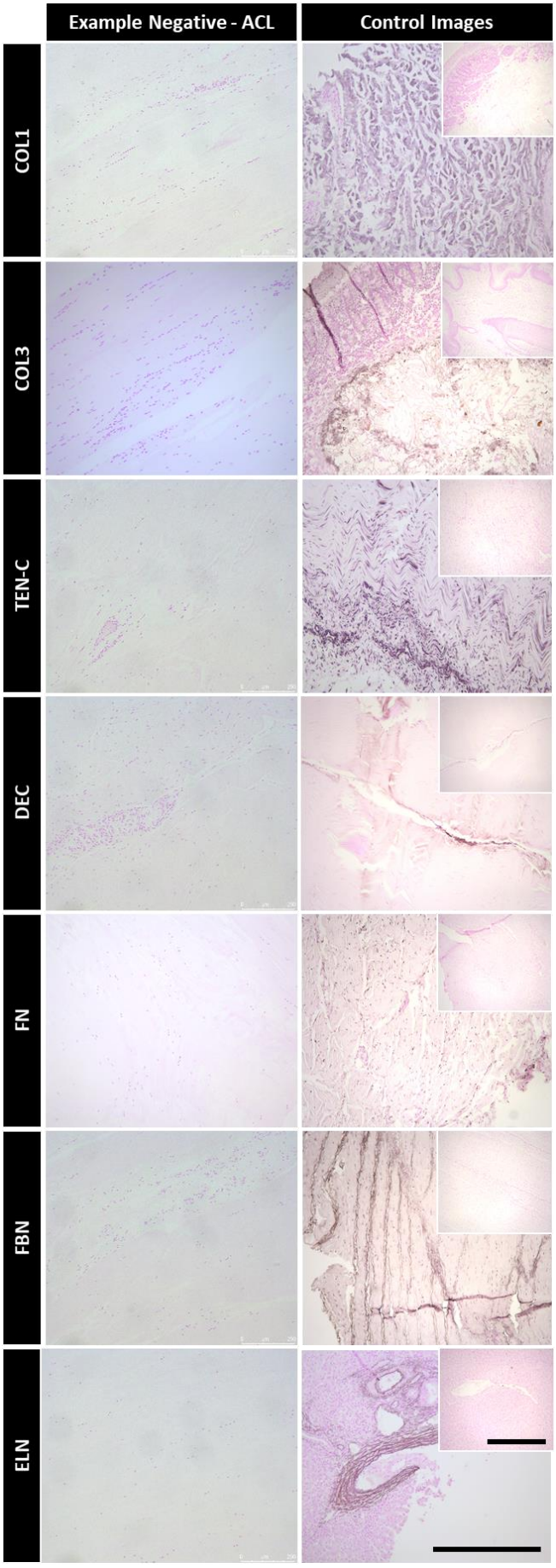
Example Negative - ACL
Control Images
COL1
COL3
TEN-C
DEC
FN
FBN
ELN

Appendix 16 Cell Morphologies of hACLs

Bright-field images of cells stained with 0.5% crystal violet, from a densely attached (**A**) and a sparsely attached (**B**) batch. Scale bars represent 250 µm.

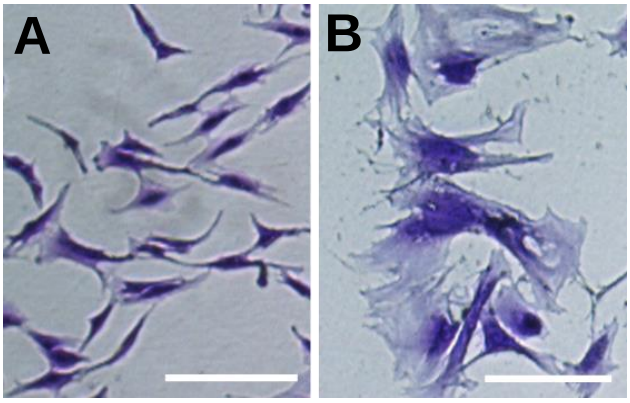

Appendix 17 Standard Curves from Chapter 6

Lamda standard curve used for calculation of dsDNA concentration in samples, using QuantIT Picogreen assay (**A**) and the standard curve used to calculate the concentration of ECM-associated sulphated GAGs in human ACL ligamentocyte cultures (**B**).